Modelling the pharmocokinetic distribution of macromolecules

Snell, Paul Robert

Award date:
1994

Awarding institution:
University of Bath

MODELLING THE PHARMACOKINETIC DISTRIBUTION OF MACROMOLECULES

Submitted by Paul Robert Snell Bsc Msc

for the degree of PhD

of the University of Bath

1994

.....

ProQuest LLC
789 East Eisenhower Parkway
P.O. Box 1346
Ann Arbor, MI 48106-1346

Abstract

A physiological pharmacokinetic model was developed to investigate the fate of macromolecular drugs after intravenous injection. The purpose of the model was to examine the effect of molecular radius on the distribution of both negatively charged protein and uncharged macromolecular drugs in man, both in the absence and presence of hepatic metabolism. This was achieved by taking into account the regional capillary permeabilities to different size macromolecules, and the physiology and flow rates within each compartment. Mathematical models of capillary permeability were developed to allow the fitting of appropriate physiological experimental data from the literature. The latter models were used to develop intercompartmental rate constants used in the physiological three-compartment pharmacokinetic model. The major objective was to predict via simulations the effect of molecular radius on biodistribution, in particular access to interstitial fluids. In addition, the proposed model allowed calculation, for molecular radii from 20-70Å, of the fraction of the dose present in the blood and the liver, the fractions of the dose excreted via the kidneys and metabolised by the liver, and the total fraction of the dose eliminated, as a function of time. A necessary objective of the study was the development of a computer programme named 'MACROHOURS' which had two main purposes; firstly to aid in the solution of cubic functions within the physiological three-compartment pharmacokinetic model equations, and secondly to perform simulations once the solutions to the model equations had been established.

Simulations suggested that generally molecular radii of 40-55Å produce the greatest fraction of a macromolecular drug dose in the interstitial fluids, and that radii less than 30Å are excreted too rapidly to gain significant access to tissues. For a macromolecular drug which is metabolised very quickly, then optimum molecular radii for tissue uptake can be as low as 35Å. Protein macromolecules (i.e. negatively charged species) were found to be better candidates than uncharged macromolecules for delivering the

greatest fraction of the dose to tissues. In the case of the protein macromolecules in the absence of hepatic metabolism or when the metabolic rate was low, the upper size range could be extended to 65Å radius to give high concentrations in the tissues over very long time periods.

The model was used in subsequent work to compare simulations with experimental animal data of plasma clearance of proteins and drug conjugates in the rat. For albumin-methotrexate conjugates it was possible to estimate their rate of hepatic metabolism and use this to predict tissue uptake. Comparison of clearance data for proteins of various dimensions was less successful, due to variable metabolism. It was concluded that the model would be strengthened by obtaining more physiological data for the animal specifies of interest.

Acknowledgements

I would like to thank my supervisors, Drs. Colin Pouton and Lidia Notarianni for their constant support and enthusiasm throughout the time spent on this thesis. I would also like to thank Dr. R. England. I would like to thank SERC for financial support and the University of Bath for providing research facilities. I would also like to thank my parents for their support and for always being there. Finally, I would like to thank Wendy Pearce and her staff for their help in the typing of this thesis.

Contents

Abbreviations

a	Molecular radius of macromolecule (Å)
F/P ratio	Glomerular filtrate/plasma concentration ratio
L/P ratio	Lymph/plasma concentration ratio
V_C	Volume of blood or central compartment (compartment No.1) (ml)
V_L	Volume of lymph or total interstitial compartment (compartment No.2) (ml)
V_H	Blood volume of the liver or hepatic compartment (compartment No.3) (ml)
GFR	Glomerular filtration rate (ml/min)
LFR	Lymphatic flow rate (ml/min)
BLFR	Blood to lymph flow rate (ml/min)
Liver/Plasma ratio	Liver/plasma concentration ratio
Plasma/Liver ratio	Plasma/liver concentration ratio
Plasma/Lymph	Plasma/lymph concentration ratio
Total blood flow rate to the liver	Total blood flow rate to the liver (ml/min)
Total blood flow rate from the liver	Total blood flow rate from the liver (ml/min)
R	Respective F/P or L/P ratio
R_0	Parameter defined in Model A representing the theoretical value of R at a=0.

n, k	Parameters used in Models A, B and C to control the shape of the curve (k representing the gradient)
ao	Parameter defined in Model B representing the molecular radius at which R=1.0 (Å)
mrrh	Parameter defined in Models C representing the molecular radius at which R=½.
f	Parameter defined in Model C4 representing a value at which R becomes linear
D_o	Dose (unity)
k_{excr}	First-order compartmental parameter controlling the rate of renal excretion of drug (min^{-1})
k_{12}	First-order inter-compartmental parameter determining the rate of movement of drug from blood to lymph (min^{-1})
k_{21}	First-order inter-compartmental parameter determining the rate of movement of drug from lymph to blood (min^{-1})
k_{13}	First-order inter-compartmental parameter determining the rate of movement of drug from blood to liver (min^{-1}).
k_{31}	First-order inter-compartmental parameter determining the rate of movement of drug from the liver to blood (min^{-1}).
k_m	First-order compartmental parameter controlling the rate of metabolism from the liver (hepatic clearance) (min^{-1}).
A_P	Amount (mass) of drug in blood compartment with respect to time
A_L	Amount (mass) of drug in lymph compartment with respect to time
A_{II}	Amount (mass) of drug in liver compartment with respect to time
γ, α, β	Roots of the cubic equation (equation 16)
C_P	Concentration of drug in blood compartment with respect to time

A_{EXCR}	Amount (mass) of drug excreted by the kidneys with respect to time
A_M	Amount (mass) of drug metabolised (hepatically cleared) by the liver with respect to time.
A_E, A_{ELIM}	Total amount (mass) of drug eliminated with respect to time
k_{filt}, a_{filt}, n_{filt}	Values of k, ao and n obtained from the fit of Model B to the selected F/P ratio data
k_{lymph}, a_{lymph}, n_{lymph}	Values of k, ao and n obtained from the fit of Model B to the selected L/P ratio data
a_i	Coefficients of the cubic equation
b_{n-1}, b_{n-1-r}	New coefficients of the cubic equation after application of synthetic division following the location of the first root by the Newton-Raphson technique.

Chapter 1

Introduction

Macromolecular prodrugs, pharmacokinetics and cancer chemotherapy

1.1 Therapeutic failures in controlling the spread of cancer micrometastases

One of the most critical and difficult problems in the management of cancer is the control and treatment of cancer micrometastases [1, 2]. It is the ability of these tiny malignant tumour cells to disseminate from a locally growing primary tumour and to form secondary tumours at near and distant sites in the body that is the most life-threatening aspect of cancer [1-3]. Completion of this process means that cells released from the primary tumour must survive a series of complex interactions with host cells and tissues which are now widely accepted in the literature [1, 3-7]. Typically, these are the growth and invasion of malignant cells at primary sites, followed by their penetration into local tissue, lymphatics and small blood vessels. Once in these new compartments, malignant cancer micrometastases cells can detach from the site of penetration as either single cells or small emboli and be transported to near and/or distant secondary sites, where they can implant in and invade surrounding tissues. Here they survive in and respond to their new microenvironments, where they can proliferate, giving rise to a further tumour or tumours (secondary tumours) which subsequently metastasize themselves, producing more cancer micrometastases which continue to spread in this way (multiple secondaries) [1, 3-7].

In the treatment of cancer micrometastases there are frequent therapeutic failures [1, 2]. The lymphatic system together with the blood circulatory system is the main route by which cancer micrometastases traverse the body [2]. All cancer micrometastases take this route, regardless of whether they are micrometastases which have been produced by, and have broken away from, either a primary or a secondary tumour. Having detached from the primary tumour the cancer micrometastases 'float' in the interstitial fluid (tissue fluid) and either enter the blood circulation directly, or more frequently they enter into the lymphatic system [1-7]. In the former case, the cancer micrometastases either arrest in the walls of minor blood vessels and grow into a secondary tumour there, which then subsequently metastasizes, and/or extravasate freely into surrounding normal tissue, developing into a secondary tumour there. In the more common latter case, once in the lymphatic system the cancer micrometastases

either remain there, becoming trapped at the site of near and/or distant draining lymph nodes, developing into a secondary tumour which then metastasizes (the site of the lymph node closest to the primary tumour is often the location of the first secondary tumour), and/or are carried through the lymph node and lymphatic system, and are eventually emptied into the bloodstream. Once in the bloodstream via this route they subsequently extravasate freely into normal tissues in other parts of the body, developing into a secondary tumour there (the most frequent organ site of metastasis is often the first organ encountered by the circulating cancer micrometastases, and in distant metastasis this is often the lung). Consequently even if any visible tumour is either removed completely by surgery (if surgery is possible), or is destroyed with irradiation during radiotherapy, or is treated successfully using cytotoxic anticancer drugs during chemotherapy, or by various combinations of these treatments (depending upon the type of cancer and the location of the tumour), many cancer micrometastases of obvious great potential threat will still be lurking somewhere within the lymph compartment, i.e. the lymphatic system and the interstitial fluid (i.e. the total interstitial or extravascular fluid) [1, 2]. Hence in order to control and treat cancer successfully, these cancer micrometastases within the lymph need to be killed before they have a chance to develop into tumours either there, or following their distribution via the lymphatic and blood circulatory systems to any other parts of the body. Thus, a complete eradication of cancer micrometastases disseminated to a wide area of lymphatic involvement is required which is an extremely difficult task to accomplish [2]. The only efficient way to achieve this is to specifically target cytotoxic anticancer drugs to the lymph, since of the main cancer treatment methods, cytotoxic anticancer drugs used in chemotherapy are the most practical forms of treatment if the disease has become too widespread or secondaries are present (such drugs will need to have a high lymphotropic character [2]). Both surgery and radiotherapy can necessarily for practical and physiological reasons only be directed towards localised tumours together with some of the surrounding local tissue and associated local draining lymph nodes, rather than towards controlling the spread of cancer micrometastases [1]. This is

because in most cases of cancer the disease is often only diagnosed following the discovery of a visible growth, and by this time many cancer micrometastases could have already traversed further within the lymphatic system (and indeed the blood circulatory system), and will no longer be confined just to the local lymph nodes and local normal tissue surrounding the tumour from which they originally detached. The cancer micrometastases are also because of their extremely small size (radius less than 150 μm), effectively invisible, making them impossible to locate individually, and also easily transportable, usually moving freely into and out of both the lymphatic and blood circulatory systems. As will be outlined in Section 1.2 along with some of the associated key pharmacokinetic studies in the literature, site-specific drug-delivery in the field of cancer chemotherapy is routinely distinguished into either actively or passively targeted macromolecular anticancer drug systems.

The situation is further complicated by the fact that in contrast to the targeting of anticancer drug systems to solid (vascularised) tumours, which have been shown to possess their own peculiar vascular properties, namely, (a) tumour angiogenesis resulting in an immature or vestigial tumour capillary basement membrane and hence a leaky tumour vasculature (hypervasculature) [8-10], (b) hyperpermeability of tumour blood vessels [11-16], mediated by enhanced vesicular transport or via transendothelial channels [11, 14], with the underlying physiological purpose to import sufficient fibrin which is essential for a functional tumour interstitium and development [12], and promoted by the existence of a tumour-secreted factor (Vascular Permeability Factor) [14, 17-20], a protein with sequence homology to platelet derived growth factor (PDGF) [21, 22], and/or kinin action [2, 23], (c) a complete absence of any organised lymphatic drainage system [2, 8, 24-28], resulting in elevated tumour interstitial pressure and hence minimal tumour drainage, and (d) architectural incompleteness of tumour blood vessels resulting in increased extravasation rates [8, 29]; the targeting of anticancer drug systems to the lymph is dependent upon normal vascular properties [2]. Hence when one considers the spread of cancer micrometastases via the lymph and the

targeting of anticancer drug systems to the cancer micrometastases located there, normal vascular properties must be considered [2]. The key to this problem is molecular size, although other factors such as charge also influence the process, and requires consideration to be given to the exchange of macromolecules across the microcirculation, and this is described in Chapter 2.

1.2 Site-specific drug delivery in cancer chemotherapy

Site specific drug delivery is routinely categorised into either 'active' or 'passive' drug-targeting [30, 31]. In the field of cancer chemotherapy the former approach is characterised by the use of specific targeting residues, the best known of which are monoclonal antibodies and their various fragments and conjugates, which recognise many tumour-associated antigens. Conversely the latter approach relies on the physicochemical properties of the particular drug system to dispose it towards an elevated therapeutic index. The aim of both the active and passive approaches to drug-targeting is to maximise the therapeutic response to a drug by delivering it specifically to the target site, whilst minimising the toxic effects at non-target sites [32].

Until very recently, the main thrust of work in the field of cancer chemotherapy has been in the active-targeting area. This has led to the development of many sophisticated monoclonal antibody systems (many of which are of murine origin), which are protein based and macromolecular in nature, and which can be used specifically to mobilize endogenous defences and to direct attached low molecular-weight therapeutic anticancer agents, such as cytotoxic protein drugs, toxins, and radionuclides, to tumours. Indeed, they have already established themselves as valuable diagnostic agents for both primary and secondary tumour growths when bound to these low molecular-weight anticancer agents [33, 34]. Monoclonal antibodies used only in their naked form generally have little activity on the growth of the tumour themselves. There are many experimental studies of monoclonal antibody systems in the literature directed towards a variety of tumour types (many in mice bearing xenografts of various

human carcinomas), using various routes of administration (mostly intravenous) and a variety of different fragments and conjugates, and utilizing various linkages (usually covalent bonding). Typical of these, and perhaps indeed the more appropriate to this study, are some of the more recent pharmacokinetic studies [35-71, 118-120].

Despite great advances in the technology of antibody production and in synthetic chemistry, and also in the performance of a large number of clinical trials, the obvious potential therapeutic benefits of these actively targeted monoclonal antibody systems does however remain to be realised. They have generally proved disappointing for several reasons, namely they (a) can never really be loaded with enough antibody to effect complete tumour death since high levels of circulating tumour antigen can form complexes with the administered antibody, leading to rapid clearance from the blood and reduction in tumour localisation, (b) show variable and often only relatively satisfactory degrees of specificity of monoclonal antibody-tumour antigen binding and tumour localisation due to (a), and also due to the fact that some antibodies are more tumour specific than others, (c) are prone to some localisation at other sites due to nonspecific uptake by the reticuloendothelial cells in some organs (e.g. lung and spleen), and also due to some antibody aggregation or cross-reactivity with normal tissue, (d) produce immunity to antibody if used extensively, (e) cause several unwanted site-effects, the most principal of which is myelosuppression, and (f) exhibit different and often only relatively satisfactory pharmacokinetics due to their limited and diverse size ranges [72-75]. There have recently been several reviews describing the many concepts and aspects involved in the use of monoclonal antibodies as therapeutic agents, and giving many of the recent studies and a historical summary of some of the key earlier studies, together with a discussion on the current clinical pharmacokinetic status using these actively-targeted systems [73, 75-80]. To date, the most interesting feature of monoclonal antibodies and their fragments and conjugates is that when they are administered intravenously for diagnosis or treatment of a cancer, they tend to distribute heterogeneously within the tumour substance [81-102]. This nonuniformity

of distribution often reflects the intrinsic heterogeneity of the tumour mass with respect to factors such as antigen density, vascularization, capillary permeability, degree of necrosis, time, and interstitial pressure [14, 81-85, 89, 92, 107, 245]; but also may reflect inefficient penetration from the blood vessels into the tumour [86, 90, 92, 93, 101, 102]. In most cases the transport of bindable antibody through the tumour interstitium is retarded by its specific binding to tumour antigen. This has led to the concept of a "binding site barrier" [86, 87, 90, 91, 97], since although formation of antigen-antibody complexes per se does not present a mechanical barrier to the uncomplexed monoclonal antibody, binding to antigens in the immediate proximity of the blood vessels does however significantly decrease the number of free, diffusable molecules available for penetration deeper into the tumour substance. Indeed, recent modelling [86-88, 90, 91, 94-98] and experimental [81, 83, 84, 101, 103-106, 245] studies have infact shown that antibody molecules (and other ligands) can be effectively prevented from penetrating the substance of a tumour by the very fact of their successful binding to tumour antigen, and that greater antigen density, higher monoclonal antibody affinity, and faster monoclonal antibody internalisation and metabolism by cells will increase the barrier effect, all else being equal [103].

Other examples of pharmacokinetic studies involving the use of actively-targeted systems include the sugar residues [108-113]. Carbohydrate and mannose receptors are found in liver hepatocyte and kupffer cells respectively [114-117].

In contrast to the extensive interest which has been shown towards the development of actively-targeted monoclonal antibody systems, the development of passively-targeted drug systems in cancer chemotherapy has until recently received comparatively little attention. This is however now changing, and has recently led to the development of several sophisticated soluble macromolecular drug conjugate systems which utilize various linkages (usually either biodegradable or covalent bonding) and administration routes (mainly systemic), are directed towards a variety of tumour types, and whose use offers many new therapeutic strategies. Typical examples of these, and perhaps indeed

the more appropriate to this study, are SMANCS (Styrene-Maleic Anhydride-Neocarzinastatin) [24, 25, 28], and the pharmacokinetic studies currently available in the literature involving the use of other passively-targeted macromolecular drug conjugate systems. Such pharmacokinetic literature is currently available for mitomycin C-dextran conjugates (MMC-D) [124-131], polyethyleneglycol (PEG)-interleukin 2 conjugates [132-134], albumin conjugates of methotrexate [135] and 5-fluorouracil-acetic acid [136], various dextran-enzyme [137-140] and antibody-polymer [141-143] conjugates, and copolymers of N-(2-hydroxypropyl) methacrylamide (HPMA) containing adriamycin [144], or doxorubicin (DOX) or daunorubicin (DNR) and sugar residues such as galactosamine [145, 146, 169], or daunomycin (DNM) and anti-Thy 1.2 antibody [147], or transferrin, anti-transferrin receptor antibody or anti-Thy 1.2 antibody [148]. In addition to these conjugates, several other passively-targeted macromolecular drug conjugate systems have now been reported [121-123], including an oxidized dextran-anthracycline conjugate (OXD-DOX), a divinyl ether-co-maleic anhydride copolymer-neocarzinostatin conjugate (DIVEMA-NCS or Pyran-NCS), a human immunoglobulin G-melphalan conjugate (K-18), a DIVEMA-DOX copolymer, a pyran-DOX conjugate, an albumin-daunorubicin conjugate, a gelatin-interferon α conjugate, a polyaspartic acid-DOX conjugate, poly-lysine-methotrexate conjugates, and anthracycline conjugates of DNA or dextran, however, the pharmacokinetic literature currently available on each of these systems is somewhat limited. In each of these passively-targeted soluble macromolecular drug conjugate systems the carrier macromolecule (polymer) which may be either of natural origin e.g. a protein such as albumin or a carbohydrate like dextran or DNA, or of synthetic origin e.g. polyethyleneglycol or HPMA etc [149, 162], and which usually constitutes at least 80% of the conjugates total molecular weight [121], significantly and favourably alters the biodistribution of the attached low molecular weight protein anticancer agent. This results in the attached anticancer agent exhibiting increased blood stability and circulation times, reduced rates of renal excretion, a reduced volume of distribution, increased and often substantially improved tumour accumulations of drug, increased lymphatic concentrations of drug, decreased

drug toxicity, decreased antigenicity, decreased immunogenicity, and hence increased therapeutic efficacy, compared to when the respective attached anticancer agent is administered in its free form. This enhanced tumour accumulation (and increased lymphatic concentration) is a direct result of the greatly improved pharmacokinetic properties which are achieved by attaching the anticancer agent to a macromolecular carrier, and are also indeed a result of the peculiar vascular properties of tumours themselves, and can generally be explained by the phenomenon termed as the 'Enhanced Permeability and Retention' (EPR) effect [25], and its associated corollaries. The EPR effect, which results from the combination of poor tumour tissue drainage with increased tumour vascular permeability, is outlined in more detail in Chapter 2. The passive drug-targeting approach in cancer chemotherapy is consequently now attaining profound significance and interest since the inadequate pharmacokinetic properties which have generally limited the clinical use of most low molecular-weight protein anticancer drugs (agents) now seem to be manipulable by tailoring these drugs by attaching them to various natural or synthetic soluble macromolecular carriers (polymers) [2, 24, 28, 121-123, 150]. The potential advantages of this approach to cancer chemotherapy are obviously quite considerable, even more so if they can be used in conjunction with known tumour vascular permeability and hence tumour macromolecular drug accumulation enhancing agents such as the hypertension inducing agent angiotensin II which selectively increases blood flow in tumour tissue [2, 151, 152], or kininase II inhibitor which inhibits kinin degradation and thus promotes both the leakage of macromolecules out of blood vessels and the accumulation of fluid in tumours [23, 153], or even both of these tumour vascular permeability enhancing agents combined [154]. To date however, the peculiar vascular properties of tumours and the EPR effect still remain to be fully exploited, and so far the investigation and development of such macromolecular conjugate systems has been surprisingly limited [121-123]. The many aspects of passive tumour-targeting using soluble macromolecular drug conjugate systems, together with the historical development which led to this approach of drug-targeting in cancer chemotherapy and all associated studies, have

recently been described in some excellent reviews [2, 24, 28, 121-123]. There have also recently been some excellent reviews discussing the studies, useage, important aspects, and pharmacokinetics of most of the commonly used low molecular-weight anti tumour protein drugs [155-159].

The key to successful pharmacokinetic properties for the passively-targeted macromolecular drug systems, and indeed for the actively-targeted macromolecular drug systems as well, is molecular radius size, although other factors such as charge, hydrophobicity, and the stability of the molecular bonds and linkages also influence the process [2, 24, 28, 121-123, 160]. In the case of both the actively and passively targeted systems the respective optimal monoclonal antibody or monoclonal antibody fragment size and optimal soluble macromolecular carrier size, and hence the respective optimal conjugate size, have yet to be determined when targeting these systems to tumours under abnormal tumour vascular conditions. The optimal macromolecular size or size range which can deliver the greatest fraction of a macromolecular drug systems dose to the lymph under normal vascular conditions has yet to be considered. Also, almost all of the work in cancer chemotherapy using the active-targeting approach, and most of the work using the passive-targeting approach has been directed primarily towards the delivery of anticancer agents to vascularised tumours, which as already outlined possess their own peculiar vascular properties, rather than specifically to cancer micrometastases in the lymph (under normal vascular conditions), and have thus concentrated more on achieving the best therapeutic tumour accumulations of drug rather than making the achievement of the best lymph accumulations their primary or sole objective. The main exception to this being the passively-targeted soluble macromolecular drug conjugate system SMANCS [24], which is specifically designed to be lymphotropic as well as being tumouritropic by binding to serum albumin in vivo [161]. Clearly the ideal actively or passively-targeted macromolecular conjugate system will be both highly tumouritropic and lymphotropic [2]. The increased lymphatic concentrations of drug usually observed with the other passively-targeted

macromolecular drug conjugate systems, and indeed some of the actively-targeted systems, is usually an important but nevertheless secondary objective (unless of course the targeted tumour is a lymphoma). In general, due to their increased blood circulation times and reduced rates of renal excretion, and also due to the peculiar vascular properties of tumours and the EPR effect, macromolecular drug systems larger than the renal threshold (60-70kDa) appear to accumulate relatively well in tumours and exhibit the better pharmacokinetic properties (and lymphatic concentrations) [2, 24, 25, 28, 121-123] . Even more so if the conjugate system or the attached carrier macromolecule bears a negative [124, 128, 162, 163], or non-cationic [25, 129, 164] charge. A negative or neutral electric charge appears to be better since polycationic polymers are rapidly captured by the first pass effect and also during circulation [129]. As outlined in more detail in Chapter 2, the reason for this is that the endothelial surfaces of the blood capillaries are covered with negatively charged components such as chondroitin sulfate, heparan sulfate and glycocalyx, which therefore repels negatively charged molecules or polymers and thus aids in the extension of their blood circulation times, but makes polycationic molecules or polymers very bioadhesive. The peculiar tumour vascular properties mean there are often fewer restrictions on size compared to the normal vascular properties under which the targeting of macromolecular drug systems to the lymph must be considered [2]. The exchange of macromolecules across the microcirculation under normal vascular conditions is described in detail in Chapter 2. Additionally, carrier macromolecules which are of natural origin have the advantage of being usually biodegradable and generally demonstrating little polydispersity [168]. Synthetic carrier macromolecules are not usually biodegradable unless they have been specifically synthesised to include biodegradable bonds [165], as is the case for most of the afore-mentioned passively-targeted macromolecular drug conjugate systems which utilize synthetic polymers, and because they are man-made they are likely to be polydisperse. An advantage which synthetic polymers have over natural polymers is that they are less likely to evoke an immunogenic response in vivo [166], and they can be tailor-made to requirements of molecular weight, charge and hydrophobicity [167].

Also, the majority of the pharmacokinetic studies using the actively-targeted monoclonal antibody systems, and virtually all of the pharmacokinetic studies using the passively-targeted soluble macromolecular drug conjugate systems, have been performed in animals rather than humans. In the case of the passively-targeted soluble macromolecular drug systems the fact that the use of macromolecular carriers is a new innovation has meant that only a few are currently scheduled for thorough clinical evaluation, including SMANCS (in Japan) and HPMA-DOX (in the UK) [121-123], and there is consequently relatively little published data available for these drug systems. One of the direct consequences of this from the point of view of trying to predict which macromolecular drug sizes are most effective in delivering the greatest fraction of a macromolecular drug dose to the lymph and hence to any cancer micrometastases present there, and indeed from the point of view of macromolecular drug disposition in general, is that there is a considerable lack of any particularly useful pharmacokinetic and tissue distribution data describing the time course of either actively or passively-targeted macromolecular drug systems in the human body for any of the key compartments of the body, i.e., the blood, the lymph, and the liver (the liver represents the site where any major drug toxicity may occur), or for the main elimination processes, i.e. renal excretion and hepatic metabolism (hepatic clearance), which are important in both macromolecular drug distribution and the targeting of anticancer agents to micrometastases in the lymph. Most of the tissue distribution data which are available in the literature for both the actively and passively-targeted macromolecular drug systems is for animals rather than humans, often consists of only a few data points or plots without any published data, and is usually clearance data or tumour accumulation data rather than distribution data for key tissues. Similarly, most pharmacokinetic parameters which are quoted in the literature (the four main pharmacokinetic parameters being clearance, volume of distribution, half-life and bioavailability) are those associated with, and therefore more appropriate to, the targeting of macromolecular drug systems to solid tumours, rather than to cancer micrometastases in the lymph. Any pharmacokinetic models given in the literature, of

which there are very few indeed, often take the form of simple classical pharmacokinetic models or non-compartmental pharmacokinetics (usually model-independent pharmacokinetics) to analyse the particular experimental data, but which due to this type of model are really generally inappropriate or inadequate for macromolecular drug disposition since they usually assume rapid distribution and equilibration. This general lack of particularly useful human or indeed animal macromolecular drug distribution data and inappropriate or inadequate pharmacokinetic models is also generally observed in much of the non-chemotherapy macromolecular drug pharmacokinetic literature, of which [170-194] are typical examples, and also for the interleukins [195-201] and interferons [202-210] as well. For the reasons outlined in section 1.3, more appropriate are the theoretical/predictive models in the literature, i.e. the physiological pharmacokinetic models, although as will be outlined in Chapter 5, in which the key models relevant to this study, i.e. the macromolecular anticancer drug and drug-targeting pharmacokinetic models are discussed in more detail, these physiological models do however also possess some important disadvantages when considering macromolecular drug disposition.

New pharmacokinetic models are therefore needed which can predict the fate of any macromolecular drug in the human body as a function of time (under normal vascular conditions) for any of the key compartments of the body (blood, lymph, and liver) and for the main elimination processes (renal excretion and hepatic clearance) which are important in both macromolecular drug distribution and the targeting of anticancer agents to micrometastases in the lymph (and which can also be used for fitting purposes if desired as well). The success of any macromolecular drug system depends upon such predictive macromolecular drug disposition models.

1.3 Pharmacokinetic models and processes

Pharmacokinetics is the study of the time course of drug and metabolite levels in different fluids, tissues, and excreta of the body, and of the mathematical relationships

required to develop models to interpret such data. It is the study of "what the body does to a drug".

Before the many complex relationships involved in pharmacokinetic processes were understood, drugs were administered purely on an empirical basis. What happened to a drug after it entered the body, or how its fate might influence the therapeutic effect, was not appreciated. The birth of modern pharmacokinetics occurred in 1937 with the publication of two classic papers [240, 241], which gave the basic equations for drug absorption, distribution, and elimination following various types of administration. The next major resurgence of interest in pharmacokinetics, and one that continues to this day, occurred in the late 1950s and early 1960s. Today, pharmacokinetic concepts are used at all stages of drug discovery, development, and therapy, and pharmacokinetic principles are being used routinely in the design and optimization of drug formulation and dosage regimens.

Pharmacokinetics has tended to diverge into four major philosophical approaches: classical linear compartment modelling, physiological compartment modelling, nonlinear compartment modelling, and noncompartmental modelling. Each of these different modelling approaches is described in this section. However, due to the voluminous amount of literature on the many different aspects of the subject of pharmacokinetics, and subsequently to avoid re-writing the major pharmacokinetic textbooks or important recent reviews or theoretical papers in which the various histories, theoretical concepts and processes, and most of the studies associated with these different modelling approaches are either already well established (ie. the classical linear compartmental modelling and nonlinear modelling approaches) or recently given (ie. the physiological modelling and noncompartmental modelling approaches), the following parts of this section consequently make reference to such major pharmacokinetic textbooks or key reviews or theoretical papers, as appropiate. Nevertheless, since the major objective of this study was the development of a physiological pharmacokinetic model, the part of this section which discusses the

physiological modelling approach is necessarily and appropriately more detailed. The purpose of the development of any pharmacokinetic model is to describe or predict the time course of drug disposition throughout the body.

In the classical linear compartmental modelling approach, which is the oldest established of the pharmacokinetic modelling approaches and is consequently the approach which has received the most attention and has subsequently produced the most published literature, the body is represented as one or more compartments between which a drug or metabolite can be distributed. These compartments may be spacial or chemical in nature. In most cases however, the compartments are used to represent a body volume, or a group of similar tissues or fluids with similar degrees of blood perfusion or with similar affinities for a particular drug. The compartments do not usually represent particular anatomic elements, and the complete model is often only a simple abstraction of body processes, tending to serve a descriptive function, usually with regard to drug profiles in plasma or urinary excretion. In these classical linear pharmacokinetic models, referred to as 'classical pharmacokinetic models', the 'volumes' of each compartment are assumed to be invariant, and drug distribution and elimination are assumed to be first-order processes with first-order rate constants which are also invariant.

As a consequence of this, the change in concentration of drug at a given time is dependent upon the concentration of drug present at that time, the area under a curve of blood level against time is proportional to the dose administered (assuming 100% bioavailability), the rate that the drug is cleared from the body is concentration dependent, the percentage of body drug load that is cleared per unit time is constant, and the drug has an elimination half-life. (If this is not the case then nonlinear compartment models apply.) Classical modelling approaches are usually based on the curve fitting of plasma concentration data ($\log_{10}$ plasma concentration versus time) with single or multi-exponential equations, depending on the profile of the data, to obtain values of hybrid microscopic disposition constants. These hybrid microscopic disposition constants determine how many compartments, and therefore

how many exponential terms, will be necessary in the model to describe the data, and are obtained either by the method of residuals (" feathering" or "exponential stripping"), or more accurately by nonlinear least squares regression analysis. Once the hybrid microscopic disposition constants are known, important pharmacokinetic parameters such as volume of distribution, clearance, half-life, and bioavailability can be determined. The hybrid microscopic disposition constants are used in conjunction with the method of Laplace transforms, inverse Laplace transforms, partial fraction theory and Cramer's rule to solve simultaneously for the differential equations describing the rate of change in the amount (or concentration) of drug as a function of time in peripheral compartments (in the case of more than one compartment) as well as the central compartment, and for the individual model rate constants. An alternative, but more general, method for performing these calculations with any first- or zero-order input process and with elimination occurring from any compartment is also available [213]. It involves the use of general input and disposition functions, a general theorem of partial fractions for solving Laplace transforms in pharmacokinetic analysis [214], and the use of a multiple dosing function. However, the use of this method does have some imposed restrictions [213, 214]. In any linear classical pharmacokinetic model where only the central compartment (a driving force compartment) is available for sampling the maximum number of solvable rate constants, Z, is given by the expression $Z = 2(n-1) +1$, where n is the number of driving force compartments in the model, and only one of the Z rate constants may unambiguously describe elimination of a drug from the model [213]. The ability to sample unchanged drug in additional non driving force compartments such as the urine would allow one to determine additional rate constants, though in most cases, these additional rate constants will only be part of a previously hypothesized elimination rate constant, and will not allow the investigator to determine the validity of the hypothesized model. For many drugs, particularly after bolus intravenous administration, a multi-compartment model provides a more accurate description of drug plasma profiles than a one compartment model. The multi-compartment is frequently represented by a two-compartment model, although three

compartment models are also sometimes used. Classical compartmental models consisting of more than three compartments are generally not used because, firstly, most plasma data can be adequately described by less than three compartments, i.e. a 'central' compartment (plasma or blood compartment), and either one or two peripheral compartments which represent tissues in which the drug equilibrates at rapid, slow, or intermediate rates, and secondly, the mathematics becomes too complicated. Often the object of using classical compartment models is to obtain estimates of rate constants using nonlinear regression. This becomes a meaningless exercise when the number of parameters is too large. Therefore it is advisable to use the simplest appropriate model. Since the clinical analysis of most drugs is performed using the classical linear compartment modelling approach, a large number of papers have appeared in the pharmaceutical literature, describing the treatment of data, at first for the one-compartment model, then for the two-compartment model, and finally for various permutations of the three-compartment model. Most of these studies are now well established in the literature and are given, together with extensive detailed descriptions of the mathematical and pharmacokinetic processes involved in the classical compartmental modelling approach, including the different possible permutations of each type of model and the historical perspectives of this modelling approach, in the major pharmacokinetic textbooks [215-218].

In the physiological modelling approach the body is divided into compartments based on true anatomical regions or volumes. Unlike the classical linear compartmental modelling approach, in which drug movement between compartments is based largely on reversible or irreversible first-order processes, drug movement using the physiological modelling approach is based on blood flow rates through particular organs or tissues and experimentally determined blood-tissue concentration ratios or drug diffusion rates between blood and tissue, and usually mass balance equations. The main advantages of physiological pharmacokinetic models compared with classical linear pharmacokinetic models is that drug movement can be predicted (simulated) in

specific selected organs or tissues, and parameter values can be altered to allow for changes in physiological function and disease states. They address more specifically and accurately the actual time course of drug or metabolite disposition in particular body organs or tissues. The pharmacokinetic parameters used are realistic because they are based on observed or predicted physiological values. Total, free or bound concentration profiles can be predicted for selected regions of the body. The differences between animal and human experiments are easier to interpret. Also insight can be obtained regarding specific organ elimination processes and parameter values can be 'scaled' for different animal species and humans. They allow the often more abundant and detailed data available for animals to be used and related to humans. In brief, they provide more information based on specific tissue localization of drugs. The main disadvantages of physiological pharmacokinetic models is that the associated mathematics can become very complex, unwieldy, and difficult to solve. Frequently, because of the large number of compartments and parameters that are involved in determining the model that is thought to be the most appropriate for the system to be studied, the model equations can only be solved by numerical techniques, either on personal computers, or often, on powerful main-frame computers, by using specifically written, powerful, or modified versions of, various published numerical computer programme packages. In such multi-compartment and multi-parameter physiological pharmacokinetic models this numerical rather than analytical method of solution means that exact or specific equations describing the amount (or concentration) of drug in each compartment as a function of time are not usually obtainable for any model, especially for those consisting of three compartments or more. Consequently physiological pharmacokinetic models tend necessarily to be used more for predictive purposes rather than for fitting purposes. Another disadvantage is that it is extremely difficult to validate a physiological model in animals and virtually impossible in humans because large numbers of tissue samples are required at different time intervals after dosing (it is often difficult to obtain these tissue samples, even more so tissue samples that are free of blood). In vitro testing is sometimes required to

establish or validate model parameters. Model development requires a large data base for each drug or drug group in a particular species, and some of this information is not always available or easily obtainable. Species differences may also cause some complications. Often some of the physiological parameters used in the model are not available in the literature and have to be estimated. The blood flow rates and tissue volumes used are generally average values for a particular species, many of which, under normal conditions, are available in the literature, however, drugs are often given under disease conditions, and the drug may also affect the physiological conditions because of pharmacological actions, and these factors can sometimes perturb the model and lead to difficulty in interpretation. Also, despite their complexity, physiological models still contain many simplifying assumptions, certainly of a more microscopic nature than the comparatively gross assumptions associated with the classical compartment modelling approach (typical simplifying assumptions in the physiological models are often associated with the diffusion of drug into tissues, and the complete mixing with organs). In brief, because of the large number of compartments and parameters that are usually involved using this type of modelling approach, physiological models are necessarily more complicated than classical compartment models. The complications are such that physiological models have been developed for very few drugs, and are justified only to investigate specific tissue localization of drugs or to examine the detailed mechanisms of drug excretion or metabolism. This modelling approach is subsequently not of general application in most situations, but is used to solve particular distribution problems for drugs when tissue distribution is important, or when sites of elimination are critical. Thus, the physiological model applies naturally to anticancer drugs (and to drugs acting on the central nervous system), and consequently most of the published work has been done in this area. Most of this work has been in the form of either blood flow rate-limited models or membrane-limited models (although both flow-limited and membrane-limited compartments can exist within the same overall model, eg. [219, 220]). In the blood flow rate-limited models, for example [221-256], it is usually assumed that drug

transport across physiological membranes is very fast, drug distribution into a specific organ is limited only by blood flow rate into that organ (blood-tissue and tissue-blood concentration ratios are often assumed to be equal to unity), the concentration of drug in the emergent or venous blood from a particular organ is in equilibrium with the drug concentration in the intracellular fluid in that organ, and hence each organ can be represented by a simple single compartment. Membrane-limited models on the other hand assume that drug transport across physiological membranes and equilibration is not rapid. Membrane-limited models tend to generally fall into one of two categories; firstly, there are the compartmental based models in which drug transport across physiological membranes is controlled either by passive diffusion, or by saturable, active transport or Michaelis-Menten type processes, for example [256-261], and secondly and more recently, there are the geometrical models [86-98, 262, 263], in which drug transport across the physiological membranes in the particular geometric situation being studied is usually embodied in one or more equations which may be in the form of either a reaction-diffusion partial differential equation, a first-order rate equation, or a simple biexponential expression, or various combinations of these equations, and which also often invoke as part of the model system or equations, the Kedem and Katchalsky [264, 265] equations, or similar mass balance equations for the diffusive and convective transport of molecules across membranes, adapted in various ways depending upon the particular geometrical situation being studied and the assumptions being made. Almost all of the physiologically based models which have been applied to non-anticancer drugs, and most of the models which have been applied to free (non-macromolecular targeted) anticancer drugs, of which [221, 224-226, 228, 229, 231, 235, 258] and [219, 220, 222, 223, 227, 230, 232-234, 236-239, 257, 259-261, 263] respectively are typical and perhaps the most frequently cited examples, together with a summary of this approach to pharmacokinetic modelling, including the history behind its development, have been described in a couple of excellent recent reviews [266, 267]. There has also fairly recently been a good review discussing the estimation of tissue-to-plasma partition coefficients often used in some of these

models [268]. A few of the non-macromolecular physiological modelling studies, and a description of some of the mathematical and pharmacokinetic processes involved in this type of modelling (the geometrical approach excepted), are also given in some of the major pharmacokinetic textbooks [269, 270]. Some of the mathematical and pharmacokinetic processes involved in this type of modelling (the geometrical approach again being the main exception) are also given in one of the afore mentioned reviews [267]. However, as already indicated in section 1.2, the key pharmacokinetic models in the literature which are relevant and appropriate to this study are the theoretical/predictive macromolecular anticancer drug system and drug-targeting pharmacokinetic models, ie. [86-98, 244-256, 262] (all of the geometric models are included in these references), and these are discussed in more detail in Chapter 5. Due to the reasons outlined above, each of these models is physiologically based.

Despite the wide diversity of the classical and physiological pharmacokinetic models, all of these models, with the exception of the physiological membrane-limited models which involve saturable or Michaelis-Menten type kinetics eg. [256-261], incorporate the common assumption that drug elimination from the body is a first-order process. Another assumption is that the rate constant for elimination is a true constant and is independent of drug concentration. In these cases, the rate that drug is cleared from the body is concentration dependent, the percentage of body drug load that is cleared per unit time is constant, and the drug has an elimination half-life. Many drugs, particularly those following oral administration, are however eliminated from the body by mechanisms that are potentially saturable and in these situations nonlinear compartment models apply (true first-order, nonsaturable elimination usually occurs only with drugs that are excreted in the urine via passive glomerular filtration). Most nonlinear compartment models are classical compartment models (usually of either one or sometimes two compartments) whose $\log_{10}$ plasma concentration versus time profile has shown the drug to be cleared by zero-order or Michaelis-Menten-type kinetics, i.e. not exhibiting a characteristic, constant elimination half-life. The nonlinear

physiological pharmacokinetic models, although less common, eg. [256-261], also exhibit these characteristics. In both of these types of nonlinear model the apparent half-life changes continuously with drug concentration in plasma. Several methods are available to obtain initial estimates for the Michaelis constants, and these, together with most of the classical, well established examples and studies which involve the application of nonlinear compartmental models, and descriptions of the mathematical and numerical methods employed in the solution of these models (numerical nonlinear fitting and integration programmes, and standard integration methods are usually used), are again given in the major pharmacokinetic textbooks [271-274]. There has also very recently been a review giving most of the classical, well established studies which have employed nonlinear compartmental methods, and most of the typical more recent studies as well, together with a description of some of the mathematical processes involved in this type of modelling, and a discussion of the clinical implications of nonlinear pharmacokinetics [275].

Model-independent pharmacokinetics represents a recent trend away from complex modelling systems towards a less complex noncompartmental approach, based purely on a mathematical description of blood or plasma profiles of drugs or metabolites, and the calculation of useful pharmacokinetic values without invoking a particular model. Model-independent pharmacokinetics is being applied if a simple single or multi-exponential equation is used to describe the plasma or blood concentration profile of a drug, and further interpretation of this fitted equation is avoided. In this equation each exponential term(s) consists of a single pre-exponential coefficient and a single exponent, and these parameters can be used to calculate several important pharmacokinetic values such as the volume of the blood compartment, the terminal elimination half-life, the area under the drug-concentration curve, and the plasma clearance [276]. The overall drug distribution volume at steady-state, although more difficult to calculate, is also obtainable in model-independent [277], and model and rate constant-independent form [278]. This parameter is useful because it describes, in a

model-independent manner, the distribution characteristics of a drug that has equilibrated into the various tissues and body fluids. Hence, the essence of this model-independent approach to pharmacokinetics is that it avoids the use of kinetic parameters that cannot readily be validated or which have little anatomical or physiological significance. This approach is useful in situations where kinetic parameters such as absorption and elimination rates and clearances are required, but specific distribution characteristics are less important. This is often the case in classical compartmental modelling, and it is consequently in this situation that the model-independent approach is usually invoked (the classical one-compartment model can be thought of as the simplest model-independent approach).

Another noncompartmental pharmacokinetic approach is also available. It is based upon the theory of statistical moments and mean residence times, and can be used to calculate absorption, distribution and elimination parameters by utilising plasma concentration-time profile data [279-284]. It is also implicated in the latter of the model-independent approaches described above, ie. [278]. Descriptions of the mathematical processes and concepts involved in this modelling approach, together with almost all associated studies, are given in the above theoretical papers [279-284], and in some very recent literature sources [285-287].

The most recent noncompartmental pharmacokinetic approach is population pharmacokinetics, which is based upon the concept of Bayesian parameter estimation [288], and involves the use of fractional data from individual patients to derive population pharmacokinetic parameters which are then used to derive individual patient parameters (via Bayesian estimation) again using fractional data from (different) individual patients. It utilizes specific software designed to handle such data, and is useful where drug concentrations are measured during relatively complicated dosage regimens, not at steady-state, and where only a few (1 or 2) concentration measurements are permissible. In these situations pharmacokinetic parameters (principally clearance and volume of distribution) can be estimated in an individual

patient so that drug dosages can be adjusted to achieve specific target concentrations, by using the Bayesian method which allows the fragmentary concentration information to be used in conjunction with pre-existing information on the population characteristics (means and variances) of the pharmacokinetic parameters. This noncompartmental Bayesian parameter estimation and population pharmacokinetic approach, along with many typical examples of clinical studies which have employed population pharmacokinetic analysis, and a summary of the historical background which led to this latest approach, are given in some recent reviews [286, 289-292].

1.4 Objectives of this thesis

Naturally occurring or synthetic macromolecular drugs are potentially a new generation of drugs in the field of cancer chemotherapy, either as carriers for low molecular-weight anticancer agents or as drugs in their own right. The experimental and theoretical literature shows that both classical and non-classical pharmacokinetic models are relatively poorly developed or often inappropriate when applied to macromolecular drugs. The literature also shows that most of the work concerning these actively and passively targeted macromolecular drug systems has been directed towards solid tumours which are known to possess their own peculiar vascular properties, rather than considering their targeting under normal vascular conditions specifically to the lymph, and hence to any cancer micrometastases located there. There is also a lack of any particularly useful pharmacokinetic or tissue distribution data describing the time course of these macromolecular drug systems in the human body under normal vascular conditions for any of the key compartments (tissues) of the body, or for the main elimination processes, which are important in both macromolecular drug distribution and the targeting of anticancer agents to cancer micrometastases in the lymph. Key parameters affecting macromolecular drug distribution under normal vascular conditions, the most important of which being molecular size, need to be investigated. New pharmacokinetic models need to be developed which will predict the distribution and fate of macromolecular drugs in the

body. Models are required for different macromolecule sizes, appropriate for proteins and uncharged polymers, and which are able to distinguish metabolism from excretion.

The major objective of this study was therefore to develop a new physiological pharmacokinetic model based on the movement of macromolecules under normal vascular conditions between three important compartments of the body, i.e. the blood, the lymph, and the liver, and modelling the two major elimination processes, i.e. renal excretion and hepatic metabolism (hepatic clearance), which are important in both macromolecular drug disposition and the targeting of anticancer agents to cancer micrometastases in the lymph. The model was required to take into account that for macromolecules excretion and hepatic metabolism was effectively occurring from separate compartments. An objective of the model was to allow prediction of the effect of molecular radius on the distribution of both protein and uncharged macromolecular drugs in the human body, both in the absence and presence of hepatic metabolism. This was to be achieved by taking into account the regional capillary permeabilities to different size macromolecules, and the physiology and flow rates within each compartment, and involved the development of smaller mathematical models, the fitting of these to appropriate physiological experimental data in the literature, and the building of these smaller models and their parameters of best-fit, and other mathematical expressions which were also developed as part of the modelling process, into the proposed new physiological three-compartment pharmacokinetic model. A major aim was to predict via simulations the molecular radii which are most effective in delivering the greatest fraction of a macromolecular drug dose into the target site. The usual target site in cancer chemotherapy being the lymph, and subsequently any cancer micrometastases present there. In addition to predicting the fraction of the macromolecular drug dose present in the lymph, the proposed new physiological three-compartment pharmacokinetic model would also allow calculation for each molecular radius size, the fraction of the dose that is present in both the blood and the liver, the fractions of the dose which have been excreted via the kidneys and metabolised by the

liver, and the total fraction of the dose eliminated, as a function of time. A necessary objective of this study was therefore to develop a computer programme which had two main purposes; firstly to aid in the solution of cubic functions within the new physiological three-compartment pharmacokinetic model equations, and secondly to perform simulations once the solutions to the model equations had been established.

Chapter 2

Development of models in relation to relevant physiology

2.1 Introduction

A physiological three-compartment pharmacokinetic model was developed in several stages. Initially mathematical models were developed to describe the relationship between molecular radius and the ratios of concentration of macromolecules present in the glomerular filtrate versus blood, and in the lymph versus blood. The latter models were devised with reference to the available data from the physiology literature. Data were available describing glomerular filtrate/plasma ratios and lymph/plasma ratios for proteins and non-ionic polymers in a variety of animal species. The best model(s) and associated parameters of best-fit were then used in the proposed pharmacokinetic model to predict the first-order inter-compartmental parameters k_{excr} and k_{12} which describe the rate of mass transfer of macromolecules from the blood to the glomerular filtrate, and from the blood to the lymph respectively. Other mathematical expressions used to represent the remaining first-order inter-compartmental parameters in the proposed pharmacokinetic model were also developed and built into the model at the appropriate stage. Prior to the development of the physiological three-compartment pharmacokinetic model, as one of the aids to its validation, simplified one-and two-compartment pharmacokinetic models were developed to describe the effect of molecular radius on the distribution of macromolecules in more simplified models of the body. The complexity of the three-compartment pharmacokinetic model required the development of a computer programme which had two main purposes; firstly to aid in the solution of the cubic functions within the model equations, and secondly to perform simulations once the solutions had been established. The physiological three-compartment pharmacokinetic model and the associated computer programme described here therefore represent the final stage of a systematic sequence of developments. At each state of development the appropriate physiological data were introduced into the model.

This chapter describes the development, strategies and solution of all the models used, and describes the systematic sequence in which the modelling was performed. Models

describing the relationship between molecular radius and the glomerular filtrate/plasma concentration ratios (F/P ratios) and lymph/plasma concentration ratios (L/P ratios) of macromolecules are presented in section 2.2. The section also summarises the strategies and methods used in their development, and the criteria for selection of the physiological data to be fitted. A review is presented of the main physiological, structural and physicochemical factors important to macromolecular drug distribution including extravasation in the different regional capillary beds appropriate to this study. The physiological three-compartment pharmacokinetic model and its solution are presented in section 2.3, together with a summary of the methods used in validation and the development of the computer programme. A summary of the key features of the new model are presented in section 2.4.

2.2 Modelling of lymph/plasma and filtrate/plasma ratios as a function of molecular radius

2.2.1 Introduction

The first stage of development was to propose mathematical models to describe the relationship between molecular radius and the concentration ratios of macromolecules extravasating from the blood to the glomerular filtrate, and from the blood to the lymph. The first task was to select the most appropriate experimental data describing the relationship between molecular radius and extravasation. Measurements have been made of the ratio of drug concentration between the blood and the glomerular filtrate (F/P ratio data), and also between the blood and the lymph (L/P ratio data). Selection of data required a thorough survey of the literature regarding the exchange of macromolecules across the microcirculation. The selection of this data together with a summary of the main physiological, structural and physicochemical factors important in macromolecular drug distribution, are described in subsection 2.2.2. Subsection 2.2.3 then describes the experiments performed to establish the best models describing the relationship between molecular radius and the F/P and L/P ratios. Nonlinear regression

analysis was performed to obtain parameters of best-fit. Subsection 2.2.4 summarises the main conclusions of this part of the work.

2.2.2 Extravasation of macromolecules from different capillary beds.

2.2.2.1 Introduction

The exchange of macromolecules across the microcirculation has fascinated physiologists for many decades and consequently there is a considerable amount of literature on many aspects of the subject. The theory and techniques used to assess macromolecule permeability, the regional differences in capillary permeability, and the mechanisms and pathways of macromolecule exchange, have recently been extensively reviewed [293], and many important features governing the egress of macromolecules from the blood circulation are known [293-296]. The features and mechanisms which have important implications for the therapeutic use of soluble macromolecular drugs and their distribution in biological systems have also been reviewed [32, 121, 297-299]. However, despite a large literature on the subject, the movement of macromolecules through the different capillary membranes remains unclear to a certain extent. The physiological features discussed in this subsection therefore represent a summary of what are generally believed to be the main physiological and physicochemical factors important in the distribution of therapeutic macromolecules, and their extravasation in the different regional capillary beds appropriate to this study.

2.2.2.2 General characteristics of blood capillaries

Current literature describes three main types of capillary in mammalian species; continuous (normal), fenestrated, and sinusoidal (discontinuous) [293]. Each capillary type has characteristic permeabilities to macromolecules, with the continuous capillaries being the least permeable and the sinusoidal capillaries being the most permeable [293]. In each class of capillary the size of the macromolecule is the main determinant of its vascular permeability, with increasing macromolecule size resulting in a decreasing likelihood of extravasation [293]. Indeed there are effective molecular

size limits above which macromolecules have negligible permeability through the various endothelial layers. However, other factors, the most notable of which being molecular charge, also influence the rate of extravasation [293].

The lumenal surface of each capillary is composed of flattened endothelial cells, approximately 20-40 μm long, 10-15 μm wide and 0.1-0.5 μm thick. A glycosaminoglycan coat about 10-20 nm thick covers the lumenal surface of each endothelial cell. The function of this glycosaminoglycan coat is still not fully understood, although it has been suggested that it may influence extravasation [295], particularly in fenestrated endothelia, as it is believed to be negatively charged [300]. The capillary endothelium plays an important role in regulating the distribution of macromolecular drugs and has characteristic permeability depending upon the particular organ or tissue [301]. A significant contribution to control of extravasation is provided by the extracellular basement membrane [293], present at the basalateral surface of continuous and fenestrated endothelia, but absent in sinusoidal capillaries [302].

The two possible routes of extravasation common to each class of capillary are believed to be (1) passage through the intercellular gaps (the size of which depends upon the capillary type), known as the paracellular route, and (2) transcapillary pinocytic processes (pinocytic vesicles occupy a relatively large volume of the endothelial cell and are considered to move freely (kinetically) from one side of the capillary membrane to another, and fuse with the plasma membrane, carrying with them plasma, including some dissolved macromolecules [293]). The paracellular route may be significant for extravasation of medium sized molecules (molecular-weight (MW) between 1,000-20,000 Da) from continuous endothelia, but as size increases the vesicular transport becomes more important e.g. the transport of albumin (MW 69,000) from continuous endothelia is thought to be mainly vesicular. Electron microscopy studies reveal that some organs (e.g. endocrine glands, the kidney, the mesentery bed of the small intestine) have distinct pores in their capillary endothelia [303, 304], so called

fenestrae. Passage of macromolecules through fenestrae is likely to be the dominant process in these tissues [293]. Sinusoidal capillaries, which are found almost exclusively in organs of the reticuloendothelial system (liver, spleen and bone marrow) [303, 304], have pronounced gaps [303, 305, 306], which allow virtually free passage of particles up to 50-100 nm in diameter [293]. The structural features and possible transport pathways for macromolecules across the continuous, fenestrated, and sinusoidal capillaries are shown in figure 2.1

Figure 2.1. Diagrammatic representation of possible transport pathways for macromolecules across (a) continuous, (b) fenestrated, and (c) discontinuous or sinusoidal capillaries. For the continuous capillary (a), pathways 1-4 represent a pioncytic vesicle, an interendothelial cell junction, a transendothelial cell channel, and the basement membrane, respectively. For the fenestrated capillary (b), pathways 1-5 represent the pinocytic route, an open fenestration, a diaphragmed fenestration (the diaphragm usually carries a net negative charge, although it can also be neutral), an interendothelial cell junction, and the basement membrane, respectively. For the discontinuous or sinusoidal capillaries (c), pathways 1 and 2 represent the pinocytic route and the freely permeable interendothelial cell spaces, respectively.

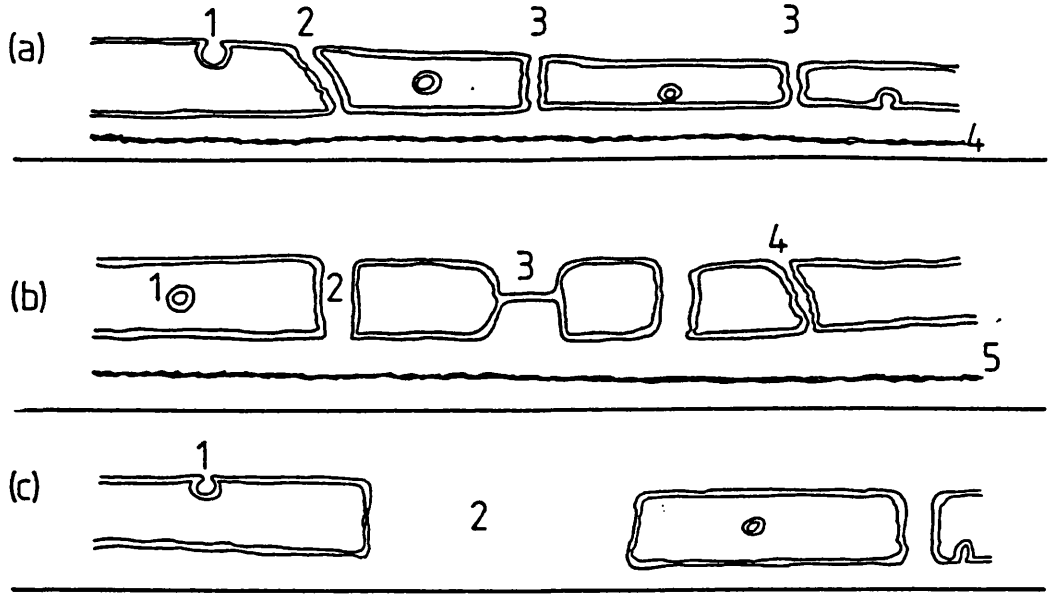

The reviews outlined earlier present detailed descriptions of the possible mechanisms and pathways of the kinetic (diffusive and convective) movement of the macromolecules through each capillary type, together with detailed descriptions of the possible nature, organisation and function of the structures that contribute to the transport characteristics of each regional capillary wall. These phenomena are summarised for each class of capillary in sections 2.2.2.3 - 2.2.2.5.

The capillary endothelial barrier has classically been described by physiologists from a phenomenological standpoint as an impermeable layer that is perforated with two types of pores [307]. These have been classified for continuous endothelia as large pores with a diameter of 50-70 nm and a frequency of 1 pore/20 μm^2 and small pores with a diameter of 6-9 nm and a frequency of 10-15 pores/μm^2. This theory has arisen from theoretical considerations using various pore-models, and led to the proposal by Kedem and Katchalsky of simple equations which equate solvent and solute flow across porous barriers [264, 265]. In addition Patlak included a selectivity factor in his equation since he believed that not all macromolecules would be able to pass through the pores at the same rate [308]. Indeed, over the years several theoretical equations have been developed to describe the exchange of molecules across capillary membranes. By far the most popular and most widely used of these, either in their original or various adapted forms, are the Kedem and Katchalsky equations which describe the diffusive and convective movement (flux) of solvents and solutes across biological membranes [264, 265]. However, as will be discussed in Chapter 5, when the Kedem and Katchalsky equations are used within physiological pharmacokinetic models, their inclusion presents some important disadvantages particularly in the context of macromolecular drug distribution. In general, the experimental data describing hydrodynamic size limits of the main extravasation pathways in each capillary type, which have usually involved the simultaneous measurement of the concentration of macromolecules in plasma and lymph, has supported the two pore theory, and some physiological estimates for small and large-pore populations in fenestrated and discontinuous

endothelia have also been suggested (pore radii 46-53 Å and 180-250 Å respectively for fenestrated endothelia, and approximately 90 Å and 330 Å for discontinuous endothelia). However, more recent investigations using electron microscopy have failed to identify two pore types in each class of capillary. Currently the large pores are believed to be explained by plasmalemmal vesicles, transendothelial channels or fenestrae. The smaller pores, although more difficult to equate, are believed to be explained by the gap junctions which are found in post-capillary junctions [307]. Consequently, most capillaries are considered to be heteroporous. Detailed descriptions of this pore work is given in a couple of excellent reviews [293, 309].

2.2.2.3 Extravasation from continuous capillaries

Capillaries with continuous endothelia and an uninterrupted basement membrane are the most widely distributed in mammalian tissues. They are found in skeletal, heart, and smooth muscles, and in lung, skin, subcutaneous tissue, and serous and mucous membranes [303, 304]. The ultrastructural appearance of these capillaries has generally led physiologists to assume that they offer more restriction to macromolecule transport than other capillary types. Hence their permeability characteristics have received far more attention, mainly in the form of experiments to determine lymph/plasma (L/P) ratio.

In the majority of continuous endothelial layers, the cells are connected together tightly by protein junctions and fusion of their glycocalyx layers. The resulting intercellular gaps in the capillary bed are generally impermeable to macromolecules greater than 20 Å diameter [300, 310], although junctions are typically looser in the post-capillary venules [307, 311-315], where 25%-30% of the junctions appear open with gaps measuring approximately 20-60 Å in width. Transcapillary vesicular traffic and/or transendothelial channels (formed by the fusion of two or more pinocytotic vesicles) are believed to account for the extravasation of macromolecules greater than approximately 20-60 Å diameter. Pinocytic, plasmalemmal or transcytotic vesicles are

thought to have internal radii of approximately 200-250 Å. However, as in all classes of capillary, the density and frequency of vesicles within a cell is dependent upon the organ within which it is found, with endothelial cells found in capillaries at the venular end, or within venules themselves, often demonstrating the highest density of vesicles. For instance the vesicle population in tissues which possess continuous capillaries is for example greater in muscle than in the lung, and greater in the lung than the brain [307, 313, 314, 316-318]. The relative frequency of transendothelial channels also increases from the arterial end to the venous end of the capillary [307, 316, 319, 320]. This variable density and frequency of vesicles and transendothelial channels, together with the tight intercellular junctions, and the presence of an uninterrupted basement membrane, results in the continuous capillaries exhibiting the lowest permeability characteristics of all the capillary types. The tight intercellular junctions mean that vesicular transport from high endothelial venules tends to be the dominant extravasation route in continuous capillaries, although evidence both for and against this as the major pathway has been presented [321-325]. The high endothelial venules are also implicated in chemotactic movement of leukocytes from capillaries, though a relationship between the two processes is not clear.

2.2.2.4 Filtration through the fenestrated capillaries of the kidney

Capillaries with fenestrated endothelia and a continuous basement membrane are found in organs whose functions demand high rates of fluid exchange i.e. the kidney, small intestine, salivary glands and other exocrine and endocrine glands [303, 304]. The physiological and physicochemical aspects of macromolecule permeability have been studied in most detail for the glomerular endothelium (mainly in the form of F/P ratio studies). This endothelium is known to be relatively permeable, and hence has provided much of the theoretical and experimental framework for the current concepts of exchange across fenestrated endothelia. Details of the nature of the endothelia in the

other organs listed above is relatively scarce, which limits current understanding of how varied are fenestrated capillaries.

Glomerular filtration plays a key role in the distribution and excretion of macromolecular drugs [121, 293]. The capillaries of the renal glomerulus are structurally unique and are designed to permit rapid extravasation of small polar molecules [326, 327]. This specialised endothelium features a large number of intercellular fenestrae (pores) [328, 329]. The endothelium is supported by a thick basement membrane to which adhere interdigitating foot processes of tubular epithelium (podocytes), which are separated by distinct spaces [328, 329]. The spaces between the podocytes are spanned by a diaphragm (the filtration slit membrane) [328, 329]. The basement membrane exerts a strong overall negative charge because of the presence of many sialylated glycoproteins and mucopolysaccharides [330, 331]. Fenestrae are also gated by negatively charged macromolecules which together with the basement membrane are considered to be the main limiting restrictive barriers to the movement of macromolecules from the blood to the glomerular filtrate of the Bowman's space [331], although the epithelial filtration slit membranes may also play a contributory role [327, 331, 332]. Consequently, molecular size is the main determinant of whether a substance will be filtered or not, with molecular charge also influencing the rate of filtration [293, 331].

Fenestrated capillaries are freely permeable to water and small solutes such as glucose and urea, have limited permeability to larger macromolecules (with permeability decreasing as molecular size increases), and are almost completely impermeable to the cellular elements of blood [326, 327]. Water and dissolved material entering the interstitium passes into the kidney tubule where most of the water, hydrophobic small molecules, (and some macromolecules) are reabsorbed by the tubular epithelial cells [326, 327]. These reabsorbed materials pass into the post-glomerular capillaries, whilst other products are lost into the urine. A largely protein-free ultrafiltrate passes into the Bowman's space from the glomerular capillaries [327]. The capillary filtration rate is

known as the glomerular filtration rate (GFR) which differs between animal species, but is well quoted in the literature as being about 125 ml/min for man under normal conditions [326, 333-339]. Detailed descriptions of the structural and functional basis of the glomerular permeability is provided in several treatises [391, 340-345].

Materials are able to escape from the glomerular capillaries mainly through the fenestrae which are circular openings with radii of 250-500 Å within the attenuated body of the endothelial cells [328, 329]. The glomerular fenestrae are unique since they are devoid of the 'diaphragms' which commonly subtend the fenestrae of other tissues [302]. (Over 60% of the fenestrae found in the other organs which possess a fenestrated endothelium are believed to be provided with a 'diaphragm' (or gate) and are consequently relatively more restrictive to the movement of macromolecules than the remaining diaphragm-less or open fenestrae; the open fenestrae in these tissues are believed to offer minimal restriction to the transport of macromolecules with radii between 25 and 150 Å [303, 304, 307, 320, 346, 347]). The frequency of the fenestrae in the glomerular capillaries (and in the capillaries of the other tissues which possess a fenestrated endothelium) increases from the arterial end to the venous end of the capillary [307, 320, 346, 347]. Another mechanism of extravasation is believed to be via pinocytotic vesicles which allow access of molecules between 25 and 150 Å radii into their vesicular structure. The rate of transport of macromolecules by this vesicular process has been shown to be approximately 3-8 times slower than exit through the fenestrae [307, 320, 346, 347], and will clearly be a function of size. Extravasation of macromolecules through the intercellular junctions is likely to be relatively unimportant given the pressure of the fenestrae because the intercellular junctions are believed to be impermeable to molecules greater than radii 25Å [346, 347]. The main barrier to the extravasation of larger macromolecules in the fenestrated glomerular capillaries seems to be the basement membrane [293, 331, 346, 347], which is generally very poorly permeable to macromolecules greater than about 40-45 Å radius.

The size-selective properties of the glomerular capillaries have mainly been derived from studies of differential solute clearance. Generally the urinary excretion of the test macromolecule is compared with that of a reference solute, such as inulin. Inulin, a hydrophilic polysaccharide of low molecular-weight, is commonly used since it appears in the glomerular filtrate at the same concentration as in plasma. Assuming both the test and reference solutes are neither actively secreted nor reabsorbed, the fractional clearance is equivalent to the concentration of the macromolecule in the glomerular filtrate relative to that in the plasma water i.e. $\frac{C_F}{C_P}$, and is usually referred to as the F/P ratio.

A survey of the literature from such studies revealed that the most comprehensive sets of data available are for dextrans (anionic [348], uncharged [348], cationic [349]) in the rat, and for proteins in the dog [326]. This datum is summarised in tables 2.1 and 2.2 respectively and is used in the modelling studies described in subsection 2.2.3. Figure 2.2 illustrates these data graphically. These F/P ratios were obtained in healthy animals under normal conditions. There is limited F/P ratio data for humans, or indeed for other animal species. However, the available datum does suggest that the relationship between molecular radius and fractional clearance of macromolecules from the blood to the glomerular filtrate is similar between mammalian species, although the relationship is different for each respective class of macromolecule. The restricted glomerular filtration of albumin is crucial to its physiological function and its molecular dimensions are similar in mammalian sepcies, which also suggests that extravasation in the kidney is similar amongst mammals.

Table 2.1 F/P ratio data for dextrans (anionic [348], uncharged [348], cationic [349]) in the rat

Molecular radius (Å)	F/P ratio Anionic Dextran	Uncharged Dextran	Cationic Dextran
18	0.56	1.0	1.0
20	0.35	0.97	0.99
22	0.19	0.87	0.97
24	0.11	0.73	0.93
26	0.06	0.60	0.87
28	0.032	0.45	0.80
30	0.02	0.32	0.74
32	0.013	0.22	0.66
34	0.007	0.15	0.56
36	0.003	0.09	0.44
38	0.0009	0.045	0.32
40	0.0004	0.022	0.20
42	0.0002	0.008	0.11
44	0.0001	0.002	0.04

Table 2.2 F/P ratio data for protein macromolecules in the dog [326]

Substance	Molecular radius (Å)	F/P ratio
Lysozyme	19	0.75
Myoglobin	18.8	0.75
β Lactoglobulin	21.6	0.39
Ovalbumin	27.3	0.20
Bence Jones protein	27.7	0.09
Hemoglobin	31.8	0.04
Serum albumin	35.5	0.003

Figure 2.2 Relationship between F/P ratio and molecular radius for dextran (anionic, uncharged, cationic) and protein macromolecules in the rat and dog.

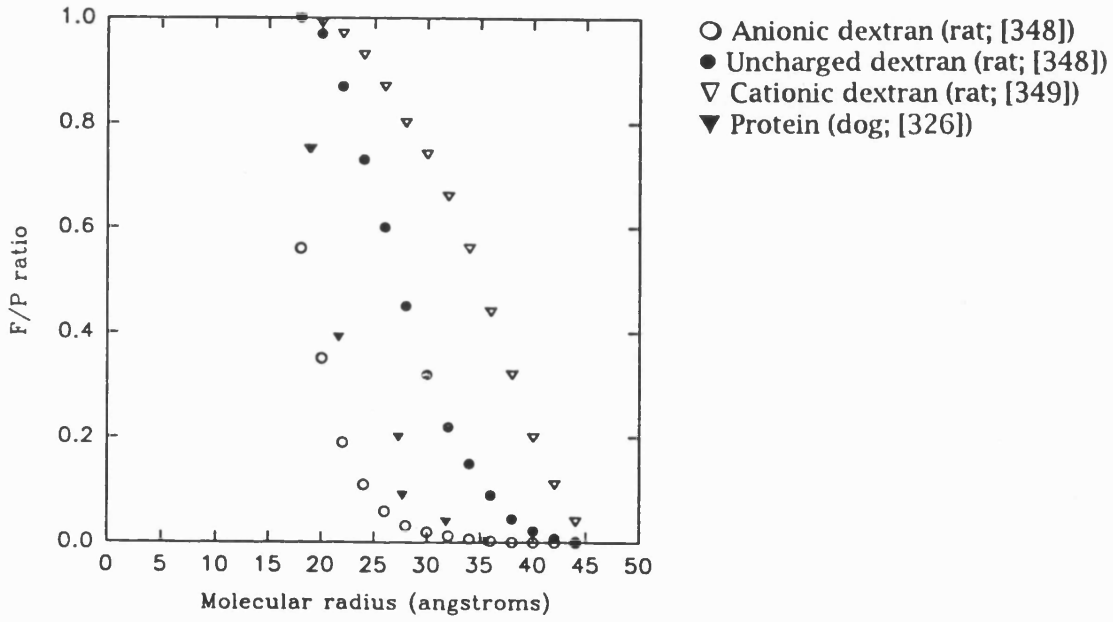

The F/P ratio is unity for molecules of radius less than about 15-20 Å. However, for molecular radii (*a*) greater than about 15-20 Å the F/P ratio declines with increasing molecular size, the rate of decline being partly dependent on molecule charge. At *a* equals approximately 40-50 Å the F/P ratio approaches zero and excretion becomes difficult to quantify. The available data also indicate the effect of charge on transglomerular movement of macromolecules. For each molecular radius the F/P ratio is greater for cationic dextran than uncharged dextran, greater for uncharged dextran than anionic dextran, and somewhat similar for both anionic dextran and endogenous protein molecules. This reflects the net negative charge on most proteins at neutral pH. For example, the F/P ratio for serum albumin which has a molecular radius of 35.5 Å (molecular weight 69,000Da), and pI of about 5, is approximately one-twentieth that of uncharged dextran molecules of the same molecular radius. This suggests that the fixed negatively charged components of the glomerular capillary wall impede/repel negatively charged molecules and thereby hinder or prevent their filtration. In contrast they facilitate relatively faster movement of positively charged macromolecules, into the Bowman's space from the blood [348-352]. There appears to be an effective molecular size cut-off for all molecules, with the cut-off for glomerular filtration of proteins and negatively charged molecules occurring at the size of serum albumin, whilst the cut-off for neutral and positively charged molecules occurs at slightly larger radii of *a* equals 42-45 Å. Consequently any macromolecules with a radius of above about 4.4 nm are generally not transported from the blood into the urine [353], and there is restricted glomerular filtration of macromolecules smaller than this size [326, 348, 349, 354].

Other factors which have been found to influence the ability of macromolecules to pass through the glomerular endothelium, to a considerably lesser extent, are the physical flexibility of the molecular structure [326], and the stability of the intramolecular bonds of the macromolecule [353, 355]. For example, the pressure gradient across the glomerular endothelium (estimated at up to 26 N/sq m [298]) may cause deformation

of flexible molecules [356], hence because many uncharged macromolecules such as PVP and dextran tend to take on a comparatively loose tertiary structure with little intramolecular bonding, they may deform more easily than the more rigid protein macromolecules and therefore may be able to pass more easily through spaces which would otherwise restrict them [356-359]. However, this idea does not meet with universal acceptance, and some authors have estimated that the applied pressure difference across the glomerular endothelium is insufficient to induce any significant molecular deformation, and that deformability of molecules is not an important parameter in regulating extravasation [360].

2.2.2.5 Extravasation through the sinusoidal capillaries of the liver

The distribution of discontinuous or sinusoidal capillaries in the body is much more limited than other capillary types. They are found almost exclusively in the liver, spleen and bone marrow [303, 304]. These capillaries are characterised by large gaps in the endothelial wall, and the basement membrane is absent or discontinuous.

In the sinusoidal vasculature of the liver the endothelial gaps (intercellular junctions) have diameters ranging between 0.1 and 1 μm [303, 305, 306].These large gaps are believed to account for almost all of the extravasation which takes place in the liver. Pinocytotic vesicles are also present in significant numbers in the endothelial layer of the liver sinusoidal capillaries, but they are probably associated with uptake into the endothelium itself and are generally considered to be of negligible significance in terms of macromolecule transport into the liver [303].

Macromolecules pass freely from the sinusoidal blood capillaries into the space of Disse and hence to the functional units of the liver (the hepatocytes and Kupffer cells). Macromolecules are also able to move freely from the space of Disse back to the sinusoidal blood capillaries. Indeed, this phenomenon is perhaps the main reason why there are few data relating the concentration of macromolecules in the hepatic blood capillaries to their concentration in the extravascular spaces of the liver. The free-passage in both directions might be expected to lead to a concentration ratio close to unity unless the molecules are very large. In reality there are some constraints on movement which lead to concentration ratios less than unity [293], but there is insufficient datum available at present to be of use in the modelling studies described here. The data available also suggests that plasma/liver concentration ratios are very sensitive to blood pressure [361-363], making their measurement subject to considerable variation.

Macromolecules may interact with Kupffer cells which are fixed macrophages within the hepatic vascular system [116]. Hydrophobic colloids are phagocytosed rapidly by

these cells and the degree of uptake will depend on the physicochemical properties of the macromolecule in question. Hydrophilic polymers lacking mannose residues or other residues recognised by Kupffer cells will generally avoid uptake by these cells of the mononuclear phagocytic system (or reticuloendothelial system), and will gain acccess to the space of Disse.

Once in the extravascular spaces of the liver macromolecules either move into the hepatocyte cells where they undergo the processes of metabolism or bile secretion, or they remain within the space of Disse unaltered. In general larger macromolecules tend to remain in the space of Disse longer than smaller macromolecules [293], because diffusional processes play a role [361, 364, 365]. The pressure in the sinusoidal capillaries is low so that virtually all of the plasma proteins which have entered the space of Disse can also easily move directly (freely) back into the bloodstream, and those which do not are returned via the lymphatic system which is connected directly to the space of Disse. The extreme permeability of the liver sinusoidal capillaries brings both arterial and venous blood into close contact with the hepatocytes and Kupffer cells, thus facilitating rapid exchange of the subsequent high concentration of nutrient materials between the blood and the liver cells. Hydrophobic low molecular weight molecules gain access by passive diffusion where metabolism can occur. In the case of polar macromolecles, unless a specific receptor for the molecule exists, it is likely that the only mechanism of uptake by hepatocytes is pinocytosis. Thus uptake of molecules such as plasma proteins and their subsequent metabolism may be comparatively slow. Molecules which bind non-specifically to membrane lipids or glycolipids would be expected to be taken up more rapidly by adsorptive endocytosis, and asialoglycoproteins, for example, would be taken up by receptor-mediated endocytosis [114, 115]. Detailed descriptions of the structural and functional units and characteristics of the liver are given in a couple of voluminous literature sources [366, 367].

Most literature reports that in a 70 kg man approximately 1100 ml/min of blood flow through the liver sinusoidal capillaries from the portal vein [368], and that about an additional 340 ml/min flow into the liver sinusoidal capillaries from the hepatic artery [368], making a total blood flow to the liver of approximately 1440 ml/min [368-369]. In a 70 kg man the total volume of blood in the body vasculature is approximately 5600 ml [370], and the normal blood volume of the liver is 560 ml (i.e. about 10% of the total blood volume [368]). In the modelling studies described below the total volume of blood in the body was represented by the parameter V_c (i.e. the volume of the blood was defined as the central compartment) and the blood volume of the liver was represented by the parameter V_H (i.e. the volume of the liver which is subject to extraction was defined as the hepatic compartment). The central compartment was assumed to have a volume equal to the total blood volume, since macromolecules are not able to diffuse freely to and from the vasculature. For simplicity during this study it was assumed that for all macromolecules, irrespective of their size, there was free movement from the sinusoidal blood capillaries into the extravascular spaces of the liver, and also free movement back again. Hence the capillary permeability ratio of polar macromolecules extravasating from the sinusoidal blood capillaries into the extravascular spaces of the liver, and the corresponding concentration ratio of the movement back again, are both assumed to be equal to one. However the model developed was designed to allow estimates of liver/plasma filtration ratios to be built into the model, should reliable data for sinusoidal filtration of macromolecues be available in the future. This study also assumed that the total blood flow rate from the liver is equal to the total blood flow rate to the liver (i.e. 1440 ml/min in man). This is a reasonable assumption, since if this were not the case then there would either be a build-up or a deficit of blood in the liver.

When the term metabolism is used here it refers to the metabolic clearance of macromolecules from the liver rather than the periphery. This is likely to be the site of metabolism which has most influence on distribution unless metabolic enzymes are

present in the plasma. The background to this study relates more to slowly metabolised molecules rather than to proteins or peptides with very short half-lives in the plasma so plasma metabolism was not included in the model. Likewise peripheral metabolism, which in reality would be significant for that proportion of the dose which entered cells of the periphery, was ignored for simplicity. Peripheral metabolism could be included in a numerical solution of more complex models in future studies. In this study an algebraic solution was desired which necessitated a reductionist approach. Thus the rate of the metabolism (k_m) used here refers to a first order rate of loss from the pool of macromolecules within the liver. For macromolecules of interest this could be estimated experimentally in vitro using isolated enzymes. However, in this study a hypothetical approach was used to simulate the effect of metabolic rate by studying the influence of a range of rates. The assignment of the liver as the compartment from which metabolism occurred allowed the relative clearance due to excretion to be separated from that due to metabolism.

2.2.2.6 Movement of macromolecules into the extracellular interstitial fluid and lymphatic system

The mechanisms by which large molecules cross capillary walls and gain access to the interstitial fluids and lymphatic system has intrigued physiologists for many years, yet even today, the mechanisms and processes of this movement still remain unclear [293]. It has long been assumed that the composition of lymphatic fluid is identical to that of interstitial fluid under steady-state conditions [371]. This has been shown to be the case by sampling prenodal lymph at steady-state [372, 373], and is generally believed to be the case for postnodal lymph obtained at steady-state as well, although postnodal lymph may sometimes have been modified slightly within the lymph nodes [374]. However, direct comparisons of interstitial fluid samples with lymph collected simultaneously from the same tissue generally support the contention that the concentrations of macromolecules in lymph and interstitial fluid are identical [293], and most literature consequently assumes that the compositions of lymphatic and

interstitial fluids are the same. In practice it is extremely difficult to distinguish or establish the exact locations where the interstitial fluid and lymphatic system meet and to sample the fluids. Accordingly most lymph permeability studies necessarily treat blood to lymph transport as a single process, even though it actually proceeds in two stages, blood to interstitial space, and interstitial space to lymphatic system. Some reabsorption of water is implied in the first process, though there is no direct route back into blood for macromolecules which have entered tissues. This modelling study therefore also assumes that blood to lymph transport is a single process, and subsequently also assumes that the term lymph (or lymph compartment) refers to the lymphatic system and interstitial fluid combined as one, i.e. the total extracellular or interstitial fluid. This assumption has often been made in the literature.

Published literature suggests that the lymph draining from different organs contain varying concentrations of macromolecules and that the concentration of a macromolecule in the lymph compartment is a function of its molecular size [293, 301, 375]. The principal barrier between blood and lymph transport is at the blood capillary wall, rather than at the lymphatic capillary or within the interstitial space [376]. Once extravasation from the blood-capillaries has taken place, molecules within the interstitial fluid can re-enter the bloodstream either directly via back-diffusion, or they can enter the lymphatic drainage system [121, 376]. Smaller macromolecules are able to take the former route [298], whilst the larger macromolecules (greater than about 15-25Å molecular radius) are forced to take the latter route due to their size [32, 377-380]. Hence there is a considerable degree of selection of macromolecules depending upon their molecular size [293], and the lymphatic circulatory system plays a vital role by returning extravasated blood proteins back to the bloodstream [376], and by recovering macromolecules from tissues [381-383]. At any instant approximately 50% total body albumin (total mass 120g) is in the extravascular space [384]. The lymphatics originate in tissues as open ended capillaries, lined by a single layer of endothelium [376], into which macromolecules move largely by convective uptake. They begin in the areas

containing tissue fluid beyond the blood capillaries and the tissue cells, have enlarged interendothelial cell junctions and lack a well-formed basement membrane [376-378], and are consequently believed to be freely permeable to macromolecules within the interstitial fluid [121]. Accordingly, the lymphatic system represents the main route by which metastatic tumour cells gain access to the blood circulation and are transported within the body [2], since they, as well as most macromolecules, have relatively easy access into the lymphatic system. The lymphatic fluid is drained via a complex series of lymphatic vessels and nodes, which empty back into the venous circulation [376]. Hence all macromolecules within the lymph compartment are returned back to the bloodstream in due course.

Extravasation across continuous endothelia is a critical process influenced by hydrodynamic size [293]. Following extravasation from the blood capillaries the rate of movement of macromolecules through the interstitial fluid and into the lymphatics generally remains unclear [293]. Molecular size appears to be the main factor determining this rate of movement, at least from subcutaneous sites, with the larger macromolecules tending to also be hindered more by interstitial fluid components [385], although charge and flexibility may also influence the process [385-387]. In general the movement of both positively and negatively charged molecules is believed to be retarded in some way, since the positively charged molecules tend to interact with negatively charged interstitial components, and the negatively-charged molecules to be repelled by many tissue components [385]. These concepts suggest therefore that uncharged molecules may move most quickly through the interstitial space.

Very little information is available regarding the relative rate of movement of macromolecules from the blood to the lymph, however, several literature sources report the lymphatic flow rate (LFR or lfr) as being approximately 2 ml/min for a 70 kg man [388, 389]. Since there is free movement for all macromolecules from the lymphatics back into the blood, then the effective concentration ratio (plasma/lymph ratio) of this movement is unity. Consequently it is reasonable to assume that all macromolecules

can move freely from the lymph compartment back into the blood (via the lymphatic system) at a rate controlled by the lymphatic flow rate. The assumption made in this study therefore is that the blood to lymph flow rate (BLFR or blfr) is assumed to be equal to the lymph to blood flow rate (i.e. the lymphatic flow rate) i.e. BLFR = LFR (= 2 ml/min in an average 70 kg man). This will certainly be an understatement of the volume of plasma water which leaves the vasculature, since there is some reabsorption of water into the venuous circulation. However the effective passage of macromolecules into lymph will not be underestimated in the modelling studies, since the physiological data used (i.e. lymph/plasma ratio) samples the lymph itself. The discussion above also explains why it is neccessary to assume that blood to lymph transport is a single process. In this study the total volume of the lymph compartment i.e. the lymphatic system and interstitial fluid is represented by the parameter V_L. Most literature reports that the volume of total interstitial or extracellular fluid in a 70 kg man is 11200 ml, i.e. 16% total body weight [390]. The values of LFR, BLFR and V_L are of course different for other animal species.

Although this study is primarily concerned with predicting which molecular sizes are optimal in achieving the greatest fraction of a macromolecular drug into the lymph, and hence to any cancer micrometastases there, it is perhaps also appropriate here to briefly outline the situation for vascularised tumours. Macromolecular distribution to larger solid tumours is believed to be different, since as has already been highlighted in more detail in Chapter 1 (Section 1.1), solid tumours lack any recognised system of lymphatic drainage [2, 8, 24-28], and recruit their own blood capillaries and exhibit wide variation in the structure and arrangment of tumour blood vessels [14, 15]. Molecules within the tumour interstitial fluid can be drained either via entry into the postcapillary venules or are driven by elevated interstitial pressures through the tumour interstitium, eventually oozing from the periphery and then being drained by the lymphatics in surrounding normal tissue. This means that macromolecules which have been able to enter the vascularised solid tumour interstitium by extravasation, and which are unable to return

to the postcapillary circulation, do not have any effective method of drainage. These macromolecules are generally unable to penetrate the dense mass of necrotic tissue within the tumour, and consequently tend to remain close to the living tissue within the tumour. The consequence is that the vascularised tumours tend to act as molecular sieves, preferentially retaining hydrophilic macromolecules. This concept forms part of the basis of the "Enhanced Permeability and Retention" (EPR) effect [25], which may be exploited for selective tumour therapy. Enhanced permeability is believed to be common because the features regulating extravasation of materials through tumour endothelium are different from those in normal tissue; there are often fewer restrictions on size (although substrate charge may be an important factor), but the high interstitial pressures [27, 89, 91, 92, 391, 392], resulting in decreased rates of fluid translocation and convective transport, mean that diffusion of macromolecules becomes a significant factor governing their rate of entry into the tissue [391, 393, 394]. Also vascularised tumours tend to have larger interstitial spaces than normal (non-neoplastic) tissues, and their interstitial matrix frequently shows variable composition, notably in its content of macromolecules such as hyaluronic acid which is thought to retard fluid movement [393]. Many tumours are reported to have levels of hyaluronic acid substantially lower than in normal tissues [391], suggesting that rates of macromolecular movement in tumours may be relatively higher [385]. The peculiar vascular properties of tumours which are responsible for these unusual characteristics have already been outlined in section 1.1. It is clear that these characteristics could be exploited, but the main concern of chemotherapy should be to eradicate micrometastases before they develop into larger vascular tumours. To exploit the EPR effect the tumour must have developed into a nodule of considerable size (perhaps 1 cm in diameter). Therefore the phenomenon of macromolecular EPR should be regarded as an added bonus of the use of macromolecular drugs. Attention should be focussed primarily on delivering macromolecules to micrometastatic lesions within tisssues, which requires passage across normal endothelia.

Most of the capillary permeability studies which have been performed with different size macromolecules compare the concentration of an intravenously infused test macromolecule in the lymph compartment (usually by sampling the lymphatic fluid, although the interstitial fluid has also been sampled) to that in the plasma, i.e. $\frac{C_L}{C_P}$, and usually refer to this ratio as the L/P ratio. Although some other methods have been employed to evaluate capillary permeability, the L/P ratio studies are the most frequently used, and have produced the best available data. A survey of the literature from such L/P ratio studies concluded that the best available data both in terms of quality and quantity related to measurements in the lung [395-409] and subcutaneous skin [306, 372, 373, 410-415]. The capillaries found in these tissues are of the continuous type, with continuous endothelia and an uninterrupted basement membrane. This ultrastructural appearance has generally led physiologists to assume that they offer more restriction to macromolecule movement than other capillary types, and consequently their permeability characteristics have received far more attention. There are some data for other tissues with continuous capillary beds (i.e. skeletal muscle [375, 416-426]) and also some data for tissues with fenestrated (i.e. gastrointestinal organs [419, 427-434]) or discontinuous (i.e. liver [301, 361, 375, 419, 427, 432 –440]) endothelia. However the datum available does not allow a full understanding of the effects of size on extravasation from fenestrated or sinusoidal capillaries.

A summary of the available L/P ratio data is discussed in a recent review [293]. Figures 2.3.1 to 2.3.5 show the most useful data for the lung, subcutaneous skin, skeletal muscle, gastrointestinal organs, and liver respectively.

Figure 2.3.1 Relationship between L/P ratio and molecular radius for various macromolecules in the lungs of different mammals.

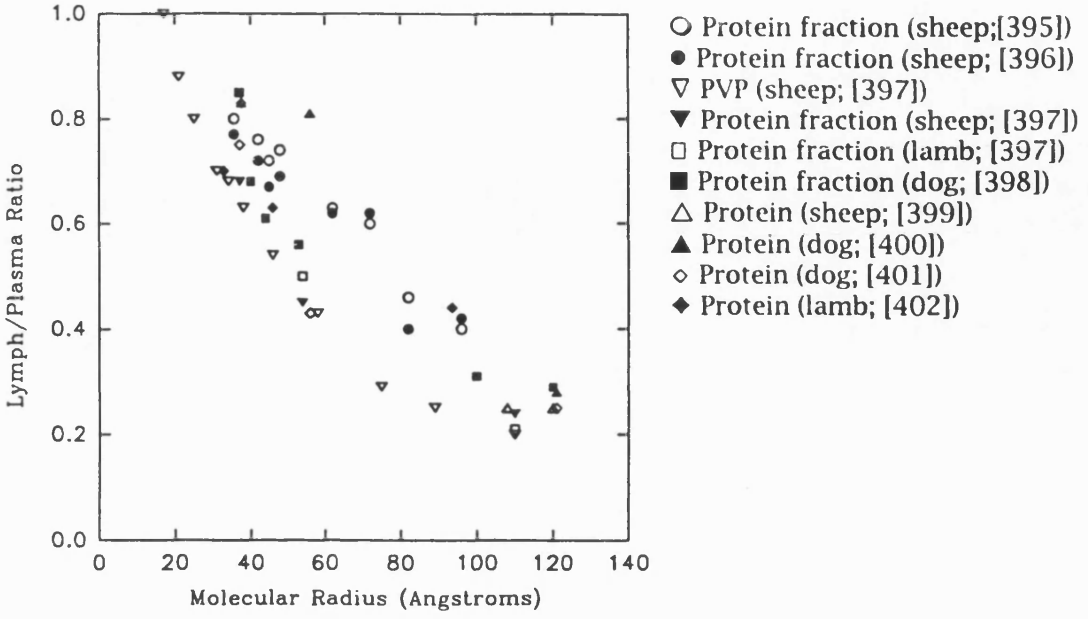

Figure 2.3.2 Relationship between L/P ratio and molecular radius for various macromolecules in the subcutaneous tissue of different mammals.

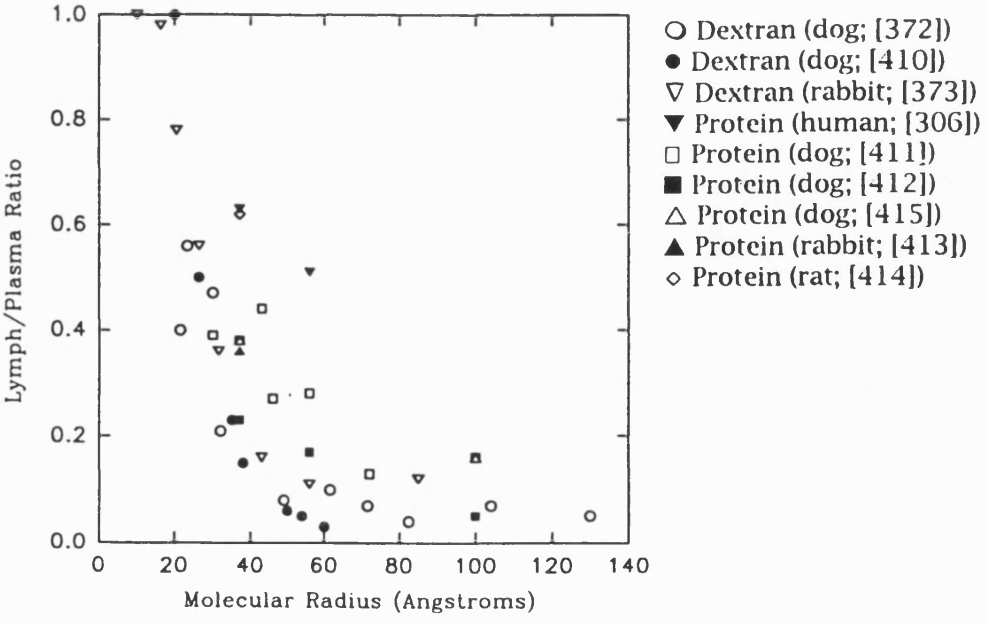

Figure 2.3.3 Relationship between L/P ratio and molecular radius for various macromolecules in the skeletal muscle of different mammals.

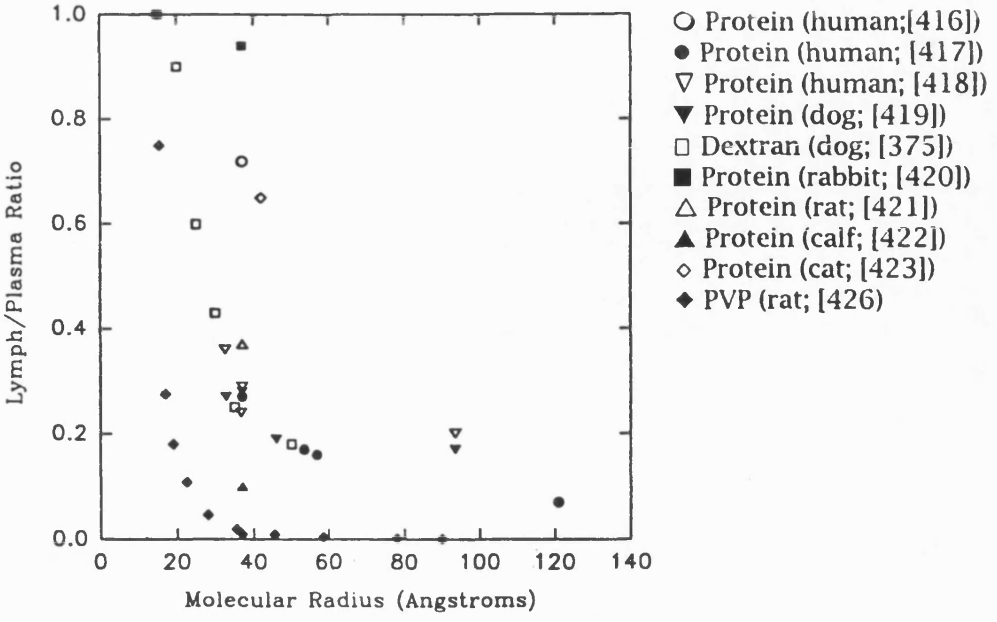

Figure 2.3.4 Relationship between L/P ratio and molecular radius for various macromolecules in the gastrointestinal organs of different mammals.

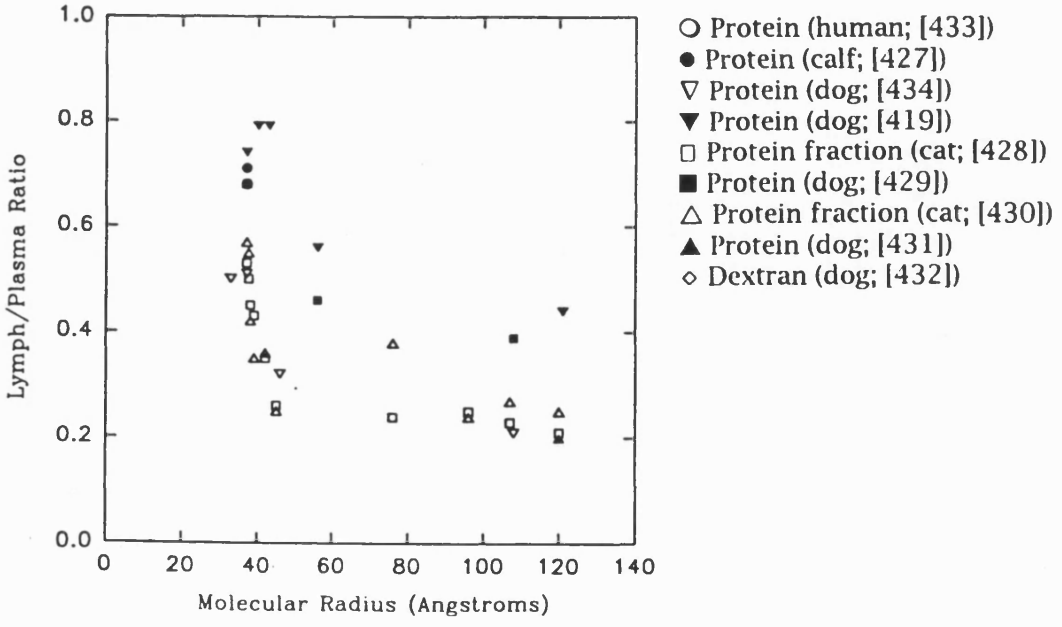

Figure 2.3.5 Relationship between L/P ratio and molecular radius for various macromolecules in the liver of different mammals.

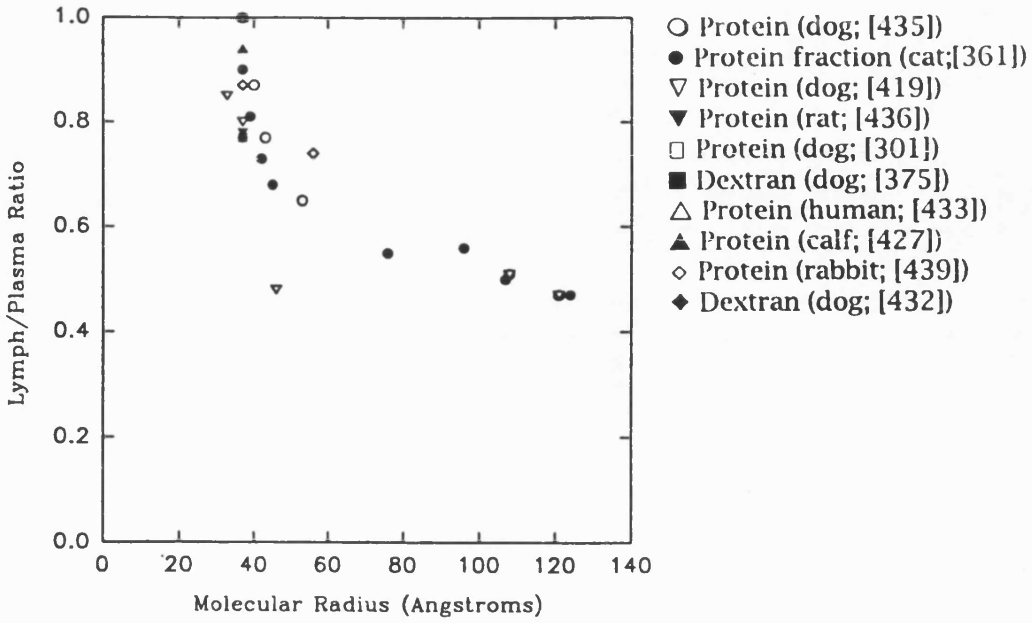

Figure 2.3.1 shows the lung L/P ratio data as a function of molecular radius for several protein, endogenous protein fraction, and povidone (PVP) macromolecules in sheep and dog. There is no human data. The capillaries in the lung demonstrate selectivity, since in all cases the L/P ratio decreases with increasing molecular size. The datum suggests that the lymph collected in the two animals were similar. For molecules with molecular radius less than 17Å there is free filtration. As molecular radius increases from approximately 37 to 110 Å, L/P ratio decreases from approximately 0.7 to 0.25. In addition these data demonstrate that the L/P ratio decreases to approximately 0.4 at a molecular radius of 60Å and thereafter decreases at a much slower rate as the radius of the molecules increases. This relationship is similar to that observed in most other tissues. Clearly a molecule of the dimensions of albumin (a = 37Å) has good access to the lung.

Figure 2.3.2 illustrates the relationship between L/P ratio and molecular radius in the subcutaneous tissue of dog, rat and rabbit, for protein and dextran macromolecules. Limited human data are also available for proteins. The data show no clear delineation between species and no distinciton in the ratios derived from lymphatic fluid or interstitial fluid. As a whole the data show a rapid decline in L/P ratio for solute radii below 40Å. Above 40Å, L/P ratio remains somewhat constant up to a solute radius of 130Å. There is free-filtration for molecules with molecular radii 10-20Å and less.

Figure 2.3.3 represents a plot of the best of the available L/P ratio data as a function of molecular radius for skeletal muscle. The data are for dextran, protein, and PVP macromolecules in the dog, cat, rat and rabbit. Some limited human data are also available. Although skeletal muscle comprises the largest percentage of the total body mass, surprisingly little information is available regarding the permeability characteristics of capillaries in this tissue. This is because it is frequently very difficult to acquire lymph that is uncontaminated by sources outside of muscle. The available data for proteins show that the value of the L/P ratio decreases from approximately 0.7 to 0.07 as the molecular radius increases from 37Å to 120Å. Similar relationships

between L/P ratio and solute radius are observed for the PVP and dextran fractions. The available data once again demonstrate selectivity and there is free-filtration for molecules with molecular radii less than approximately 15Å.

Figure 2.3.4 illustrates the relationship between L/P ratio and molecular radius for various protein and endogenous protein fraction macromolecules in dog, calf and cat gastrointestinal organs. There is very limited human data. The limited data show a steep fall in permeation of solute in the size range below a radius of 60Å. Above 60Å there is an extension in residual permeability with little decrement in L/P ratio for molecules with radii as large as 135Å. The lack of data for low molecular radii solutes make prediction of sizes at which free-filtration occurs difficult.

Figure 2.3.5 shows the relationship between L/P ratio and molecular radius for various protein and endogenous protein fraction macromolecules in the liver for several animal species, although the data are somewhat limited. Hepatic lymph is unique because it flows at a high rate and has the greatest protein concentration of all regional lymphs [293]. Under normal experimental conditions the ratio of total protein concentration in lymph to that in plasma generally ranges between 0.8 and 0.95, whereas a L/P ratio of 1.0 is commonly reported for albumin. In spite of the high L/P ratio values for albumin and total protein, analyses of L/P ratio for macromolecules of various sizes indicate that there is selectivity at the liver blood-lymph barrier under normal conditions, although the lack of useful data currently available make it difficult to confirm this. The datum does however show that the liver sinusoids are very permeable. There appears to be free-filtration for molecules with molecular radii less than approximately 37Å and even molecules with radii greater than 70-120Å produce high L/P ratios. The unique features of hepatic lymph does however make interpretation of this data difficult and correspondingly limits its usefulness.

Figures 2.3.1 to 2.3.5 therefore illustrate a number of interesting featues, the most obvious of which is that all capillaries demonstrate selectivity to macromolecules. In all

cases the L/P ratio decreased with increasing molecular radius size, but the capillary permeability varied between tissues. The data also show that the differences between lymph collected in various mammalian species were limited suggesting therefore that the data for non-human mammals are a good estimate of L/P ratios for humans. There are clear differences in the L/P ratio data between tissues of different capillary types, the liver sinusoidal capillaries being permeable to molecules of radius greater than 70Å. There are also some differences between tissues of the same general capillary type i.e. the subcutaneous skin appears to be much more restrictive (tighter) in terms of permeability than the lung. However, there are also some general similarites between different tissues i.e. the lung L/P ratio data show some general similarity to the L/P ratio data for the gastrointestinal organs.

Figures 2.3.1-2.3.5 show that the L/P ratio data for tissues other than the lung and the subcutaneous skin is not as comprehensive and therefore not as useful for the proposed physiological modelling. There are fewer data for these other tissues, and also a large proportion of what is available tends to be in a single or a few data points per experimental report. L/P ratio studies which report data for a range of different macromolecules by the same researcher were considered to be more useful as model data though an understanding of the accuracy of the data can be gained by comparing data from single point studies or by pooling data. In order to investigate the effect of molecular radius on the distribution of both protein and uncharged macromolecular drugs in the body, L/P ratio data were needed for both classes of macromolecules, and ideally the pairs of data would be for the appropriate animal species. However, such data are not available. As in the case of the F/P ratio data, there are very little L/P ratio data for humans. In the absence of human data it was necessary to use the best available animal data. There were various considerations for and against the selection of the best data, and indeed whether or not to pool any data from various species. For these modelling studies it was decided to use the lung and subcutaneous skin data which covered a wide range of molecular radii. This datum is presented in tables 2.3 to

2.6 respectively and is used in the modelling studies described in subsection 2.2.3. The lung and subcutaneous skin are also tissues possessing continuous capillaries, and this type of capillary offers more restriction to macromolecule movement and distribution than other capillary types. The lung data are particularly appropriate to this study since the lung is often the site where cancer micrometastases develop into secondary tumours.

Table 2.3 Pooled endogenous protein L/P ratio data for the sheep lung [395-396] (postnodal lymph measured at normal lymph flow).

Endogenous protein fraction	Molecular radius (Å)	L/P ratio	
		[395]	[396]
I	35.3	0.8	0.77
II	42	0.76	0.72
III	45	0.72	0.67
IV	48	0.74	0.69
V	62	0.63	0.62
VI	72	0.60	0.62
VII	82	0.46	0.40
VIII	96	0.40	0.42

Table 2.4 Endogenous protein L/P ratio data for the dog lung [398] (prenodal lymph measured at normal lymph flow)

Endogenous protein fraction	Molecular radius (Å)	L/P ratio
I	37	0.85
II	40	0.68
III	44	0.61
IV	53	0.56
V	100	0.31
VI	120	0.29

Table 2.5 **(PVP) Povidone L/P ratio data for the sheep lung [397] (postnodal lymph measured at normal lymph flow)**

PVP	Molecular radius (Å)	L/P ratio
A	110	0.20
B	89	0.25
C	75	0.29
D	58	0.43
E	46	0.54
F	38	0.63
G	34	0.68
H	31	0.70
I	25	0.80
J	21	0.88
K	17	1.00

Table 2.6 **Pooled uncharged dextran L/P ratio data for the dog and rabbit subcutaneous skin [372-373, 410]**

	Molecular radius (Å)	L/P ratio
Dextran [372] (dog, prenodal lymph measured at steady-state)	21.5	0.40
	23.3	0.56
	30	0.47
	32	0.21
	49	0.08
	61.5	0.10
	71.5	0.07
	82.5	0.04
	104	0.07
	130	0.05
Dextran [410] (dog, prenodal lymph measured at steady-state)	20	1.00
	26.4	0.50
	35	0.23
	38	0.15
	50	0.06
	54	0.05
	60	0.03
FITC-dextran [373] (rabbit, interstitial fluid measured at steady-state)	10.1	1.00
	16.3	0.98
	20.5	0.78
	26.4	0.56
	31.5	0.36
	43	0.16
	56	0.11
	85	0.12

2.2.3 Development of mathematical models of the effect of hydrodynamic radius on L/P and F/P ratios

2.2.3.1 Introduction

The purpose of this section was to develop mathematical expressions on an empirical basis which could describe the dependence of L/P and F/P ratios on hydrodynamic radius.

The parameters of best-fit for each of the models studied in this subsection were obtained using the nonlinear curve fitting computer programme Minsq [441]. A brief introduction and description of Minsq [441] is given in part 2.2.3.2. The models studied are presented in parts 2.2.3.3-2.2.3.5. A summary of the main conclusions is then presented in part 2.2.3.6.

2.2.3.2 Methods and strategies used in the selection of the best model(s) and determination of the parameters of best-fit.

Minsq [441] is a menu driven nonlinear curve fitting programme published by MicroMath Inc. Various options become available to the user only after they become logically possible during the sequence of events. The programme runs under MS-DOS on IBM clone PCs. The model equation(s) and associated data are entered by the user via the relevant menu options. Inital parameter estimates must also be entered before least-squares minimisation curve-fitting can take place. For a simple relationship the parameter estimates need not be accurate. However, a complex equation will require good parameter estimates. In this situation if the initial parameter estimates are not appropriate then Minsq [441] will fail to find the optimal parameter values. Minsq [441] employs a least-squares minimisation procedure to find a local minimum of the sum of squared deviations between observed data and model predictions/simulations. The algorithm employed is many times faster than more common microcomputer algorithms and is based on sequential searches using one parameter at a time. The algorithm is a hybrid that combines the reliability of a steep descent method with the speed (near convergence) of the Gauss-Newton method. Minsq [441] also has a

nonlinear simplex algorithm which can be selected for searching through the parameter space for the general location of a minimum, so that initial parameter estimates are improved prior to selecting the least-squares minimisation option. In performing its minimisation Minsq [441] weights each datum point according to a weighting factor inversely proportional to the observed value raised to some power given by the weighting factor, i.e. for the i^{th} point $w(i)=1/(\text{observation (i)})^{WF}$, where WF is the weighting factor. A weighting factor of zero (the default) causes all points to be weighted equally and does not introduce any bias into the fit, whilst a weighting factor of 2 results in weights inversely proportional to the squares of the observed values. The latter choice is appropriate when measurement errors are thought to be proportional to the observed data values. The other major menu options within Minsq [441]are the simulation run, graphics and statistics options. The simulation option simulates the model using the current parameter values and gives a weighted sum of squared deviations values, wss (as do the simplex and least squares options). The graphics options displays the data visually and can be used to generate hard copies of graphs. Both the simulation and graphics options should be used when trying to find the best initial choice of parameters. The statistics option is available after a least-squares minimisation fit has been performed, and provides a variety of statistical information on the parameters of best-fit.

The purpose of the curve fitting described here was to arrive at a suitable mathematical model for the dependence of F/P or L/P ratio on hydrodynamic radius (a).

i.e. $F/P = f(a)$

and $L/P = f'(a)$

A series of putative mathematical models were explored using an empirical approach to determine the most appropriate relationship.

As indicated above, before any sensible simulations could be performed on Minsq [441], good initial parameter estimates for each respective model and data sets are required. Consequently the strategy used to determine these good initial parameter estimates for each of the models presented in this subsection, and the subsequent selection of the most appropriate model, is described in parts (i) to (v) below:

(i) The first step was to choose from each of the F/P and L/P ratio data sets either a single or pair of data points which could be used in the calculations to find good initial parameter estimates. Each data point consisted of a given molecular radius (independent variable) with its associated F/P or L/P ratio value (dependent variable). The choice of whether one or two data points were selected depended both on the mathematical form of each of the models and their parameters, and on the data sets themselves. In general and indeed where possible, for each of the chosen data sets a data point with a molecular radius close to serum albumin was selected. In the cases when two data points were chosen, the second data point was usually chosen to cover a reasonable spread of the data, thus avoiding selection of two points too close to each other, and hence increasing the chances of finding good initial parameter estimates. For consistency, the same data point(s) (as appropriate) from each of the respective F/P ratio and L/P ratio data sets were selected to be used in the initial parameter estimation procedure in each of the models presented in this subsection.

(ii) For each data set the chosen data point(s) (as appropriate) in (i) were then substituted into the appropriate model equation. Equations were then solved by hand to yield the model parameters. In the models whose general form involved an exponent n, i.e. models A and B (as shown later), this procedure was repeated for varying positive whole numbers of n (n=1, 2, 3, . . .), so that for each choice of n, initial estimates for the model parameters were obtained. n was forced to take the value of positive whole numbers because otherwise the equations would become too complex.

(iii) In the cases of models whose general form involved a power *n*, i.e. models A and B (as shown later), the next step was to decide for each of the chosen F/P ratio and L/P ratio data sets which power of *n* and its associated initial parameter estimates were most appropriate. This was achieved by simulating with Minsq [441] the appropriate model equation for each data set for each power of *n* and its associated initial parameter estimates. The simulation which produced the lowest wss value, between the observed and model predicted data, generally corresponded to the best choice of *n* and its associated initial parameter estimates. Although for the reasons outlined in (v), a graphical plot of the general shape of the curve had to be considered in conjunction with this. When the best choice of initial parameter estimates was still unclear, one of the least-squares methods outlined in (iv) was also used.

(iv) Once the choice of initial parameter estimates had been made, the next step was to use Minsq [441] to perform least-squares minimisation procedures to find the optimal parameters of best-fit. Minsq [441] offers two ways of performing this operation, both of which are perfectly acceptable. One method, the quicker of the two, is to go direct to a least squares minimisation fit. The other method, which takes longer but ensures the absolute best-fit, is to make use of all the tools provided by Minsq [441] by first simulating the model using parameter estimates, then performing a simplex search to further improve the initial parameter estimates, before carrying out the least-squares minimisation. Both methods were found to be acceptable if good initial parameter estimates were obtained. In general the wss value obtained after the least-squares minimisation fit was lower, and therefore better, if the simplex search was used. However there were often no significant differences between parameter estimates. For the sake of thoroughness both methods were used throughout the modelling experiments. A weighting factor of zero was used for all the fits throughout this subsection, unless otherwise stated, so that no bias was introduced into the fitting. The parameters of best-fit used in the later pharmacokinetic modelling studies (described in Chapter 3) were those obtained using a simulation run, a simplex search,

then the least squares minimisation fit. When there was an exponent '*n*' involved in the model, it was held constant during the least-squares fitting process at its most appropriate positive whole number value as determined in (iii).

(v) Once the least-squares fits had been performed it was possible to select the best model(s) to describe the relationship between molecular radius and the F/P or L/P ratios. The selection of the best model(s) was based on the wss value between the observed data and model predictions following the least-squares fits. The model which produced the lowest wss value following the least-squares minimisation was considered to be the best model, although the graphics option was also employed to generate plots to support this assumption. In some cases models with similar wss values were observed to fit different parts of the data well. Thus some subjective assessment was necessary by considering the shape of the fit, to establish that the fit was reasonable for all the data. The 'model selection criteria' (MSC) value given in the statistics option of Minsq [441] was also used to support this selection.

The MSC is a modified Akaike Information Criterion (AIC), and is defined by the formula:

$$MSC = \ln\left[\frac{\sum_{i=1}^{n} w_i \left(Y_{obsi} - \overline{Y}_{obs}\right)^2}{\sum_{i=1}^{n} w_i \left(Y_{obsi} - Y_{cal_i}\right)^2}\right] - \frac{2p}{n}$$

where n is the number of observations and p is the number of parameters (or equivalently, the number of degrees of freedom). The AIC is defined by the formula,

$$AIC = n \bullet \ln\left(\sum_{i=1}^{n} w_i \left(Y_{obs_i} - Y_{cal_i}\right)^2\right) + 2p$$

and attempts to represent the "information content" of a given set of parameter estimates by relating the coefficient of determination to the number of parameters (or equivalently, the number of degrees of freedom) that were required to obtain the fit.

When comparing two models with a different number of parameters, this criterion places a burden on the model with more parameters to not only have a better coefficient of determination, but quantifies how much better it must be for the model to be deemed more appropriate. The AIC is dependent on the magnitude of the data points as well as the number of observations. The advantage the MSC has over the AIC is that the MSC will give the same rankings between models as the AIC and has been normalised so that it is independent of the scaling of the data points, thus overcoming the disadvantages which the AIC has. In general, the higher the MSC value, the more appropriate the model (representing a higher "information content" of the model), with MSC values greater than about 1.5 being adequate. For each mathematical model examined a large volume of statistical information was obtained, however, not all of this is presented in the parameter of best-fit tables, since the MSC is the recommended criterion in preference to any of the other statistical measures of goodness of fit (eg coefficient of determination, correlation, R-squared, etc).

2.2.3.3 Model A

The first and simplest mathematical model proposed to describe the relationship between molecular radius and F/P or L/P ratio had the general form:

$$R = R_0 \exp\left(-k(a)^n\right) \qquad \text{(A)}$$

where R is the respective F/P or L/P concentration ratio, a is the molecular radius of the macromolecule (Å), R_0 is a parameter representing the theoretical value of R at $a = 0$, and the parameters n and k control the shape of the curve with k representing the gradient (exponential gradient).

Model A was then fitted to each of the F/P ratio data sets presented in tables 2.1 and 2.2 and also to each of the L/P ratio data sets presented in tables 2.3, 2.4 and 2.5. The data points used to initiate the fitting procedure, the best initial parameter estimates, and the optimal parameters of best-fit (mean ± sd) for all of these fits, together with the wss values and the MSC where possible are presented in table 2.7. Figures 2.4A and

2.4B illustrate these results in plot form for the parameters of best-fit obtained following a simulation run, a simplex search, then the least squares minimisation.

Table 2.7

Initial parameter estimates and parameters of best-fit for Model A

		Model A:			
		(*a*, ratio) data point(s) selected to initiate calculation of initial parameter estimates	Initial parameter estimates	Parameters of best-fit Simulation → Least Squares	Simulation → Simplex → Least squares
$\frac{F}{P}$ ratio data	Anionic dextran [348] (rat)	(20, 0.35) (36, 0.003)	*n* =1 *k*=0.2974575 *R*0=134.19988 (wss 0.0055927)	*n* =1 *k*=0.26855 ± 0.0053119 *R*0=71.330 ± 7.2257 (wss 0.00051592) (MSC 6.2623)	*n* =1 *k*=0.26855 ± 0.0053119 *R*0=71.330 ± 7.2257 (wss 0.00051592) (MSC 6.2623)
	Uncharged dextran [348] (rat)	(20, 0.97) (36, 0.09)	*n* =4 *k*=1.5645E-6 *R*0=1.2459033 (wss 0.0056695)	*	*n* =4 * *k*=1.5631E-6 *R*0=1.2140 (wss 0.003368)
	Cationic dextran [349] (rat)	(20, 0.99) (36, 0.44)	*n* =6 *k*=3.83817E-10 *R*0=1.0146199 (wss 0.0046919)	**	*n* =6 ** *k*=3.83817E-10 *R*0=1.0146199
	Protein [326] (dog)	(18.8, 0.75) (27.7, 0.09)	*n* =1 *k*=0.2382318 *R*0=66.093853 (wss 0.015767)	*n* =1 *k*=0.20946 ± 0.021139 *R*0=38.960 ± 16.076 (wss 0.0080614) (MSC 3.7726)	*n* =1 *k*=0.20946 ± 0.021139 *R*0=38.961 ± 16.076 (wss 0.0080614) (MSC 3.7726)
$\frac{L}{P}$ ratio data	Pooled endogenous protein fractions [395, 396] (sheep lung)	(35.5, 0.77) (96, 0.42)	*n* =1 *k*=0.0100187 *R*0=1.0988914 (wss 0.029437)	*n* =1 *k*=0.010456 ± 0.00096528 *R*0=1.1524 ± 0.061905 (wss 0.025334) (MSC 2.1475)	*n* =1 *k*=0.010456 ± 0.00096528 *R*0=1.1524 ± 0.061905 (wss 0.025334) (MSC 2.1475)
	Endogenous protein fractions [398] (dog lung)	(37, 0.85) (100, 0.31)	*n* =1 *k*=0.0160105 *R*0=1.5370572 (wss 0.053204)	*n* =1 *k*=0.013361 ± 0.0027238 *R*0=1.2146 ± 0.16940 (wss 0.020736) (MSC 1.7644)	*n* =1 *k*=0.013361 ± 0.0027238 *R*0=1.2146 ± 0.16940 (wss 0.020736) (MSC 1.7644)
	PVP [397] (sheep lung)	(89, 0.25) (21, 0.88)	*n* =1 *k*=0.0185067 *R*0=1.2979711 (wss 0.0067842)	*n* =1 *k*=0.019522 ± 0.00078146 *R*0=1.3325 ± 0.035584 (wss 0.0056258) (MSC 4.4646)	*n* =1 *k*=0.019522 ± 0.00078146 *R*0=1.3325 ± 0.035584 (wss 0.0056258) (MSC 4.4646)

* Least squares fit not possible, simplex parameters quoted as they offered small improvements on initial parameter estimates.

** Least squares fit not possible, simplex offered no improvement on initial parameter estimates quoted.

Figure 2.4A Model A fitted to the selected F/P ratio data.

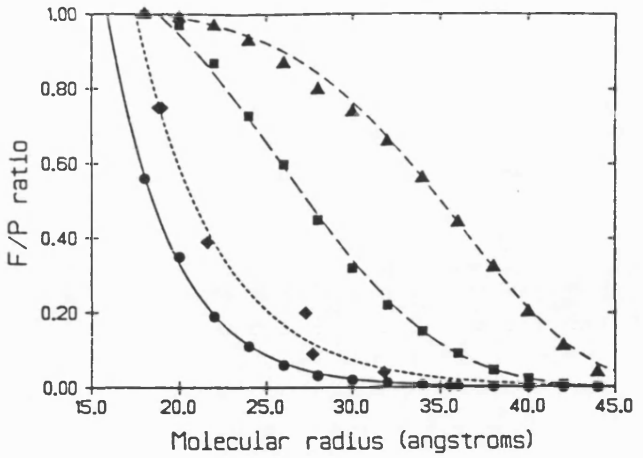

● Anionic dextran (rat; [348])
■ Uncharged dextran (rat; [348])
▲ Cationic dextran (rat; [349])
◆ Protein (dog; [326])

Figure 2.4B Model A fitted to the selected Lung L/P ratio data

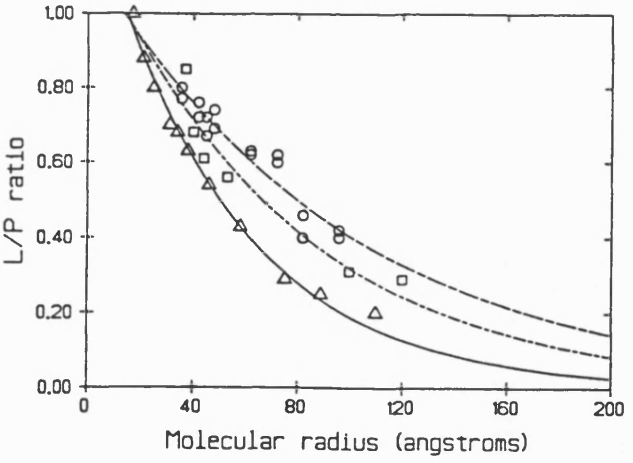

O Pooled protein fraction (sheep; [395; 396])
□ Protein fraction (dog; [398])
△ PVP (sheep; [397])

With n = 1Model A was found to fit most of this datum reasonably well with good wss and MSC values in most cases, although its general form presented two disadvantages:

(i) In the cases of the uncharged [348] and cationic [349] dextran data least squares minimisation fits were not possible. This is almost certainly due to the relatively large values of n required and the very small values of the parameter k in each case, making the calculations very difficult to perform. In the case of the uncharged dextran data set [348], the simplex search offered a small improvement on the initial parameter estimates, but in the case of the cationic dextran data set [349] no improvement on the initial parameter estimates was possible.

(ii) Although the pre-exponential coefficient R_0 in model A is mathematically correct, from a physiological point of view it is a meaningless value since the maximum value the extravasation concentration ratio R can have is in practice, $R = 1.0$ (free-filtration). The consequence of using model A was to generate values of R_0 >1 such that for values of molecular radii between zero and an unknown radius at which free-filtration ceases to occur, Model A produces F/P ratio values which are nonsense. Furthermore, the general form of Model A does not include any parameter which represents the maximum molecular radius at which free-filtration occurs.

The considerations outlined above led to the development of the more complex mathematical model, Model B.

2.2.3.4 Model B

The second model studied had the general form:

$$R = \exp\left(-k(a - ao)^n\right) \qquad \text{(B)}$$

where R is the respective F/P or L/P concentration ratio, a is the molecular radius of the macromolecule (Å), ao is the parameter representing the molecular radius at which the ratio R is 1.0, and n and the parameter k control the shape of the curve, with k representing the gradient (exponential gradient).

Model B has the following important advantages over Model A:

(i) The presence of the parameter ao meant there was no need for a pre-exponential coefficient in Model B. This is an advantage because such a parameter has no physiological meaning. It should be noted that an important factor in the selection of all of the models presented in this subsection, was the desire to model the data adequately whilst keeping the number of parameters to a minimum.

(ii) The introduction of the parameter ao provides important information from the physiological point of view, since ao ensures that for each fit the value of the molecular radius at which the concentration ratio R equals 1.0 is obtained (i.e. at $a = ao$). Hence free-filtration can be assumed to occur for all molecular radii smaller than that respective ao value, whereas for molecular radii greater than ao the extent of extravasation decreases with increasing molecular radius. An important assumption with Model B therefore is that $a \geq ao$ (the actual value of ao will of course be different for each data set the model is fitted to). It can be assumed that $R = 1.0$ (i.e. free-filtration) for all molecular radii within the range $0<a<ao$.

(iii) In the cases of the uncharged dextran F/P ratio data [348] and the cationic dextran F/P ratio data [349] (which proved difficult to fit to Model A) and as a consequence of (i) and (ii), the power of n was reduced, (and correspondingly the

respective parameter k in each case became larger) which enabled the least-squares minimisation fits to be performed for all of the chosen data sets.

Model B was fitted to each of the F/P ratio data sets presented in tables 2.1 and 2.2, and to each of the L/P ratio data sets presented in tables 2.3 to 2.6. The results obtained from these fits are presented in table 2.8. Figures 2.5A and 2.5B illustrate the results of the fits to the F/P ratio data and the lung L/P ratio data respectively in plot form. Only single data points were used to initiate the fitting procedure in this case, because it was often easy to estimate the size of *ao* from the datum itself.

Table 2.8
Initial parameter estimates and parameters of best-fit for Model B

		Model B:			
		(*a*, ratio) data point(s) selected to initiate calculation of initial parameter estimates	Initial parameter estimates	Parameters of best-fit Simulation → Least Squares	Simulation → Simplex → Least squares
$\frac{F}{P}$ ratio data	Anionic dextran [348] (rat)	(36, 0.003)	*n* =1 *ao*=16 *k*=0.2904571 (wss 0.0017984)	*n* =1 *k*=0.26850 ± 0.0052882 *ao*=15.890 ± 0.070982 (wss 0.00051593) (MSC 6.2623)	*n* =1 *k*=0.26851 ± 0.0052884 *a*0=15.890 ± 0.070977 (wss 0.00051593) (MSC 6.2623)
	Uncharged dextran [348] (rat)	(36, 0.09)	*n* =2 *ao*=18 *k*=0.0074319 (wss 0.0034985)	*n*=2 *k*=0.0072930 ± 0.0014658 *ao*=17.579 ± 0.10185 (wss 0.00049785) (MSC 7.9236)	*n* =2 *k*=0.007333 ± 0.00014778 *a*0=17.612 ± 0.10185 (wss 0.00049917) (MSC 7.9236)
	Cationic dextran [349] (rat)	(36, 0.44)	*n* =3 *ao=18* *k*=0.0014077 (wss 0.016428)	*n*=3 *k*=0.00014097 ± 1.8627E-5 *ao*=17.458 ± 0.76359 (wss 0.010087) (MSC 4.7226)	*n* =3 *k*=0.00011562 ± 1.3312E-5 *a*0=16.291 ± 0.70815 (wss 0.0079578) (MSC 4.9597)
	Protein [326] (dog)	(35.5, 0.03)	*n* =1 *ao=17* *k*=0.314007 (wss 0.133377)	*n* =1 *k*=0.20950 ± 0.021068 *ao*=17.487 ± 0.26103 (wss 0.0080615) (MSC 3.7726)	*n* =1 *k*=0.20941 ± 0.021055 *a*0=17.486 ± 0.26119 (wss 0.0080615) (MSC 3.7726)
$\frac{L}{P}$ ratio data	Pooled endogenous protein [395-396] fractions (sheep lung)	(35.5, 0.77)	*n* =1 *ao=14* *k*=0.0100187 (wss 0.028842)	*n* =1 *k*=0.010458 ± 0.00096525 *ao*=13.568 ± 3.9650 (wss 0.025334) (MSC 2.1475)	*n* =1 *k*=0.010454 ± 0.00096511 *a*0=13.558 ± 3.9671 (wss 0.025334) (MSC 2.1475)
	Endogenous protein fractions [398] (dog lung)	(37, 0.85)	*n* =1 *ao*=15 *k*=0.00738722 (wss 0.17899)	*n* =1 *k*=0.013386 ± 0.0027232 *ao*=14.711 ± 7.6999 (wss 0.02074) (MSC 1.7642)	*n* =1 *k*=0.013375 ± 0.0027251 *a*0=14.581 ± 7.7374 (wss 0.020736) (MSC 1.7644)
	PVP [397] (sheep lung)	(38, 0.63)	*n* =1 *ao*=17 *k*=0.0220016 (wss 0.011915)	*n* =1 *k*=0.019537 ± 0.00078171 *ao*=14.711 ± 0.88002 (wss 0.0056261) (MSC 4.4645)	*n* =1 *k*=0.019532 ± 0.0007815 *a*0=14.711 ± 0.88015 (wss 0.0056259) (MSC 4.4646)
	Pooled uncharged dextran (dog and rabbit subcutaneous skin) [372-373, 410]	(35, 0.23)	*n* =1 *ao*=20 *k*=0.0979783 (wss 3.2289)	*n* =1 *k* =0.0558385 ± 0.0060309 *ao*=13.131 ± 1.1771 (wss 0.3004) (MSC 1.9649)	*n* =1 *k* =0.054927 ± 0.0059965 *a*0=13.092 ± 1.1907 (wss 0.30031) (MSC 1.9652)

Figure 2.5A Model B fitted to the selected F/P ratio data.

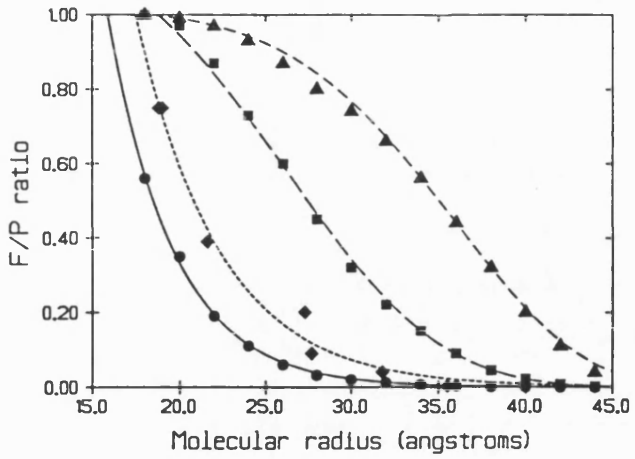

● Anionic dextran (rat; [348])
■ Uncharged dextran (rat; [348])
▲ Cationic dextran (rat; [349])
◆ Protein (dog; [326])

Figure 2.5B Model B fitted to the selected lung L/P ratio data.

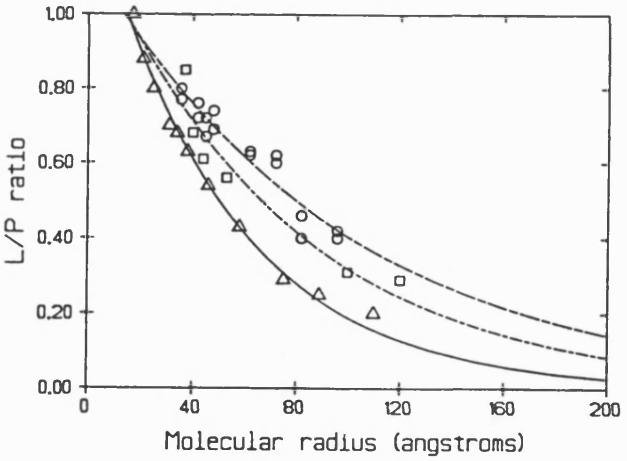

O Pooled protein fraction (sheep; [395; 396])
□ Protein fraction (dog; [398])
△ PVP (sheep; [397])

Model B was also fitted to each of the F/P ratio data sets presented in tables 2.1 and 2.2 using Minsq [441] with a weighting factor of 2.0, and these results are presented in table 2.9. In each case using a weighting factor of 2.0 tended to improve the quality of the fit slightly at higher molecular radii, but compared to a weighting factor of zero, did not fit nearly so well over the rest of the data, producing higher wss and lower MSC values. Consequently a weighting factor of 2.0 was not pursued any further.

The results in table 2.8 and figures 2.5A and 2.5B show that Model B fitted all of the data well, with low wss and high MSC values in every case. The wss and MSC values in table 2.8 were similar to those for Model A presented in table 2.7, though model B could be fitted to all of the data sets, giving it a clear advantage over model A. Interestingly, the similarities between the values of the parameters generated for the anionic dextran F/P ratio data [348] and the protein F/P ratio data [326] appear to clearly support the connection between fractional clearance and molecular charge as outlined in part 2.2.2.4. (Protein macromolecules which generally have net negative charge are believed to behave similarly to negatively charged polymers of the same size, due to the negative charge which is believed to be present on the luminal surface of the glomerular endothelium, as outlined in subsection 2.2.2.4.) The optimum values of n and the parameter k also depended on charge with the smallest value of n, $n = 1$, and the larger values of k reflecting the more restrictive permeability characteristics (steeper general curve shape) for the anionic dextran [348] and protein [326] F/P ratio data. Larger values of n and smaller values of k modelled the more freely permeable characteristics of the uncharged [348] and cationic [349] dextran F/P ratio data. A similar trend was also shown in table 2.7 (where appropriate).

Table 2.9

Initial parameter estimates and parameters of best-fit for Model B and the selected F/P ratio data using a weighting factor of 2.0

		Model B using a WF = 2.0			
		(*a*, *R*)data points selected to initiate calculation of initial parameter estimates	Initial parameter estimates	Parameters of best-fit: Simulation → Least Squares	Parameters of best-fit: Simulation → Simplex → Least squares
$\frac{F}{P}$ ratio data	Anionic dextran' (rat) [348]	(36, 0.003)	*n* =1 *ao*=16 *k*=0.2904571 (wss 0.0017984)	*k*=0.26850 ± 0.0052882 *ao*=15.890 ± 0.070982 (wss 0.00051593) (MSC 6.2623)	*n* =1 *k*=0.26851 ± 0.0052884 *ao*=15.890 ± 0.070977 (wss 0.00051593) (MSC 6.2623)
	Uncharged dextran (rat) [348]	(36, 0.09)	*n* =2 *ao*=18 *k*=0.0074319 (wss 0.0034985)	*n*=2 *k*=0.0072930 ± 0.0014658 *ao*=17.579 ± 0.10185 (wss 0.00049785) (MSC 7.9236)	*n* =2 *k*=0.007333 ± 0.00014778 *ao*=17.612 ± 0.10185 (wss 0.00049917) (MSC 7.9236)
	Cationic dextran (rat) [349]	(36, 0.44)	*n* =3 *ao=18* *k*=0.0014077 (wss 0.016428)	*n*=3 *k*=0.00014097 ± 1.8627E-5 *ao*=17.458 ± 0.76359 (wss 0.010087) (MSC 4.7226)	*n* =3 *k*=0.00011562 ± 1.3312E-5 *ao*=16.291 ± 0.70815 (wss 0.0079578) (MSC 4.9597)
	Pooled protein (dog) [326]	(35.5, 0.03)	*n* =1 *ao=17* *k*=0.3140077 (wss 0.133377)	*n* =1 *k*=0.20950 ± 0.021068 *ao*=17.487 ± 0.26103 (wss 0.0080615) (MSC 3.7726)	*n* =1 *k*=0.20941 ± 0.021055 *ao*=17.486 ± 0.26119 (wss 0.0080615) (MSC 3.7726)

Various other conclusions can be drawn by reference to the parameters of best fit. The similarities between the estimates of parameters in table 2.8 for extravasation of the pooled endogenous protein fractions in the sheep lung [395, 396], and the corresponding data for the dog lung [398] reflect the similarities between different animal species. The differences between the parameters of best-fit for the pooled endogenous protein fractions in the sheep lung [395, 396] and the PVP in the sheep lung [397] indicate the dependence of L/P on charge. The PVP data for the sheep lung [397] and the pooled uncharged dextran data for the dog and rabbit subcutaneous skin [372, 373, 410], reflect the differences in permeability of different tissue endothelia.

In summary Model B appeared to fit all of the data well and its general form had several important advantages over Model A. However, before choosing Model B as the best model to fit all of the data, further types of models with a common general form were also developed to see if any further improvements could be made. These models are presented in 2.2.2.5.

2.2.3.5 Models C

Visual observation suggests that the general form of plots of F/P or L/P ratios against molecular radius are sigmoidal. The idea behind the models presented here was to derive an equation which would produce a sigmoidal plot which might produce a better representation of F/P or L/P at low radii. Ideally low radii should all have a F/P or L/P value of unity. When a critical radius was reached the F/P or L/P ratio would start to decline and ultimately reach an asymptote. This would ideally allow the generation of physiologically relevant ratio values between zero and one for all molecular radii, including very small radii. This is in contrast to Models A and B since the general form of both these models meant that physiologically unrealistic ratio values ($R > 1.0$) were obtained at low molecular radii, notably below the maximum radius at which free-filtration occurs. This objective initially led to the consideration of three further models whose basic general form can be represented as:

$$R = \frac{1}{1+x} \qquad \text{(C)}$$

where as x (which can be thought of as the molecular radius) becomes very large, the ratio R approaches zero, and conversely as x approaches zero, the ratio R approaches a value of $R = 1.0$ (with $R = 1.0$ at $x = 0$).

Three different models based on this concept were investigated:

$$R = \frac{1}{1+z^{(a-mrrh)}} \qquad \text{(C1)}$$

$$R = \frac{1}{1+10^{k(a-mrrh)}} \qquad \text{(C2)}$$

$$R = \frac{1}{1+e^{k(a-mrrh)}} \qquad \text{(C3)}$$

where in each case, R is the respective F/P or L/P concentration ratio, a is the molecular radius of the macromolecule (Å), *mrrh* is the parameter representing the molecular

radius at which the ratio equals one half, and k and z are parameters controlling the shape of the curve (both representing the gradient).

Models C1, C2 and C3 were initially fitted to the uncharged dextran data for the rat [348] only (presented in table 2.1) in order to establish which was the better of the three. All three of the models were found to work equally well, producing wss and MSC values almost identical to each other, with Model C3 being marginally the better of the three. However, the wss and MSC values for each of models C1, C2 and C3 indicated a poorer fit of the data than that achieved with Model B or indeed Model A, where applicable, to the data. The data points used to initiate the fitting procedure, the best initial parameter estimates, and the optimal parameters of best-fit (mean ± sd) for each of these fits, together with the wss and MSC values are presented in table 2.10

Model C3 was subsequently selected to test with most of the other data. A criterion in selecting Model C3 in preference to Models C1 and C2 was also the presence of an exponential term in Model C3 which would make it easier to differentiate than Models C1 and C2 should such a situation ever arise. Model C3 was then subsequently fitted to each of the F/P ratio data sets presented in tables 2.1 and 2.2 and to the L/P ratio data sets presented in tables 2.3, 2.4 and 2.5. The data points used to initiate the fitting procedure, the best initial parameter estimates, and the optimal parameters of best-fit (mean ± sd) for each of these fits, together with the wss and MSC values are presented in table 2.11. Figures 2.6A.1-2.6A.4 and 2.6B.1-2.6B.3 illustrate these results in plot form for the parameters of best-fit obtained using a simulation run, a simplex search, then the least-squares minimisation.

Table 2.10 **Initial parameter estimates and parameters of best-fit following the fitting of Models C1, C2 and C3 to the uncharged dextran F/P ratio data for the rat [348]**

	(*a*, *ratio*)data points selected to initiate calculation of initial parameter estimates	Initial parameter estimates	Parameters of best-fit	
			Simulation → Least Squares	Simulation → Simplex → Least squares
Model C1	(20, 0.97) (36, 0.09)	z=1.44 *mrrh*=29.61 (wss 0.12900)	z=1.3661 ± 0.020308 *mrrh*=27.636 ± 0.16966 (wss 0.0089469) (MSC 5.0375)	z=1.3648 ± 0.020200 *mrrh*=27.623 ± 0.16985 (wss 0.0089393) (MSC 5.0384)
Model C2	(20, 0.97) (36, 0.09)	k=0.16 *mrrh*=29.61 (wss 0.13082)	k=0.13560 ± 0.0064524 *mrrh*=27.637 ± 0.16961 (wss 0.0089503) (MSC 5.0371)	k=0.13509 ± 0.0064156 *mrrh*=27.623 ± 0.16984 (wss 0.0089393) (MSC 5.0384)
Model C3	(20, 0.97) (36, 0.09)	k=0.36 *mrrh*=29.61 (wss 0.12682)	k=0.31172 ± 0.014820 *mrrh*=27.637 ± 0.16972 (wss 0.0089462) (MSC 5.0376)	k=0.31105 ± 0.014722 *mrrh*=27.623 ± 0.16984 (wss 0.0089393) (MSC 5.0384)

Table 2.11

Initial parameter estimates and parameter of best-fit for Model C3

		Model C3			
		(*a*, *ratio*)data points selected to initiate calculation of initial parameter estimates	Initial parameter estimates	Parameters of best-fit Simulation → Least Squares	Simulation → Simplex → Least squares
$\frac{F}{P}$ ratio data	Anionic dextran [348] (rat)	(20, 0.35) (36, 0.003)	*k*=0.32 *mrrh*=18.09 (wss 0.0045551)	*k*=0.39401 ± 0.0097679 *mrrh*=18.515 ± 0.060305 (wss 0.00070056) (MSC 5.9563)	*k*=0.39394 ± 0.0097638 *mrrh*=18.516 ± 0.060299 (wss 0.00070056) (MSC 5.9563)
	Uncharged dextran [348] (rat)	(20, 0.97) (36, 0.09)	*k*=0.36 *mrrh*=29.61 (wss 0.12682)	*k*=0.31172.± 0.014820 *mrrh*=27.637 ± 0.16972 (wss 0.00089462) (MSC 5.0376)	*k*=0.31105.± 0.014772 *mrrh*=27.623 ± 0.16984 (wss 0.00089393) (MSC 5.0384)
	Cationic dextran [349] (rat)	(20, 0.99) (36, 0.44)	*k*=0.30 *mrrh*=35.20 (wss 0.029217)	*k*=0.24764.± 0.010144 *mrrh*=34.585 ± 0.17769 (wss 0.0076964) (MSC 4.9931)	*k*=0.24765.± 0.010145 *mrrh*=34.586 ± 0.17769 (wss 0.0076964) (MSC 4.9931)
	Protein [326] (dog)	(18.8, 0.75) (27.7, 0.09)	*k*=0.38 *mrrh*=21.67 (wss 0.023206)	*k*=0.34790.± 0.056446 *mrrh*=21.465 ± 0.45776 (wss 0.020462) (MSC 2.8411)	*k*=0.34784.± 0.056431 *mrrh*=21.466 ± 0.45780 (wss 0.020462) (MSC 2.8411)
$\frac{L}{P}$ ratio data	Pooled endogenous protein fractions [395-396] (sheep lung)	(35.5, 0.77 (96.0,0.42)	*k*=0.03 *mrrh*=83.25 (wss 0.034889)	*k*=0.027423.± 0.002239 *mrrh*=80.325 ± 2.0663 (wss 0.021148) (MSC 2.3281)	*k*=0.027423.± 0.002239 *mrrh*=80.325 ± 2.0663 (wss 0.021148) (MSC 2.3281)
	Endogenous protein [398] fractions (dog lung)	(37, 0.85) (100, 0.31)	*k*=0.04 *mrrh*=80.11 (wss 0.11278)	*k*=0.024713.± 0.0055618 *mrrh*=73.170 ± 7.1550 (wss 0.031177) (MSC 1.3566)	*k*=0.024696.± 0.0055601 *mrrh*=73.175 ± 7.1586 (wss 0.031177) (MSC 1.3566)
	PVP [397] (sheep lung)	(21, 0.88) (89, 0.25)	*k*=0.05 *mrrh*=64.83 (wss 0.15667)	*k*=0.041989.± 0.0058902 *mrrh*=55.799 ± 3.2568 (wss 0.057199) (MSC 2.1454)	*k*=0.042106.± 0.0059097 *mrrh*=55.596 ± 3.2447 (wss 0.057176) (MSC 2.1458)

Figure 2.6A.1 Model C3 fitted to the rat anionic dextran F/P ratio data [348].

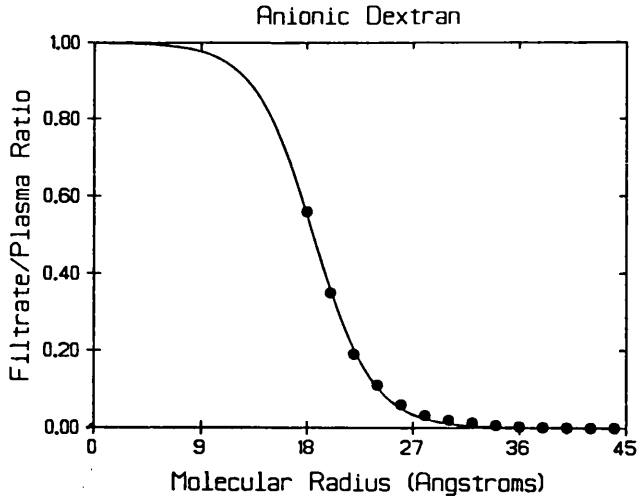

Figure 2.6A.2 Model C3 fitted to the rat uncharged dextran F/P ratio data [348].

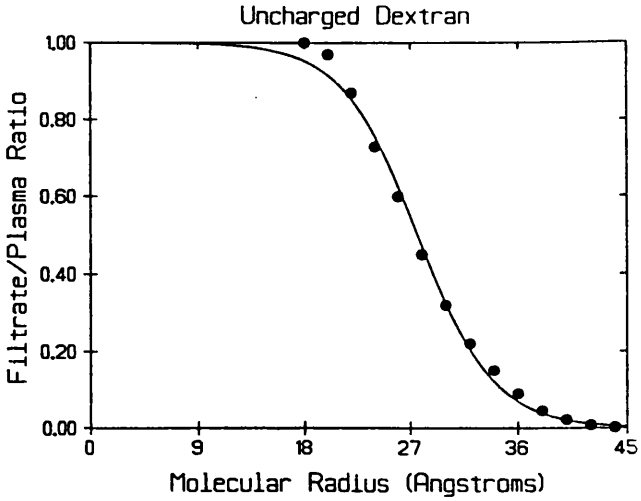

Figure 2.6A.3 Model C3 fitted to the rat cationic dextran F/P ratio data [349].

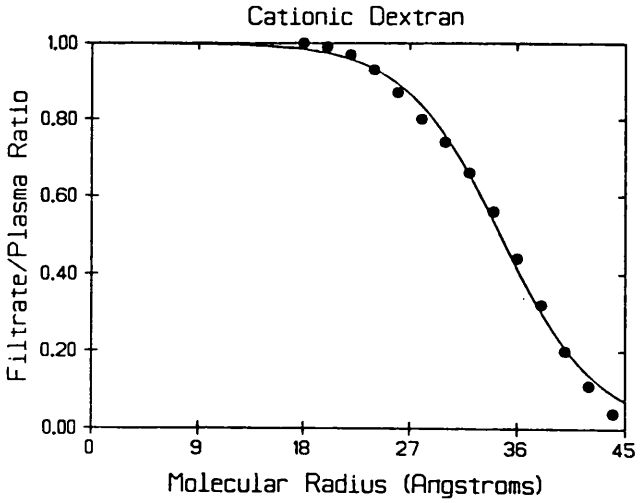

Figure 2.6A.4 Model C3 fitted to the dog protein F/P ratio data [326].

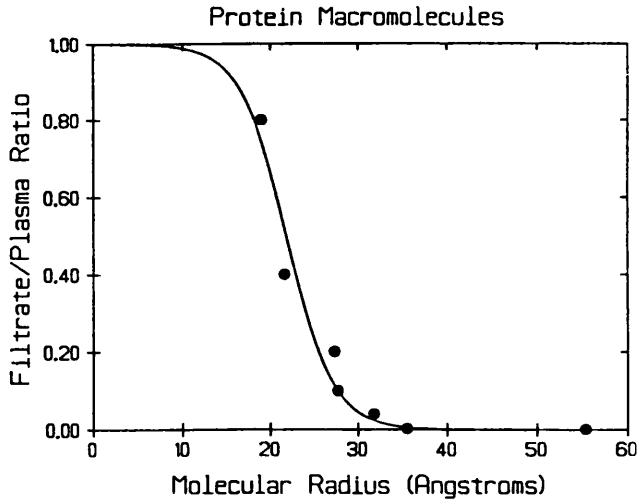

Figure 2.6B.1 Model C3 fitted to the pooled sheep endogenous protein fraction lung L/P ratio data [395, 396].

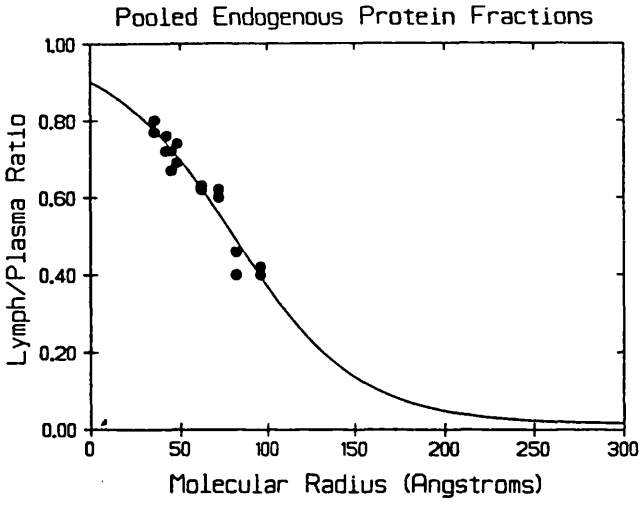

Figure 2.6B.2 Model C3 fitted to the dog endogenous protein fraction lung L/P ratio data [398].

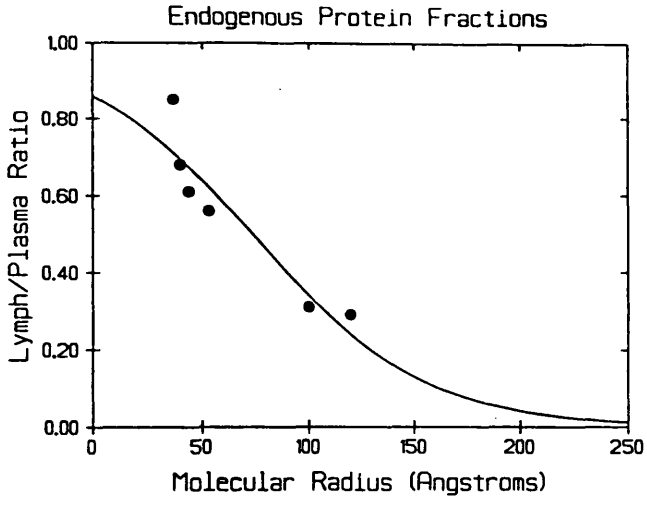

Figure 2.6B.3 Model C3 fitted to the sheep PVP lung L/P ratio data [397].

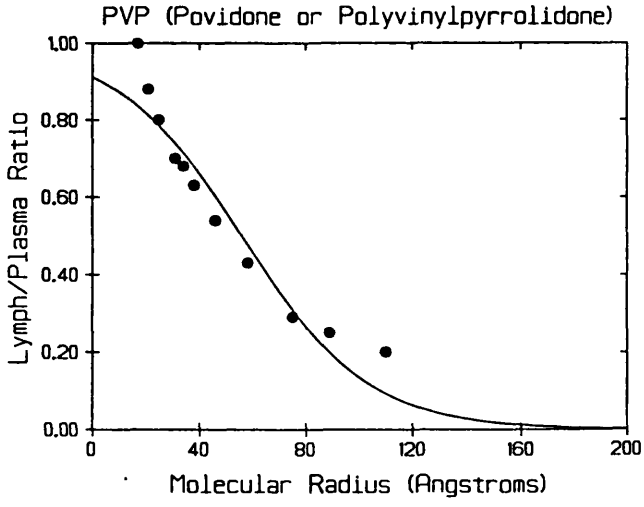

Table 2.11 and figures 2.6A.1-2.6A.4 and 2.6B.1-2.6B.3 show that Model C3 appeared to fit the data well, with the fits to the F/P ratio data sets being generally better than the fits to the L/P ratio data sets. However, the wss and MSC values were not as good as the corresponding values following the fitting of Model B and Model A and on closer inspection one can see why. It was impossible to find a value of k (or z) which fitted the high ratio values since the curve began to decline before the data had been reached. Even the presence of the parameter *mrrh*, a similar parameter to *ao* in Model B, did not overcome this problem.

A further development led to a modified form of Model C3 i.e. Model C4 whose general form was as follows:

$$R = f + (1-f)\left(\frac{1}{1+e^{k(a-mrrh)}}\right) \qquad \text{(C4)}$$

where f represents a ratio value R at which the curve levels off and becomes linear, and all the other parameters are as defined before. It was thought that this might be a better model for the L/P data.

Model C4 was fitted to each of the L/P ratio data sets presented in tables 2.3, 2.4 and 2.5. The data points used to initiate the fitting procedure, the best initial parameter estimates, and the optimal parameters of best-fit (mean ± sd) for each of these fits, together with the wss and MSC values are presented in table 2.12. Figures 2.7A -2.7C illustrate these results in plot form for the parameters of best fit obtained using a simulation run, a simplex search, then the least-squares minimisation.

Table 2.12

Initial parameter estimates and parameter of best-fit for Model C4

		Model C4			
		(a, R)data points selected to initiate calculation of initial parameter estimates	Initial parameter estimates	Parameters of best-fit Simulation → Least Squares	Simulation → Simplex → Least squares
$\frac{L}{P}$ ratio data	Pooled endogenous protein fractions [395, 396] (sheep lung)	(35.5, 0.77) (96.0, 0.42)	k=0.03 $mrrh$=83.25 f=0.2 (wss 0.17885)	k=0.027741.± 0.010304 $mrrh$=79.164 ± 35.946 f=0.015303 ± 0.47104 (wss 0.021146) (MSC 2.2032)	k=0.027568.± 0.010294 $mrrh$=79.796 ± 36.810 f=0.0070053 ± 0.48082 (wss 0.021146) (MSC 2.2032)
	Endogenous protein [398] fractions (dog lung)	(37, 0.85) (100, 0.31)	k=0.04 $mrrh$=80.11 f=0.2 (wss 0.16964)	k=0.092954.± 0.036473 $mrrh$=44.871 ± 2.7902 f=0.30013 ± 0.047687 (wss 0.012681) (MSC 1.9229)	k=0.091021.± 0.036201 $mrrh$=45.003 ± 2.8574 f=0.29865 ± 0.047952 (wss 0.012699) (MSC 1.9214)
	PVP [397] (sheep lung)	(21, 0.88) (89, 0.25)	k=0.05 $mrrh$=64.83 f=0.2 (wss 0.30130)	k=0.076063.± 0.011958 $mrrh$=40.680 ± 2.3539 f=0.22544 ± 0.036637 (wss 0.019377) (MSC 3.0461)	k=0.077249.± 0.012143 $mrrh$=40.401 ± 2.3048 f=0.22886 ± 0.036055 (wss 0.019335) (MSC 3.0482)

Figure 2.7A Model C4 fitted to the pooled sheep endogenous protein fraction lung L/P ratio data [395, 396].

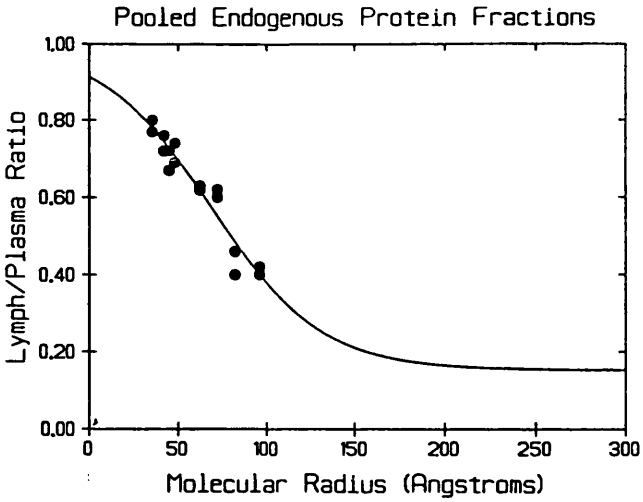

Figure 2.7B Model C4 fitted to the dog endogenous protein fraction lung L/P rati data [398].

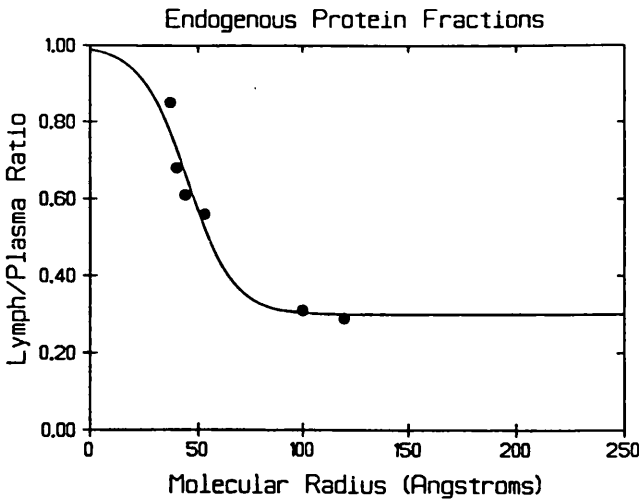

Figure 2.7C Model C4 fitted to the sheep PVP lung L/P ratio data [397].

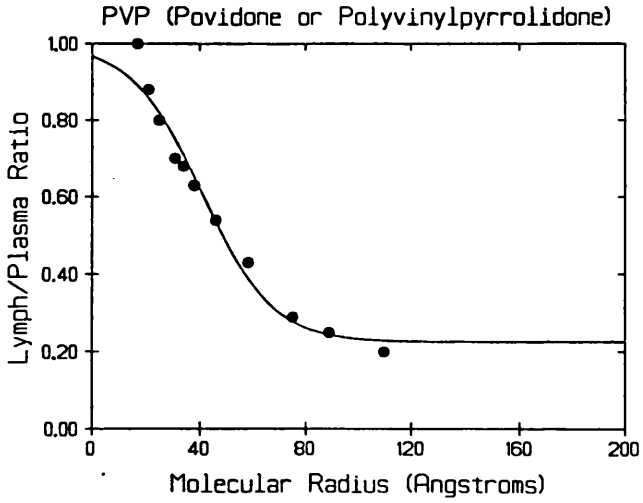

Table 2.12 and figures 2.7A -2.7C show that although the wss and MSC values when Model C4 was fitted to the L/P ratio data sets were on the whole better than those when Model C3 was used, they were not as good as those obtained with Model B. The general shape of the curve produced by Model C4 and its f parameter was such that at some value of f, the curve was forced to level off towards a constant value (representing filtration independence). This can be observed for L/P data at high radii, but it was not possible to generate realistic parameter estimates using the least squares method.

The main concern of the modelling described in this section was to establish which model best fitted the range of radii spanned by the experimental data, rather than being too concerned about very low or very high molecular radii outside the range of experimental data. A model which produces exactly a ratio of $R = 1.0$ for all molecular radii between zero and the maximum radius at which free-filtration occurs, and then declines down through the data, was not mathematically possible to develop, and although Models C1, C2 and C3 come relatively close to this for the F/P ratio data, for the reasons already outlined, Model B was still the best of the models.

2.2.3.6 Conclusions

The relationship between molecular radius and regional extravasation concentration ratios of macromolecules was modelled directly by each of models A, B and C. The general form of these models was based purely on this relationship, with the number of parameters in each model being deliberately kept to a minimum. Model A, Model B, and Models C represent the three possible different and most logical approaches to this type of modelling. The primary concern of each of these models was to ensure the best possible fits over the actual range of the chosen F/P ratio and L/P ratio data sets, since it was within this range that the molecular radii of the macromolecular drugs in which this study was most concerned lie. In this respect, Model B was the best for each of the data sets. Consequently Model B was selected along with its appropriate chosen respective protein and uncharged parameters of best-fit to be developed at the appropriate stage of the modelling (as described in section 2.3) into the respective physiological expressions for the parameters k_{excr} and k_{12} which determine the rate of movement of both protein and uncharged macromolecular drugs from the blood to the glomerular filtrate (the excretion process) and from the blood to the lymph (the target site) respectively (see page 91 for diagram). An important assumption of Model B is that $a \geqslant ao$. Another important assumption made by Model B, and indeed each of Models A, C1, C2, C3 and C4 is that each drug macromolecule is uniformly spherical (with molecular radius a). The parameters of best-fit selected for Model B were those obtained following the method of a simulation run, a simplex search, and then the least squares fit, and using a weighting factor of zero. The fits of Model B to the uncharged dextran rat F/P ratio data [348], the pooled protein macromolecule dog F/P ratio data [326], the pooled endogenous protein fraction sheep lung L/P ratio data [395, 396], the PVP sheep lung L/P ratio data [397], and to the pooled uncharged dextran dog and rabbit subcutaneous skin L/P ratio data [372, 373, 410], the results of which were all given in table 2.8, were selected to be used throughout the rest of this study to investigate the fate of protein and uncharged macromolecular drugs in the body. The

parameters obtained following the fitting of Model B to the anionic [348] and cationic [349] dextran rat F/P ratio data were used to show the effect of charge on glomerular filtration, they were not used in the major simulations described later in chapter 3 because firstly there was no corresponding anionic or cationic L/P ratio data available to use, and secondly because this study was concerned with the two main types of macromolecular drug or drug carrier distribution, uncharged polymers and proteins. The parameters obtained following the fitting of this model to the endogenous protein fraction dog lung L/P ratio data [398], were used only in part 2.2.3.4 to illustrate some important permeability characteristics, and were not used for the major simulations described later in chapter 3 because the data were not so good as the pooled endogenous protein fraction sheep lung L/P ratio data.

2.3 The development, solution and validation of a novel physiological three-compartment pharmacokinetic model

2.3.1 Introduction

The major objective of this study was to develop a physiological pharmacokinetic model consisting of three compartments (tissues) of the body representing the blood, lymph and liver. The model was chosen to allow the two major elimination processes, i.e. renal excretion and hepatic metabolism (hepatic clearance), to be determined separately. The major rationale for design of the physiological model was the desire to examine the effect of molecular radius on the distribution of both protein and uncharged macromolecular drugs in the body both in the absence and presence of hepatic metabolism, taking into account the relevant different regional capillary membrane permeabilities to different size macromolecules. A practical objective of the study was to predict via simulations, the molecular radii which are most effective in distributing the greatest fraction of a macromolecular drug dose to a particular target site, the interstitial fluids or lymph, and thus to the site of cancer micrometastases present there. In addition to showing the fraction of the macromolecular drug dose present in the lymph, the model was required to show for each molecular radius size (within the range determined by the modelling process) over almost any desired interval of time, the fractions of the dose present in the blood and the liver, and also the fractions which have been excreted via the kidneys and metabolised by the liver. Another objective was to solve the model preferably using analytical techniques and where necessary numerical techniques so that equations describing the amount (or fraction) of the macromolecular drug dose in each compartment (tissue) with respect to time could be obtained. The study also involved the development of a specific computer programme written in BASIC which had two main purposes, firstly to aid in the solution of the model equations, and secondly to perform the simulations described in chapter 3. The advantages and disadvantages of this novel physiological three-compartment pharmacokinetic model over the key theoretical/predictive

macromolecular anticancer drug and drug-targeting pharmacokinetic models in the literature, are discussed in chapter 5.

This current section of this chapter describes the development, solution and validation of this new physiological three-compartment pharmacokinetic model. The model, the associated equations, their method of solution and the development of the computer programme are described in 2.3.2. Also in 2.3.2 attention is paid to the use of Model B for calculating expressions for the parameters k_{excr} and k_{12}. 2.3.2 also describes the development of the other mathematical expression used in the modelling process. The methods used to validate the model are described in 2.3.3. A summary of the main features of the model is then presented in 2.3.4.

2.3.2 The model

2.3.2.1 Description and definition of terms

Consider the following model,

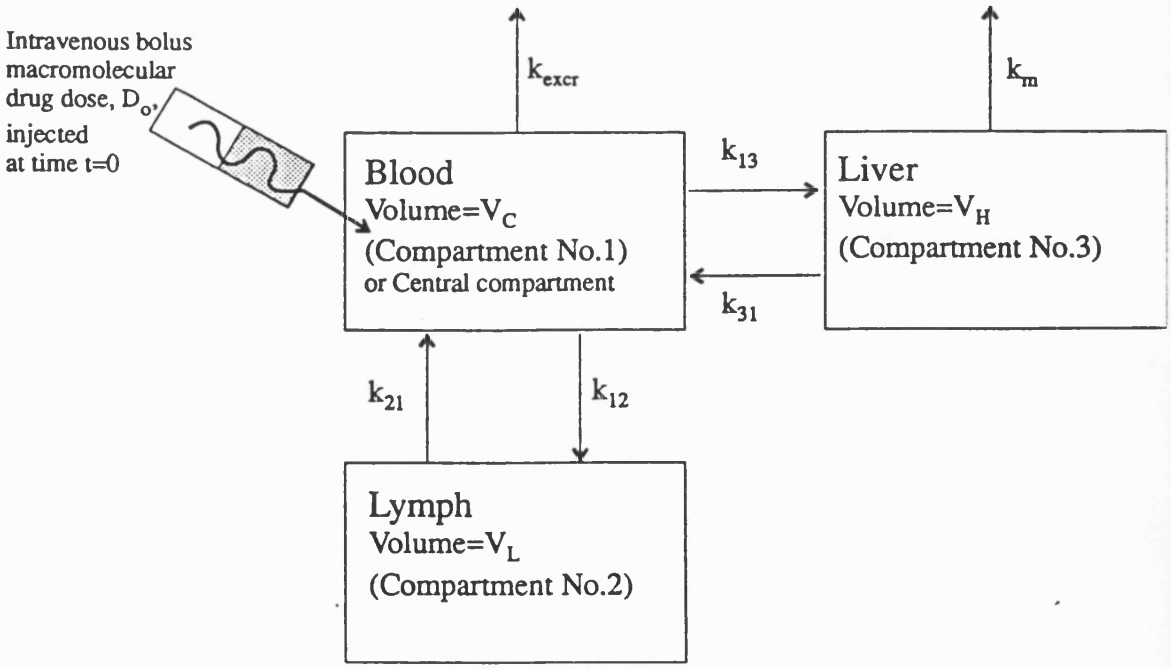

where an intravenous (i.v.) bolus dose D_0 (mg) is injected into the blood compartment (compartment No. 1 or central compartment) at time $t = 0$. Therefore at time $t = 0$ there will be no drug in the lymph or liver compartments (compartments No. 2 and No. 3 respectively). Let A_P be the amount (mass) of drug in the blood compartment at time t, and let a_1 be its Laplace transform. Similarly, let A_L be the amount (mass) of drug in the lymph compartment at time t, and let a_2 be its Laplace transform. Also let A_H be the amount (mass) of drug in the liver compartment at time t, and let a_3 be its Laplace transform. Since the dose D_0 of the drug is in the blood compartment at time $t = 0$ the following set of initial conditions at time $t = 0$ can be defined; $A_P = D_0$ at $t = 0$, $A_L = 0$ at $t = 0$, and $A_H = 0$ at $t = 0$.

Let the volume of the blood compartment be V_C, the volume of the lymph compartment be V_L, and the volume of the liver compartment be V_H. Now the rate of movement of the drug between the three compartments is controlled by the inter-compartmental parameters k_{12}, k_{21}, k_{13} and k_{31} respectively (which are first-order rate constants), and similarly the rates of excretion and metabolism (the elimination processes) of the drug are controlled by the first order parameters k_{excr} and k_m respectively. Hence k_{12} determines the rate of movement of the drug from the blood to the lymph, k_{21} determines the rate of movement of the drug from the lymph to the blood, k_{13} determines the rate of movement of the drug from the blood to the liver, k_{31} determines the rate of movement of the drug from the liver to the blood, k_{excr} determines the rate of movement of the drug from the blood to the glomerular filtrate (excretion via kidneys), and k_m represents the rate of metabolism (hepatic clearance) of the drug from the liver.

The set of differential equations which describe the model with respect to time are therefore,

$$\frac{dA_P}{dt} = -(k_{12} + k_{13} + k_{excr})A_P + k_{21}A_L + k_{31}A_H \qquad 1$$

$$\frac{dA_L}{dt} = k_{12}A_P - k_{21}A_L \qquad 2$$

$$\frac{dA_H}{dt} = -(k_{31} + k_m)A_H + k_{13}A_P \qquad 3$$

The method of solution of this set of differential equations is described in 2.3.3.3. However, before describing the solution of the model equations, it is appropriate to define the mathematical expressions (models) representing the parameters k_{excr} and k_{12}, and the expressions for the other intercompartmental parameters, and also to outline the assumptions made. These issues are presented in 2.3.2.2 below.

2.3.2.2 Development of mathematical expressions (models) to represent k_{excr} and k_{12}, and other inter-compartmental parameters.

Following the selection of Model B as the best model to describe both the selected F/P ratio and L/P ratio data sets, the next step in the modelling process was to use this relationship to define the parameters k_{excr} and k_{12}. This was achieved by considering the pharmacokinetic principle of clearance of a drug from an organ (tissue) given by the relationship $Cl_{organ} = V_D\, k_{organ}$ (equation 4) where V_D is the volume in which the drug is distributed and k_{organ} is the rate at which the drug leaves the organ.

(i) A mathematical expression (model) for k_{excr}

A mathematical expression (model) for k_{excr} was developed as follows,

$$k_{excr} = \frac{Cl_{\text{from blood to glomerular filtrate}}}{V_C}$$

and also,

$$Cl_{\text{from blood to glomerular filtrate}} = \frac{F}{P}\ \text{ratio} \times \text{GFR}$$

Therefore, $$k_{excr}V_C = \frac{F}{P}\ \text{ratio} \times \text{GFR}$$

so $$k_{excr} = \frac{\frac{F}{P}\text{ratio} \times GFR}{V_C}$$

Now from the modelling process described in section 2.2 Model B can be substituted for the F/P ratio to give,

$$k_{excr} = \frac{\exp\left(-k(a-ao)^n\right) \times GFR}{V_C} \qquad 5$$

Hence the parameter k_{excr} now determines the rate of movement of macromolecular drugs from the blood to the glomerular filtrate, taking into account the different permeability of the fenestrated capillaries of the kidney to different size macromolecules by entering the desired molecular radius of the macromolecule *a* (with $a \geq ao$) and the appropriate parameters of best-fit. Since GFR is in units of ml/min, V_C is units of ml, and Model B is dimensionless, then k_{excr} is in units of min^{-1}.

(ii) A mathematical expression (model) for k_{12}

Following the same principle used in (i), a mathematical expression (model) for k_{12} was developed as follows,

$$k_{12} = \frac{Cl_{\text{from blood to lymph}}}{V_C}$$

and also,

$$Cl_{\text{from blood to lymph}} = \frac{L}{P} ratio \times BLFR$$

Therefore $$k_{12} V_C = \frac{L}{P} ratio \times BLFR$$

so $$k_{12} = \frac{\frac{L}{P} ratio \times BLFR}{V_C}$$

Now from the modelling process described in section 2.2, Model B can be substituted for the L/P ratio to give,

$$k_{12} = \frac{\exp\left(-k(a-ao)^n\right) \times BLFR}{V_C} \qquad 6$$

Hence the parameter k_{12} determines the rate of movement of macromolecular drugs from the blood to the lymph, taking into account the different regional permeabilities of the capillaries (lung or subcutaneous skin continuous capillaries) to different size macromolecules. For the reasons outlined in section 2.2 this study assumes BLFR = LFR. Since BLFR is in units of ml/min, V_C is in units of ml, and Model B is dimensionless, then k_{12} is in units min^{-1}.

(iii) A mathematical expression (model) for k_{21}

A mathematical expression (model) for k_{21} was developed as follows,

$$k_{21} = \frac{Cl_{\text{from lymph to blood}}}{V_L} \qquad \text{and also} \qquad Cl_{\text{from lymph to blood}} = 1 \times LFR$$

Therefore $$k_{21} = \frac{1 \times LFR}{V_L} \qquad (7)$$

For the reasons outlined in section 2.2 this study assumes that the concentration ratio of macromolecules moving from the lymph to the blood is one, i.e. there is free movement from lymph to blood for all macromolecules, and that this rate of movement occurs at the same rate as LFR. k_{21} is in units of min^{-1} because LFR is in units of ml/min and V_L is in units of ml.

(iv) A mathematical expression (model) for k_{13}

A mathematical expression (model) for k_{13} was developed as follows,

$$k_{13} = \frac{Cl_{\text{from blood to liver}}}{V_C} \qquad \text{and also} \qquad Cl_{\text{from blood to liver}} = 1 \times \text{ Total blood flow rate to the liver}$$

Therefore $$k_{13} = \frac{1 \times \text{ Total blood flow rate to the liver}}{V_C} \qquad (8)$$

The parameter k_{13} determines the rate of movement of macromolecular drugs from the blood to the extravascular spaces of the liver. For the reasons outlined in section 2.2 this study assumes that the concentration ratio of macromolecules extravasating from the blood to the extravascular spaces of the liver is one i.e. free movement for all

macromolecules from the blood to the extravascular spaces of the liver, and that this rate of movement therefore occurs at the same rate as the total blood flow rate to the liver. In practice the Liver/Plasma ratio is dependent on molecular radius at high radii but the extent of experimental data available do not allow Liver/Plasma ratio to be modelled effectively. Since the total blood flow rate to the liver is in units of ml/min, and V_C is in units of ml, then k_{13} is in units of min^{-1}.

(v) A mathematical expression (model) for k_{31}

A mathematical expression (model) for k_{31} was developed as follows,

$$k_{31} = \frac{Cl_{\text{from liver to blood}}}{V_H} \quad \text{and also} \quad Cl_{\text{from liver to blood}} = 1 \times \text{Total blood flow rate from the liver}$$

$$\text{Therefore} \qquad k_{31} = \frac{1 \times \text{Total blood flow rate from the liver}}{V_H} \qquad 9$$

The parameter k_{31} determines the rate of movement of macromolecular drugs from the extravascular spaces of the liver to the blood stream. For the reasons outlined in section 2.2 this study assumes that the concentration ratio of macromolecules moving from the extravascular spaces of the liver back into the bloodstream is one, i.e. there is free movement from the extravascular spaces of the liver to the blood, and that this rate of movement therefore occurs at the same rate as the total blood flow rate from the liver, where it is also assumed that the total blood flow rate from the liver equals the total blood flow rate to the liver. Since the total blood flow rate from the liver is in units of ml/min, and V_H is in units of ml, then k_{31} is in units of min^{-1}.

(vi) A mathematical expression (model) for k_m

A mathematical expression (model) for k_m was not fixed because macromolecular drugs would be expected to be metabolised at different rates. The approach taken here was to vary the value of k_m to model the influence of this parameter on macromolecular disposition (see Chapter 3).

2.3.2.3 Solution of the model equations and development of the computer programme

The complexity of the set of differential equations 1, 2 and 3 describing the three-compartment model meant that they had to be solved by the method of Laplace transforms, where in general notation, the Laplace transform $f(s)$ of a function $F(t)$ is given by

$$L[F(t)] = f(s) = \int_0^\infty F(t)e^{-st}dt$$

where the function $F(t)$ is multiplied by e^{-st} and then the product is integrated over time from $t=0$ to $t=\infty$. The Laplace transform rules used in the solution of the model equations 1, 2 and 3 were,

(i) the rule for constants

i.e. $L[cF(t)] = cL[F(t)]$ if c is a constant 9.1

(ii) the rule for linearity

i.e.

$$L[c_1F_1(t)+c_2F_2(t)+\ldots+c_nF_n(t)] = c_1L[F_1(t)]+c_2L[F_2(t)]+\ldots c_nL[F_n(t)] \quad 9.2$$

(iii) the rule for first-derivatives

i.e. $L\left[\frac{dF}{dt}\right] = L[F'(t)] = sL[F(t)] - F(0)$ 9.3

where $F(0)$ is the value of $F(t)$ at time $t = 0$.

and the rule used for taking the inverse Laplace transform was,

(iv) since $L[ce^{-\phi t}] = \frac{c}{s+\phi}$ where c is a constant and ϕ is a parameter (≡ a constant)

then $L^{-1}\left[\frac{c}{s+\phi}\right] = ce^{-\phi t}$ 9.4

The full solution of equations 1, 2 and 3 by the method of Laplace transforms is described in Appendix A1 because the solution is a lengthy procedure. Both Cramers rule and the theory of partial fractions had to be used in the solution process, yielding

the following equations describing the amount (mass) of the macromolecular drug dose, in the blood, lymph, and liver compartments with respect to time.

$$A_p = \frac{D_0(k_{21}-\gamma)(k_{31}+k_m-\gamma)e^{-\gamma t}}{(\gamma-\alpha)(\gamma-\beta)} + \frac{D_0(k_{21}-\alpha)(\alpha-(k_{31}+k_m))e^{-\alpha t}}{(\gamma-\alpha)(\alpha-\beta)} + \frac{D_0(k_{21}-\beta)(k_{31}+k_m-\beta)e^{-\beta t}}{(\gamma-\beta)(\alpha-\beta)}$$

10

$$A_L = \frac{D_0 k_{12}(k_{31}+k_m-\gamma)e^{-\gamma t}}{(\gamma-\alpha)(\gamma-\beta)} + \frac{D_0 k_{12}(\alpha-(k_{31}+k_m))e^{-\alpha t}}{(\gamma-\alpha)(\alpha-\beta)} + \frac{D_0 k_{12}(k_{31}+k_m-\beta)e^{-\beta t}}{(\gamma-\beta)(\alpha-\beta)}$$

11

$$A_H = \frac{D_0 k_{13}(k_{21}-\gamma)e^{-\gamma t}}{(\gamma-\alpha)(\gamma-\beta)} + \frac{D_0 k_{13}(\alpha-k_{21})e^{-\alpha t}}{(\gamma-\alpha)(\alpha-\beta)} + \frac{D_0 k_{13}(k_{21}-\beta)e^{-\beta t}}{(\gamma-\beta)(\alpha-\beta)}$$

12

where γ, α and β can be expressed in terms of the inter-compartmental parameters in the following system of expressions,

$$\alpha+\beta+\gamma = k_{12}+k_{21}+k_{13}+k_{31}+k_{excr}+k_m \quad 13$$

$$\alpha\beta+\alpha\gamma+\beta\gamma = k_{21}k_{31}+k_{21}k_m+k_{12}k_{31}+k_{12}k_m+k_{13}k_m + k_{13}k_{21}+k_{excr}k_{31}+k_{excr}k_m+k_{excr}k_{21} \quad 14$$

$$\alpha\beta\gamma = k_{13}k_{21}k_m+k_{excr}k_{21}k_{31}+k_{excr}k_{21}k_m \quad 15$$

which upon solving produces the following cubic equation in general notation *f*(*x*) say as follows,

$$f(x) = a_3x^3+a_2x^2+a_1x+a_0 = 0 \quad 16$$

with

$$a_3 = 1 \quad 17$$

$$a_2 = -(k_{12}+k_{21}+k_{13}+k_{31}+k_{excr}+k_m) \quad 18$$

$$a_1 = (k_{21}k_{31}+k_{21}k_m+k_{12}k_{31}+k_{12}k_m+k_{13}k_m+k_{13}k_{21}+k_{excr}k_{31}+k_{excr}k_m+k_{excr}k_{21}) \quad 19$$

$$a_0 = -(k_{13}k_{21}k_m+k_{excr}k_{21}k_{31}+k_{excr}k_{21}k_m) \quad 19a$$

whose roots are actually γ, α, and β, with $\gamma > \alpha > \beta > 0$. All the other terms in each of equations 10, 11 and 12 are as defined in parts 2.3.2.1 and 2.3.2.2. Equation 16 was

solved numerically using the Newton-Raphson and synthetic division techniques to find the roots γ, α and β, using procedures described later.

Other related equations were developed as described below. The following equation for the concentration of the macromolecular drug in the blood compartment with respect to time can be obtained from equation 10,

$$C_P = \frac{D_0(k_{21}-\gamma)(k_{31}+k_m-\gamma)e^{-\gamma t}}{V_C(\gamma-\alpha)(\gamma-\beta)} + \frac{D_0(k_{21}-\alpha)(\alpha-(k_{31}+k_m))e^{-\alpha t}}{V_C(\gamma-\alpha)(\alpha-\beta)} + \frac{D_0(k_{21}-\beta)(k_{31}+k_m-\beta)e^{-\beta t}}{V_C(\gamma-\beta)(\alpha-\beta)} \qquad 20$$

Having obtained the equations for A_P, A_L and A_H, the total mass of macromolecular drug eliminated with respect to time was described by the following equation,

$$A_E = D_0 - (A_P + A_L + A_H) \qquad 21$$

The rate of change in the amount (mass) of the macromolecular drug excreted by the kidney with respect to time was described by the following differential equation,

$$\frac{dA_{EXCR}}{dt} = k_{excr} A_P \qquad 22$$

and the rate of change in the amount (mass) of the macromolecular drug metabolised (hepatically cleared) by the liver with respect to time was described by the following differential equation,

$$\frac{dA_M}{dt} = k_m A_H \qquad 23$$

Equations 22 and 23 were both solved individually by direct integration between time $t = 0$ and $t = t$ to give the following equations for the amount (mass) of the macromolecular drug excreted by the kidneys with respect to time (A_{EXCR}) and the amount (mass) of the macromolecular drug metabolised (hepatically cleared) by the liver with respect to time (A_M),

$$A_{EXCR} = k_{excr} D_0 \left\{ \frac{(k_{21}-\gamma)(k_{31}+k_m-\gamma)}{\gamma(\gamma-\alpha)(\gamma-\beta)} + \frac{(k_{21}-\alpha)(\alpha-(k_{31}+k_m))}{\alpha(\gamma-\alpha)(\alpha-\beta)} + \frac{(k_{21}-\beta)(k_{31}+k_m-\beta)}{\beta(\gamma-\beta)(\alpha-\beta)} \right.$$

$$\left. - \frac{(k_{21}-\gamma)(k_{31}+k_m-\gamma)e^{-\gamma t}}{\gamma(\gamma-\alpha)(\gamma-\beta)} - \frac{(k_{21}-\alpha)(\alpha-(k_{31}+k_m))e^{-\alpha t}}{\alpha(\gamma-\alpha)(\alpha-\beta)} - \frac{(k_{21}-\beta)(k_{31}+k_m-\beta)e^{-\beta t}}{\beta(\gamma-\beta)(\alpha-\beta)} \right\}$$

24

$$A_M = k_m k_{13} D_0 \left\{ \frac{(k_{21}-\gamma)}{\gamma(\gamma-\alpha)(\gamma-\beta)} + \frac{(\alpha-k_{21})}{\alpha(\gamma-\alpha)(\alpha-\beta)} + \frac{(k_{21}-\beta)}{\beta(\gamma-\beta)(\alpha-\beta)} - \frac{(k_{21}-\gamma)e^{-\gamma t}}{\gamma(\gamma-\alpha)(\gamma-\beta)} \right.$$

$$\left. - \frac{(\alpha-k_{21})e^{-\alpha t}}{\alpha(\gamma-\alpha)(\alpha-\beta)} - \frac{(k_{21}-\beta)e^{-\beta t}}{\beta(\gamma-\beta)(\alpha-\beta)} \right\}$$

25

Since equations for A_{EXCR} and A_M were obtained, then the total amount of the macromolecular drug eliminated with respect to time, i.e. A_E, was also equivalently described by the following equation,

$$A_E = A_{EXCR} + A_M \qquad 26$$

where A_E can also be written as,

$$A_E = A_{ELIM} \qquad 27$$

For the simulations described in chapter 3, and consequently also in the computer programme developed to perform these simulations described below, the dose D_0 of the macromolecular drug was set to unity, i.e. $D_0 = 1$, so that the fractions of a macromolecular drug dose in each of the blood, lymph and liver compartments, and the fractions of the dose excreted by the kidneys and metabolised by the liver, were predicted with respect to time for each molecular radius.

A computer programme (MACROHOURS) was written to solve for γ, α and β and to allow rapid calculation of the equations for A_P, A_L, A_H, A_{EXCR}, A_M and A_E. The programme was written in BASIC V a modified and expanded BASIC language which runs on the Acorn Archimedes RISC processor.

Figure 2.8 shows the overall plan and structure of the computer programme MACROHOURS, which illustrates the main subroutines (procedures (PROC)) involved. The main features of these subroutines are summarised in parts (a) to (h) below, and the complete listing of the computer programme MACROHOURS is given in Appendix A3, to which the reader is referred.

Figure 2.8 Plan of the computer programme MACROHOURS.

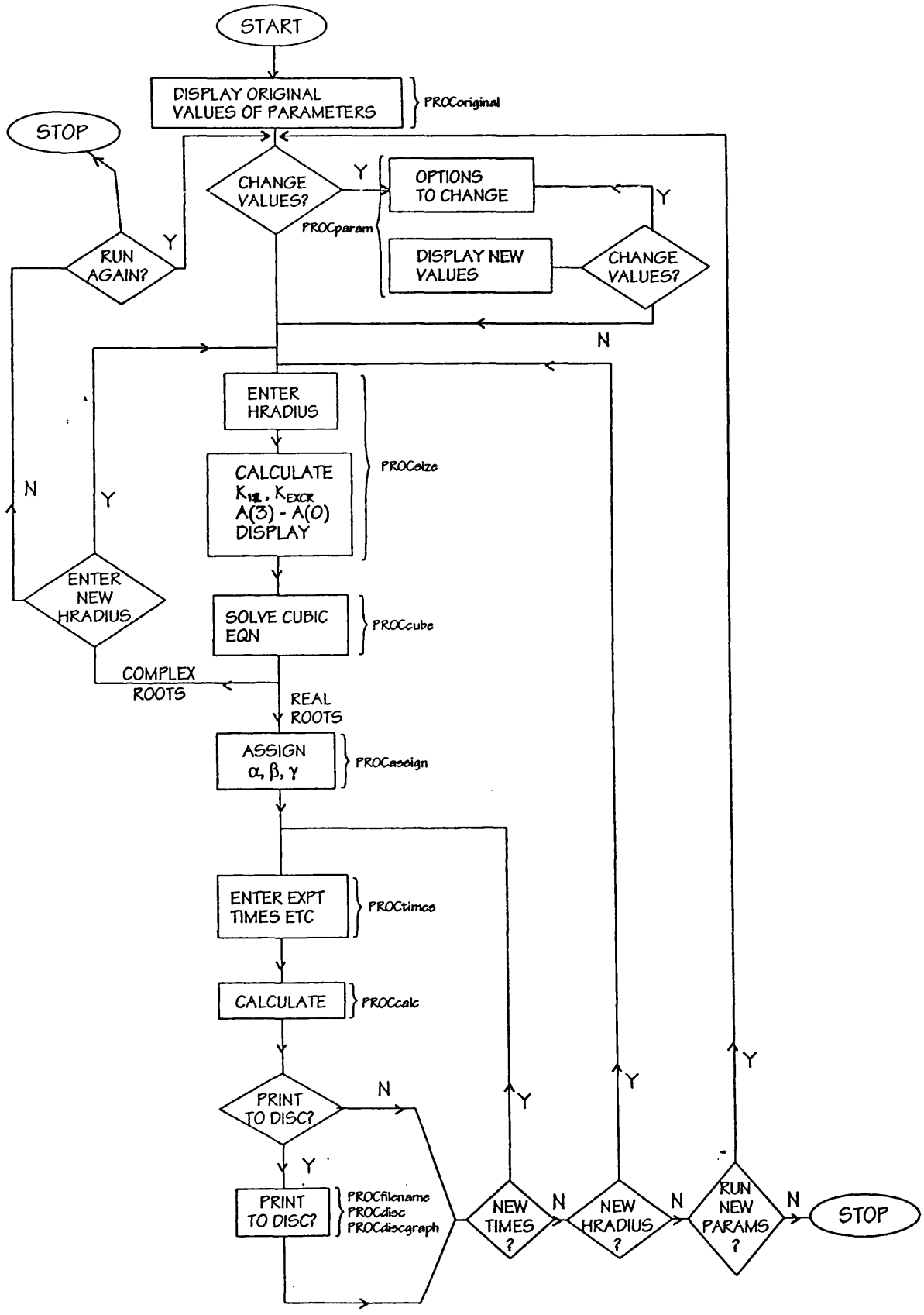

(a) The preliminary definitions

The main function of the first few lines prior to the first subroutine PROCoriginal was to dimension the matrix A and the vectors AA, B, and XW. The matrix A contains all the values of the functions to be calculated by the following subroutines. The vector AA contains the coefficients a_i of the cubic equation. The vector B contains the values of the new coefficients after the application of synthetic division. The vector XW stored the values of all the roots as they were determined. All the vectors were given the dimension of 20 for convenience, although a dimension of 3 would have been sufficient. The names of all the subroutines (procedures) to be used in the programme were required to be listed at this stage.

(b) The subroutines PROCoriginal and PROCparam

The subroutines PROCoriginal and PROCparam display on the screen the current baseline values of the parameters D_0, GFR, BLFR, V_C, k_{21}, k_{13}, k_{31}, k_m, k_{filt}, a_{filt}, n_{filt}, k_{lymph}, a_{lymph} and n_{lymph}, and their units, which have necessarily been built into the programme. The user is then given the option to change any, or all of these parameters accordingly. For example, the values k_{filt}, a_{filt}, n_{filt}, k_{lymph}, a_{lymph} and n_{lymph}, which the programme uses to represent the filtration (i.e. subscript filt) and lymph (i.e. subscript lymph) parameters of best-fit *k*, *ao* and *n* respectively following the fitting of Model B to the selected F/P ratio and L/P ratio data sets, would have to be changed accordingly depending upon whether the distribution of protein or uncharged macromolecular drugs was being simulated. The values of the parameters GFR, BLFR and V_C, and therefore correspondingly k_{21}, k_{13} and k_{31} would also have to be given different values if the simulations were for mammals other than man, as indeed would k_m. Baseline parameters in the programme represent uncharged macromolecules in man with the dose D_0 set to unity.

(c) The subroutine PROCsize

Having entered the desired protein or uncharged parameters of best-fit together with the other appropriate baseline parameters, the subroutine PROCsize then requests the user to enter the desired molecular radius of the macromolecule *a* to be simulated for. The subroutine PROCsize then calculates the values of the parameters k_{excr} and k_{12} (since *a* determines the values of these parameters), and then calculates the values of the coefficients a_i of the cubic equation 16 via equations 17 to 19a respectively. These values of the coefficient a_i are printed on the screen. (The programme uses the term HRADIUS to represent the molecular radius *a*.)

(d) The subroutines PROCcube, PROCsubcube and PROCrootfind

The subroutines PROCcube, PROCsubcube and PROCrootfind calculate the three roots of equation 16 for the selected molecular radius value. This is achieved by solving equation 16 numerically using the Newton-Raphson and synthetic division techniques described in parts (i) and (ii) respectively below:

(i) The first root of equation 16 is calculated using the Newton-Raphson formula

$$x_{n+1} = x_n - \frac{f(x_n)}{f'(x_n)} \qquad 28$$

with an initial starting value for the root of $x_1 = 0.5$ and the convergence limit for the root set at $|f(x_n)| < IE-14$, where $f(x_n)$ in this case is equation 16 evaluated at x_n for iteration number *n*, and $f'(x_n)$ is its derivative, and where x_{n+1} is calculated from x_n so that each successive newly found value is used as the starting point for each subsequent repetitive iteration. This repetitive application is repeated until either a root has been found satisfying the convergence criterion $|f(x_n)| < IE-14$, or of course $f(x_n) = 0$, or the number of iterations has exceeded the iteration limit. In MACROHOURS the convergence criterion has been set at $IE-14$ because this is the lowest order of magnitude with which the Acorn Archimedes computer can work (this also applies to PCs), The number of iterations was set to run from 0 to 400 in steps of 2. Hence, if within the set number of iterations $|f(x_n)| < IE-14$ (or of course

$f(x_n) = 0$) then this represents a root of equation 16. If however a root has not been found within the set number of iterations, then this indicates that the convergence is very slow, and taking too long, and the user is subsequently requested to enter a new convergence limit, i.e. *IE* - 13, *IE* - 12 etc as appropriate to find the root. In practice the first root, and indeed the other roots, are usually found within approximately the first 40 or so iterations (function calls) with the convergence limit set at *IE* - 14, hence 0 to 400 iterations in steps of 2 is usually more than adequate. A starting value of $x_1 = 0.5$ is used because the Newton-Raphson technique will obviously not commence unless such a value is given, and $x_1 = 0.5$ is a sensible initial estimate, as indicated by the general form of equation 16. Any sensible starting value within the range of search could have been used to initiate the procedure, because the roots arrived at will of course be the same, although the order in which they are found and the number of iterations it takes to find them may vary. The three roots of equation 16 must be real, distinct and greater than zero, hence in MACROHOURS the range of search for the roots is defined to be between $x = -10$ and $x = 10$. The lower value of $x = -10$ was used for safety in case the smallest root was to be extremely close to, but not actually zero itself. The term $\left[\frac{-f(x_n)}{f'(x_n)}\right]$ in equation 28, which represents the correction term applied to the previous estimate of the root at each iteration, means that the value of x_{n+1} is obtained by moving from x_n to x_{n+1} in the direction of the tangent $f'(x_n)$ of the function $f(x_n)$, hence ensuring the eventual convergence to a root. The nature of the model and the inter-compartmental parameters, and consequently the general shape of the curve given by equation 16 mean that convergence is always guaranteed, with the convergence to a root being fast when the denominator in this term $\left[\frac{-f(x_n)}{f'(x_n)}\right]$ is large (due to a strong vertical trajectory near the root), and slower when the denominator in this term is smaller (due to a less vertical, more horizontal trajectory near a root).

(ii) Once the first root of equation 16 has been found using the Newton-Raphson technique described in part (i) above, this root is then removed (factored out) from

equation 16 by the process of synthetic division described below, thus reducing equation 16 to a quadratic equation (degree 2) with new coefficients. In general notation, for a polynomial of n^{th} degree the new coefficients after application of synthetic division are given by,

$$\left.\begin{aligned} b_{n-1} &= a_n \\ b_{n-1-r} &= a_{n-r} + b_{n-r}x^* \end{aligned}\right\} \; r = 1,2,\ldots,(n-1) \qquad 29$$

where x^* is the first root to be determined by part (i). The polynomial, in this case the cubic equation 16, is then reduced by one degree,

$$n = n - 1 \qquad 29.1$$

and the newly calculated coefficients of this reduced equation by degree one are renamed,

$$a_i = b_i \qquad \text{for} \qquad i = 0,1,\ldots,n \qquad 29.2$$

Part (i) is then repeated to find the next root, and once this has been found, this root is then factored out by synthetic division. This process is repeated until all roots of the original polynomial have been found.

Therefore, in general notation, if the first root of equation 16 is found by part (i) to be x^* say, then since equation 16 has degree $n = 3$, then removing this root x^* from equation 16 by synthetic division gives an equation of degree 2 (a quadratic equation) whose new coefficients are calculated as follows,

$$\begin{aligned} b_2 &= a_3 \\ b_1 &= a_2 + b_2 x^* \\ b_0 &= a_1 + b_1 x^* \end{aligned}$$

(where a_i's are as defined by equation 17, 18 and 19 previously) and these newly calculated coefficients of the resulting quadratic equation are then renamed $a_i = b_i$ for $i = 0,1,2$. Hence having factored out the first root x^*, the next root is then calculated from this quadratic equation by repeating part (i) again. This second root is then factored out from the quadratic equation by synthetic division again to give the third and final root.

To check the validity of the roots determined MACROHOURS checks the quadratic equation for the presence of complex roots, and if there are any, the user is requested to enter a new molecular radius value. MACROHOURS also prints on the screen the number of steps (function calls) it takes to arrive at each of the three roots.

(e) The subroutine PROCassign

Once the three roots of equation 16 have been calculated for the selected molecular radius, the subroutine PROCassign then defines the largest of these three roots to be γ, the middle (next largest) to be α, and the smallest root to be β since by definition $\gamma > \alpha > \beta > 0$.

(f) The subroutine PROCtimes

Having assigned the values γ, α and β such that $\gamma > \alpha > \beta > 0$, MACROHOURS then requests the desired time period for which the simulation is to be performed. The user is requested to enter the initial (starting) time for the simulation run, the final (end) time for the simulation run, and the time increment (all in hours).

(g) The subroutine PROCcalc

The subroutine PROCcalc simulates each of equations 20, 10, 11, 12, 24, 25, 26 and 21 for the desired molecular radius over the selected time period. Thus giving the fraction of the dose in each of the blood (equation 10), lymph (equation 11) and liver (equation 12) compartments, and also the fractions of the dose which have been excreted by the kidneys (equation 24) and metabolised by the liver (equation 25). The total fraction of the dose eliminated (equations 26 and 27, where of course equation 26 equals equation 27), and the concentration of the dose in the blood compartment (equation 20).

(h) The subroutines PROCfilename, PROCdisc and PROCdiscgraph

The simulated results can then be printed to disc (inserted into drive 0 or A). Having entered the desired filename, the results are saved onto floppy disc as two ASCII files

under the names 'filename' and 'Gfilename'. The former files can be printed out to give a table of simulated results (raw data) for the fractions of the dose in each compartment together with a summary of the baseline parameters used and the values of the three roots γ, α, β. Files with prefix G can be imported into a worksheet of a suitable plotting programme to construct the desired plots. The figures presented in chapter 3 were all constructed by importing each appropriate 'G-file' into worksheets of the plotting programme Sigma Plot (Jandel). In this way the transfer of data are accomplished without introducing errors.

Once the simulated results have been saved to disc (if desired), then either a new simulation time period, or a different molecular radius value, or new baseline parameters can be entered, and the procedures described in parts (a) to (h) are then repeated as appropriate.

One restriction of the use of MACROHOURS is that for the very large molecular radii of greater than about 70Å, the fractions of the dose excreted can be so small (less than IE-14), that the computer cannot calculate these values. Hence the programme can be used when $ao \leqslant a \leqslant 70$ Å.

2.3.3 Validation of the model and the computer programme

The physiological three-compartment pharmacokinetic model and the computer programme MACROHOURS were validated in two ways which are described in parts (a) and (b) as follows:

(a) Validation using full length calculation

The main method by which the model and the computer programme MACROHOURS were validated, was by long hand calculation. The uncharged dextran F/P ratio and PVP L/P ratio parameters of best-fit for Model B were used to calculate the respective expressions k_{excr} and k_{12} for man (i.e. GFR = 125 ml/min, V_C = 5600 ml and BFLR = 2ml/min) for a selected molecular radius value. The intercompartmental parameters k_{21}, k_{13} and k_{31} were calculated for man whilst k_m was set equal to zero i.e. the case of no metabolism. The coefficients a_3, a_2, a_1 and a_o of the cubic equation 16 given by equations , 17, 18, 19 and 19a respectively, were then calculated accordingly.

Equation 16 was then differentiated to give,

$$\frac{df(x)}{dx} = 3a_3x^2 + 2a_2x + a_1 \qquad 30$$

which is a quadratic equation and which was then evaluated at $\frac{df(x)}{dx} = 0$ for the selected molecular radius using the general equation for solving quadratic equations,

$$x = \frac{-B \pm \sqrt{B^2 - 4AC}}{2A} \qquad 31$$

(where in this case $A \equiv 3a_3$, $B \equiv 2a_2$ and $C \equiv a_1$) to give two values of x, x_{T1} and x_{T2} which represent the values of x at which the two turning points of the curve given by equation 16 occur, i.e. the two turning points occur at $(x_{T1}, f(x_{T1}))$ and $(x_{T2}, f(x_{T2}))$. To perform these calculations a small computer programme in BASIC was written called 'PAUL9' and which is presented in Appendix A4.1

2.3.3 Validation of the model and the computer programme

The physiological three-compartment pharmacokinetic model and the computer programme MACROHOURS were validated in two ways which are described in parts (a) and (b) as follows:

(a) Validation using full length calculation

The main method by which the model and the computer programme MACROHOURS were validated, was by long hand calculation. The uncharged dextran F/P ratio and PVP L/P ratio parameters of best-fit for Model B were used to calculate the respective expressions k_{excr} and k_{12} for man (i.e. GFR = 125 ml/min, V_C = 5600 ml and BFLR = 2ml/min) for a selected molecular radius value. The intercompartmental parameters k_{21}, k_{13} and k_{31} were calculated for man whilst k_m was set equal to zero i.e. the case of no metabolism. The coefficients a_3, a_2, a_1 and a_o of the cubic equation 16 given by equations , 17, 18, 19 and 19a respectively, were then calculated accordingly.

Equation 16 was then differentiated to give,

$$\frac{df(x)}{dx} = 3a_3x^2 + 2a_2x + a_1 \qquad 30$$

which is a quadratic equation and which was then evaluated at $\frac{df(x)}{dx} = 0$ for the selected molecular radius using the general equation for solving quadratic equations,

$$x = \frac{-B \pm \sqrt{B^2 - 4AC}}{2A} \qquad 31$$

(where in this case $A \equiv 3a_3$, $B \equiv 2a_2$ and $C \equiv a_1$) to give two values of x, x_{T1} and x_{T2} which represent the values of x at which the two turning points of the curve given by equation 16 occur, i.e. the two turning points occur at $(x_{T1}, f(x_{T1}))$ and $(x_{T2}, f(x_{T2}))$. To perform these calculations a small computer programme in BASIC was written called 'PAUL9' and which is presented in Appendix A4.1

	x	$f(x)$
:	:	:
for x = 0.001 to 0.01 step IE-3 which gives	2E-3	2.31705214E-6
	3E-3	-4.4454585E-6
	:	:
therefore for x = 2E-3 to 3E-3 step IE-4 which gives	:	:
	2.4E-3	2.89813077E-7
	2.5E-3	-3.58222781E-7
	:	:
therefore for x = 2.4E-3 to 2.5E-3 step IE-5 which gives	:	:
	2.44E-3	3.7376541E-8
	2.45E-3	-2.71446545E-8

and so on, until eventually either $f(x) = 0$ or more commonly $|f(x)| < IE-14$. When $|f(x)| < IE-14$ (the convergence limit), or indeed of course when $f(x) = 0$ then this represents the first root of equation 16.

The first root was then removed from equation 16 using the process of long division so that equation 16 was reduced to a quadratic equation whose two roots could be calculated by hand using the general formula given by equation 31. The largest of these three roots is then assigned to be γ the middle (next largest) root is assigned to be α, and the smallest root is assigned to be β.

This process was repeated for the uncharged macromolecules using the same baseline parameters and parameters of best-fit etc described above for man for molecular radii values of a = 20 Å, 25 Å, 30 Å, 35 Å and 40 Å. The values of the three roots γ, α and β calculated in each case by this brute-force method were then compared to the corresponding respective roots γ, α and β calculated by MACROHOURS for these selected uncharged molecular radii in the case of no metabolism. In each respective case the values of the roots agreed exactly, hence validating the numerical component of the programme MACROHOURS. For obvious reasons this time consuming validation

method was only used for the afore-mentioned selected molecular radii and parameters.

(b) Validation using a collapsing method

The second way the model and the programme MACROHOURS were validated was to collapse the three-compartment pharmacokinetic model into a two-compartment pharmacokinetic model which had been developed at an earlier stage of the modelling process. The fractions of the dose predicted for a two-compartment model were calculated using Minsq [441] in early studies and these could be compared with data calculated using MACROHOURS.

For example, the differential equations describing the physiological two-compartment pharmacokinetic model are as follows,

$$\frac{dA_P}{dt} = -(k_{12} + k_{excr})A_P + k_{21}A_L \qquad 33.1$$

$$\frac{dA_L}{dt} = k_{12}A_P - k_{21}A_L \qquad 33.2$$

which upon solving by the method of Laplace transforms (see appendix A5.2 for skeleton solution) gave,

$$A_P = \frac{D_0\{(k_{21} - \pi_2)e^{-\pi_2 t} - (k_{21} - \pi_1)e^{-\pi_1 t}\}}{(\pi_1 - \pi_2)} \qquad 33.3$$

$$A_L = \frac{D_0 k_{12}\left(e^{-\pi_2 t} - e^{-\pi_1 t}\right)}{(\pi_1 - \pi_2)} \qquad 33.4$$

$$\text{where } \pi_1 = \frac{(k_{12} + k_{21} + k_{excr}) + \sqrt{(k_{12} + k_{21} + k_{excr})^2 - 4k_{21}k_{excr}}}{2} \qquad 33.5$$

$$\text{and } \pi_2 = \frac{(k_{12} + k_{21} + k_{excr}) - \sqrt{(k_{12} + k_{21} + k_{excr})^2 - 4k_{21}k_{excr}}}{2} \qquad 33.6$$

$$\text{with } \pi_1 > \pi_2 > 0 \qquad 33.7$$

$$\text{so that } A_{ELIM} = D_0 - A_P - A_L \qquad 33.8$$

$$\text{and } C_P = \frac{D_0\{(k_{21} - \pi_2)e^{-\pi_2 t} - (k_{21} - \pi_1)e^{-\pi_1 t}\}}{V_C(\pi_1 - \pi_2)} \qquad 33.9$$

Hence in order to collapse the new physiological three-compartment pharmacokinetic model into equations 33.3, 33.4. 33.8 and 33.9 for the physiological two-compartment

pharmacokinetic model, k_{13}, k_{31} and k_m were entered in MACROHOURS as zero. The three roots then calculated by MACROHOURS would then have the largest root γ being equivalent to the root π_1 in the physiological two-compartment pharmacokinetic model, with the middle (next largest) root α being equivalent to the root π_2, and the smallest (third) root would take a value of zero. The fractions of the dose predicted in the compartments A_P, A_L, A_{ELIM} and C_P was then be compared in each case. This analysis was performed for uncharged macromolecules for the same molecular radii values, parameters of best-fit, and baseline parameters as used in validation (a), over a simulation time period from zero to 48 hours in 4 hour intervals. In each case the simulated results using MACROHOURS for the collapsed version of the new physiological three-compartment pharmacokinetic model agreed with the results calculated using Minsq [441] and the physiological two-compartment pharmacokinetic model.

A skeleton solution of both the physiological one and two compartment pharmacokinetic models which were developed as part of the modelling process is given in Appendix A5.1 and A5.2 respectively. A full solution and description is not given because; firstly, these two more simplified models of the body were not the main objectives of this study (although they were a necessary part of the modelling process for validation purposes), secondly, their solution by the method of Laplace transforms can in theory be extracted, by setting the appropriate parameters to zero, from the solution of the new physiological three-compartment pharmacokinetic model presented in Appendix A1. and thirdly, although they are physiological pharmacokinetic models, if the intercompartmental parameters are treated strictly as first-order rate constants rather than taking their assigned physiological values for each molecular radius value, then their solution follows the solution of classical one and two compartment pharmacokinetic models in the pharmacokinetic textbooks. The mathematical expressions developed for k_{excr} and k_{12}, and indeed k_{21}, were first introduced and tested

into these two more simple physiological pharmakokinetic models, as appropriate. Initial simulations were performed on Minsq [441].

2.3.4 Conclusions

The novel physiological three-compartment pharmacokinetic model, with the associated computer programme MACROHOURS, represent the development of the model for macromolecular distribution, which was used in later experiments. The model was designed to predict via the simulation performed using MACROHOURS, the molecular radii which are most effective in getting the greatest fraction of a macromolecular drug into the target site, the lymph, and thus to any cancer micrometastases present there. In addition to predicting the fraction of the macromolecular drug dose present in the lymph, the new physiological three-compartment pharmacokinetic model will also predict for each molecular radius (within the range determined by the modelling process) the fractions of the dose present in the blood and the liver, and the fractions which have been excreted via the kidneys and metabolised by the liver, and the total fraction of the dose eliminated. The new physiological pharmacokinetic model is unique in that it predicts the fate of both protein and uncharged macromolecular drugs in the body, taking into account the different regional capillary permeability to different size macromolecules and the different physiology and flow rates. The model is also unique in that it enables calculation of the separate contributions of renal excretion and hepatic metabolism. The advantages and disadvantages of this new physiological three-compartment pharmacokinetic model over the key theoretical/predictive macromolecular anticancer drug and drug-targeting pharmacokinetic models in the literature are discussed in chapter 5.

Chapter 3

Simulations using the physiological three compartment pharmacokinetic model

3.1 Introduction

The aim of the simulations presented in this chapter was to examine the effect of molecular radius on the distribution of macromolecules in man, and hence to predict the molecular radii which are likely to be most effective in accessing the interstitial fluids. In addition to calculating the fraction of the macromolecular dose present in the lymph, the simulations were required to predict for each molecular radius, the fraction of the dose present in both the blood and the liver, and the fractions excreted unchanged via the kidneys, and metabolised (hepatically cleared) by the liver, as a function of time. This would allow the fate of a macromolecular drug dose in the body to be predicted for all molecular radii within the 20-70Å range over any desired time period. Section 3.2 investigates the effect of molecular radius on the distribution of both protein and uncharged macromolecules in the absence of metabolism. In section 3.3 the strategy for determining some realistic rates of metabolism is described, and these rates of metabolism are then used later in section 3.3 to investigate the effect of molecular radius on the distribution of macromolecules in the presence of metabolism. For these studies the lung was used as a model for tissues with continuous endothelia. In section 3.4 the data for L/P ratio in subcutaneous tissues was used to investigate the influence of more restrictive tissue endothelia on the predictions of pharmacokinetic distribution. Section 3.5 presents the main conclusions.

In each set of simulations the molecular radius was varied from 20Å to 70Å in intervals of 5Å (and 1Å intervals in some cases) and distribution was simulated over 48 hours (4 hour intervals), 240 hours (12 hour intervals), and in sections 3.2 and 3.4, 1008 hours (72 hour intervals). These time periods and intervals were found to be the most useful for examination of the overall trends. The raw datum generated from these simulations is given in Appendix B which is presented separately in lever-arch file form. The figures presented in this chapter have been selected to emphasize particular points. In some of these figures some early data time points (at 1 and 2 hours for the 48 hour simulations; at 1, 3 and 6 hours for the 240 hour simulations; and at 12, 24, 36 and 108 hours for

the 1008 hour simulations) from other simulations performed in this study (given in Appendix B) have also been included to show the early profiles of disposition in more detail. The figures described in each of the subsections of this chapter are presented at the end of each subsection. All the simulations in this chapter are for a 70kg man and used the known or assigned physiological values which were presented in Chapter 2.

3.2 The effect of molecular radius on the distribution of protein and uncharged macromolecules in the absence of metabolism

3.2.1 Introduction

In this section the effect of molecular radius on the distribution of both protein and uncharged macromolecules in the absence of metabolism, i.e. $k_m = 0.0\ min^{-1}$, is studied. The simulations presented here can be thought of as representing the 'ideal case' for an inert macromolecular drug which is not metabolised by the liver such as polyoxyethylene. In practice proteins would be subject to metabolism in vivo, but it was useful to simulate their distribution in the hypothetical case of zero metabolism in preliminary studies. The respective protein and uncharged parameters of best-fit and the other baseline parameters used in this set of simulations are given in table 3.1. The simulated results are described and discussed in subsection 3.2.2, and a summary of the subsequent trends is presented in subsection 3.2.3.

TABLE 3.1 **The baseline parameters used in the simulations to investigate the effect of molecular radius on the distribution of protein and uncharged macromolecules in the absence of metabolism**

D_0	1 unit (dimensionless)
k_{excr}	$GFR = 125\,\text{ml/min}$ $V_C = 5600\,\text{ml}$ and Model B with $n_{filt} = 1, ao_{filt} = 17.486, k_{filt} = 0.20941$ for protein macromolecules and $n_{filt} = 2, ao_{filt} = 17.612, k_{filt} = 0.007333$ for uncharged macromolecule
k_{12}	$BLFR = 2\,\text{ml/min}$ $V_C = 5600\,\text{ml}$ and Model B with $n_{lymph} = 1, ao_{lymph} = 13.558, k_{lymph} = 0.010454$ for protein macromolecules and $n_{lymph} = 1, ao_{lymph} = 14.711, k_{lymph} = 0.019532$ for uncharged macromolecules
k_{21}	$1.78571E-4\,\text{min}^{-1}$ { $\frac{\text{Plasma}}{\text{Lymph}}$ filtration ratio = 1 LFR = 2 ml/min V_L = 11200 ml
k_{13}	$2.57143E-1\,\text{min}^{-1}$ { $\frac{\text{Liver}}{\text{Plasma}}$ filtration ratio = 1 Total blood flow rate to liver = 1440 ml/min V_C = 5600 ml
k_{31}	$2.57143E0\,\text{min}^{-1}$ { $\frac{\text{Plasma}}{\text{Liver}}$ filtration ratio = 1 Total blood flow rate from liver = 1440 ml/min V_H = 560 ml
k_m	$0.0\,\text{min}^{-1}$

3.2.2 Results and Discussion

The simulations for both the protein and uncharged macromolecules clearly predict the importance of molecular radius in determining the distribution of a macromolecular drug in the body. This is illustrated in figures 3.1 A.1 - 3.1 A.11 and 3.1 B.1 - 3.1 B.4 for the protein macromolecules and figures 3.2 A.1 - 3.2A.11 and 3.2 B.1 - 3.2 B.4 for the uncharged macromolecules. These figures show that although the absolute fractions of the dose in each of the blood, lymph and liver compartments and the fraction of the dose excreted are different for both macromolecule types (protein and uncharged), the common trend is that as the molecular radius increases there is a corresponding increase in the fraction of the dose accumulating in the lymph compartment, and a corresponding decreasing fraction of the dose being excreted. At high molecular radii the time taken for distribution to the lymph may be considerable, but as there is reduced excretion and no metabolism, the dose is predicted to accumulate in the interstitial fluids.

Figures 3.1A.1-3.1A.11 and 3.2A.1-3.2A.11 each represent the fraction of dose in each compartment versus time for a particular molecular radius. The rapid plasma clearance of low molecular weight hydrophilic compounds (a=20-25Å) is predicted due to extensive glomerular filtration, which is very much more rapid and dominant than lymphatic uptake for these smaller size macromolecules. The data are replotted to show the influence of molecular radius on the fraction of dose present in each compartment in figures 3.1B.1-3.1B.4 and 3.2B.1-3.2B.4. These plots are presented using an extended timescale in figures 3.3A-3.3D, 3.4A-3.4D, and 3.5A-3.5B.

In the absence of metabolism the largest macromolecule produced the greatest fraction of the dose in the blood and liver, and the smallest macromolecule produced the least fraction of the dose in these compartments, for the whole duration of the simulation period. Loss from these compartments can take place by excretion or uptake into the lymph, both of which are influenced by molecular radius. Since clearance by both

mechanisms decreases as molacular radius increases, the overall plasma clearance must also decrease with increasing molecular radius. Consequently, as shown by figures 3.1B.4 and 3.2B.4 it is the smallest macromolecule which is also excreted most, and the largest macromolecule which is excreted least, for the whole duration of the simulation period. However, as shown by figures 3.1 B.2 and 3.2 B.2, although the ultimate fraction of the dose in the lymph does increase with increasing molecular radius, the accumulation of large molecules in the lymph can take a considerable time so that over the first few days the highest levels in the lymph are provided by intermediate molecular radii 45Å-50Å, rather than the macromolecule with the largest molecular radius.

Figures 3.1B.4 and 3.2B.4 emphasise the role of hydrodynamic radius in determining the rate of excretion of protein and uncharged molecules. At 25Å, 90.2% of the dose for the protein macromolecules and 98.3% of the dose for the uncharged molecules is excreted within 12 hours, but when the radius is doubled to 40Å, less than 11.3% and 29% of the dose respectively is excreted in the same period.

The trends outlined above are due to the fact that as the molecular radius increases it becomes more difficult for the macromolecules to pass through the capillary membranes (extravasate) from the blood into the lymph, and from the blood into the kidney glomerulus (these rates of movement being modelled and controlled by the expressions for k_{12} and k_{excr} respectively, as described in Chapter 2). However there is a differential effect, the glomeruli being less permeable to large molecules. At a molecular radius of 55Å and greater (as shown by figures 3.1 A.7 and 3.1 B.4 for the protein macromolecules and figures 3.2 A.7 and 3.2 B.4 for the uncharged macromolecules), excretion becomes almost insignificant and uptake into the lymph becomes the only mechanism causing loss from the blood and liver compartments. (Most literature sources report the glomerular filtrate cut-off somewhere between radii 45-60Å radius [333-339]). The greater fractions of the dose observed in the lymph for the larger macromolecules can be explained by the greater fractions of the dose in the

blood compartment for these sizes, since these macromolecules are either at or above the size of the renal threshold, and are therefore excreted very slowly or not at all, and so remain in the blood much longer than the rapidly excreted smaller macromolecules (the k_{21} parameter models and controls the rate of return back to the blood from the lymph, and is the same for all radii).

Figures 3.1 B.3 for the protein macromolecules and 3.2 B.3 for the uncharged macromolecules indicate that there is never greater than 10% of the macromolecular dose in the liver at any one time. This is due to the greater size of k_{31} in relation to k_{13} (k_{31} is ten times greater than k_{13} since V_H is one-tenth the size of V_C), so once the macromolecule has equilibrated between the blood and the liver (rate determined by k_{13}), the overall mass transfer to and from the liver is equivalent. This can be explained since the net blood flow rates, i.e. the total blood flow rates to and from the liver, are the same. This rapid distribution between the blood and the liver reflects the relative ease with which even the largest macromolecules pass out of the discontinuous capillary membranes from the blood into the liver sinusoids and back again, and is the reason why in most 'classical pharmacokinetic models' the liver is included as part of the central compartment. Since equilibration between the blood and liver is rapid, this explains why the peak fraction of the dose in the liver occurs at short times irrespective of molecular radius. Although the graphs do not show the period between 0 and 1 hour in detail, the peak fraction of the dose in the liver will in fact be 10% of the dose very soon after intravenous injection because V_H is one-tenth the size of V_C and k_{13} is high. Hence the peak time for the liver fraction will always be short and will always occur very soon after an i.v. bolus.

The net effect of the above distribution phenomena is that the larger macromolecules remain within the whole system much longer than smaller sized macromolecules. The smallest macromolecules ($a < 25$Å) are transfered from blood to lymph much faster than the larger macromolecules but are lost from the system via excretion before they even have a chance to accumulate significant amounts in the lymph. Hence it is the

radii within an intermediate size range of 45-50Å which tend to produce the greatest fraction of the macromolecular dose in the lymph over the first few days. However in the absence of metabolism, as excretion is the only form of elimination, the larger macromolecules (i.e. >55Å) are cleared very slowly and eventually accumulate in the lymph to high levels.

Figure 3.1 B.2 for the protein macromolecules shows that at the end of the 48 hour period significant amounts of the macromolecular drug dose have accumulated in the lymph for molecular radii 40Å and greater. At 48 hours we see that between 30-37% of the dose is in the lymph for molecular radii 40Å and greater, and that the fraction of the dose in the lymph is in fact still increasing for molecular radii 35Å and greater. Figure 3.1 B.2 also shows that over about the first 40 hours a molecular radius of 45Å produces the greatest fraction of the dose in the lymph, but from about 40 hours onwards to the end of the 48 hour simulation time it is molecules of 50Å which do so. This trend is also shown in figure 3.2 B.2 to be similar for the uncharged macromolecules. Figure 3.2 B.2 shows that at the end of the 48 hour period significant amounts of the macromolecular drug dose have accumulated in the lymph for molecular radii 40Å and greater (between about 20-30% of the dose for radii greater than 45Å) and that the fraction of the dose in the lymph is still increasing for molecular radii 40Å and greater. For uncharged molecules excretion of molecules with $a \leqslant 35$Å is considerable and at $a = 35$Å the uncharged species would be expected to have different pharmacokinetics to negatively charged proteins (figs. 3.1B.2 and 3.2B.2).

Both figures 3.1 B.2 and 3.2 B.2 show that there is a clear 'band of curves' of molecular radii 45Å-70Å producing significant fractions of the macromolecular dose in the lymph, with the intermediate radii sizes 45Å - 50Å producing the greatest fractions there at any one time. The figures also show that although a macromolecule of radius 40Å is in amongst the most effective radii sizes, in the unlikely case of a total absence of metabolism and over longer time periods, 40Å becomes less effective, being excreted more rapidly and thus cleared from the tissues after extended time periods. Figures 3.1

B.2 and 3.2 B.2 also show that when comparing protein molecular radii with the same size uncharged molecular radii, the fraction of the dose present in the lymph is greater for the protein macromolecules than the uncharged macromolecules over the 48 hour period. This is mainly due to the effect of the dominant negative charge within the glomerular basement membrane of the kidney which repels negative or similarly charged molecules, i.e. proteins, thus reducing their rates of renal excretion and consequently increasing their blood circulation times so that they have a better chance of extravasating into the lymph than the relatively more quickly excreted uncharged molecules of the same size. Thus a macromolecular drug which is uncharged should be selected using different criteria. The figures also illustrate the fact that in the absence of metabolism the fraction of the dose present in the lymph over 48 hours has only reached a peak for the smaller macromolecules. Therefore simulations over longer time periods were performed (figures 3.3A-D and 3.4A-D).

Figure 3.3 B for the protein macromolecules shows that at the end of a 240 hour simulation period the fraction of the dose in the lymph was still increasing for molecular radii 60Å and greater, and shows that over the first 40 hours a molecular radius of 45Å produced the greatest fraction of the dose in the lymph. From about 40 to 72 hours a molecular radius of 50Å produced highest levels (as indicated by figure 3.1 B.2 over 48 hours), and from about 72-204 hours a molecular radius of 55Å produced the greatest fraction of the dose in the lymph. At 240 hours the largest mass in the lymph (51.6% of the dose) was produced by a molecular radius of 60Å. Thus in the extreme case of a totally inert molecule which is not subject to metabolism the largest molecules would ultimately have a moderate advantage over intermediate sized molecules. Figure 3.4B shows similar predictions for uncharged polymers where from about 204 hours onwards to the end of the 240 hour period, the highest mass in the lymph was provided by a molecular radius of 55Å (44.6% of the dose in the lymph at 240 hours).

An interesting point suggested by the simulations over each of the chosen time periods which is worth noting (shown by figures 3.3 A-3.3 D and 3.4 A- 3.4 D for example), is that in the absence of metabolism if proteins are compared with uncharged molecules of the same size, we see that for radii less than 45Å, the fraction of the dose found in the blood and the liver compartments is greater for the protein macromolecules than the uncharged macromolecules over most times. However for molecular radii 45Å and greater the fraction of the dose found in the blood and liver compartments is less for proteins than uncharged macromolecules. For molecular radii less than 50Å (simulations over 48 hours in 1Å intervals found the exact radius to be 47Å), the fraction of the dose excreted is greater for the uncharged molecules than proteins, but then for molecular radii 47Å and greater the fraction of the dose excreted is less for the uncharged macromolecules than the proteins. Also at a molecular radius of about 45Å (simulations over 48 hours found the exact radius to be 44Å), in the absence of metabolism, the fractions of the dose in the blood and liver compartments are almost equal for both the protein and uncharged macromolecules at most times.

One possible explanation for the above pattern for macromolecules of molecular radius 20Å to 45-47Å may be that since excretion via the kidneys is the only form of elimination, the influence of charge has a large effect on the plasma clearance, proteins being retained by the repulsive interactions with fenestrated endothelia of the glomerulus. But once the macromolecules have reached the size when excretion becomes less prevalent (most literature reports this as being somewhere between 45-60Å [333-339]), the effect of the negative charge within the glomerular basement membrane is not so important and other factors begin to play a more dominant role. The simulations suggest that the larger uncharged macromolecules (>50Å radius) are not excreted as quickly as the larger protein macromolecules of the same radius. These phenomena also play a part even in the presence of metabolism. The simulations in sections 3.3 and 3.4 will show that for each of the chosen rates of metabolism the above pattern is generally repeated over either all (in the case of the slowest rate of

metabolism) or at least some of the simulation time period, and that when metabolism occurs the fraction of the dose metabolised is also greater for the protein macromolecules than the uncharged macromolecules for all radii less than 45Å. This is presumably since there is a larger mass in the liver pool to be metabolised. For all radii 45Å and greater uncharged macromolecules are predicted to be metabolised most.

To conclude this section on the simulations in the absence of metabolism, figures 3.5 A and 3.5 B for the fraction of the macromolecular dose in the lymph for the protein and uncharged macromolecules respectively and which represent the simulations over the longest chosen time period (1008 hours), also illustrate the trends outlined earlier.

Figure 3.5 A shows that for proteins by the end of the 1008 hour period the fraction of the dose in the lymph had reached a peak and started to decline again for all radii 70Å and less, and that the greatest mass in the lymph at any one time occurred at a molecular radius of 60Å. Simulations in 1Å intervals found the optimum radius to be 58Å, producing 51.6% of the dose in the lymph at about 216 hours. At the end of the 1008 hour period a molecular radius of 65Å resulted in the most drug left in the lymph, i.e. about 50% of the dose (simulations in 1Å intervals found the exact radius to be 66Å, giving 50.1% of the dose there at 1008 hours). Similarly figure 3.5 B for the uncharged macromolecules showed a similar picture. The optimum molecular radius was about 55Å, i.e. about 45% of the dose in the lymph at 288 hours (simulations in 1Å intervals found the optimum radius to be 53Å, giving 45.2% in the lymph at about 288 hours). At 1008 hours a molecular radius of 55Å gave the greatest fraction of the dose in the lymph, 44.2%.

Figures 3.5 A and 3.5 B predict that for uncharged molecules the intermediate size macromolecules (a = 55-60Å) are the most effective in getting the greatest fraction of the dose to the lymph at all times. For proteins, 60-65Å radii become more effective towards the end of this very long time period.

The simulations over 1008 hours enabled the molecular radii which produced the greatest peak fraction of the dose at any one time in the lymph in the absence of metabolism to be discovered for both the protein and uncharged macromolecules, i.e. radii 58Å and 53Å respectively. In reality all macromolecular drugs are probably metabolised in some way and these cases are considered in section 3.3. However it is useful to understand the behaviour of hypothetical inert macromolecules so that the influence of metabolism can be appreciated when introduced.

Figures 3.1A.1-3.1A.11

The effect of molecular radius on the distribution of protein macromolecules in the body over 48 hours in the absence of metabolism.

3.1A.1

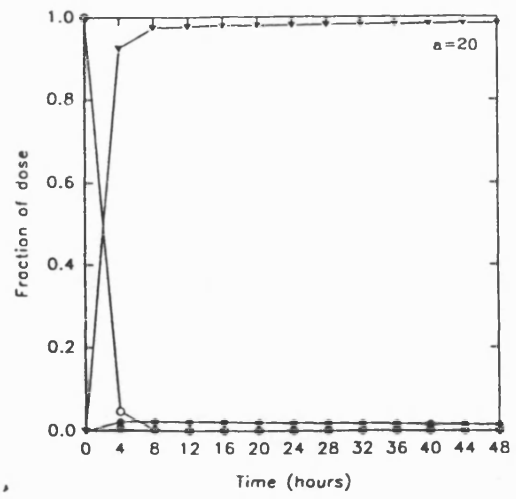

3.1A.2

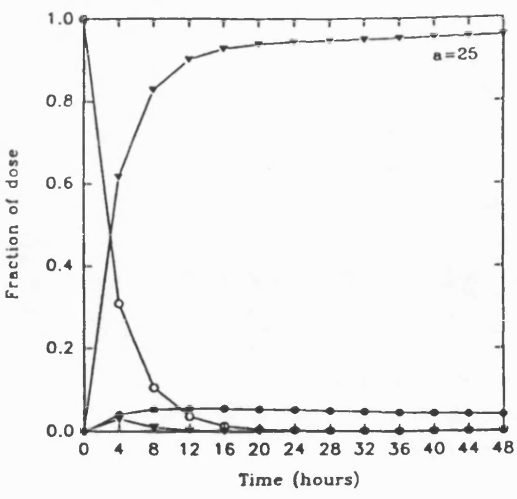

3.1A.3

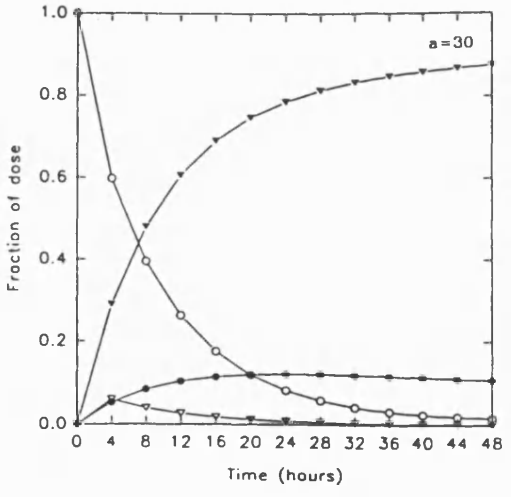

3.1A.4

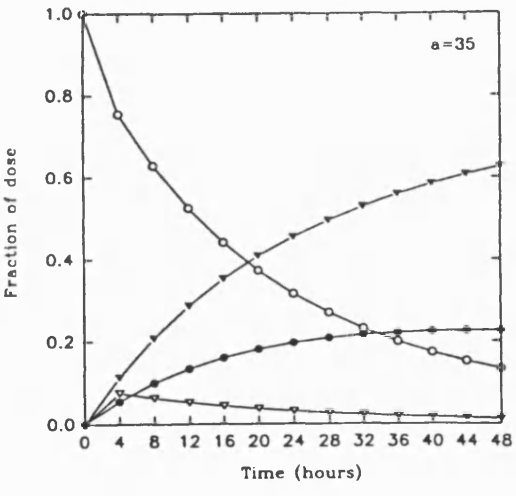

3.1A.5

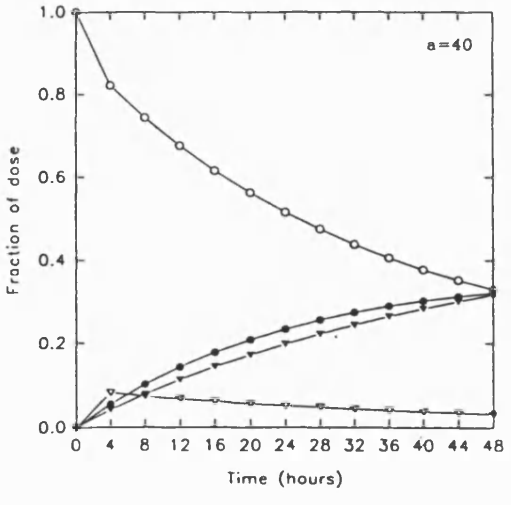

3.1A.6

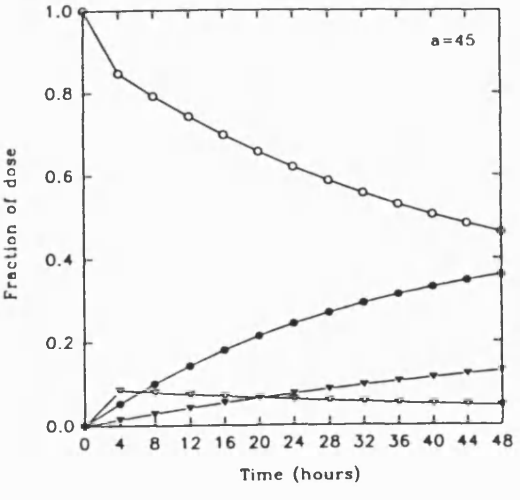

3.1A.7

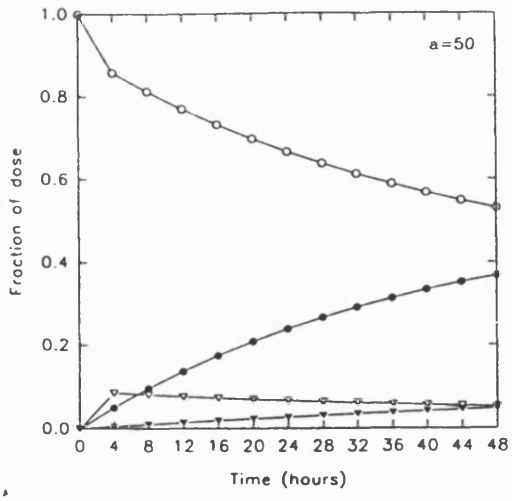

3.1A.8

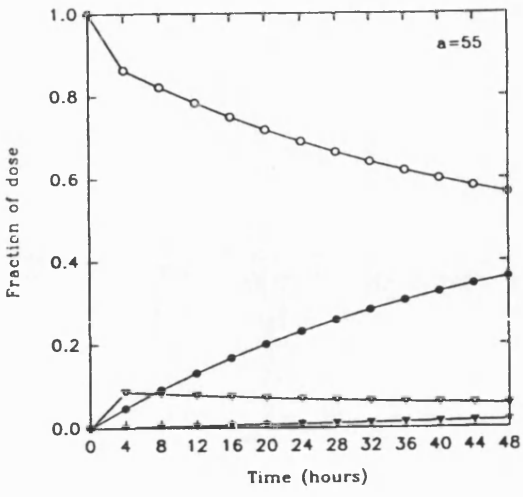

3.1A.9

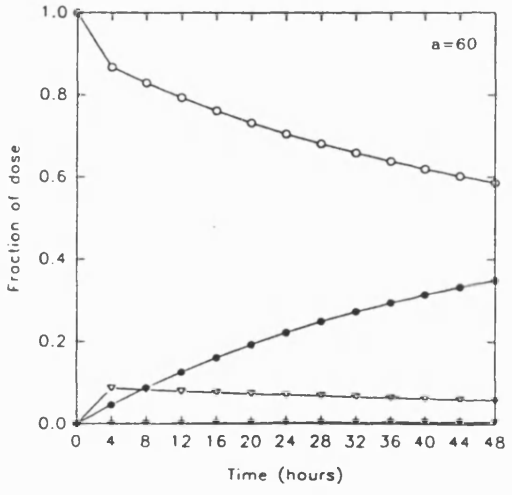

3.1A.10

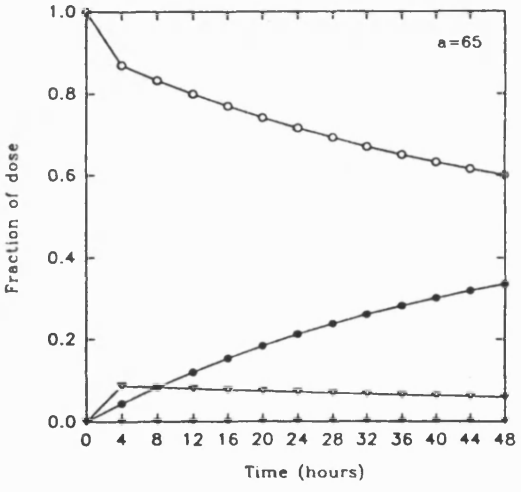

3.1A.11

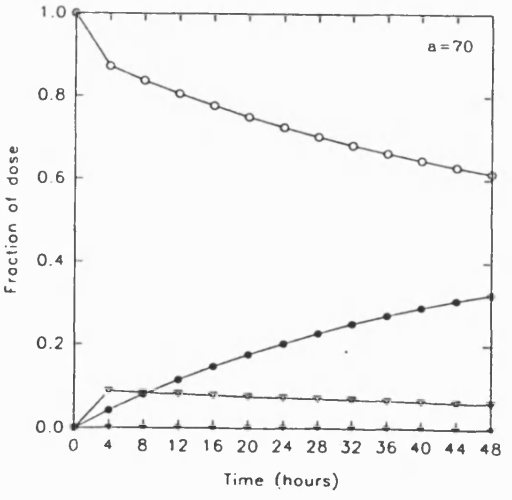

a molecular radius (Å)
Fraction of dose in:

- ○ Blood
- ● Lymph
- ▽ Liver
- ▼ Excreted

Figures 3.1B.1-3.1B.4

The effect of molecular radius on the distribution of protein macromolecules in the body over 48 hours in the absence of metabolism

3.1B.1

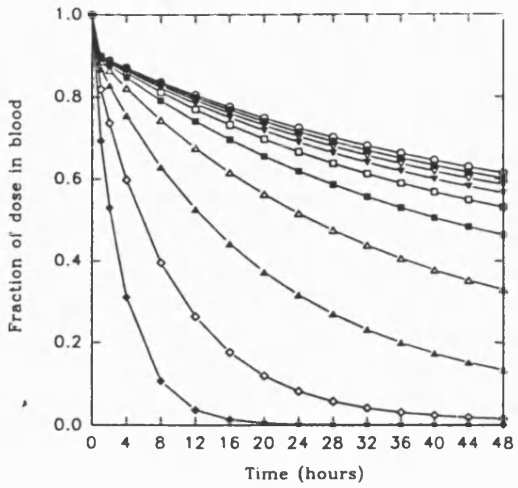

3.1B.2

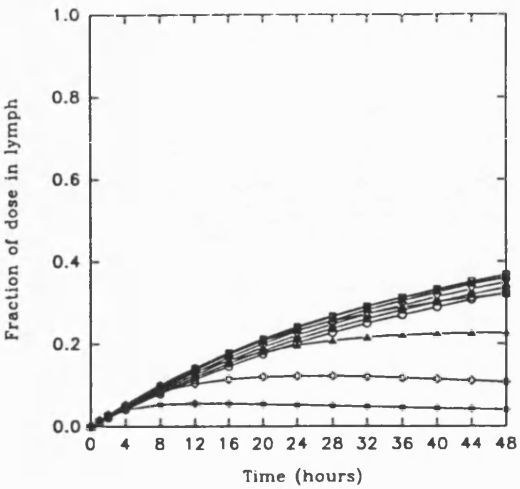

3.1B.3

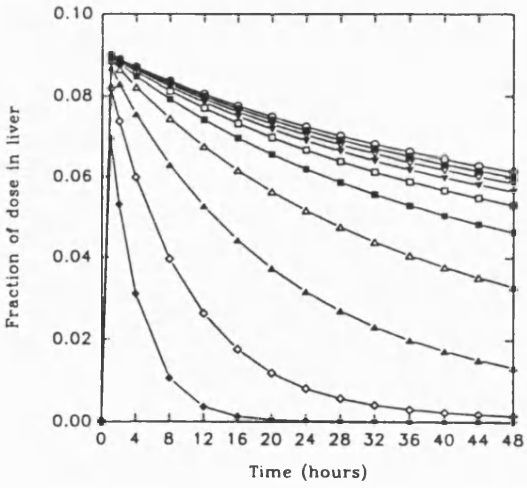

3.1B.4

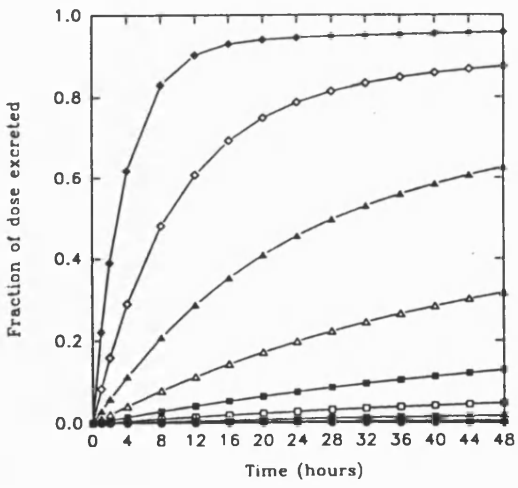

○	70Å
●	65Å
▽	60Å
▼	55Å
□	50Å
■	45Å
△	40Å
▲	35Å
◇	30Å
◆	25Å

Figures 3.2A.1-3.2A.11

The effect of molecular radius on the distribution of uncharged macromolecules in the absence of metabolism.

3.2A.1

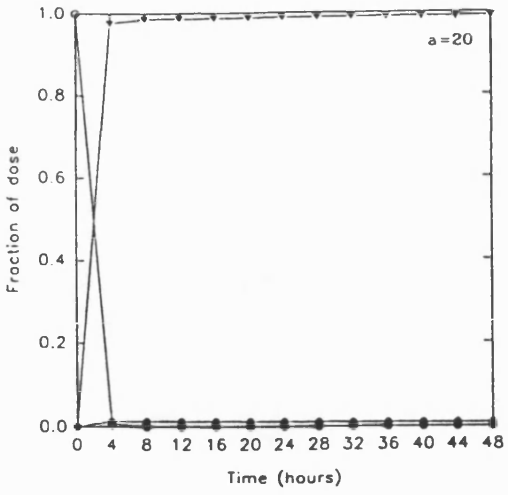

3.2A.2

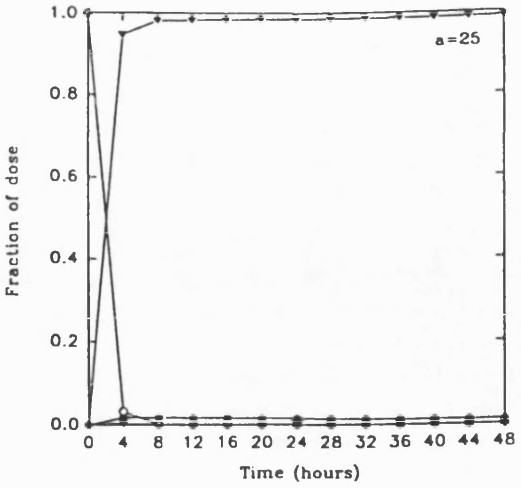

3.2A.3

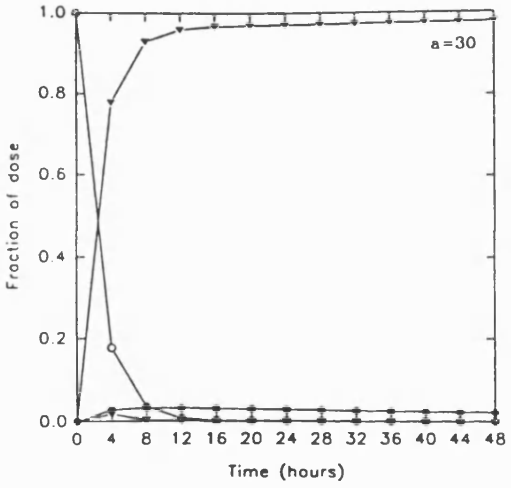

3.2A.4

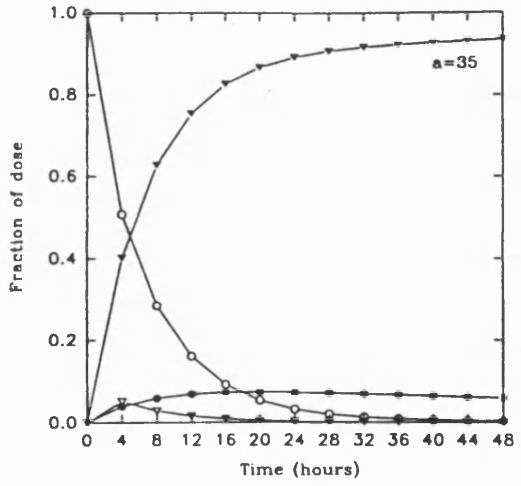

3.2A.5

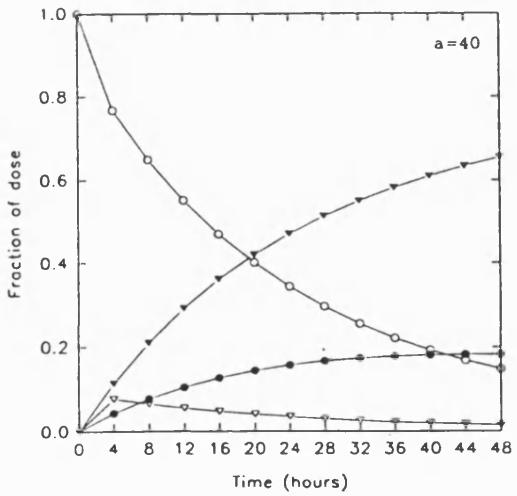

3.2A.6

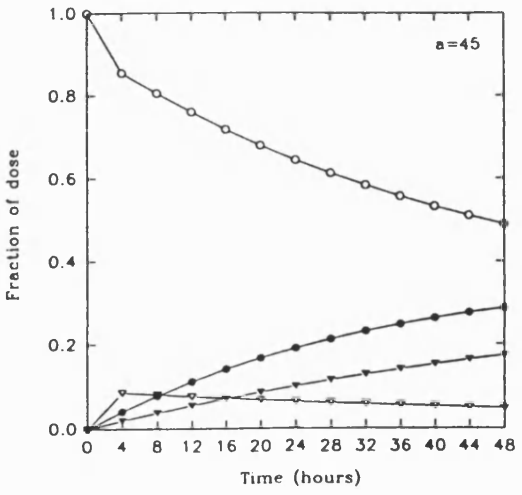

3.2A.7

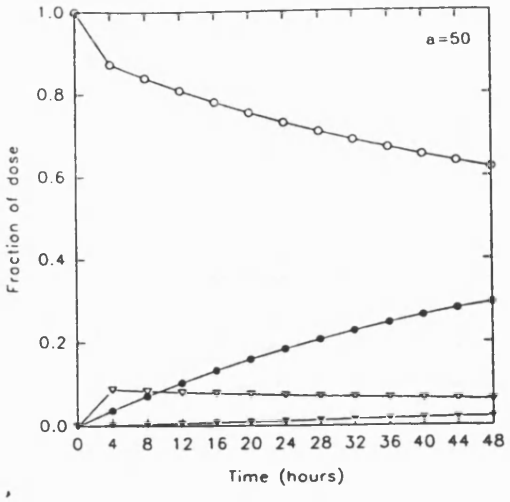

3.2A.8

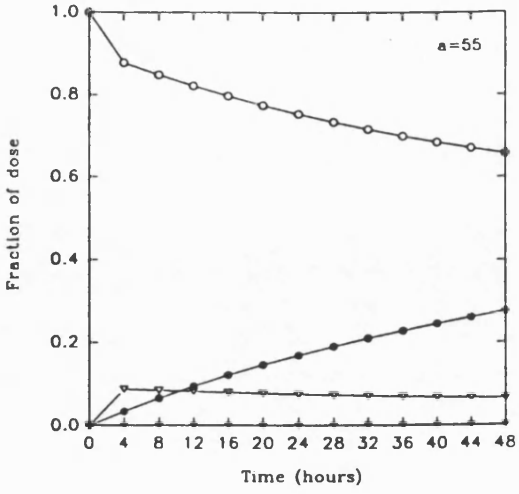

3.2A.9

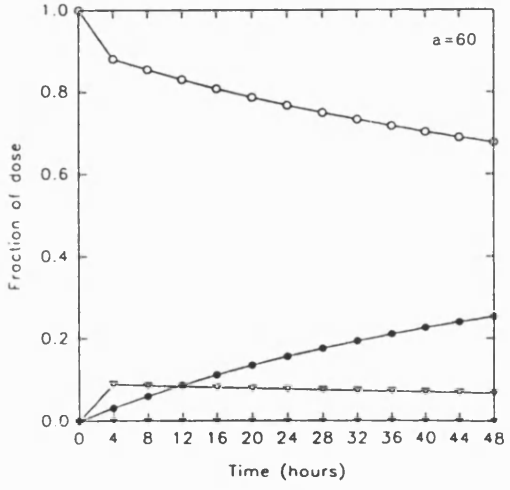

3.2A.10

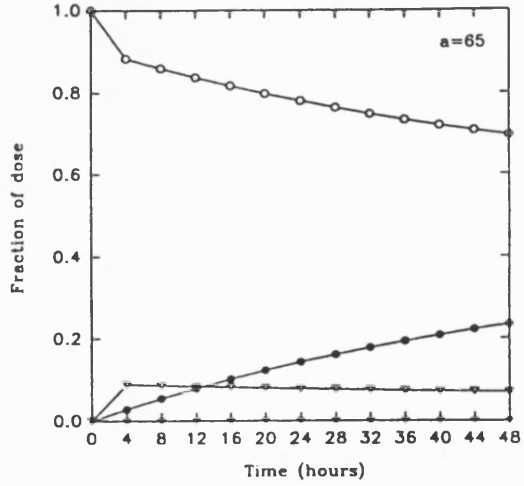

3.2A.11

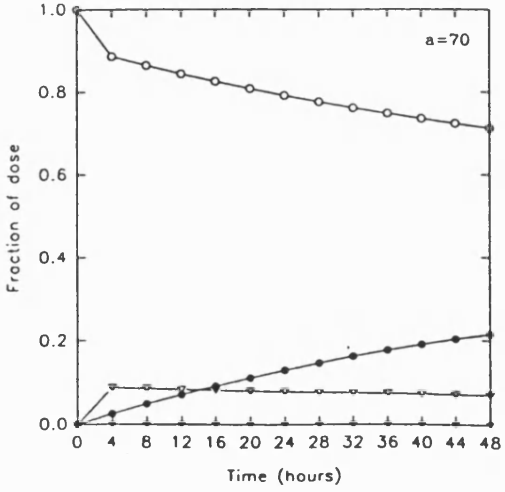

a molecular radius (Å)
Fraction of dose in:
○ Blood
● Lymph
▽ Liver
▼ Excreted

Figures 3.2B.1-3.2B.4
The effect of molecular radius on the distribution of uncharged macromolecules in the body over 48 hours in the absence of metabolism.

3.2B.1

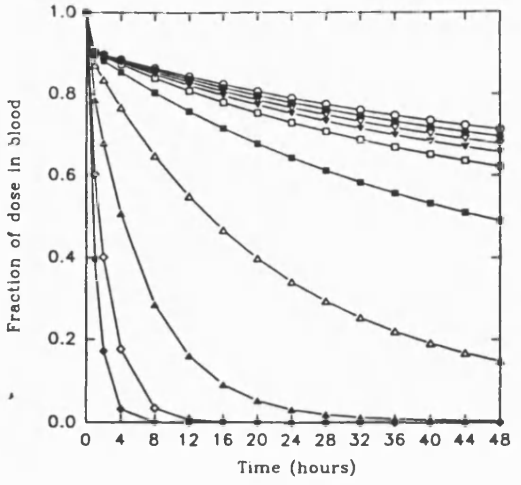

3.2B.2

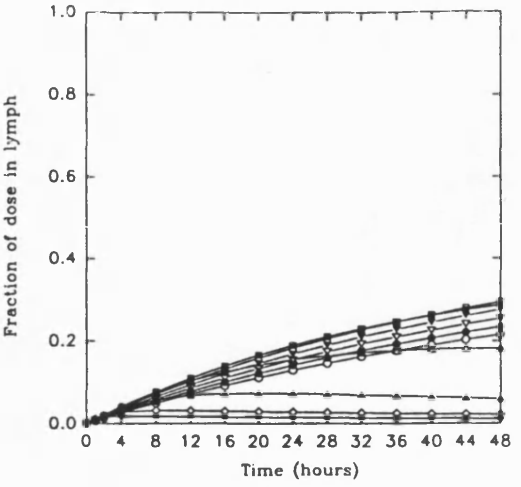

3.2B.3

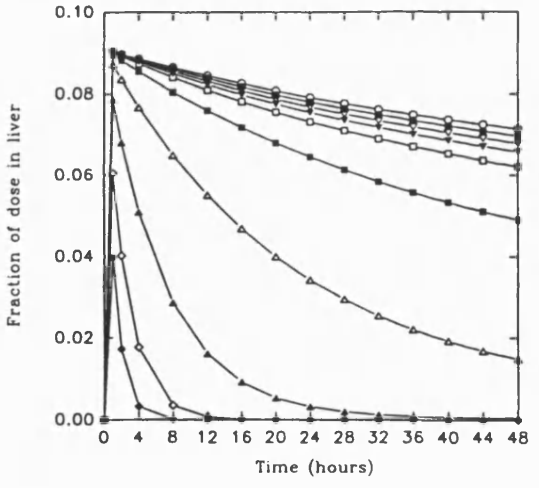

3.2B.4

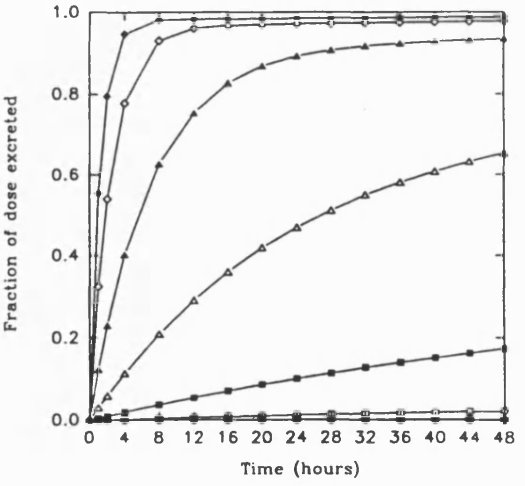

Molecular radius (Å)

○	70Å
●	65Å
▽	60Å
▼	55Å
□	50Å
■	45Å
△	40Å
▲	35Å
◇	30Å
◆	25Å

Figures 3.3A-3.3D

The effect of molecular radius on the distribution of protein macromolecules in the body over 240 hours in the absence of metabolism.

3.3A

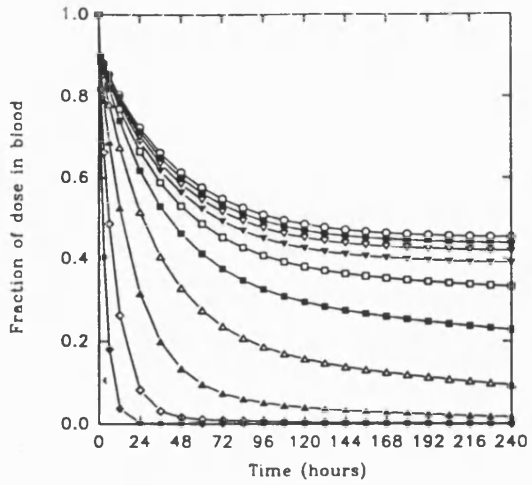

3.3B

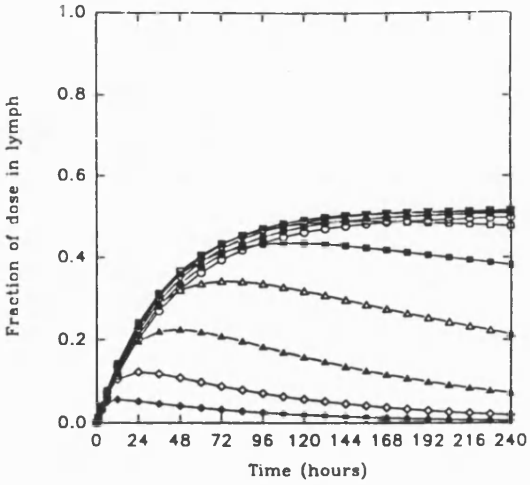

3.3C

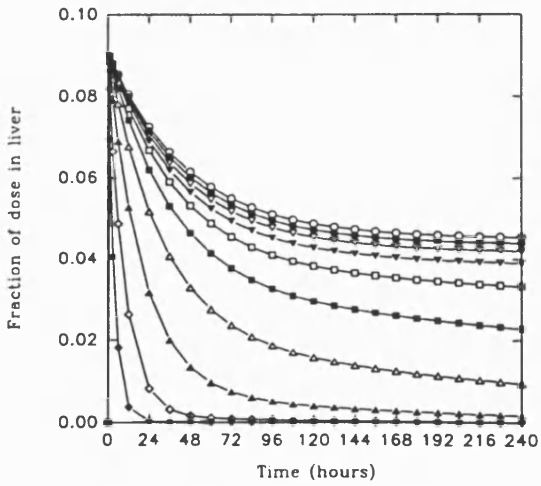

3.3D

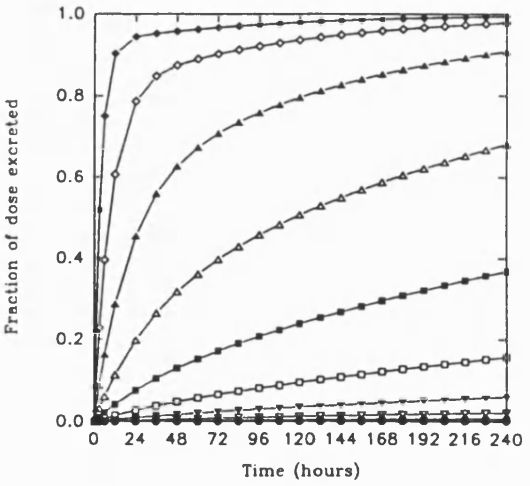

Molecular radius (Å)

○	70Å
●	65Å
▽	60Å
▼	55Å
□	50Å
■	45Å
△	40Å
■	35Å
◇	30Å
◆	25Å

Figures 3.4A-3.4D

The effect of molecular radius on the distribution of uncharged macromolecules in the body over 240 hours in the absence of metabolism.

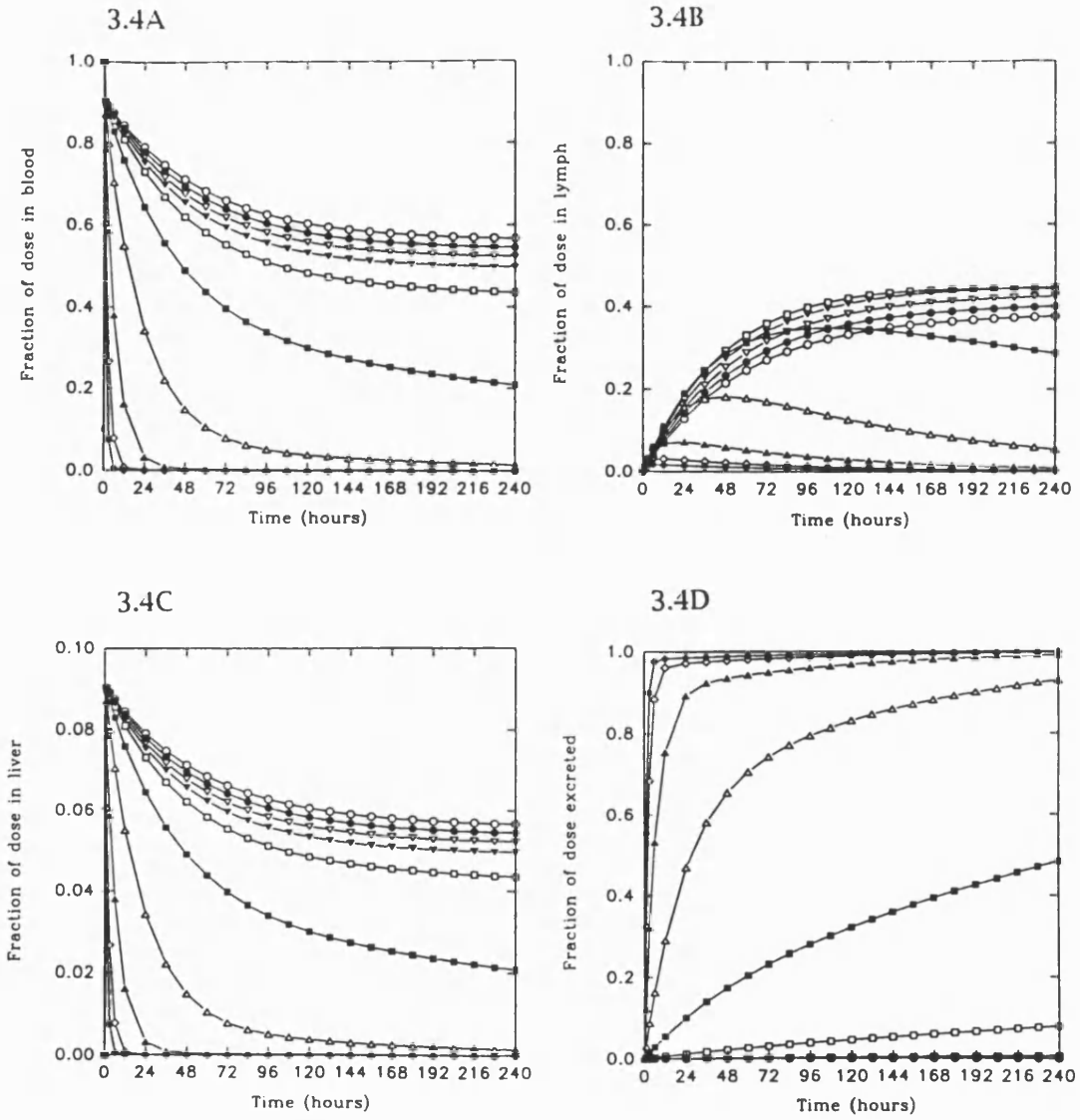

Molecular radius (Å)

○	70Å
●	65Å
▽	60Å
▼	55Å
□	50Å
■	45Å
△	40Å
▲	35Å
◇	30Å
◆	25Å

Figures 3.5A and 3.5B

The effect of molecular radius on the distribution of protein (figure 3.5A) and uncharged (3.5B) macromolecules in the lymph over 1008 hours in the absence of metabolism

3.5A

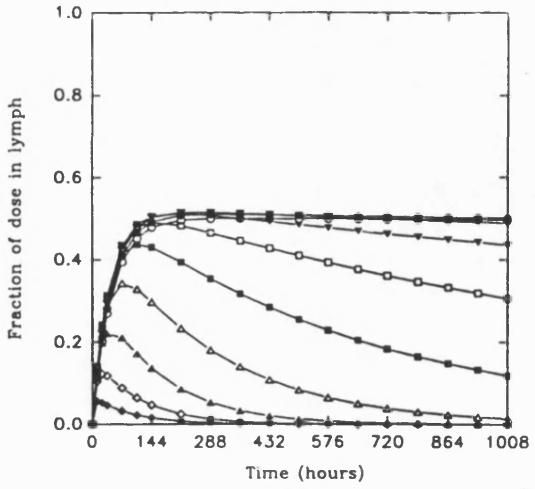

3.5B

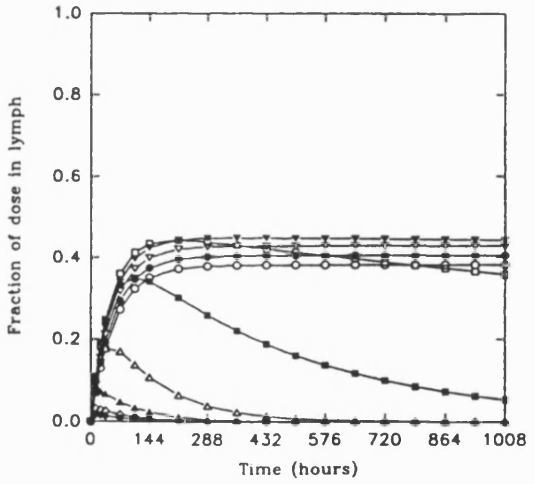

Molecular radius (Å)

○	70Å
●	65Å
▽	60Å
▼	55Å
□	50Å
■	45Å
△	40Å
▲	35Å
◇	30Å
◆	25Å

3.2.3 Conclusions

This set of simulations investigated the effect of molecular radius on the distribution of both protein and uncharged macromolecules in the body in the absence of metabolism. This set of simulations therefore represented the best or 'ideal case' since a macromolecular drug which is not metabolised will remain in the body longer than a macromolecular drug which is metabolised, and will therefore be more likely to get a greater fraction of its dose into the lymph, the target. The simulations in the absence of metabolism illustrated the following trends over each of the chosen simulation time periods:

- Although the actual fractions of the dose in each of the blood, lymph and liver compartments and the fraction of the dose excreted are different for both the protein macromolecules and the uncharged macromolecules, the trend is that as the molecular radius increases there is a corresponding increasing fraction of the dose found in each of the blood, lymph and liver compartments, and a corresponding decreasing fraction of the dose being excreted. With regard to the blood and the liver compartments, the largest macromolecule produces the greatest fraction of the dose, and the smallest macromolecule produces the lowest fraction of the dose, in these compartments for the whole of each of the simulation time periods. In the case of the fraction of the dose excreted, the largest macromolecule is excreted slowest, and the smallest macromolecule is excreted most rapidly, for the whole of each of the simulation time periods.

- Although the fraction of the dose in the lymph does increase with increasing molecular radius for both the protein and uncharged macromolecules, the general tendency is that it is not the largest molecular radius which produces the greatest fraction of the dose in the lymph over the first few days, but generally the intermediate size molecular radii (a = 55Å) that do so.

- There is a clear group of macromolecules of radii 45Å-70Å producing significant fractions of the dose in the lymph for both the protein and uncharged macromolecules.

- The biological half-lives increase with increasing molecular radius for both classes of macromolecule.

- If proteins are compared with uncharged molecules of the same hydrodynamic radius then the proteins will almost always produce a greater fraction of the dose in the lymph than the uncharged macromolecules.

The simulations in the absence of metabolism therefore suggest that the best size candidates to deliver the greatest fraction of the dose to the lymph are macromolecules within the intermediate 45-55Å molecular radii range, with the lower intermediate size molecular radii being the most effective over early times and the larger intermediate size molecular radii tending to be the more successful at the later times. In the case of protein macromolecules which are not subject to metabolism, significant tissue uptake will occur with sizes up to 65Å radius over very long time periods. In the absence of metabolism the theoretical highest peak fractions possible occur at molecular radii 60Å and 55Å for the protein and uncharged macromolecules respectively.

3.3 The effect of molecular radius on the distribution of protein and uncharged macromolecules in the presence of metabolism

3.3.1 Introduction

In this section the effect of molecular radius on the distribution of both protein and uncharged macromolecules in the presence of metabolism (hepatic clearance) is studied. In subsection 3.3.2 the choice of some realistic rates of metabolism is discussed. These rates of metabolism are then used throughout the rest of subsection 3.3.2 to investigate the effect of molecular radius on the distribution of both protein and uncharged macromolecules, with particular attention on the fraction of the macromolecular dose present in the lymph. A summary of the subsequent trends and conclusions shown in subsection 3.3.2 is then given in subsection 3.3.3.

As outlined in Chapter 2, the physiological three compartment model presented here assumes that the first order rate of metabolism k_m refers to the rate at which a macromolecule is hepatically cleared (eliminated) by the liver and lost from the system altogether. In relation to a particular macromolecular prodrug this could be estimated from known experimental data, but in the absence of particular data the approach taken here was to study a range of k_m values which is expected to span a realistic range.

3.3.2 Results and Discussion

In an effort to determine some realistic rates of metabolism initial simulations were performed using the following choices of k_m: 0.001 min^{-1}, 0.003 min^{-1}, 0.01 min^{-1}, 0.03 min^{-1} and 0.1 min^{-1}, which represent the following half-life times of the macromolecule in the liver; 11 hrs 33 mins, 3 hrs 51 mins, 1 hr 9.3 mins, 23.1 mins and 6.93 mins, where $t_{1/2} = \frac{0.693}{k_m}$ is the half-life of the macromolecule in the liver compartment. Initial simulations were performed for molecular radii 40Å and 60Å for both the protein and uncharged macromolecules over 48 hours (4 hour intervals). Molecular radii 40Å and 60Å were chosen because as a result of the simulations over

each time period in section 3.2, they appeared to represent the lower and upper limits of molecular radii between which the most interesting trends were observed. This was particularly true of the lymph, where at a molecular radius of about 40Å and greater significant fractions of the dose were beginning to accumulate in the lymph, and by about 60Å the fraction of the dose there had reached levels close to the maximum observed. A time period of 48 hours was chosen since it was one of the best time periods to depict the overall trends in pharmacokinetic distribution.

Initial simulations over 48 hours for both the protein and uncharged macromolecules at either radius (40Å and 60Å) revealed that the two faster rates of metabolism (0.03 min^{-1} and 0.1 min^{-1}) were so fast that they were probably not relevant for use in future simulations since most of the macromolecular drug dose, even for the larger molecular radius of 60Å, was eliminated before it even had a chance to distribute to the tissues. This is clearly illustrated by figures 3.6 A.1-3.6 A.5 and 3.6 B.1-3.6 B.5 for the protein macromolecules for each of the five values of k_m. (The corresponding figures for the uncharged macromolacules are not shown since they are very similar, as indicated by the raw simulated data presented in Appendix B.) Thus a macromolecular prodrug with $k_m > 0.01$ min^{-1} would have very poor access to the interstitial fluids.

For future work three metabolic rates were chosen; 0.001 min^{-1}, 0.003 min^{-1} and 0.01 min^{-1} , which spanned the range over which the significance of metabolism changed from low to high. Simulations were performed for both the protein and uncharged macromolecules over both 48 hours and 240 hours for each of the three rates of k_m for molecular radii 20-70Å in 5Å intervals.

Figures 3.7 A.1-3.7 A.6 and 3.7 B.1-3.7 B.6 for the protein macromolecules with k_m equal to 0.003 min^{-1} and 0.01 min^{-1} respectively for example, show that even in the presence of metabolism, the general trend over a considerable time span is that as the molecular radius increases there is a corresponding increasing fraction of the dose found in the blood, lymph and liver compartments, with a corresponding decreasing

fraction of the dose being excreted, though now a significant fraction of the dose is also being metabolised.

Clearly, comparing molecular radii for the slower rate of k_m (0.003 min^{-1}) with the corresponding molecular radii at the faster rate of k_m (0.01 min^{-1}), then the absolute fractions of the dose in each respective compartment are different for each rate of metabolism. An increase in k_m results in a corresponding decreasing fraction of the dose in the body overall since the total elimination half life is decreased. However, as in the absence of metabolism, the general trend, which occurs in the presence of metabolism, is that the largest macromolecule produces the greatest fraction of the dose in the circulation, and the smallest macromolecule produces the least fraction of the dose in the blood and liver compartments. As a result, the fraction of the dose metabolised by the liver is highest for the largest macromolecule and lowest for the smallest macromolecule. Thus excretion is a major factor in pharmacokinetics of macromolecules when $k_m < 0.01$ min^{-1}. The renal clearance is avoided by increasing molecular radius until the molecules are too large to excrete in significant amounts. In summary, the larger macromolecules stay within the whole system much longer than the smaller macromolecules, though the fact that discontinuous capillaries are found in the liver allowing easy movement of large macromolecules from the blood to the liver, means that larger macromolecules are more available for metabolism. Distribution of the large macromolecules will be critically influenced by metabolic rate.

Most importantly, both figures 3.7 A.1-3.7 A.6 and 3.7 B.1-3.7 B.6 illustrate that the fraction of the dose reaching the lymph increases with molecular radius size, up to intermediate radii of about 50Å. However in the presence of metabolism further increases in radius (a > 60Å) reduce the effective fraction and duration of the dose reaching the lymph compartment. Thus in the presence of metabolism, in a realistic model, it can be anticipated that there will be an optimum molecular radius for uptake into the tissues. The optimum will be the intermediate size molecular radii (45-55Å),

with the lower of these intermediate sizes being more successful over the shorter times (the exact radii for these observations are given later).

In summary, the general trends illustrated and described in section 3.2 appear to be well established even in the presence of metabolism. The corresponding figures in this set of simulations for uncharged macromolecules are not presented because the trend is well established for both macromolecule types (data are available in Appendix B).

To conclude this section on the simulations in the presence of metabolism, figures 3.8A-3.8C and 3.9A-3.9C examine closely the fraction of the macromolecular drug dose in the lymph for both the protein and uncharged macromolecules for each of the respective three chosen k_m rates. These sets of simulations over 240 hours are from a practical point of view the most useful and emphasize the trends already indicated earlier.

Figures 3.8A-3.8C and figures 3.9A-3.9C show that as the rate of metabolism increases then the absolute fraction of the dose in the lymph at any time decreases for each molecular radius. For each rate of metabolism the fraction of the dose in the lymph has peaked for each radius within the 240 hour period, with the peaks occurring at increasingly earlier times as k_m increases.

Figure 3.8A for the protein macromolecules with k_m=0.001 min^{-1} (the slowest of the three chosen rates of metabolism) shows that over about the first 42 hours a molecular radius of 45Å produces the greatest fraction of the dose in the lymph, then from about 42-96 hours a radius of 50Å does so. From about 96 hours onwards to the end of the 240 hour period a molecular radius of 55Å is most effective. There is a clear 'band of curves' for molecular radii 45-70Å producing significant fractions of the dose in the lymph, with time to peak fraction occurring at roughly the same time. Radii greater than 55Å peak at approximately 108 hours, radii 45Å and 50Å peak at 84 hours and 96 hours respectively. Figure 3.8A shows that the greatest peak fraction of the dose in the lymph at k_m=0.001 min^{-1} occurs at a molecular radius of 55Å (37.1% of the dose at 96

hours), and that the greatest mass of drug in the lymph after the 240 hour period also occurs at a radius of 55Å (29.1% of the dose).

Figure 3.8B for the protein macromolecules with k_m=0.003 min^{-1} shows a similar 'band of curves' for molecular radii 45-70Å producing significant fractions of the dose in the lymph, with a molecular radius of 40Å also achieving high levels at earlier times (over the first 60 hours). For this slightly faster rate of metabolism, over about the first 40 hours a molecular radius of 45Å gives the greatest fraction of the dose in the lymph, then from about 40-132 hours a molecular radius of 50Å was most effective. From 132 hours to the end of the 240 hour period a molecular radius of 55Å was optimal. The molecular radius of 50Å produces the greatest peak fraction of the dose in the lymph (26.4% of the dose at 60 hours). The largest fraction of drug in the lymph at the end of the 240 hour period was achieved at 55Å (12.3% of the dose). Again the time to peak within this band of curves occurred at about the same time, 60 hours, with a radius of 40Å producing an earlier peak at about 48 hours. Simulations in 1Å intervals revealed the exact radius which produces the greatest fraction of the dose in the lymph to be 49Å (26.4% of the dose at 60 hours). The greatest fraction left in the lymph at 240 hours occurred at a radius of 53Å (12.3% of the dose). Therefore since the special case simulations in 1Å intervals in section 3.2 found the greatest fraction of the dose in the lymph in the ideal case (k_m=0.0 min^{-1}) to occur at a radius of 58Å, then this suggests that the greatest fraction of the dose in the lymph at any one time will not occur at exactly the same radius for each different rate of metabolism, but instead lies within this intermediate size band.

Figure 3.8C for the protein macromolecules with k_m=0.01 min^{-1} (the fastest of the three chosen k_m rates) is perhaps the most interesting of the three figures because in addition to the trends outlined above, we now see that for this relatively fast rate of k_m, even molecular radii as small as 35Å are also becoming effective over early times in producing significant fractions of the macromolecular dose in the lymph. Though the absolute fractions reaching the lymph are substantially reduced at this metabolic rate.

Consequently for this faster rate of metabolism the 'band of curves' producing significant fractions of the dose in the lymph now corresponds to molecular radii 35-70Å with a molecular radius of 35Å being relatively successful over about the first 36 hours and then falling away gradually over the rest of the time period. The peak fractions of the dose in the lymph for each radius within this 'band of curves' once again occur at about the same time, 32 hours, except for the radius of 35Å which peaks earlier at about 28 hours. Figure 3.8C shows that over about the first 16 hours a molecular radius of 40Å produces the most drug in the lymph, then from about 16-108 hours it is a radius of 45Å doing so, and from 108-240 hours there is little to choose between the radii 45Å and 50Å, although the molecular radius of 45Å has the highest mass left in the lymph at the end of the 240 hour period (2.8% of the dose). The greatest peak fraction of the dose present in the lymph occurs at a molecular radius of 45Å (14.2% of the dose at 36 hours). Simulations in 1Å intervals in this case found the radius producing the greatest peak fraction of the dose in the lymph to be 45Å, with 47Å having the greatest fraction left at the end of the 240 hour period.

The analysis shows that as the metabolic rate increases, the optimum radius for interstitial distribution decreases. This illustrates the complex relationship between distribution and molecular radius which is usefully modelled here.

Similar trends are illustrated in figures 3.9A-3.9C for the uncharged macromolecules for each of the three rates of metabolism. For almost all of the 240 hour period it is the intermediate size molecular radii 45Å and 50Å which produce the greatest fraction of the macromolecular drug dose in the lymph. In each figure the 'band of curves' producing the most significant fractions of the dose in the lymph once again occurs for molecular radii 45-70Å with a molecular radius of 40Å also in amongst this band in the case of the fastest k_m rate (k_m=0.01 min^{-1}). Also, once again, the peak fractions of the dose for the radii within this 'band of curves' for each respective k_m rate appear to occur at approximately the same time, at about 108 hours for k_m=0.001 min^{-1} (with a radius of 45Å peaking slightly earlier at about 84 hours), at about 72 hours for

k_m=0.003 min^{-1} (with a radius of 45Å again peaking slightly earlier at about 60 hours), and at about 36 hours for k_m=0.001 min^{-1} (with a radius of 40Å peaking slightly earlier at about 28 hours). Interestingly, these times for each k_m rate for the uncharged macromolecules are very similar to the corresponding peak times for the protein macromolecules, especially in the cases of k_m=0.001 min^{-1} and k_m=0.01 min^{-1}. This suggests that these are robust estimates of peak time, since the intercompartmental rate constants for proteins and uncharged polymers are quite different due to difference in molecular charge.

Figure 3.9A for the uncharged macromolecules with k_m=0.001 min^{-1} shows that over about the first 40 hours a molecular radius of 45Å gives the greatest fraction of the dose in the lymph, but from about 40 hours to the end of the 240 hour time period a molecular radius of 50Å is most effective. Figure 3.9A also shows that a molecular radius of 50Å produces the greatest peak fraction of the dose in the lymph (31.1% of the dose at 108 hours), and that the greatest fraction of the dose present in the lymph at the end of the 240 hour period also occurs for a radius of 50Å (24.1% of the dose).

Similarly, figure 3.9B for the uncharged macromolecules with k_m=0.003 min^{-1} shows that over about the first 44 hours a molecular radius of 45Å gives the greatest fraction of the dose in the lymph, but from about 44 hours to the end of the 240 hour period once again a molecular radius of 50Å is optimal. Figure 3.9 B shows that once again a molecular radius of 50Å produces the greatest peak fractions of the dose in the lymph (21.1% of the dose at 72 hours), and that the greatest fraction of the dose left in the lymph at the end of the 240 hour period occurred at a radius of 50Å (9.5% of the dose).

Finally, figure 3.9 C for the uncharged macromolecules with k_m=0.01 min^{-1} shows that a molecular radius of 45Å produces the greatest fraction of the dose in the lymph for almost all of the 240 hour period, except for about the first 4 hours, which sees a radius of 40Å doing so. Correspondingly figure 3.9 C shows that a molecular radius of 45Å produces the greatest peak fraction of the dose in the lymph (11.1% of the dose at

36 hours), and that the greatest fraction of the dose left in the lymph at the end of the 240 hour period also occurs for a radius of 45Å (2.1% of the dose).

Figures 3.6A.1-3.6A.5 and 3.6B.1-3.6B.5

The effect of the five different k_m rates on the distribution of protein macromolecules of molecular radii 40Å and 60Å respectively in the body over 48 hours.

3.6A.1

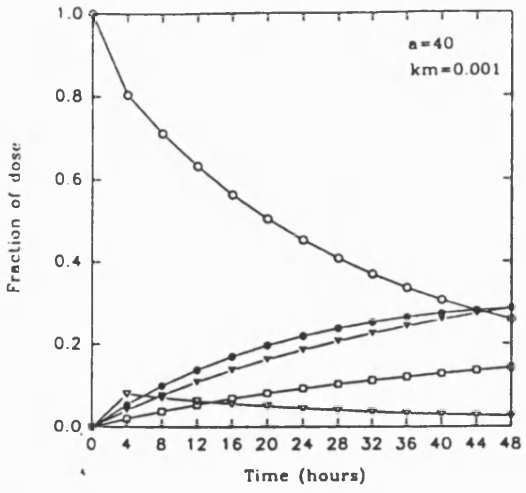

3.6A.2

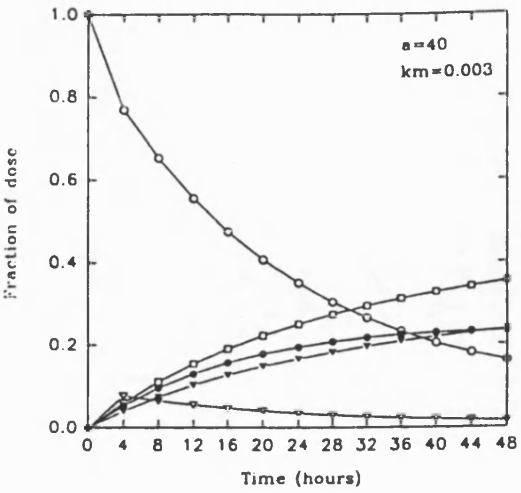

3.6A.3

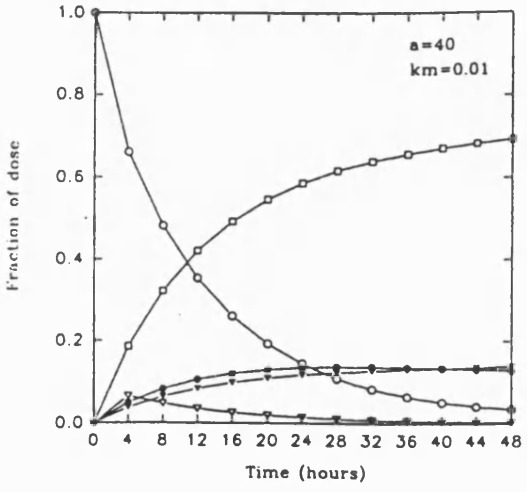

3.6A.4

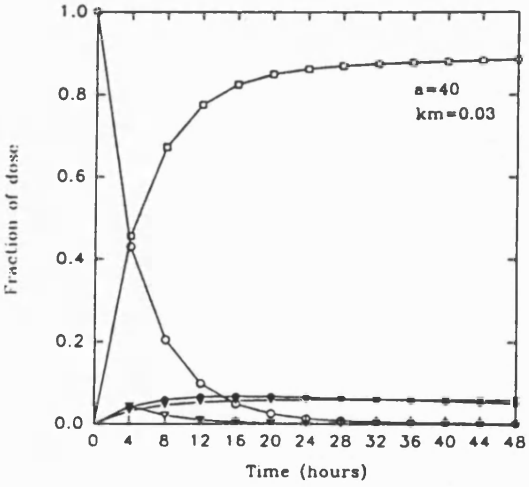

3.6A.5

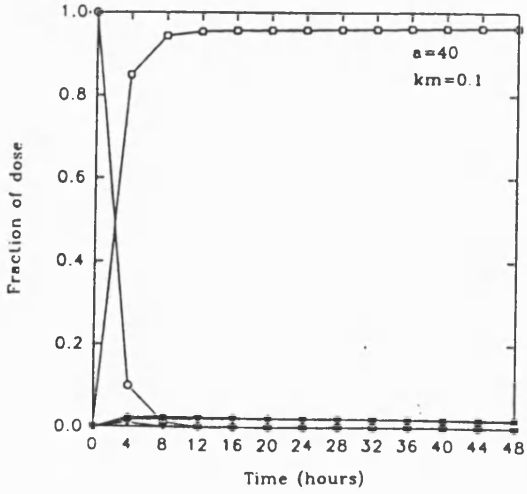

3.6B.1

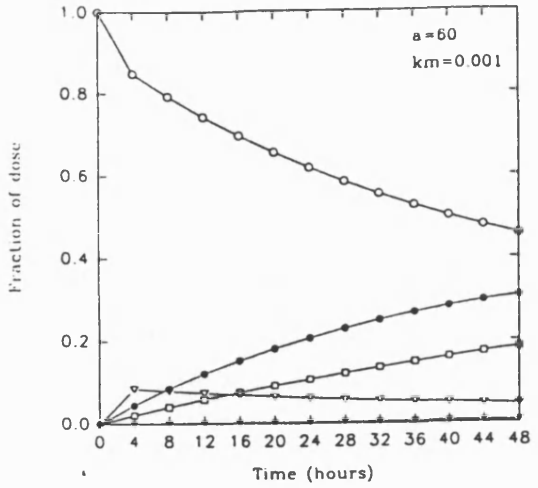

3.6B.2

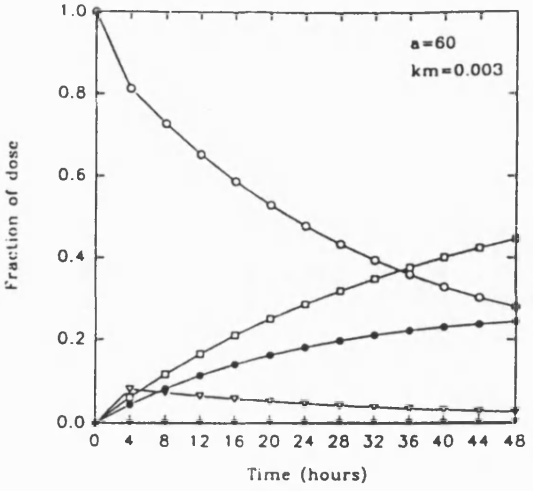

3.6B.3

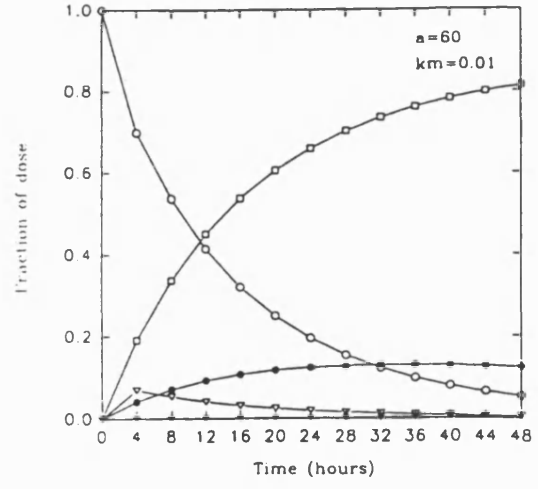

3.6B.4

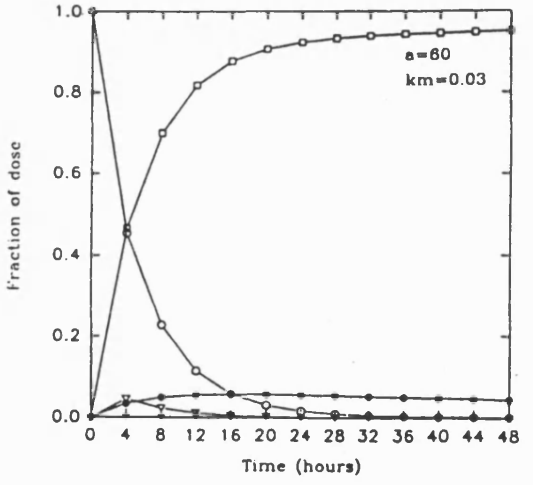

3.6B.5

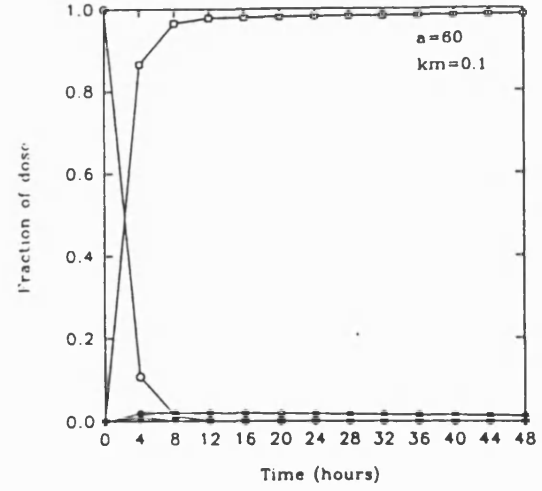

a molecular radius (Å)
Fraction of dose in:

- ○ Blood
- ● Lymph
- ▽ Liver
- ▼ Excreted
- □ Metabolised

Figures 3.7A.1-3.7A.6 and 3.7B.1-3.7B.6

The effect of molecular radius on the distribution of protein macromolecules in the body over 48 hours for k_m equal to 0.003 min^{-1} and 0.01 min^{-1} respectively

3.7A.1

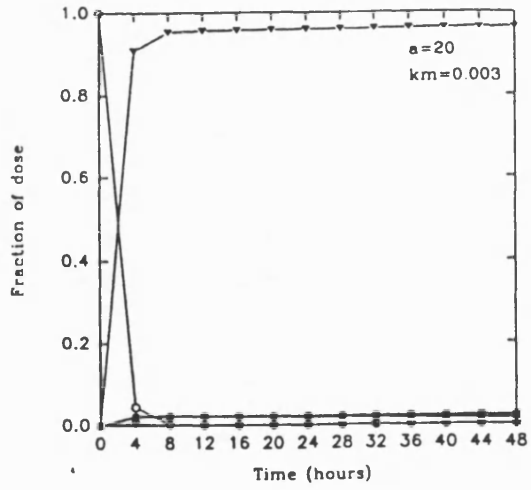

3.7A.2

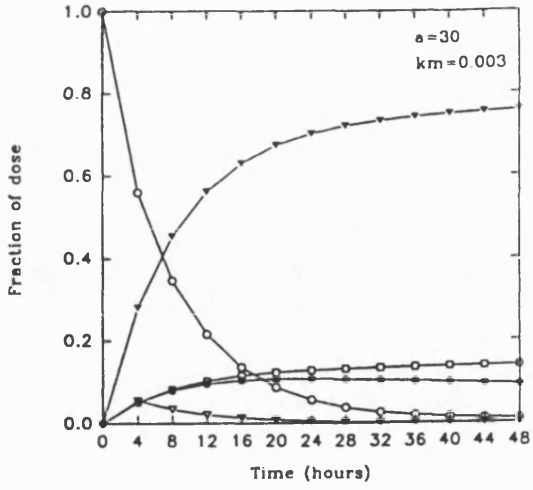

3.7A.3

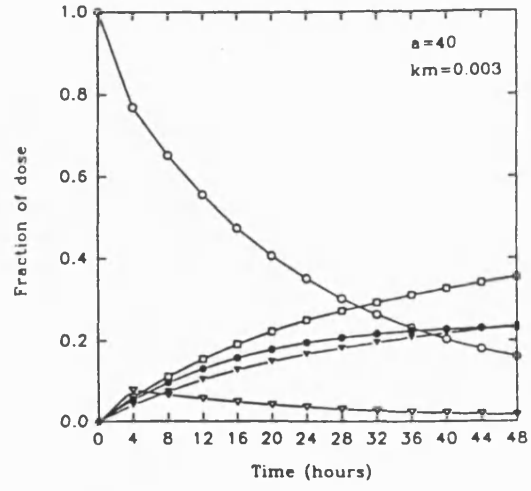

3.7A.4

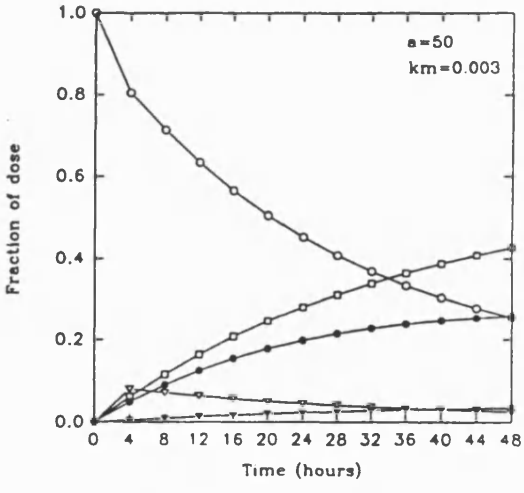

3.7A.5

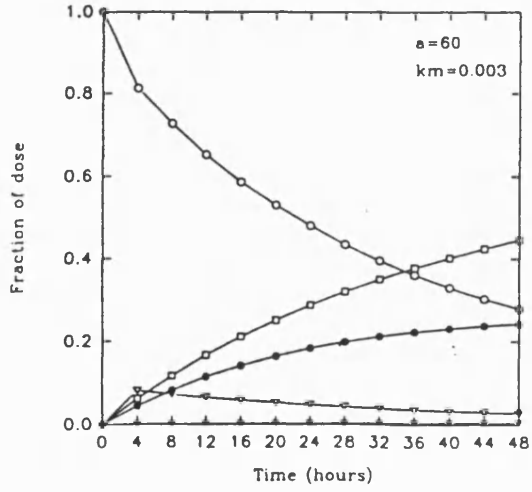

3.7A.6

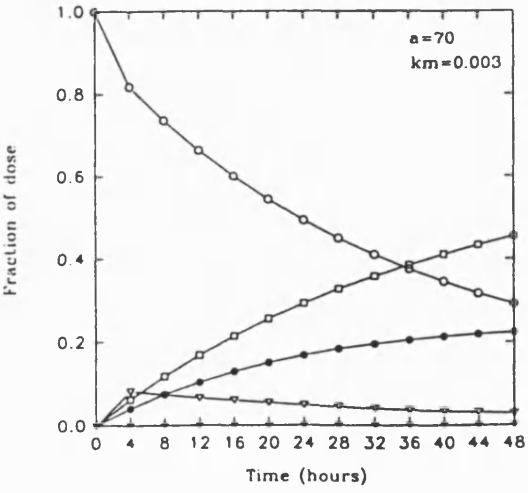

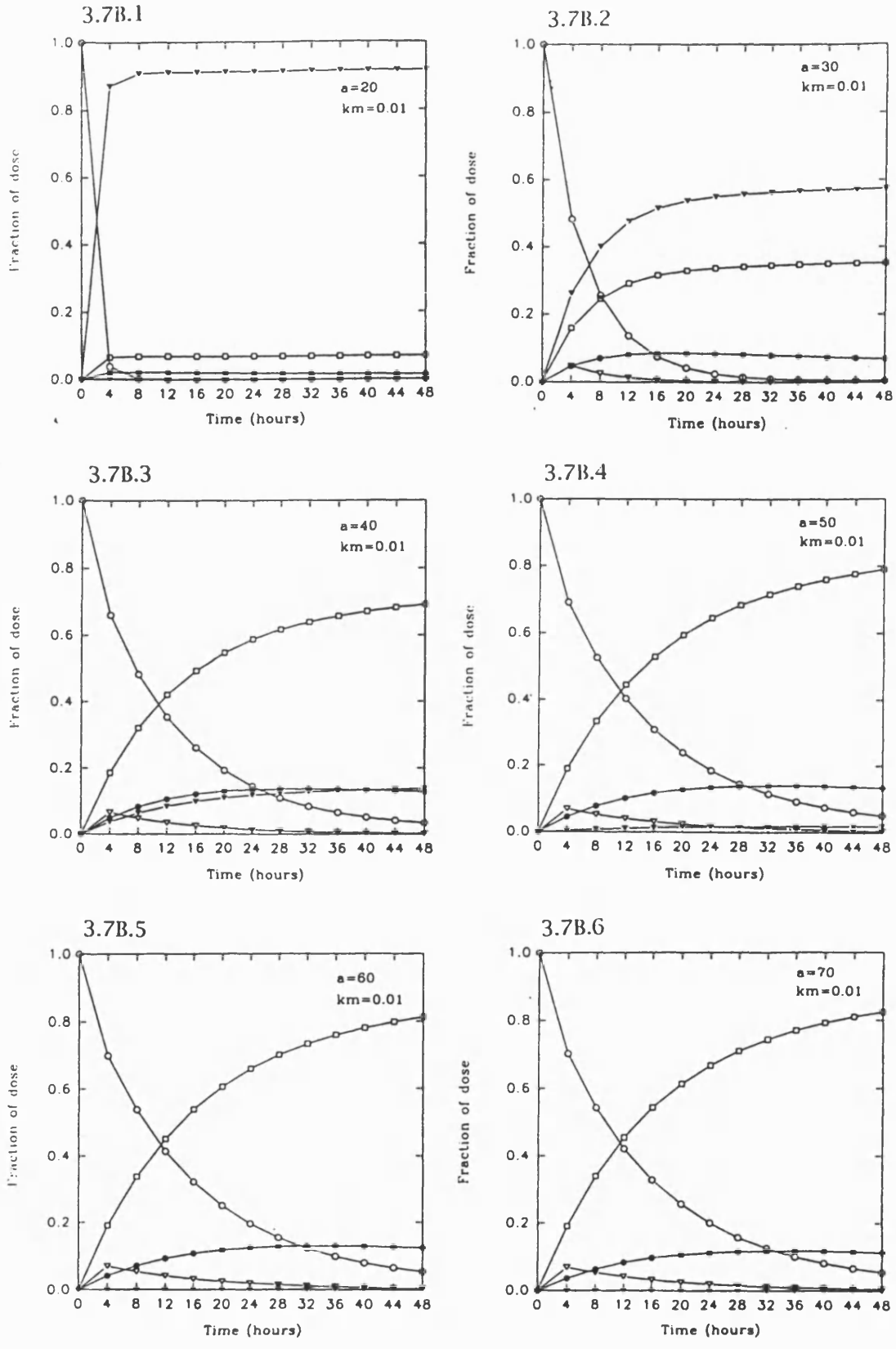

Legend as in figures 3.6A and 3.6B.

Figures 3.8A-3.8C

The effect of molecular radius on the distribution of protein macromolecules in the lymph over 240 hours for each of the three chosen k_m values.

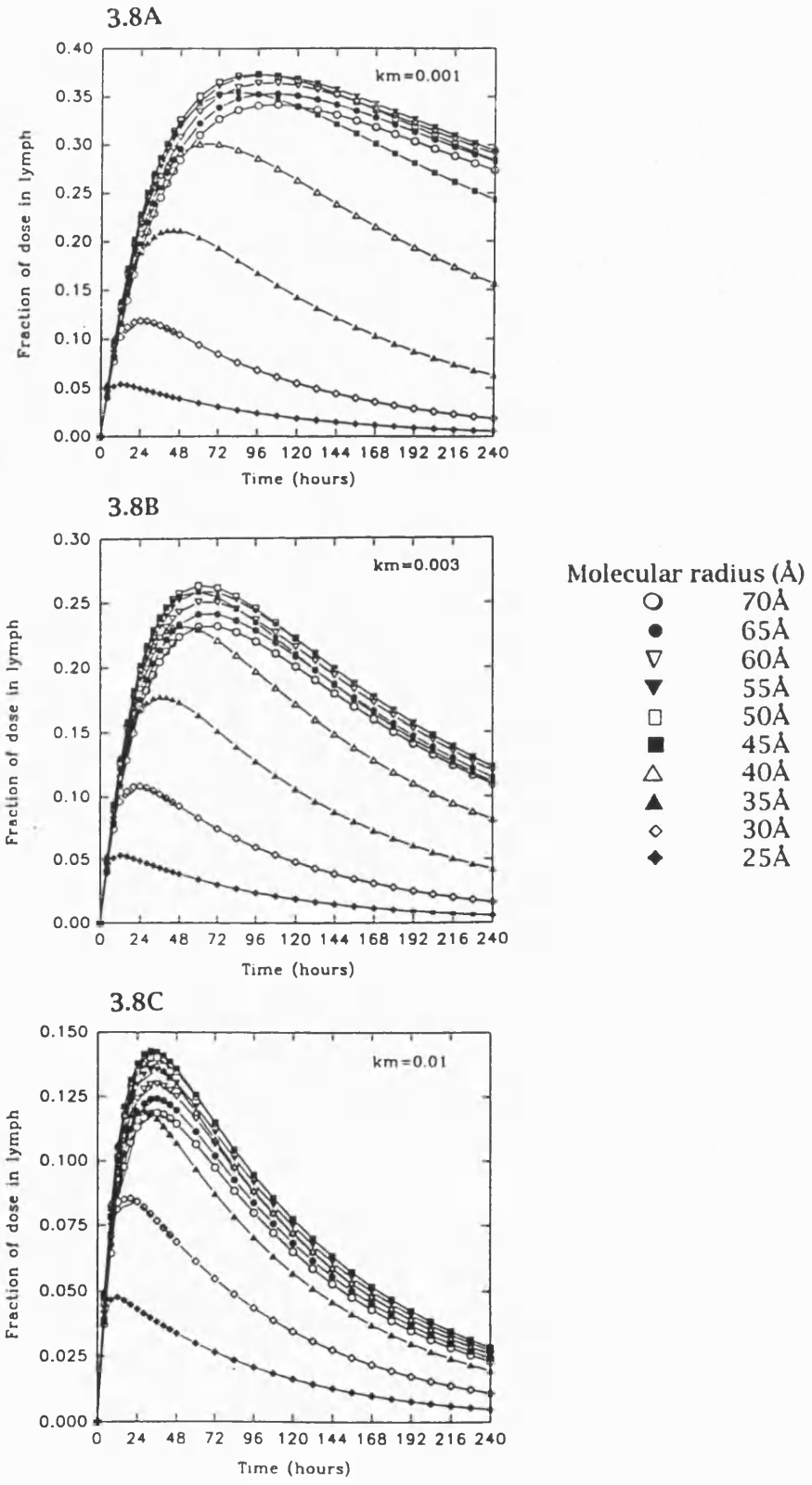

Figures 9A-9C

The effect of molecular radius on the distribution of uncharged macromolecules in the lymph over 240 hours for each of the three chosen k_m values.

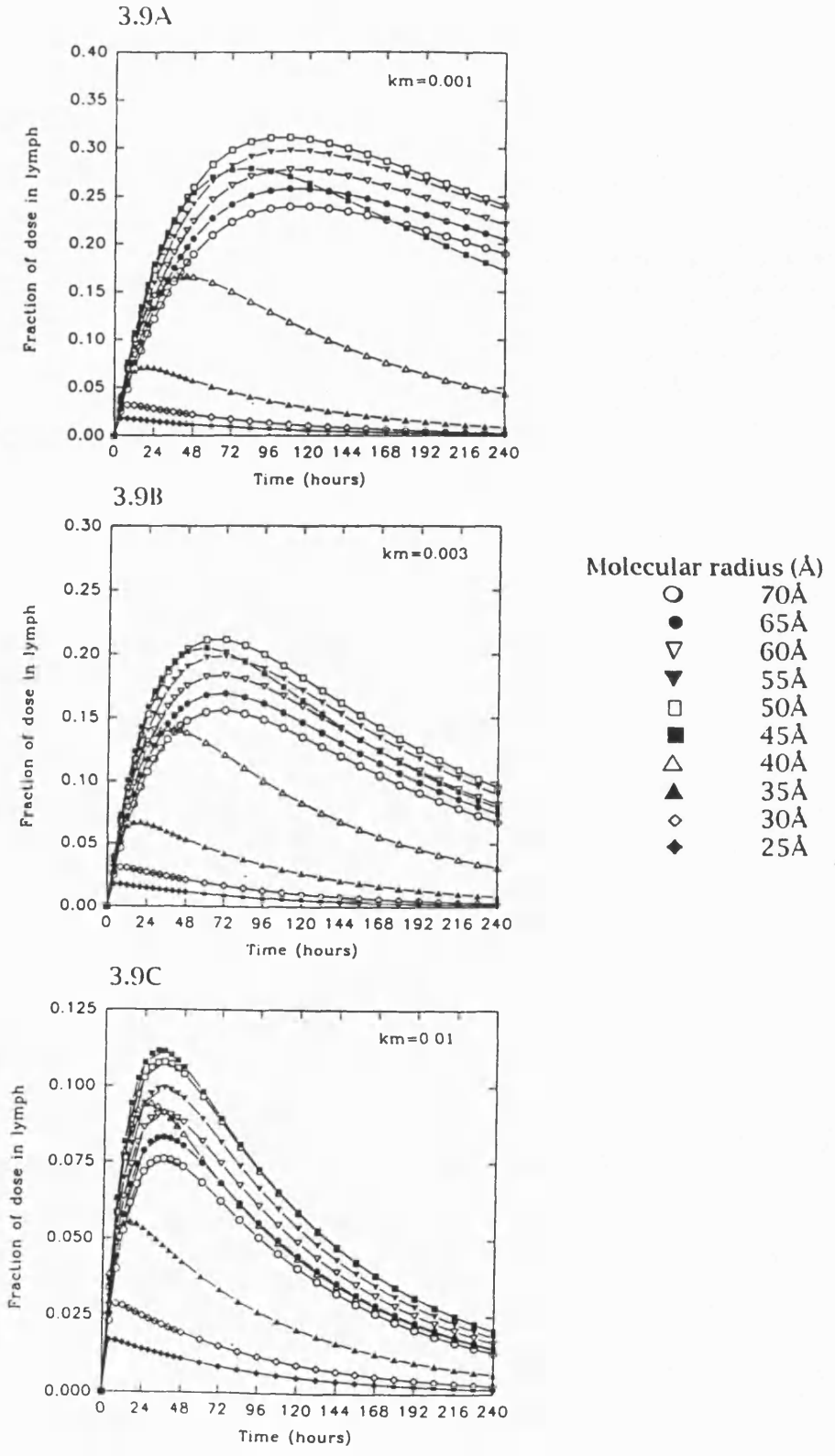

3.3.3 Conclusions

This set of simulations investigated the effect of molecular radius on the distribution of protein and uncharged macromolecules in the body in the presence of metabolism. The trends illustrated were as follows:

- Although the absolute fractions of the macromolecular drug in each of the blood, lymph and liver compartments and the fractions of the dose excreted and metabolised are different for each type of macromolecule and for each k_m rate, some general trends are evident. Increase in k_m results in a corresponding decrease in the fraction of the dose in the body overall since more drug is being eliminated. For each k_m rate as the molecular radius increases there is a corresponding increasing fraction of the dose found in each of the blood and liver compartments, as a result of the decreasing fraction of the dose being excreted. The fraction of dose reaching the lymph is influenced by the balance between extravasation and elimination, with intermediate radii producing the highest levels of lymphatic distribution.

- Although the fraction of the dose in the lymph does increase with increasing molecular radius for both macromolecule types, with increasing k_m rates resulting in a corresponding decreasing fraction of the dose in the lymph, the general trend is that it is not the largest molecular radius which produces the greatest fraction of the dose in the lymph, but is in fact the more intermediate sizes 40/45-50/55Å that do so, with the lower intermediate sizes being more successful over earlier times and at faster k_m rates, and the larger intermediate size molecular tending to become more optimal over the later times and at slower k_m rates. As the rate of metabolism increases then the actual fraction of the dose found in the lymph decreases when comparing the same molecular radii at different k_m rates. The peaks for each radius occur earlier as k_m increases (all radii for each k_m rate having reached a peak within the 240 hour period).

- A distinct group of radii 40/45-70Å produce significant fractions of the dose in the lymph for both the protein and uncharged macromolecules at each k_m rate.

- The blood half-lives increase with increasing molecular radius for both macromolecule types but decrease with each increasing k_m rate, the smallest macromolecule having the most rapid distribution and elimination phases (becoming faster as the k_m increases), and the largest macromolecule having the slowest distribution and elimination phase (becoming faster as k_m increases).

    - If protein molecular radii are compared with uncharged molecular radii of the same size for each k_m rate then the protein macromolecular drugs will always produce a greater fraction of the dose in the lymph than the uncharged macromolecular drugs.

The simulations therefore show that the general trends outlined in section 3.2 also occur in the presence of metabolism as well. They predict that for a macromolecular drug which is metabolised then the best size candidates to produce the greatest fraction of the dose in the lymph appear to be macromolecules with radii within the intermediate 40/45-50/55Å size band, with the 40/45Å sizes being more successful over earlier times, and faster k_m rates, and the larger 50/55Å sizes being the more successful over the later times and slower k_m rates. The simulations suggest that for a macromolecular drug which is metabolised very quickly then molecular radii as small as 35Å can also be effective in getting a significant fraction of the dose in the lymph at early times.

3.4 The effect of molecular radius on the distribution of the uncharged macromolecules, with and without metabolism, using the more restrictive subcutaneous skin L/P ratio parameters of best-fit.

3.4.1 Introduction

In this comparatively shorter but nevertheless important section, the effect of molecular radius on the distribution of the uncharged macromolecules using the more

restrictive subcutaneous skin L/P ratio parameters of best-fit is discussed. The purpose of this work was to determine if the trends already observed in sections 3.2 and 3.3 are repeated, and what difference, if any, results from using L/P ratio data from this different (more restrictive) tissue type. This was expected to shed light on the likely accuracy of the simulations in 3.2 and 3.3 by deliberately varying distribution parameters. As outlined in Chapter 2 the uncharged subcutaneous skin L/P ratio data [372, 373, 410] was also used here because it represented the best of the rest of the available data. Consequently the simulations in this section are performed over the same time periods as those in sections 3.2 and 3.3, with and without metabolism, also using the same k_m rates as before (0.0 min^{-1}, 0.001 min^{-1}, 0.003 min^{-1}, 0.01 min^{-1}). The parameters of best-fit and the other baseline parameters used in this section are given in table 3.2.

TABLE 3.2 **The baseline parameters used in the simulations to investigate the effect of molecular radius on the distribution of uncharged macromolecules (in the absence and presence of metabolism) using the more restrictive L/P ratio parameters of best-fit.**

D_0	1 unit (dimensionless)
k_{excr}	$GFR = 125\,\text{ml / min}$ $V_C = 5600\,\text{ml}$ and Model B with $n_{filt} = 2, ao_{filt} = 17.612, k_{filt} = 0.007333$
k_{12}	$BLFR = 2\text{ml / min}$ $V_C = 5600\text{ml}$ and Model B with $n_{lymph} = 1, ao_{lymph} = 13.092,\ k_{lymph} = 0.05492$
k_{21}	$1.78571E-4\,\text{min}^{-1}$ { $\frac{\text{Plasma}}{\text{Lymph}}$ filtration ratio $= 1$ LFR $= 2\text{ml / min}$ $V_L = 11200\text{ml}$
k_{13}	$2.57143E-1\,\text{min}^{-1}$ { $\frac{\text{Liver}}{\text{Plasma}}$ filtration ratio $= 1$ Total blood flow rate to liver $= 1440\text{ml / min}$ $V_C = 5600\text{ml}$
k_{31}	$2.57143E0\,\text{min}^{-1}$ { $\frac{\text{Plasma}}{\text{Liver}}$ filtration ratio $= 1$ Total blood flow rate from liver $= 1440\,\text{ml / min}$ $V_H = 560\,\text{ml}$
k_m	$0.0\ \text{min}^{-1}$, $0.001\ \text{min}^{-1}$, $0.003\ \text{min}^{-1}$, $0.01\ \text{min}^{-1}$

3.4.2 Results and Discussion

The raw simulated data (presented in Appendix B) for each set of simulations for each k_m rate over each time period once again showed (as in sections 3.2 and 3.3) that although the actual fractions of the dose in each of the blood, lymph and liver compartments, and the fractions of the dose excreted and metabolised are different for each k_m rate, with increasing k_m rates resulting in a decreasing fraction of the dose in the body overall, the general trend for each k_m rate was again that as the molecular radius increases there is a corresponding increasing fraction of the dose found in each of the blood, lymph and liver compartments, and a decreasing fraction of the dose being excreted. Excretion once again becomes almost insignificant at radii 55Å and greater. The more restrictive subcutaneous skin L/P ratios mean that every macromolecule, including the smaller molecular radii, are taking comparatively longer to get out of the continuous blood capillaries into the lymph, and so are more likely to be excreted or transfered into the liver to be metabolised. Hence, if we compare molecular radii in this subcutaneous skin case for each k_m rate with the corresponding same size uncharged molecular radii in sections 3.2 and 3.3 for each k_m rate, we see that in the subcutaneous skin case the fractions of the dose in the blood (and therefore the blood half-lives) are greater, the fractions of the dose in the lymph are less, the fractions of the dose in the liver are greater, and the fractions of the dose excreted and metabolised are greater. This is clearly shown if figures 3.10A-3.10D for the subcutaneous skin uncharged macromolecules with k_m=0.0 min^{-1} are compared with the corresponding figures 3.4A-3.4D in section 3.2.

Many of the features of the previous simulations were reflected here but the most important data on interstitial uptake are shown in figure 3.10 B and indeed figures 3.11 A-3.11 C and 3.12 A-3.12 C. These figures show that although the fraction of the dose in the lymph increases with increasing molecular radius size, the general trend for each k_m rate once again is that it is not the largest molecular radius which produces the greatest fraction of the dose in the lymph, but is in fact the intermediate molecular

radii 40/45-55Å. Lower intermediate sizes (including 35Å at very early times and at fastest k_m rates) are more successful over earlier times and at faster k_m rates, with the larger intermediate sizes tending to be the more successful over later times and at slower k_m rates. The clearest difference between the data produced here and that described earlier is that the access of molecules with radii greater than 55Å to the lymph is clearly more restricted emphasising the existance of an optimum radius of 45-50Å. Times to peak were similar to those generated using the lung L/P data but the absolute fractions gaining access to lymph, using skin L/P data, were considerably lower.

Figures 3.11A-3.11C in the absence of metabolism (k_m=0.0 min^{-1}) show that the fraction of the dose in the lymph has peaked for all radii less than 65Å by the end of the longest simulation period (1008 hours), with the greatest peak fraction occurring at about 288 hours for a molecular radius of 50Å (17.0% of the dose), and a molecular radius of 55Å giving the greatest fraction of the dose left there at the end of the longest time period (14.9% of the dose).

Figures 3.12A-3.12C for each k_m rate show once again that the fraction of the dose in the lymph has now peaked for all radii within the 240 hour period and that most of the peaks for the radii within the 40-70Å range (the exceptions being the 40/45Å sizes which occur earlier) again occur at about the same time for each respective k_m rate, i.e. at about 120 hours for k_m=0.001 min^{-1}, at about 72 hours for k_m=0.003 min^{-1}, and at about 36 hours for k_m=0.01 min^{-1}. Figure 3.12 A for k_m=0.001 min^{-1} shows that the greatest peak fraction of the dose in the lymph occurs for a molecular radius of 45Å at about 96 hours (10.6% of the dose) and that a molecular radius of 50Å gives the greatest fraction of the dose left there at the end of the 240 hour period (about 7.9% of the dose). Similarly figure 3.12 B for k_m=0.003 min^{-1} shows that the greatest peak fraction of the dose in the lymph occurs for a molecular radius of 45Å at about 60 hours (7.4% of the dose) and that a molecular radius of 50Å gives the greatest fraction of the dose there at the end of the 240 hour period (2.5% of the dose). Likewise, figure

3.12 C for k_m=0.01 min^{-1} shows that the greatest peak fraction of the dose in the lymph at any one time occurs for a molecular radius of 45Å at about 36 hours (3.8% of the dose) and that a molecular radius of 45Å has the greatest fraction of the dose left in the lymph at the end of the 240 hour period (0.6% of the dose).

Figures 3.10A-3.10D

The effect of molecular radius on the distribution of uncharged macromolecules in the body over 240 hours in the absence of metabolism for the more restrictive L/P ratios parameters of best-fit.

3.10A

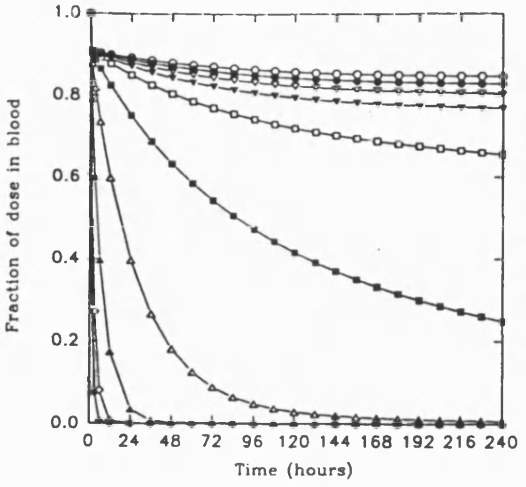

3.10B

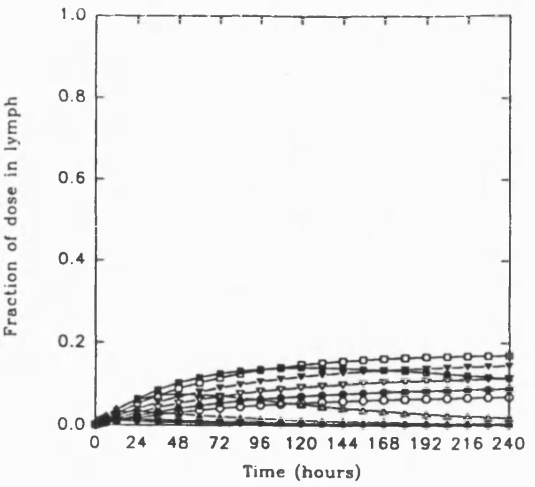

3.10C

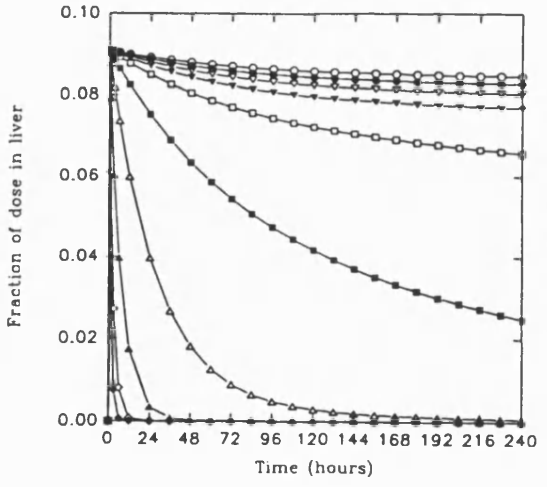

3.10D

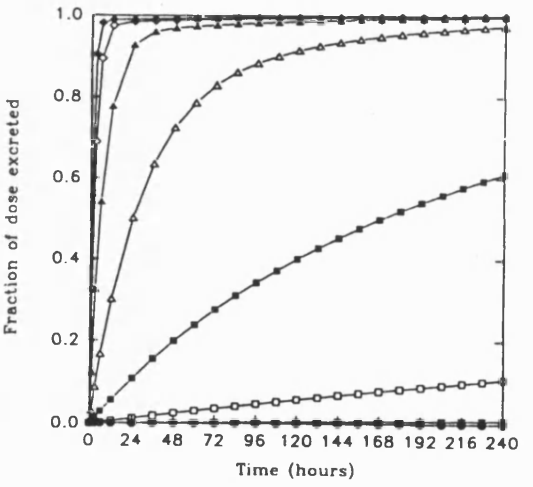

Molecular radius (Å)

○	70Å
●	65Å
▽	60Å
▼	55Å
□	50Å
■	45Å
△	40Å
▲	35Å
◇	30Å
◆	25Å

Figures 3.11A-3.11C

The effect of molecular radius on the distribution of uncharged macromolecules in the lymph over 48 hours, 240 hours and 1008 hours respectively, in the absence of metabolism for the more restrictive L/P ratio parameters of best-fit.

3.11A

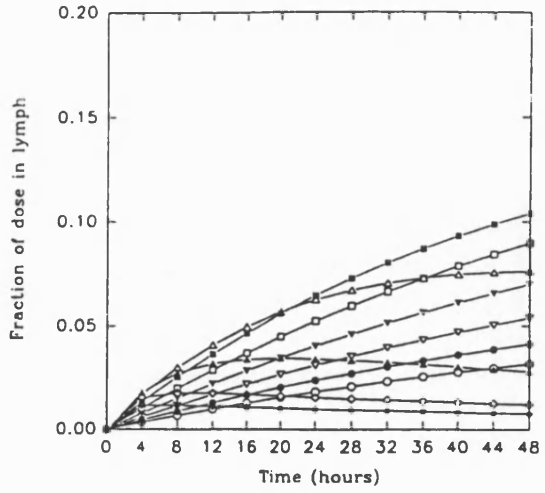

3.11B

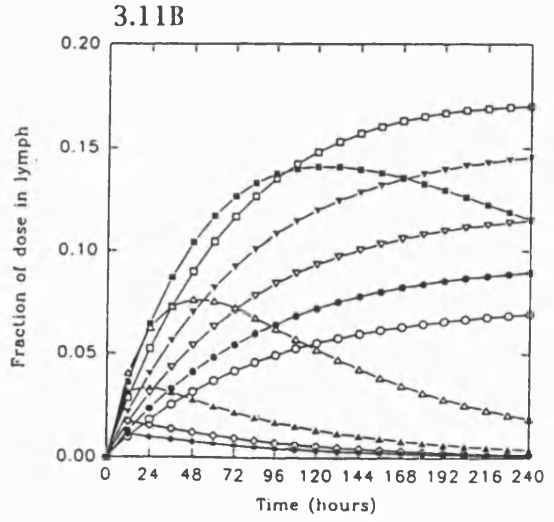

Molecular radius (Å)

○	70Å
●	65Å
▽	60Å
▼	55Å
□	50Å
■	45Å
△	40Å
▲	35Å
◇	30Å
◆	25Å

3.11C

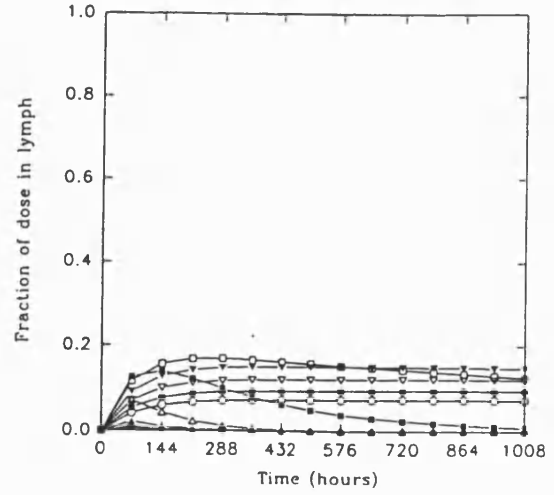

Figures 3.12A-3.12C

The effect of molecular radius on the distribution of uncharged macromolecules in the lymph over 240 hours for each of the three k_m values for the more restrictive L/P ratio parameter of best-fit.

3.12A

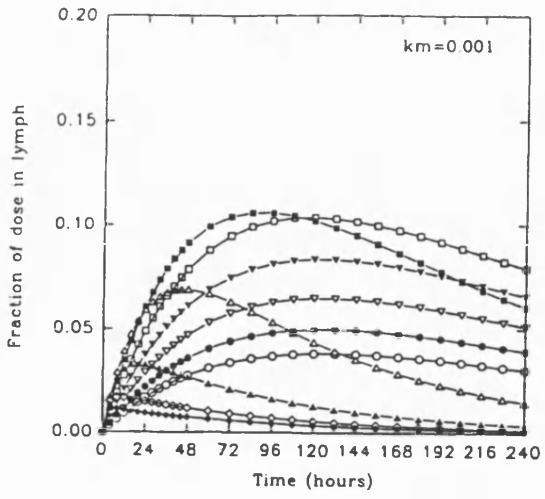

3.12B

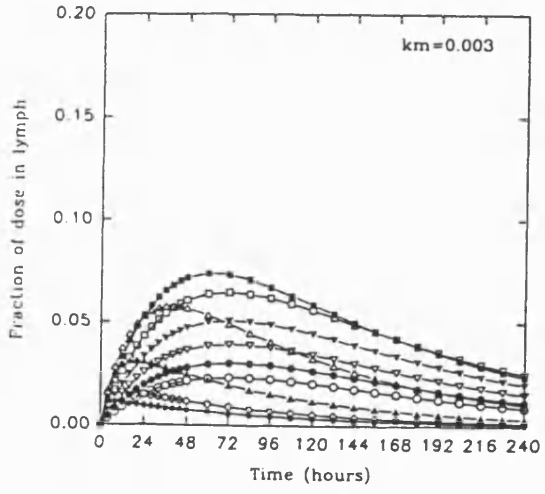

Molecular radius (Å)

○	70Å
●	65Å
▽	60Å
▼	55Å
□	50Å
■	45Å
△	40Å
▲	35Å
◇	30Å
◆	25Å

3.12C

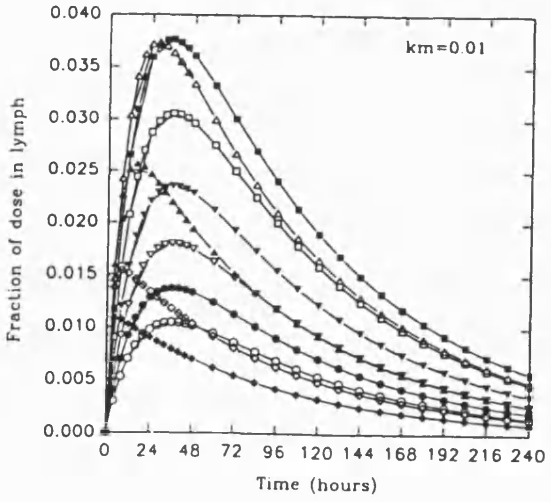

3.4.3 Conclusions

The more restrictive L/P ratios such as those from the subcutaneous skin clearly result in comparatively less of the macromolecular drug dose reaching the lymph compared with the less restrictive (more permeable) L/P ratios from the lung as used in sections 3.2 and 3.3. However, all the same trends as outlined in sections 3.2 and 3.3 are once again also repeated in this the more restrictive L/P ratio case, with the simulations once again predicting that it is the intermediate size molecular radii 40/45-55Å (including 35Å at very early times and fast k_m rates) which will produce the greatest fraction of the macromolecular drug dose in the lymph. Once again the lower intermediate size molecular radii appear to be the more successful over earlier times and at faster k_m rates, with the larger intermediate size molecular radii tending to become more successful over later times and at slower k_m rates.

3.5 Conclusions

The best size macromolecular drugs to produce the greatest fraction of the dose in the lymph are macromolecules with radii within the 40/45-50/55Å intermediate size range, with the lower intermediate sizes appearing to be the more successful over earlier times and at faster k_m rates, and the larger intermediate sizes appearing to be the more successful over later times and at slower k_m rates. For a macromolecular drug which is metabolised very quickly, even molecular radii as small as 35Å can be relatively effective at early times. Protein macromolecular drugs are better than uncharged macromolecular drugs. In the case of protein macromolecules which are not subject to metabolism significant tissue uptake will occur with sizes up to 65Å radius over very long time periods. Hence, if you are lucky enough to know roughly how quickly a particular macromolecular carrier or macromolecular drug system is metabolised, then the choice of size may depend upon whether you want a macromolecular carrier or macromolecular drug system within this intermediate size range which gets into the lymph relatively quickly but does not produce the greatest fraction of the dose there

possible and does not stay there so long, or one that takes a bit longer to get there, but once there produces a greater fraction of the dose there and stays there longer.

Chapter 4

Use of the physiological model to interpret experimental data

4.1 Introduction

The aim of this chapter is to illustrate how the model presented in this study can be used for fitting purposes. It shows how the model can be used to generate or predict the tissue distribution of macromolecules and the role of the two major elimination processes (renal excretion and hepatic clearance), following the fitting of experimental data on plasma clearance of macromolecules. In so doing, this chapter therefore also serves as another justification and validation of the work presented in this study.

The selection of the data used to illustrate this application of the model is described in section 4.2. The selection of appropriate scaled baseline parameters and the methods used to perform the fitting of the model to the selected data are also discussed in that section. In section 4.3 the results from fitting experiments are presented. Section 4.4 then presents some general remarks.

4.2 Methods

4.2.1 Selection of data to be used

Before any fitting could be performed, the first task was to select appropriate macromolecular drug distribution data from the literature. The desired data to which the model could be fitted would ideally consist of many plasma concentration versus time data points for several different size macromolecules for man. It would also be very useful if other disposition data were also available for other key compartments of the body such as the lymph or the liver, or for the two major elimination processes, (renal excretion and hepatic clearance), so that other comparisons between observed and predicted data could also be made. Preferably the data would also be expressed in terms of the fraction of the dose or percent of the dose in each tissue or eliminated as well. However, most of the macromolecular drug disposition data currently available is for animals rather than humans, and often consists of only a few plasma concentration versus time data points or a plasma concentration versus time plot without any published data. Little data are available on tissue distribution to each compartment

(blood, lymph and liver) or the two major elimination processes (renal excretion and hepatic clearance). The situation is not helped by the comparative novelty of the use of targeted macromolecular drug systems in chemotherapy, particularly with regard to passively-targeted macromolecular systems, since many of these have not reached full clinical trial stages yet. Consequently, for the fitting experiments described in this chapter it was decided to use (with permission) data for intravenous administration into male wistar rats, of five radiolabelled Bovine Serum Albumin-Methotrexate (BSA-MTX) conjugates recently described in a colleague's thesis [442]. These data comprise of many plasma concentration versus time data points, is in a usable form, and is more complete than most of the data currently available in the other literature. The five BSA-MTX conjugates selected were designated as BSA-MTX (5.1 % w/w), BSA-MTX (11.74% w/w), BSA-MTX (11.76% w/w), BSA-MTX (13.63% w/w) and BSA-MTX (13.64% w/w), where the figures in parentheses refer to the weight concentration of MTX. It was decided to pool the data for the BSA-MTX (11.74% w/w) conjugate with the data for the BSA-MTX (11.76% w/w) conjugate since these conjugates were virtually the same. Similarly, the plasma concentration versus time data for the BSA-MTX (13.63% w/w) and BSA-MTX (13.64% w/w) conjugates were pooled. Data from the same thesis [442] on i.v. administration of other radiolabelled proteins into male wister rats was also used; namely free bovine serum albumin, lactalbumin, carbonic anhydrase and chicken egg albumin. The data for the BSA-MTX (5.1% w/w) conjugate, the pooled BSA-MTX (11.74% w/w) and BSA-MTX (11.76% w/w) conjugates, and the pooled BSA-MTX (13.63% w/w) and BSA-MTX (13.64% w/w) conjugates , is presented in tables 4.1 - 4.3 respectively. The data for the free bovine serum albumin, lactalbumin, carbonic anhydrase and chicken egg albumin is presented in tables 4.4 - 4.7 respectively. Each data set has been transformed into the form most useful for this study. Consequently plasma concentration is expressed as the fraction of dose per ml of plasma.

Table 4.1 BSA-MTX (5.1% w/w) conjugate plasma concentration versus time data

Time (hours)	i.v. plasma concentration (fraction of dose/ml)
1	6.933E-2
1	9.007E-2
3	5.899E-2
3	4.129E-2
5	4.757E-2
5	3.775E-2
7	2.934E-2
7	3.335E-2
23.5	0.678E-2
23.5	0.737E-2
30.5	0.572E-2
30.5	0.590E-2
48	0.230E-2
48	0.275E-2
52.5	0.234E-2
52.5	0.236E-2
55	0.179E-2
55	0.174E-2
71.75	0.0989E-2
71.75	0.126E-2
97.5	0.0604E-2
97.5	0.0824E-2

Table 4.2 **Pooled BSA-MTX (11.74% w/w) and BSA-MTX (11.76% w/w) conjugate plasma concentration versus time data**

BSA-MTX (11.74% w/w)		BSA-MTX (11.76% w/w)	
Time (hours)	i.v. Plasma Concentration (fraction of dose/ml)	Time (hours)	i.v. Plasma Concentration (fraction of dose/ml)
1	2.955E-2	1	6.266E-2
1	2.089E-2	1	6.389E-2
3	0.584E-2	2	2.906E-2
3	0.498E-2	2	3.311E-2
6.75	0.329E-2	4	1.472E-2
6.75	0.297E-2	4	0.888E-2
19	0.116E-2	7	0.531E-2
19	0.108E-2	7	1.099E-2
24	0.0821E-2	24.5	0.449E-2
24	0.0924E-2	24.5	0.308E-2
30.5	0.121E-2	30.75	0.295E-2
30.5	0.129E-2	30.75	0.324E-2
48	0.0506E-2	48	0.187E-2
48	0.0713E-2	48	0.187E-2
54.5	0.0494E-2	52.5	0.176E-2
54.5	0.0303E-2	52.5	0.164E-2
71.75	0.0319E-2	71.5	0.107E-2
71.75	0.0215E-2	71.5	0.111E-2
76	0.0331E-2	79	0.103E-2
76	0.0182E-2	79	0.110E-2
96	0.0402E-2	96	0.0741E-2
96	0.0142E-2	96	0.0579E-2
		100	0.0801E-2
		100	0.0667E-2

Table 4.3 **Pooled BSA-MTX (13.63% w/w) and BSA-MTX (13.64% w/w) conjugate plasma concentration versus time data**

BSA-MTX (13.63% w/w)		BSA-MTX (13.64% w/w)	
Time (hours)	i.v. Plasma Concentration (fraction of dose/ml)	Time (hours)	i.v. Plasma Concentration (fraction of dose/ml)
0.75	6.921E-2	1	2.558E-2
0.75	5.919E-2	1	1.614E-2
3	5.998E-2	3	0.668E-2
3	5.784E-2	3	0.634E-2
4.75	1.351E-2	5	0.552E-2
4.75	1.730E-2	5	0.535E-2
7.5	0.499E-2	8	0.424E-2
7.5	0.562E-2	8	0.436E-2
18.5	0.198E-2	23	0.160E-2
18.5	0.184E-2	23	0.177E-2
19	0.173E-2	26.5	0.154E-2
29	0.117E-2	26.5	0.183E-2
29	0.106E-2	31.75	0.124E-2
43	0.0735E-2	31.75	0.197E-2
43	0.0637E-2	48	0.0791E-2
48	0.0725E-2	48	0.0959E-2
48	0.0541E-2	49.5	0.0712E-2
67.5	0.0471E-2	49.5	0.0793E-2
67.5	0.0625E-2	54	0.0899E-2
78.75	0.0443E-2	54	0.102E-2
78.75	0.0532E-2	71	0.0508E-2
94	0.0362E-2	71	0.0564E-2
94	0.0283E-2	79.5	0.0558E-2
96	0.0446E-2	79.5	0.0692E-2
96	0.0397E-2	96	0.0375E-2
		96	0.0353E-2
		97	0.0416E-2
		97	0.0374E-2

Table 4.4 BSA plasma concentration versus time data

Time (hours)	i.v. Plasma Concentration (fraction of dose/ml)
0.75	8.899E-2
1	7.556E-2
1	7.925E-2
3	6.685E-2
3	5.702E-2
6	4.548E-2
6	4.841E-2
23.5	2.077E-2
23.5	1.935E-2
31	1.652E-2
31	1.409E-2
48	0.755E-2
48	0.935E-2
54.25	0.589E-2
54.25	0.617E-2
72	0.351E-2
72	0.317E-2
79.5	0.265E-2
79.5	0.315E-2
97	0.244E-2
97	0.219E-2

Table 4.5 Lactalbumin plasma concentration versus time data

Time (hours)	i.v. Plasma Concentration (fraction of dose/ml)
0.25	1.0992E-2
0.25	1.205E-2
0.5	1.041E-2
0.5	1.104E-2
1	0.852E-2
1	0.839E-2
2	0.659E-2
2	0.534E-2
3	0.493E-2
3	0.391E-2
4	0.412E-2
4	0.467E-2
6	0.350E-2
6	0.362E-2
8	0.302E-2
8	0.319E-2
10	0.237E-2
10	0.270E-2
25	0.243E-2
25	0.173E-2
28	0.201E-2
28	0.139E-2
31.5	0.125E-2
31.5	0.113E-2
47.5	0.076E-2
47.5	0.087E-2
55	0.094E-2
55	0.103E-2
72	0.046E-2
72	0.037E-2

Table 4.6 Carbonic anhydrase plasma concentration versus time data

Time (hours)	i.v. Plasma Concentration (fraction of dose/ml)
1	0.980E-2
1	0.948E-2
2	0.906E-2
2	0.972E-2
4	0.640E-2
4	0.675E-2
6	0.704E-2
6	0.578E-2
10	0.431E-2
10	0.488E-2
18.75	0.298E-2
18.75	0.271E-2
21	0.263E-2
21	0.284E-2
24	0.238E-2
24	0.211E-2
30.75	0.255E-2
30.75	0.232E-2
48	0.0841E-2
48	0.106E-2
55.5	0.124E-2
55.5	0.097E-2
72	0.0653E-2
72	0.0667E-2
97.5	0.0437E-2
97.5	0.0392E-2

Table 4.7 Chicken egg albumin plasma concentration versus time data

Time (hours)	i.v. Plasma Concentration (fraction of dose/ml)
0.5	2.377E-2
1	0.896E-2
2	0.330E-2
4	0.213E-2
6	0.151E-2
24	0.087E-2

Having selected the data, the next step was to decide upon a strategy to perform the fitting, and to scale the physiological parameters from humans to values representing rats.

4.2.2. The fitting strategy

One of the most logical and sensible ways to fit the model to any experimental data would be to fit the equation describing plasma concentration versus time (equation 20 given in chapter 2) to the selected plasma clearance data, varying k_m to establish the most appropriate rate of hepatic clearance whilst keeping all the other parameters fixed. However, to use Minsq [441] or similar curve-fitting programmes to perform this operation would be inappropriate. This is due to the form of the model, i.e. the number of compartments and the number of compartmental processes, and also because the roots γ, α, β describing the solution to the model depend upon the relationship between k_{12}, k_{21}, k_{13}, k_{31}, k_{excr} and k_m, with each of these in turn depending upon their assigned baseline values. In addition k_{12} and k_{excr} also depend upon the particular molecular radius of the macromolecule. To use regression with only k_m entered as a varying parameter in equation 20 with γ, α and β kept at fixed values, or indeed to use regression with k_m and/or any of the baseline parameters entered as varying parameters whilst keeping γ, α and β at fixed values, would be inappropriate because then γ, α and β would be taking one independent fixed value each instead of taking values which depended upon the relationship between k_{12}, k_{21}, k_{13}, k_{31}, k_{excr} and k_m, or upon the designated physiological baseline parameter values. Similarly, to enter γ, α and β as varying parameters themselves either instead of, or as well as k_m and/or any baseline parameters would be inappropriate, because γ, α and β would then be taking values which were independent of the relationship between k_{12}, k_{21}, k_{13}, k_{31}, k_{excr} and k_m, and of the designated physiological baseline parameter values. The way forward was therefore to simulate plasma concentration using MACROHOURS for different k_m rates whilst keeping all other baseline parameters fixed at their assigned values. The predicted data were then printed out or imported into a plotting programme such as

Sigmaplot and observed in plot form on screen, or both, to establish the best choice of k_m to fit the selected plasma concentration versus time data. Once this k_m rate was established, it was then re-entered into MACROHOURS with the other baseline parameters, and simulations were performed over any desired time interval to predict the fraction of the dose expected to be found in each of the blood, lymph and liver, and also the fractions of the dose renally excreted and hepatically cleared (and the total fraction of the dose eliminated).

4.2.3. Selection of scaled baseline parameters

Before any fitting to equation 20 could be performed, baseline parameters first had to be scaled from their human values to values appropriate to the animal species of interest. Before describing which baseline parameters were used for the rat, it is appropriate to make some general comments about animal scaling.

There are many similarities in the anatomy and physiology of mammalian species. A general belief in this similarity has been the cornerstone of most biomedical research. All mammals share a remarkable geometric similarity. One general blood flow diagram for example could be used for several mammals, many organs and tissues are similar fractions of the body weight, and many volumes of distribution tend to be proportional to weight across species [443]. Indeed, it has been shown that some anatomical and physiological properties can in fact be correlated among mammals as exponential functions of body weight [444]. Some physiological processes vary as the 0.7 - 0.8 power of body weight; anatomic variables show a near first-degree dependence on body-weight [444]. Hence the physiological function per unit of organ weight or per unit of animal weight generally decreases as body size increases [443], (though several exceptions to this trend no doubt also exist as well). Consequently for results from any study involving scaling to be realistic, appropriate time scaling also needs to be taken into account, and this is usually done automatically when various model parameters are assigned the appropriate scaled baseline values. Major qualitative differences such

as the absence of a gallbladder in some species are the exception [443]. The two processes which influence scale among animal species are physical processes and chemical processes [443, 445]. The physical processes such as blood flows, organ volumes, tissue binding, kidney clearance etc, often vary 'comparatively' predictably among mammalian species [443, 445], and some information independent of any biochemical reactions is often available from experimental studies in the literature about these. In some very general situations it has in fact been reported that purely physical interactions of exogenous chemicals with biological tissues and fluids are expected not to show a great variation among species [443], and there is often better than order magnitude in many tissues, with the liver exhibiting the greatest discrepancy. Chemical processes on the other hand, such as metabolic reactions, vary greatly and unpredictably among species [443, 445]. Indeed, the most significant species differences that may confound pharmacokinetic predictability are in the qualitative pathways and kinetic characteristics of metabolism [443], and over the years several studies have been conducted in simple systems to investigate the effect of metabolism of molecules (usually small molecules) on inter-species scaling (reviewed by references [443, 445]). The unpredictability is because, in reality, foreign organic compounds actually tend to be metabolised in two phases [443, 446]. Phase I reactions leading to oxidation, reduction and hydrolysis products, whilst phase II reactions leading to synthetic or conjugation products that are relatively polar and thus more easily excreted by the kidneys in the urine, and in some cases by the liver in the bile. Within this general framework there are also large species variations, and it has in fact been observed that Phase I reactions are relatively common and often very unpredictable [446], whilst Phase II reactions are more limited in number than Phase I reactions but it may be possible to identify some patterns of these [446]. Humans are believed to usually metabolise drugs less rapidly than other smaller animals [447, 448]. Each of these factors therefore plays an influencing role, although to try and model or predict the two phases of metabolism as processes in their own right is obviously an extremely difficult task to accomplish. Most models are necessarily forced to either

include metabolism within one single general elimination process (occurring from the plasma), not represent it at all, or at best, represent it as an individual first-order loss process occurring somewhere from the model. The situation when considering any scaling is further complicated by the fact the physical and chemical processes interact so that the relationship of the pharmacokinetics of any given drug between one species and another may be relatively straightforward, or alternatively it may be rather obscure [445]. The relationship is more straightforward for drugs which are not metabolised since then all interactions are physical and there are no chemical processes involved. There are several good reviews in the literature describing most of the different studies and approaches which have been used in investigations of interspecies scaling [443, 445]. To date however more work is necessary before the problem of inter-species scaling can be fully understood, and there is no standard rule or method to be used or to say how it should be done. Recent allometric techniques are interesting [449], although these are generally more appropriate for small molecules eliminated soley by physical processes. More work is therefore needed in the area, before the similarities and differences underlying the distribution and elimination of molecules in different species can be fully appreciated. It appears that the clearances and distributions of molecules, particularly macromolecules, follow well-defined, size-related physiological relationships, (as illustrated by the F/P ratio and L/P ratio data described and discussed in chapter 2 and the associated models developed in this study to model this data), and that preclinical pharmacokinetic data are a good indicator of human pharmacokinetics.

For the fitting demonstrations described in this chapter the following scaled baseline parameters were used for the rat (250g male wistar rat):

(i) Volume of blood (V_C) = 12ml

This value was available in the literature [450].

(ii) Volume of lymph (V_L) = 40ml

This value represents 16% of 250g, i.e. the same percentage of body weight of total interstitial fluid (lymph) as for humans is assumed.

(iii) Volume of blood in the liver (V_H) = 1.2ml

This value represents 10% of 12ml, i.e. the blood volume of the liver is assumed to be the same percentage of the total blood volume as it is for humans.

(iv) Blood to lymph flow rate (BLFR) = Lymph to blood flow rate (LFR) = 0.00714 ml/min

These values are assumed to be the same fraction of lymph flow rate per volume of total interstitial fluid (lymph) as for humans, i.e. 1.785×10^{-4} per min

(v) Blood flow rate from the liver = Blood flow rate to the liver = 8.0 ml/min

This value was estimated from Knaak et al [451].

(vi) Glomerular Filtration Rate (GFR)

For this parameter it was difficult to assign a value since values quoted in the literature varied quite considerably between rats with different and similar body weights, e.g [326]. Therefore, it was decided to obtain the most realistic rate of GFR by fitting the equation describing plasma concentration versus time (equation 20) with k_m=0.0 min^{-1} (i.e. no hepatic clearance) to the free BSA plasma concentration versus time data, presented in table 4.4. For this fit, the scaled baseline parameters given in parts (i) - (v) were used along with the usual model baseline parameters which did not require scaling, ie Model B with n_{filt}=1, ao_{filt}=17.486, k_{filt}=0.20941, n_{lymph}=1, ao_{lymph}=13.558 and k_{lymph}=0.010454 for protein macromolecules, the dose D_0 set to unity, and the plasma/lymph filtration ratio, the liver/plasma filtration ratio, and the plasma/liver filtration ratio each also set equal to unity (free-filtration). The molecular radius of BSA is

well quoted in the literature as being 37Å [442], so this radius was used. The free BSA plasma concentration versus time data were chosen to establish the most appropriate rate for the GFR parameter because the main fitting demonstrations described in this chapter were to the BSA-methotrexate conjugates, and also the size of this protein macromolecule (radius of 37Å) meant it was less likely to be renally excreted so quickly or bind to any plasma proteins in vivo so easily as the other selected smaller free protein macromolecules, i.e. the lactalbumin, carbonic anhydrase and the chicken egg albumin. Figures 4.1A and 4.1B show the fit of equation 20 to the free BSA data using these baseline parameters with k_m=0.0 min^{-1} and GFR varying between 0.3-0.6 ml/min.

Figures 4.1A and 4.1B show that the best choice of value for the GFR appears to be GFR=0.5 ml/min and consequently this value was selected to be used for the fitting demonstrations described in section 4.3.

The set of baseline parameters to be used for the rat data are now complete, and these are summarised in table 4.8.

Figures 4.1A and 4.1B Fit to the BSA plasma concentration versus time data with k_m = 0.0min^{-1} and varying rates of glomerular filtration

Figure 4.1A (linear scale)

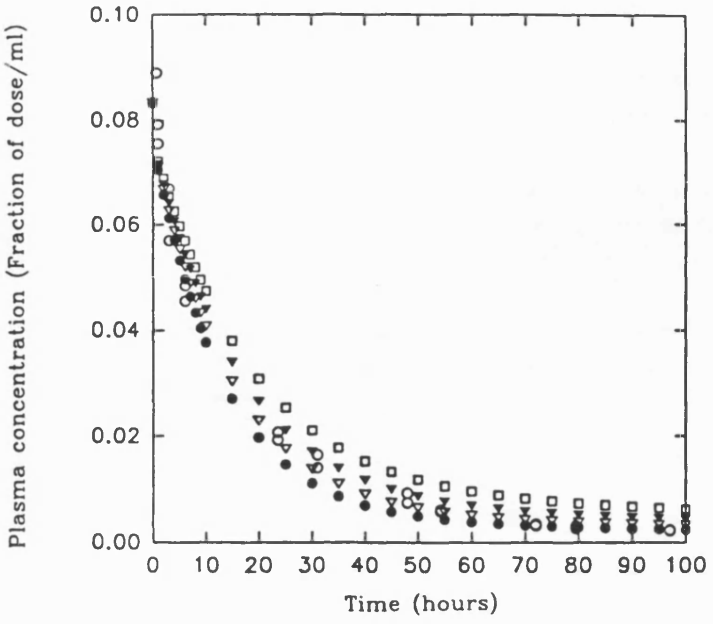

Figure 4.1B (log_{10} scale

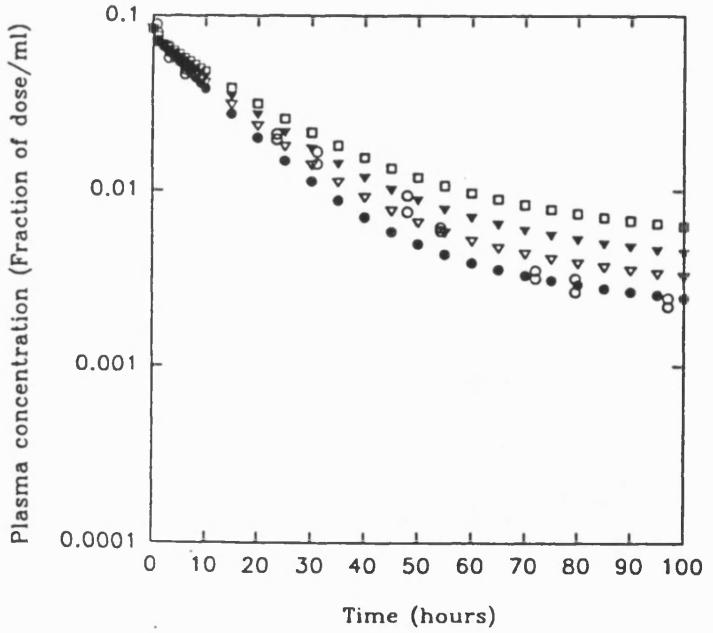

○ Observed BSA data

Predicted data

● GFR = 0.6ml/min

▽ GFR = 0.5ml/min

▼ GFR = 0.4ml/min

□ GFR = 0.3ml/min

Table 4.8 **Baseline parameters used in the fitting of the model to rat protein macromolecules and BSA-MTX conjugate data.**

D_0	1 unit (dimensionless)
k_{excr}	GFR = 0.5 ml / min V_c = 12 ml and Model B with $n_{filt} = 1$, $ao_{filt} = 17.486$, $k_{filt} = 0.20941$ for protein macromolecules
k_{12}	BLFR = 0.00714 ml / min V_c = 12 ml and Model B with $n_{lymph} = 1, ao_{lymph} = 13.558, k_{lymph} = 0.010454$ for protein macromolecules
k_{21}	$1.785E-4$ min^{-1} { $\frac{\text{plasma}}{\text{lymph}}$ filtration ratio = 1 LFR = 0.00714 ml / min V_L = 40ml
k_{13}	$6.67E-1$ min^{-1} { $\frac{\text{liver}}{\text{plasma}}$ filtration ratio = 1 Total blood flow rate to liver = 8.0 ml / min V_c = 12 ml
k_{31}	$6.67E0$ min^{-1} { $\frac{\text{plasma}}{\text{liver}}$ filtration ratio = 1 Total blood flow rate from liver = 8.0 ml / min V_H = 1.2 ml

What remains to be specified is the molecular radius of the macromolecule of interest. For some macromolecular drugs or macromolecular drug conjugate systems, the molecular size of the particular macromolecule or macromolecular conjugate system will already be known in terms of its molecular radius. For other macromolecular systems however, the molecular size may only be given or known in terms of its molecular weight. For these latter systems the molecular radius needs to be calculated or estimated from the known molecular weight. This can generally be achieved by using one of the following two methods:

Method A

By using the formulae for the volume of a sphere, i.e. $V = \frac{4}{3}\pi r^3$, and the well known relationship Density (ρ) = $\frac{\text{Mass (mw)}}{\text{Volume}}$, to obtain the expression ,

$$\text{molecular radius} \approx \sqrt[3]{3mw/4\pi\rho} \qquad 4.1$$

Therefore by using a macromolecular drug whose mass (molecular weight, *mw*) and molecular radius are well known in the literature, e.g. free BSA (*mw* 66296Da, radius 37Å), an approximate general value for the density can be estimated (e.g. density (ρ) $\approx$ 0.3 g / cm^3 for free BSA), and this general density value along with the mass of the particular macromolecular drug or macromolecular drug conjugate system can then be entered into equation 4.1 to give an approximate molecular radius size for a set of related molecules. For the free lactalbumin, carbonic anhydrase and chicken egg albumin used for some of the fitting demonstrations described in this chapter, each had an unknown molecular radius which was estimated using this method, with the density assumed to be equal to 0.3 g/cm^3. The estimated molecular radius using this method for the lactalbumin (mw 14200Da) was found to be approximately 22Å , the estimated molecular radius for the carbonic anhydrase (mw 29000Da) was found to be approximately 28Å , and the molecular radius for the chicken egg albumin (mw 45000Da) was found to be approximately 33Å .

Method B

Estimates of radius were also obtained by extrapolating the molecular radius from a relatively well known figure in the literature [326], which plots molecular radius in relation to molecular weight for some substance used to investigate glomerular filtration. Figure 4.2 illustrates this figure.

Figure 4.2 Molecular radius size in relation to molecular weight for some substances used to investigate glomerular filtration (taken from the literature [326])

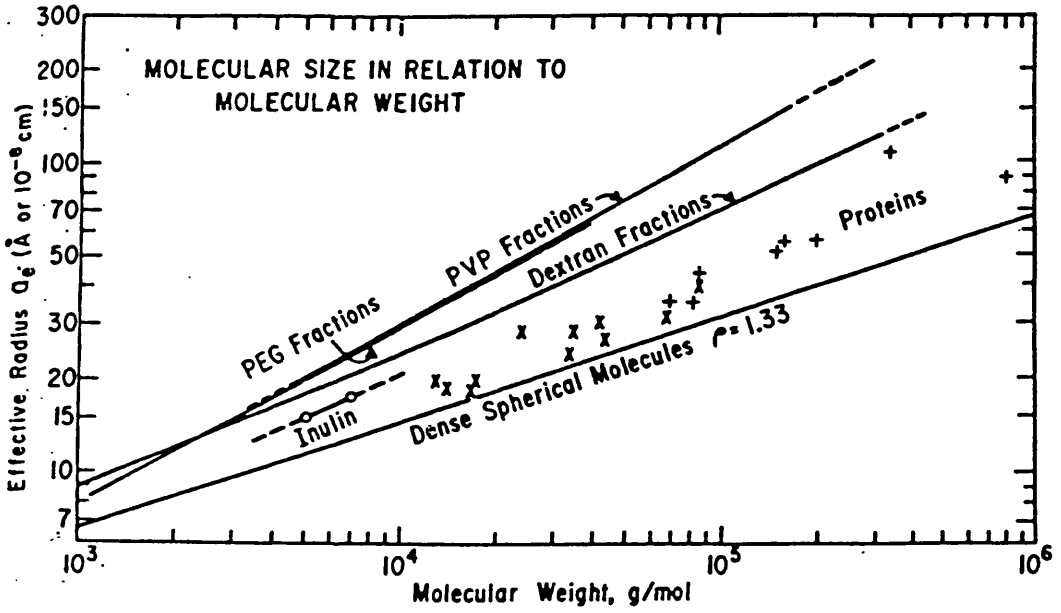

Using this figure, the molecular radius for the lactalbumin was estimated to be approximately 21Å , the molecular radius for the carbonic anhydrase was estimated to be approximately 27Å , and the molecular radius for the chicken egg albumin was estimated to be approximately 32Å .

Each BSA-MTX conjugate was assumed to have a molecular radius the same size as free BSA, i.e. a=37Å. This is an approximation which was considered reasonable since the major effects of MTX conjugation on BSA distribution were increased rates of metabolism.

4.3 Results

4.3.1. Fits of the model to the three BSA-MTX conjugates.

Using the fitting strategy described in subsection 4.2.2, the baseline parameters given in table 4.8 , and a molecular radius of 37Å, the plasma concentration was simulated using equation 20 with MACROHOURS. These results are presented in parts 4.3.1.1-4.3.1.3 (the raw simulated data is given in Appendix B).

4.3.1.1. The fit to the BSA-MTX (5.1% w/w) conjugate

For the BSA-MTX (5.1% w/w) conjugate, rates of hepatic clearance k_m=0.005-0.01 min^{-1} appeared to fit the data well, as shown by figures 4.3A.1 and 4.3A.2.

The best choice of rate of hepatic clearance to fit the data appeared to be k_m=0.008 min^{-1}. This k_m rate was re-entered into MACROHOURS with the other baseline parameters, and simulations were performed over the appropriate time interval (100 hours in this case) to predict the fraction of the dose which can be expected to be found in each of the blood, lymph and liver, and also the fractions of the dose renally excreted and hepatically cleared (and the total fraction of the dose eliminated). Figures 4.3B and 4.3.C illustrate the predicted results in plot form.

Comparisons between observed and predicted data could additionally also be used to support the choice of best k_m rate, e.g. by simulating MACROHOURS using the best choice of k_m and comparing the observed plasma concentration versus time data with the model predicted plasma concentration versus time data. For a good fit, there should be a random spread of small positive and negative differences between observed and predicted data. Table 4.9 indicates a satisfactory fit for the BSA-MTX (5.1% w/w) conjugate with k_m=0.008 min^{-1}. Both the distribution and elimination phases of the plasma concentration versus time profile are well represented.

Figures 4.3A.1 and 4.3A.2 Fit to the BSA-MTX (5.1% w/w) conjugate plasma concentration versus time data for varying rates of k_m.

Figure 4.3A.1 (linear scale)

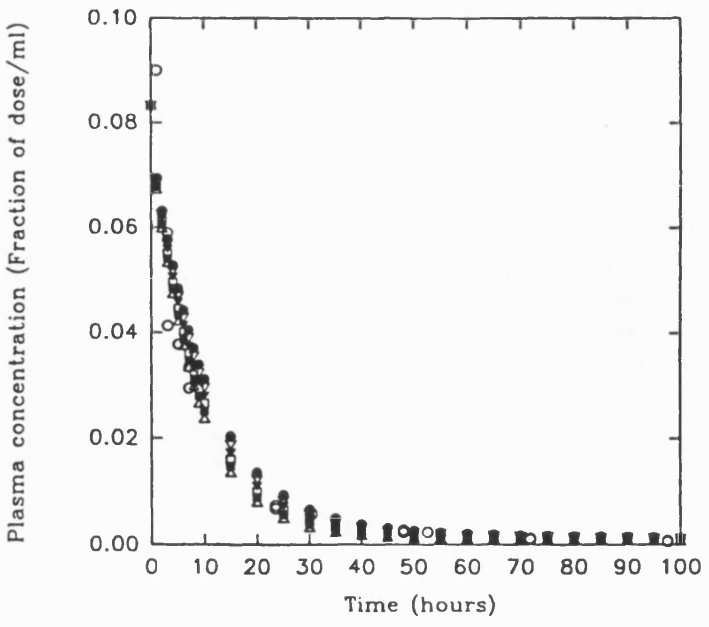

Figure 4.3A.2 (log_{10} scale)

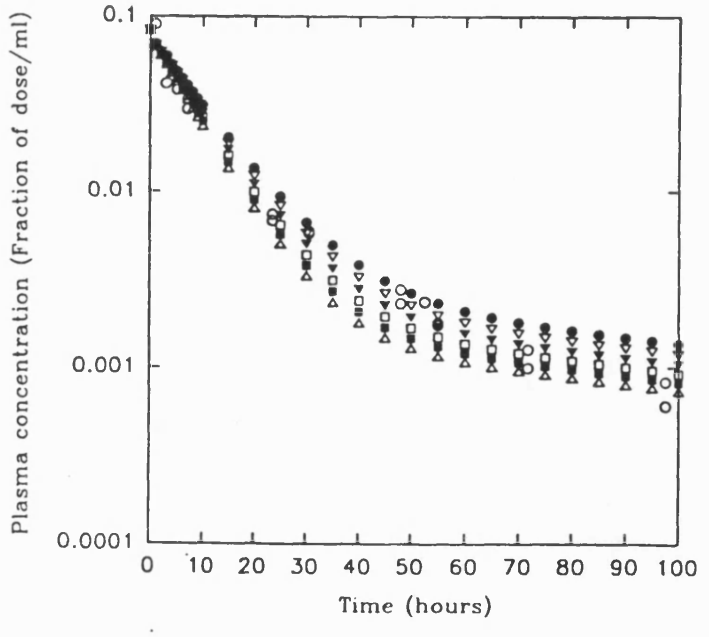

○ Observed data

Predicted data

● $k_m = 0.005min^{-1}$

▽ $k_m = 0.006min^{-1}$

▼ $k_m = 0.007min^{-1}$

□ $k_m = 0.008min^{-1}$

■ $k_m = 0.009min^{-1}$

△ $k_m = 0.010min^{-1}$

Figures 4.3B and 4.3C Predicted fraction of dose disposition data for the BSA-MTX (5.1% w./w) conjugate with $k_m = 0.008 min^{-1}$.

Figure 4.3B (linear scale)

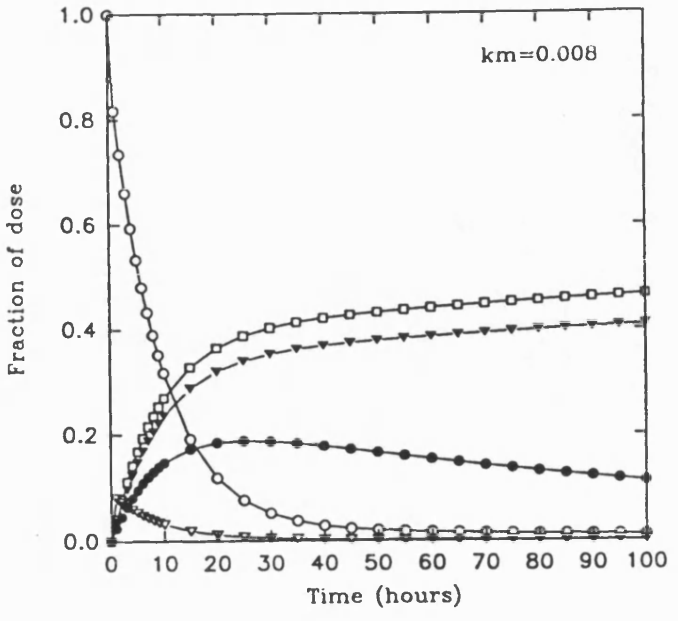

Figure 4.3C (log_{10} scale)

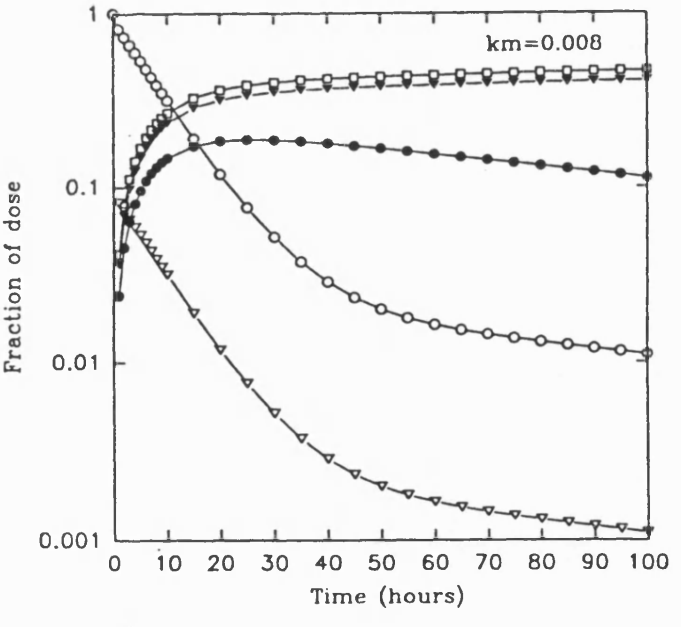

○ Blood
● Lymph
▽ Liver
▼ Excreted
□ Metabolised

Table 4.9 **Observed and predicted plasma concentration versus time data for BSA-MTX (5.1%w/w) conjugate.**

Time (hours)	Observed (O) i.v. plasma concentration (fraction of dose/ml)	Predicted (E) i.v. plasma concentration (fraction of dose/ml)	Difference (O - E)
1	6.933E-2	6.80786E-2	1.2514E-3
1	9.007E-2	6.80786E-2	2.19914E-2
3	5.899E-2	5.50093E-2	3.9807E-3
3	4.129E-2	5.50093E-2	-1.37193E-2
5	4.757E-2	4.45137E-2	3.0563E-3
5	3.775E-2	4.45137E-2	-6.7637E-3
7	2.934E-2	3.60838E-2	-6.7438E-3
7	3.335E-2	3.60838E-2	-2.7338E-3
23.5	0.678E-2	0.725859E-2	-4.7859E-4
23.5	0.737E-2	0.725859E-2	1.1141E-4
30.5	0.572E-2	0.417797E-2	1.54203E-3
30.5	0.590E-2	0.417797E-2	1.72203E-3
48	0.230E-2	0.17671E-2	5.329E-4
48	0.275E-2	0.17671E-2	9.829E-4
52.5	0.234E-2	0.15711E-2	7.689E-4
52.5	0.236E-2	0.15711E-2	7.889E-4
55	0.179E-2	0.148944E-2	3.0056E-4
55	0.174E-2	0.148944E-2	2.5056E-4
71.75	0.0989E-2	0.11783E-2	-1.893E-4
71.75	0.126E-2	0.11783E-2	8.17E-5
97.5	0.0604E-2	0.0938827E-2	-3.3482E-4
97.5	0.0824E-2	0.0938827E-2	-1.1482E-4

4.3.1.2. The fits to the BSA-MTX conjugates with high MTX content.

For the pooled BSA-MTX (11.74% w/w) and BSA-MTX (11.76% w/w) conjugates, and the pooled BSA-MTX (13.63% w/w) and BSA-MTX (13.64% w/w) conjugates, rates of hepatic clearance k_m=0.01-0.05 min^{-1} and k_m=0.01-0.04 min^{-1} respectively appeared to fit the data well, as shown by figures 4.4A.1 and 4.4A.2 and 4.4B.1 and 4.4B.2 respectively.

The best choice of rate of hepatic clearance to fit the plasma concentration versus time data for both sets of these pooled BSA-MTX conjugate data appeared to be k_m= 0.02 min^{-1}. This k_m rate was therefore re-entered into MACROHOURS and simulations were performed over an appropriate time interval (100 hours again for both pooled sets). Figures 4.4C and 4.4D illustrate the predicted results in plot form. The figures represent the predicted results for both sets of pooled BSA-MTX conjugates since the best k_m rate for each was found to be the same.

Table 4.10 for the pooled BSA-MTX (11.74% w/w) and BSA-MTX (11.76% w/w) conjugates, and table 4.11 for the pooled BSA-MTX (13.63% w/w) and BSA-MTX (13.64% w/w) conjugates show the observed and predicted plasma concentration versus time data for each set of these pooled BSA-MTX conjugates. As already indicated by figures 4.4A.1 and 4.4A.2 and figures 4.4B and 4.4B.2 respectively, these tables show that both the distribution and elimination phases of the plasma concentration versus time profiles for both sets of pooled data are relatively well represented.

Figures 4.4A.1 and 4.4A.2 Fit to the pooled BSA-MTX (11.74% w/w) and BSA-MTX (11.76% w/w) conjugates plasma concentration versus time data for varying rates of k_m.

Figure 4.4A.1 (linear scale)

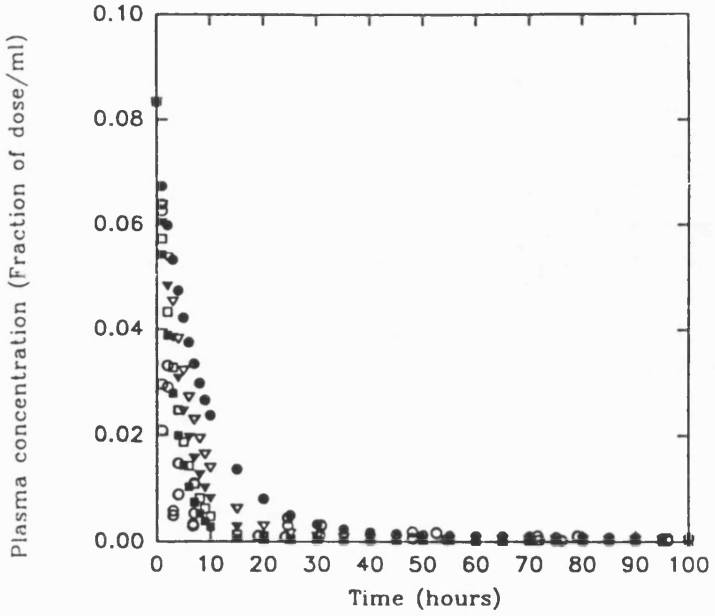

Figure 4.4A.2 (log_{10} scale)

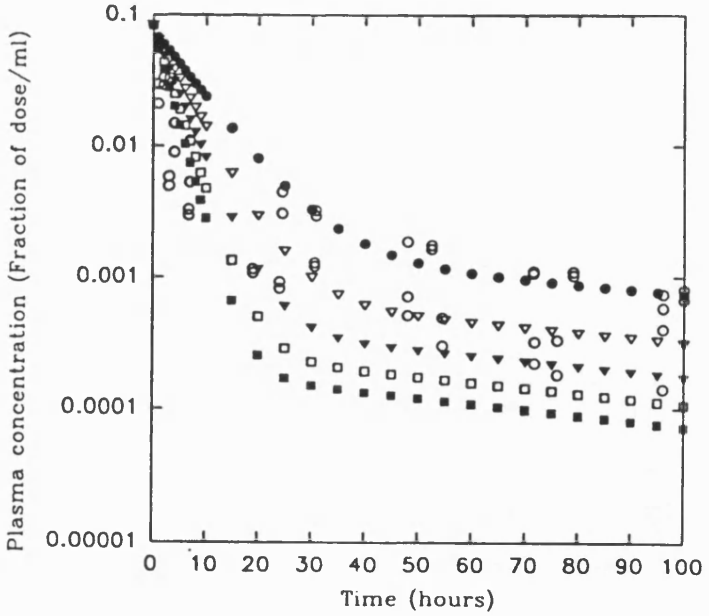

○ Observed data

Predicted data

● $k_m = 0.01 min^{-1}$

▽ $k_m = 0.02 min^{-1}$

▼ $k_m = 0.03 min^{-1}$

□ $k_m = 0.04 min^{-1}$

■ $k_m = 0.05 min^{-1}$

Figures 4.4B.1 and 4.4B.2 Fit to the pooled BSA-MTX (13.63% w/w) and BSA-MTX (13.64% w/w) conjugates plasma concentration versus time data for varying rates of k_m.

Figure 4.4B.1 (linear scale)

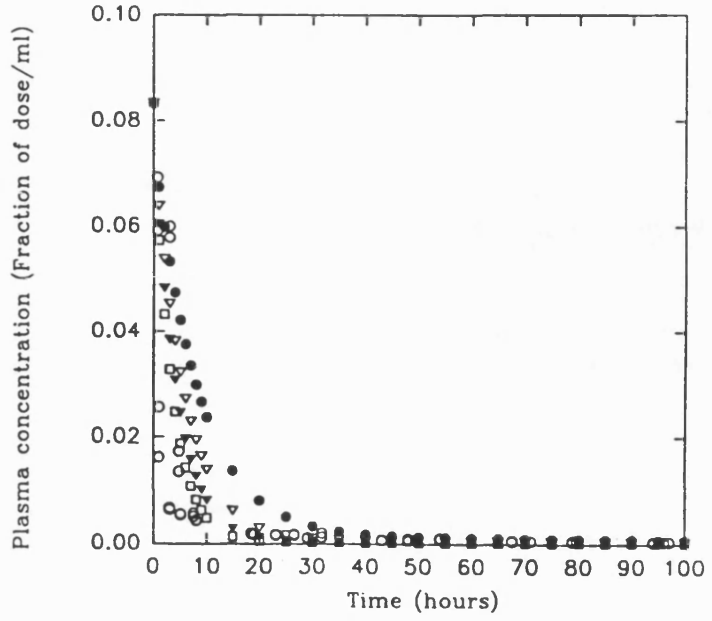

Figure 4.4B.2 (log_{10} scale)

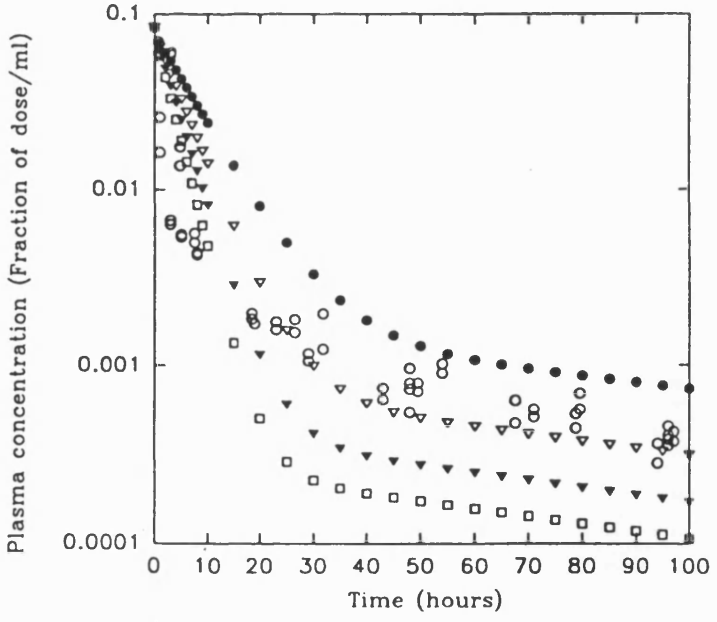

○ Observed data

Predicted data

● $k_m = 0.01min^{-1}$

▽ $k_m = 0.02min^{-1}$

▼ $k_m = 0.03min^{-1}$

□ $k_m = 0.04min^{-1}$

Figures 4.4C and 4.4D Prediction fraction of dose disposition data for the pooled BSA-MTX (11.74% w/w) and BSA-MTX (11.76% w/w) conjugates and the pooled BSA-MTX (13.63% w/w) and BSA-MTX (13.64% w/w) conjugates with $k_m = 0.02min^{-1}$.

Figure 4.4C (linear scale)

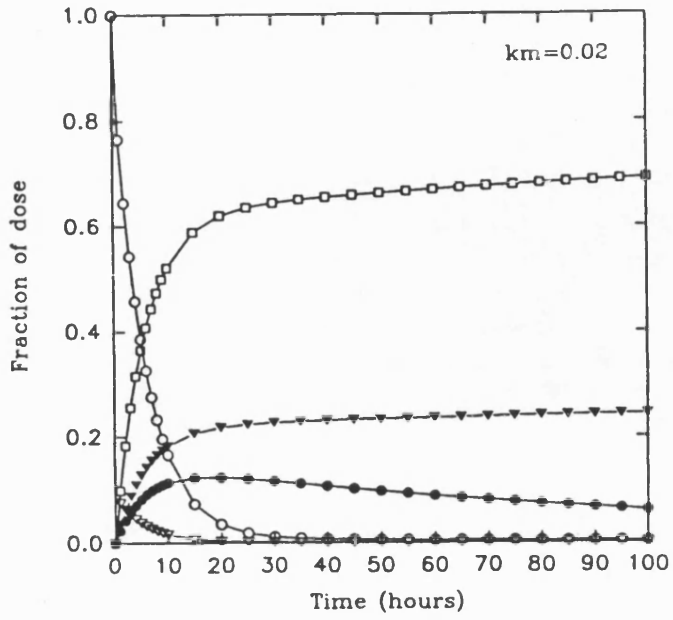

Figure 4.4D (log_{10} scale)

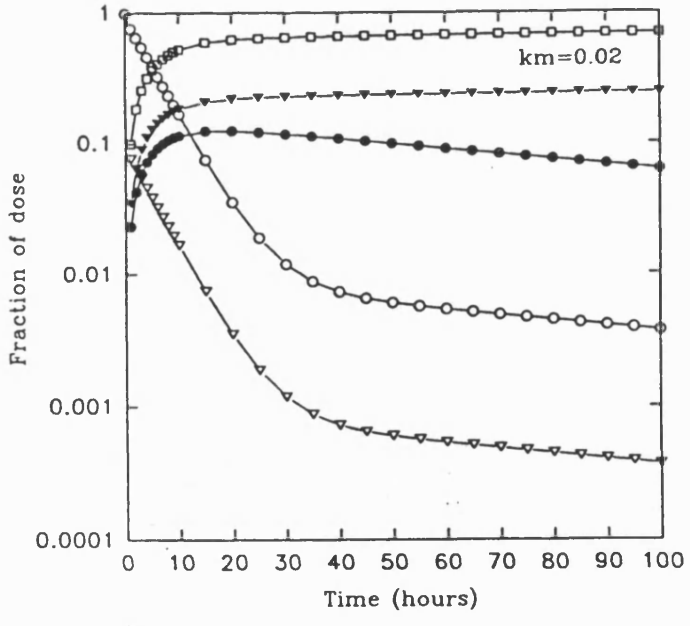

○ Blood
● Lymph
▽ Liver
▼ Excreted
□ Metabolised

Table 4.10 Observed and predicted plasma concentration versus time data for the pooled BSA-MTX (11.74% w/w) and BSA-MTX (11.76 w/w) conjugates.

Time (hours)	Observed (O) i.v. plasma concentration (fraction of dose/ml)	Predicted (E) i.v. plasma concentration (fraction of dose/ml)	Difference (O - E)
1	2.955E-2	6.37976E-2	-3.42476E-2
1	2.089E-2	6.37976E-2	-4.29076E-2
1	6.266E-2	6.37976E-2	-1.1376E-3
1	6.389E-2	6.37976E-2	9.24E-5
2	2.906E-2	5.3718E-2	-2.4658E-2
2	3.311E-2	5.3718E-2	-2.0608E-2
3	0.584E-2	4.52479E-2	-3.94079E-2
3	0.498E-2	4.52479E-2	-4.02679E-2
4	1.472E-2	3.81302E-2	-2.34102E-2
4	0.888E-2	3.81302E-2	-2.92502E-2
6.75	0.329E-2	2.38859E-2	-2.05959E-2
6.75	0.297E-2	2.38859E-2	-2.09159E-2
7	0.531E-2	2.28976E-2	-1.75876E-2
7	1.099E-2	2.28976E-2	-1.19076E-2
19	0.116E-2	0.338979E-2	-2.2297E-3
19	0.108E-2	0.338979E-2	-2.3097E-3
24	0.0821E-2	0.176543E-2	-9.4443E-4
24	0.0924E-2	0.176543E-2	-8.4143E-4
24.5	0.449E-2	0.16668E-2	2.8232E-3
24.5	0.308E-2	0.16668E-2	1.4132E-3
30.5	0.121E-2	0.0951353E-2	2.58647E-4
30.5	0.129E-2	0.0951353E-2	3.38647E-4
30.75	0.295E-2	0.0934249E-2	2.01575E-3
30.75	0.324E-2	0.0934249E-2	2.30575E-3
48	0.0506E-2	0.05132E-2	-7.2E-6
48	0.0713E-2	0.05132E-2	1.998E-4
48	0.187E-2	0.05132E-2	1.3568E-3
48	0.187E-2	0.05132E-2	1.3568E-3
52.5	0.176E-2	0.0483866E-2	1.27413E-3
52.5	0.164E-2	0.0483866E-2	1.15613E-3
54.5	0.0494E-2	0.047297E-2	2.103E-5
54.5	0.0303E-2	0.047297E-2	-1.6997E-4
71.5	0.107E-2	0.0400987E-2	6.69013E-4
71.5	0.111E-2	0.0400987E-2	7.09013E-4
71.75	0.0319E-2	0.040007E-2	-8.107E-3
71.75	0.0215E-2	0.040007E-2	-1.8507E-4
76	0.0331E-2	0.03848E-2	-5.38E-3
76	0.0182E-2	0.0384847E-2	-2.0284E-4
79	0.103E-2	0.0374495E-2	6.55505E-4
79	0.110E-2	0.0374495E-2	7.25505E-4
96	0.0402E-2	0.0321059E-2	8.0941E-5
96	0.0142E-2	0.0321059E-2	-1.7905E-4
96	0.0741E-2	0.0321059E-2	4.19941E-4
96	0.0579E-2	0.0321059E-2	2.57941E-4
100	0.0801E-2	0.030965E-2	4.9135E-4
100	0.0667E-2	0.030965E-2	3.5735E-4

Table 4.11 Observed and predicted plasma concentration versus time data for the pooled BSA-MTX (13.63% w/w) and BSA-MTX (13.64% w/w) conjugates.

Time (hours)	Observed (O) i.v. plasma concentration (fraction of dose/ml)	Predicted (E) i.v. plasma concentration (fraction of dose/ml)	Difference (O - E)
0.75	6.921E-2	6.66036E-2	2.6064E-3
0.75	5.919E-2	6.66036E-2	-7.4136E-3
1	2.558E-2	6.37976E-2	-3.82176E-2
1	1.614E-2	6.37976E-2	-4.76576E-2
3	0.668E-2	4.52479E-2	-3.85679E-2
3	0.634E-2	4.52479E-2	-3.89079E-2
3	5.998E-2	4.52479E-2	1.47321E-2
3	5.784E-2	4.52479E-2	1.25921E-2
4.75	1.351E-2	3.35481E-2	-2.00381E-2
4.75	1.73E-2	3.35481E-2	-1.62481E-2
5	0.552E-2	3.21488E-2	-2.66288E-2
5	0.535E-2	3.21488E-2	-2.67988E-2
7.5	0.499E-2	2.10453E-2	-1.60553E-2
7.5	0.562E-2	2.10453E-2	-1.54253E-2
8	0.424E-2	1.93472E-2	-1.51072E-2
8	0.436E-2	1.93472E-2	-1.49872E-2
18.5	0.198E-2	0.364242E-2	-1.6624E-3
18.5	0.184E-2	0.364242E-2	-1.8024E-3
19	0.173E-2	0.338979E-2	-1.6597E-3
23	0.160E-2	0.198966E-2	-3.8966E-4
23	0.177E-2	0.198966E-2	-2.1966E-4
26.5	0.154E-2	0.134594E-2	1.9406E-4
26.5	0.183E-2	0.134594E-2	4.8406E-4
29	0.117E-2	0.106993E-2	1.0007E-4
29	0.106E-2	0.106993E-2	-9.93E-6
31.75	0.124E-2	0.0872311E-2	3.67689E-4
31.75	0.197E-2	0.0872311E-2	1.09768E-3
43	0.0735E-2	0.056058E-2	1.7442E-4
43	0.0637E-2	0.056058E-2	7.642E-5
48	0.0725E-2	0.05132E-2	2.118E-4
48	0.0541E-2	0.05132E-2	2.78E-5
48	0.0791E-2	0.05132E-2	2.778E-4
48	0.0959E-2	0.05132E-2	4.458E-4
49.5	0.0712E-2	0.0502473E-2	2.09527E-4
49.5	0.0793E-2	0.0502473E-2	2.90527E-4
54	0.0899E-2	0.0475605E-2	4.23395E-4
54	0.102E-2	0.0475605E-2	5.44395E-4
67.5	0.0471E-2	0.0416045E-2	5.4955E-5
67.5	0.0625E-2	0.0416045E-2	2.08955E-4
71	0.0508E-2	0.040283E-2	1.0517E-4
71	0.0564E-2	0.040283E-2	1.6117E-4
78.5	0.0443E-2	0.0375346E-2	6.7654E-5
78.5	0.0532E-2	0.0375346E-2	1.56654E-4
79.5	0.0558E-2	0.0372799E-2	1.85201E-4
79.5	0.0692E-2	0.0372799E-2	3.19201E-4
94	0.0362E-2	0.0326921E-2	3.5079E-5
94	0.0283E-2	0.0326921E-2	-4.3921E-5
96	0.0446E-2	0.0321059E-2	1.24941E-4
96	0.0397E-2	0.0321059E-2	7.5941E-5
96	0.0375E-2	0.0321059E-2	5.3941E-5
96	0.0353E-2	0.0321059E-2	3.1941E-5
97	0.0416E-2	0.0318168E-2	9.7832E-5
97	0.0374E-2	0.0318168E-2	5.5832E-5

4.3.2. Fits of the model to i.v. dosage of lactalbumin, carbonic anhydrase and chicken egg albumin

In order to highlight some of the problems which can be encountered in modelling proteins and in animal scaling as well, equation 20 was also fitted to the plasma concentration versus time data of the lactalbumin, carbonic anhydrase and chicken egg albumin macromolecules, which was presented in tables 4.5-4.7 respectively. For these experiments, the same fitting strategy described in subsection 4.2.2. was used, along with the same baseline parameters given in table 4.8. The estimated molecular radii obtained using both Methods A and B described in section 4.2.3. were used for each macromolecule, and simulations were performed on MACROHOURS using a value of hepatic clearance k_m=0.0 min^{-1}. The results from these simulations are presented in plot form in figures 4.5A - 4.5C respectively (the raw simulated data are presented in Appendix B).

Figures 4.5A-4.5C show that these fits were poor. One might expect that equation 20 should fit the plasma concentration versus time data of these three free proteins as well as it fitted the free BSA shown in figure 4.1, since the same baseline parameters and rate of hepatic clearance (i.e. k_m=0.0 min^{-1}) were used. However, as shown by figures 4.5A-4.5C for these three macromolecules, neither the distribution or the elimination phases of the data were adequately modelled. There are several possible explanations for this. One possible explanation could be that some of the values assigned to the rat baseline parameters given in table 4.8. were not typical for the rats used in these three particular experiments, and consequently some baseline parameters may be slightly over- or under-estimated for these particular rats. For instance, the elimination phases of the predicted plasma concentration versus time profiles for the lactalbumin and carbonic anhydrase macromolecules could be improved by decreasing the value of GFR, whilst the elimination phase of the profile for the chicken egg albumin could be improved by increasing the value of GFR. Similarly, the distribution phase of the predicted plasma concentration versus time profile for the chicken egg

albumin, and at early times for the predicted plasma concentration versus time profiles for the lactalbumin and carbonic anhydrase macromolecules, could be improved by increasing the BLFR and LFR values, and/or by increasing the blood to liver and liver to blood flow rates, whilst the later distribution phase (after about the first 5 hours) could be improved for the latter two macromolecules by decreasing the value of BLFR and LFR and/or decreasing the blood to liver and liver to blood flow rates. An alternative and perhaps more likely explanation may be that since these three macromolecular drugs are comparatively small (i.e. smaller than the renal threshold) and are in a non-conjugated form, they may be binding to some plasma proteins in vivo, and this could alternatively account for most of the differences between observed and predicted plasma concentration versus time data in the cases of the lactalbumin and carbonic anhydrase, and some of the differences in the case of the chicken egg albumin data. Indeed, the fairly unusual plasma concentration versus time profiles of the observed data for the lactalbumin and carbonic anhydrase protein macromolecules does in fact appear to indicate that this may be the case, since by observing the data visually, it appears that some binding must be happening since for such comparatively small macromolecules one would normally expect a smaller amount of each drug to be left in the body with respect to time than is actually observed experimentally. Macromolecules of this dimension should generally be renally excreted relatively quickly, which from the observed experimental data, does not appear to be the case. Also, in the case of the chicken egg albumin data, there are relatively few plasma concentration time data points anyway, and due to the size of this macromolecule (radius 32-33Å), one would perhaps not normally expect it to be eliminated quite so quickly as the observed experimental data suggests. Consequently, any difference between observed and predicted plasma concentration versus time data or profiles in these fits, may in fact be due to unpredictable or unusual anomalies or processes, such as binding to plasma proteins, in the observed rat plasma concentration versus time experimental data itself. Other possible causes for the difference between observed and predicted plasma

concentration versus time profiles could also include unpredictable chemical processes, or they may simply be due to a combination of these explanations.

These three fits therefore illustrate some of the classic problems associated both with animal scaling, and the fitting of a theoretical model to actual experimental data. The fits show that in some situations, probably for macromolecules below the size of the renal threshold or macromolecular drugs not in a conjugated form, and in situations when any animal scaling is involved, other appropriate baseline parameters in addition to k_m may also sometimes be needed to be varied via simulations on MACROHOURS when performing any fitting of the equation describing plasma concentration versus time (equation 20) to experimental plasma concentration versus time data. The additional baseline parameters which will be needed to be varied in order to obtain the best fit, will be those about which very little is known either experimentally or in the literature. These three fits also show how unpredictable processes such as the binding of smaller macromolecules to plasma proteins in vivo can confound predictability as well.

Figures 4.5A.1 and 4.5A.2 Fit to the lactalbumin plasma concentration versus time data with $k_m = 0.0 min^{-1}$.

Figure 4.5A.1 (linear scale)

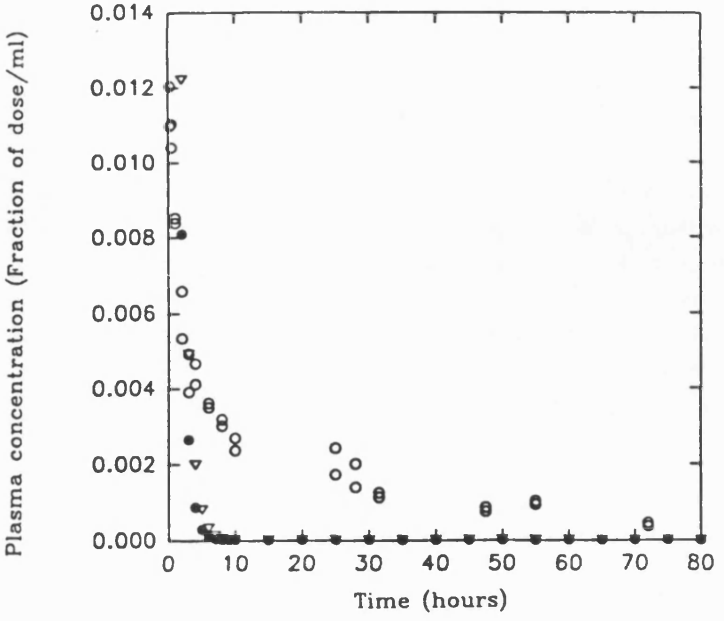

Figure 4.5B.1 (log_{10} scale)

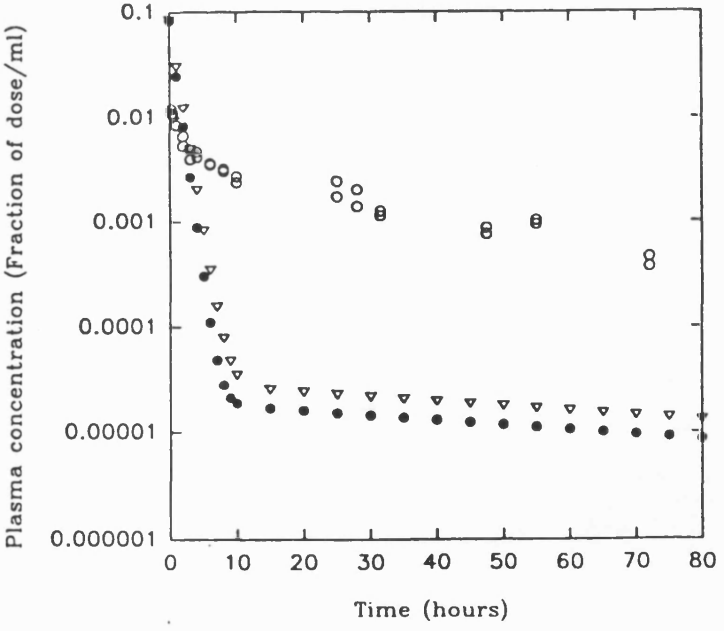

○ Observed data

Predicted data

● a = 21Å

▽ a = 22Å

Figures 4.5B.1 and 4.5B.2 Fit to the carbonic anhydrase plasma concentration versus time data with $k_m = 0.0min^{-1}$

Figure 4.5B.1 (linear scale)

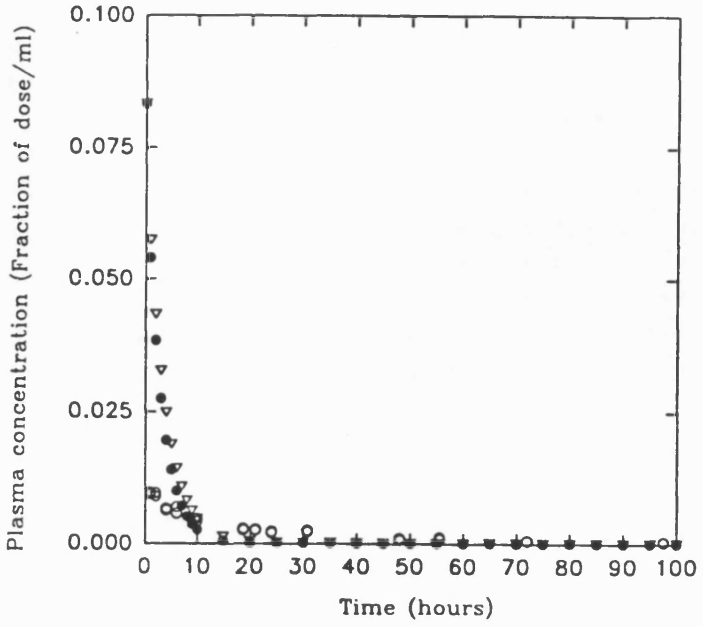

Figure 4.5B.2 (log_{10} scale)

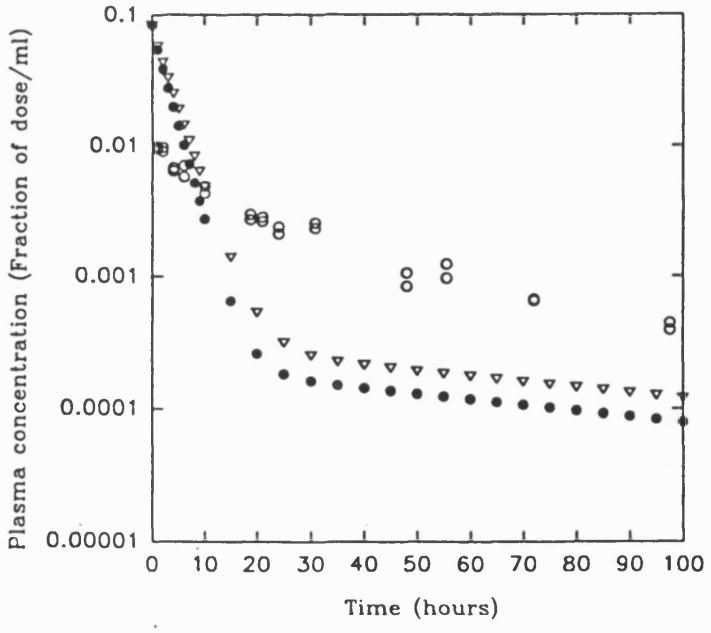

○ Observed data

Predicted data

● a = 27Å

▽ a = 28Å

Figures 4.5C.1 and 4.5C.2 Fit to the chicken egg albumin plasma concentration versus time data with $k_m = 0.0min^{-1}$

Figure 4.5C.1 (linear scale)

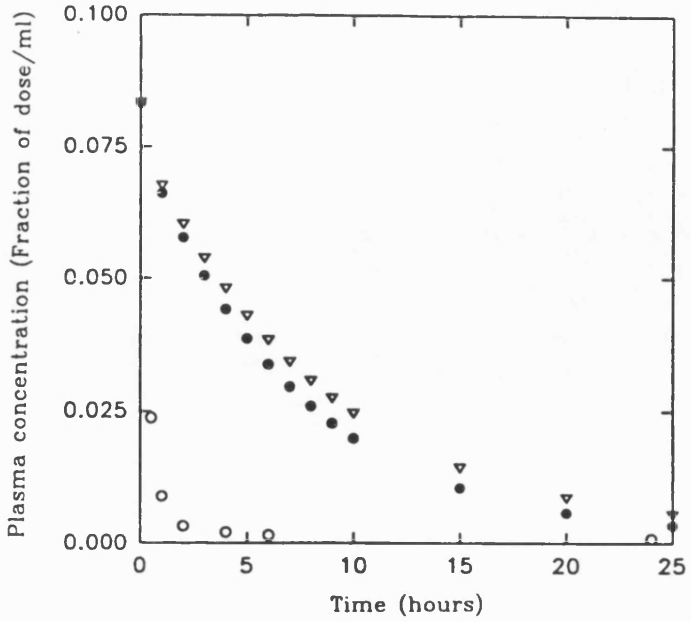

Figure 4.5C.2 (log_{10} scale)

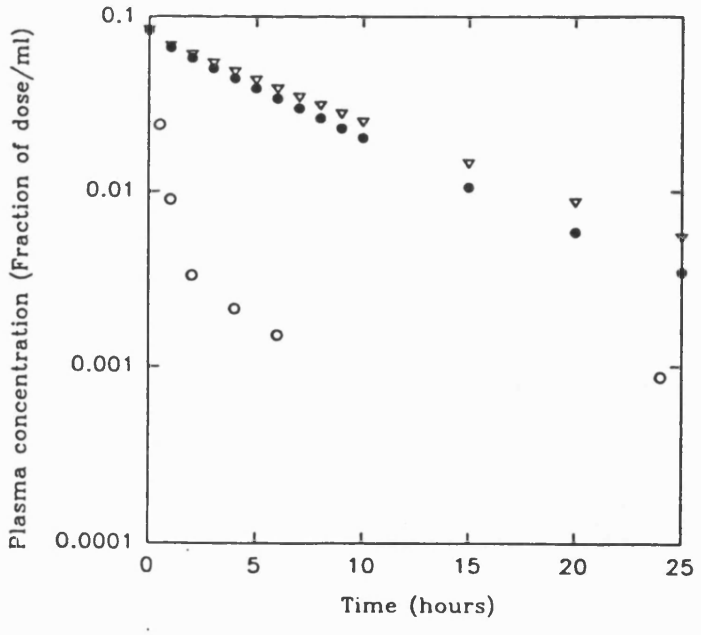

○ Observed data

Predicted data

● a = 32Å

▽ a = 33Å

4.3.3 Visual fit of the model to an i.v. plasma clearance plot of a polyethyleneglycol interleukin-2 (PEG IL-2) conjugate

A further fit performed in this study was the visual comparison of a plasma clearance plot for an intravenously administered polyethyleneglycol intrleukin-2 (PEG IL-2) conjugate, approximate molecular radius 55Å, in man [132], with the model predicted plasma clearance plot for an uncharged macromolecule of radius 55Å in man for varying rates of hepatic clearance. For this fit the uncharged baseline parameters presented in table 3.1 (given in chapter 3) and the rates of hepatic clearance selected in that chapter, i.e. k_m = 0.0 min^{-1}, 0.001 min^{-1}, 0.003 min^{-1}, and 0.01 min^{-1}, were used. Although no data were published for this PEG IL-2 conjugate [132], the plasma concentration versus time plot presented in the literature was useful, since it was in a normalised form and was over an appropriate time scale. Figure 4.6A shows this plot, whilst figure 4.6B shows the predicted fraction of dose in the plasma for the different k_m rates (the raw simulated data for figure 4.6B are presented in Appendix B).

Visual comparison of figure 4.6B for k_m= 0.01 min^{-1} with figure 4.6A shows that at 48 hours the plasma levels in each figure have decreased by two log-cycles, and that at 96 hours they have either decreased, or are on the verge of decreasing, by a further log-cycle. Consequently on this basis, the predicted fraction of dose in the plasma for an uncharged molecule of radius 55Å with k_m = 0.01 min^{-1} appears to fit reasonably well the plasma clearance of the PEG IL-2 conjugate. Other tissue distribution data can now be obtained by re-entering this k_m rate into MACROHOURS and simulating; it is not presented in this subsection since the most important tissue distribution, i.e. distribution to the lymph, was already represented in chapter 3.

This fitting demonstration was useful since it illustrated how the model can be used for fitting purposes when a plasma clearance plot and not any plasma concentration versus time data are presented. However, further visual fitting experiments of this kind were not performed, since most of the other plasma concentration versus time plots in the

literature were either in an unusable form, or were over an inappropriate time scale, or both.

Figure 4.6A Observed PEG IL-2 serum clearance data

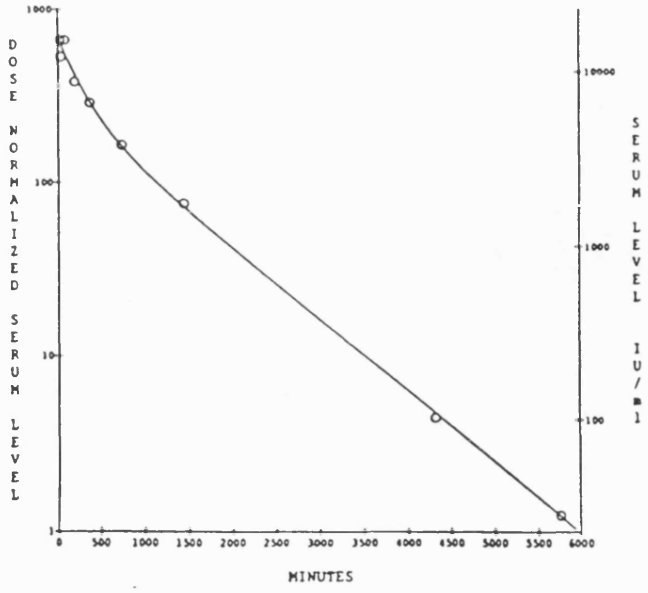

Figures 4.6B Predicted serum clearance data for varying rates of k_m for a macromolecule of the same size and charge as PEG IL-2

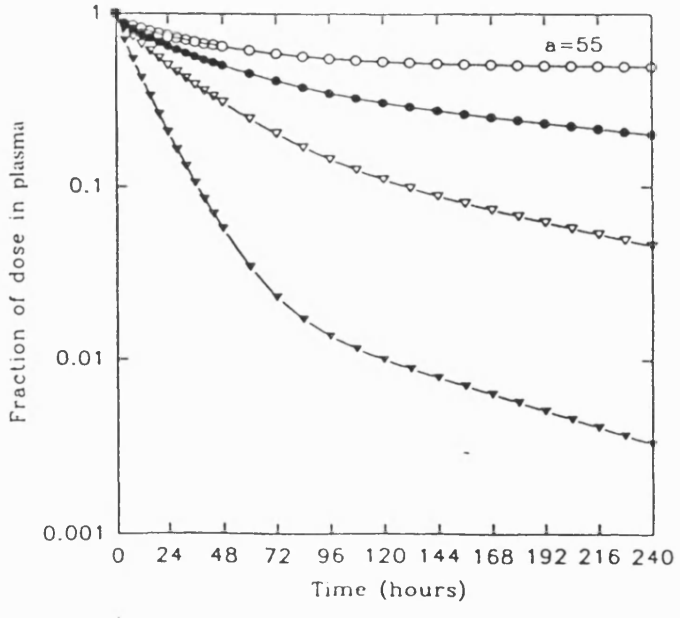

○ $k_m = 0.0 min^{-1}$
● $k_m = 0.001 min^{-1}$
▽ $k_m = 0.003 min^{-1}$
▼ $k_m = 0.01 min^{-1}$

4.4 Conclusions

This chapter demonstrated how the model presented in this study can be used for fitting purposes. It showed how the model can be used to generate or predict disposition data for the key tissues of the body (blood, lymph and liver) and the two major elimination processes (renal excretion and hepatic clearance) which are important in both macromolecular drug distribution and the targeting of anticancer agents to the lymph, following the fitting of the equation describing plasma concentration versus time (equation 20) to plasma concentration versus time data in the literature. The fits demonstrated in this chapter illustrated some of the common problems encountered with animal scaling, and the fitting of a theoretical model to real experimental data. The fits of the model to the plasma concentration versus time data of the selected BSA-MTX (5.1% w/w) conjugate, the pooled BSA-MTX (11.74% w/w) and BSA-MTX (11.76% w/w) conjugates, the pooled BSA-MTX (13.63% w/w) and BSA-MTX (13.64% w/w) conjugates, and to the free BSA, were found to be relatively successful, as was the fit to the clearance plot of the PEG IL-2 conjugate. In contrast, however, the fits of the model to the plasma concentration versus time data of the three selected protein macromolecules, i.e. the lactalbumin, carbonic anhydrase and chicken egg albumin, were not so successful. Possible reasons for this have already been discussed, The fits demonstrated here suggest that in some situations, probably for macromolecules below the size of the renal threshold or macromolecular drugs not in a conjugated form, and in situations when any animal scaling is involved, other appropriate baseline parameters in addition to k_m may also sometimes need to be varied via simulations on MACROHOURS when performing any fitting of the models equation describing plasma concentration versus time (equation 20) to experimental plasma concentration versus time data. How well the model actually fits experimental data may only be known in the future, when more human and better animal macromolecular drug disposition data from pharmacokinetic studies involving targeted macromolecular systems in the field of cancer chemotherapy, or from non-chemotherapy macromolecular drug

pharmacokinetic studies as well, becomes available, for key compartments of the body (blood, lymph, liver) and the two major elimination processes (renal excretion and hepatic clearance). The data selected to be used in the fitting demonstrations described in this chapter were as good as any that is available, and better than most, and the fits of the model to some of this selected data were comparatively successful.

Chapter 5

Discussion

In this study a new physiological pharmacokinetic model was developed to investigate the fate of macromolecular drugs in the body. The model was based on the movement of macromolecules under normal vascular conditions between three important compartments (tissues) of the body (blood, extracellular fluid or lymph, and liver) and modelling the two major elimination processes (renal excretion from the blood compartment and hepatic metabolism from the liver compartment). These aspects of distribution were considered important in macromolecular drug disposition and the targeting of anticancer agents to malignant micrometastases located in the extravascular space (lymph). The model was required to take into account that for macromolecules renal excretion and hepatic metabolism were effectively occurring from separate compartments. The purpose of the model was to examine the effect of molecular radius on the distribution of both negatively charged protein and uncharged macromolecular drugs in man, both in the absence and presence of hepatic metabolism. This was achieved by taking into account the regional capillary permeabilities to different size macromolecules, and the physiology and flow rates within each compartment. Mathematical models of capillary permeability were developed to allow fitting of appropriate physiological experimental data from the literature. The latter models were used to model intercompartmental rate constants used in the physiological three-compartment pharmacokinetic model. The major objective was to predict via simulations the molecular radii which are likely to be most effective in delivering, following an intravenous bolus injection, the greatest fraction of a macromolecular drug dose to the extravascular fluids (lymph), and hence to any cancer micrometastases present there. In addition to predicting the fraction of the macromolecular drug present in the lymph, the proposed model also allows calculation, for each molecular radius within the range determined by the modelling process ($20 \leq a \leq 70$ Å), the fraction of the dose that is present in the blood and the liver, the fractions of the dose which have been excreted via the kidneys and metabolised by the liver, and the total fraction of the dose eliminated, as a function of time. The model can also be used for fitting purposes. A necessary objective of the study was the

development of the computer programme 'MACROHOURS' which had two main purposes; firstly to aid in the solution of cubic functions within the physiological three-compartment pharmacokinetic model equations, and secondly to perform simulations once the solutions to the model equations had been established. Simulations suggested that the best dimensions which produce the greatest fraction of a macromolecular drug dose in the lymph are macromolecules within the intermediate radii range of 40/45 - 50/55 Å , with lower sizes within this range being more successful over earlier times and at faster rates of hepatic metabolism, and upper sizes being more successful over later times and at slower rates of hepatic metabolism. It was shown that for a macromolecular drug which is metabolised very quickly, then molecular radii as small as 35Å can also be as effective at early times. Protein macromolecules (i.e. negatively charged species) were found to be better candidates than uncharged macromolecules for delivering the greatest fraction of the dose to the target, the lymph, and hence to any cancer micrometastases located there. In the case of the protein macromolecules in the absence of hepatic metabolism or when the metabolic rate was low, the upper size range could be extended to 65Å radius to give high concentrations in the tissues over very long time periods.

The model presented here differs in several important respects from the key theoretical/predictive macromolecular anticancer drug and drug-targeting pharmacokinetic models in the literature. As indicated in chapter 1 (section 1.2), actively-targeted and passively -targeted macromolecular drug conjugate systems are a relatively new innovation in the field of cancer chemotherapy. Consequently there are comparatively few of these theoretical/predictive physiological pharmacokinetic models in the literature. Most of the models which are available in the literature are concerned with examining monoclonal antibody (or immunotoxin) distribution and uptake in solid tumours. These have taken the form of geometrical membrane-limited models [86, 87, 89-98, 262], although there are also some important compartmental blood flow rate-limited models [252, 253]. There are also two important general drug-targeting models

[254, 255], and a paper containing a set of general models investigating the influence of transport limitation on the amount of macromolecular drug taken up by a general target [256]. The major features of each of these models is described in more detail in the appropriate category below. The advantages and disadvantages between the model presented in this study and each of these models is also discussed at the end of each category. The general strengths and weaknesses of the model presented in this study are then summarized at the end of this chapter, together with some suggestions for future work.

General drug-targeting models.

The model presented here differs in several important respects from two important general theoretical/predictive drug-targeting pharmacokinetic models in the literature [254, 255]. These differences are discussed below.

In the earlier of the general drug-targeting models in the literature, the model by Hunt et al. [254], a physiologically based four-compartment blood flow-rate limited pharmacokinetic model was used to aid prediction of the pharmacological benefits to be derived from the administration of a drug as a targeted drug-carrier combination. This was achieved by modelling the distribution of free drug which would be released from a carrier. The distribution of the drug carrier conjugate itself was not modelled. The compartments in the model represented response, toxicity and elimination tissues, and the blood, with the blood or central compartment also representing all other tissues not accounted for by the other three compartments. Each compartment had its own volume of distribution. Effective blood-flow rates were represented as occurring between the blood and the response compartments, the blood and toxicity compartment, and between the blood and elimination compartments. Drug delivery was designated by one of two different input functions, either an intravenous input function to the blood compartment in the case of free-drug administration, or release rates (and also input functions) of free drug from the carrier into each of the four

compartments in the case when the drug is administered as a drug-carrier combination (these release rates are in fact later combined and rewritten in terms of an average in vivo drug release rate from the total carrier dose, and the fractions of drug release occurring in each of the four compartments). First-order elimination of free drug either in its original form or once it had been released from the carrier was designated as occurring from the response, toxicity and elimination compartments. The model is a simplified version of several earlier anatomic tissue perfusion models [240-243], and builds on a model presented in some earlier work [452]. Two sets of differential mass balance equations describing the model were presented for the effective concentrations of drug at each site (compartment); one set representing the case for the intravenous administration of free-drug, and the other set representing the case for the intravenous administration of the drug-carrier combination. The authors expressed elimination from the compartments in terms of known blood flows and estimable tissue extraction ratios, defined two relative blood-flow parameters, and then solved analytically both sets of differential mass balance equations at steady-state, and in terms of the area under the site-concentration time curve (AUC). The solutions to these equations, i.e. the steady-state free-drug and drug-carrier equations for each compartment, were then used to generate two new parameters: therapeutic availability (TA) and drug targeting index (DTI), which allowed predictions of the magnitude of the improved therapeutic efficacy or increased apparent potency that would result when the drug is administered as a drug-carrier combination. The DTI was defined as the expected ratio of drug delivered to response and toxicity sites when the drug-carrier combination is used, divided by the same ratio when free drug is administered intravenously. TA was defined as the ratio of the dose fraction reaching target sites when the dose is administered parenterally as a drug-carrier combination to the amount reaching the same sites when an equal dose of free-drug is administered intravenously. An improvement in the therapeutic index (TI), a statistical measurement defined as the ratio of the median toxic dose to the median effective dose, and an increase in the TA were the primary benefits sought by the authors. A measure of the former was obtained

from the value of the DTI, and this together with the TA were directly calculable following the solutions of the differential mass balance equations either at steady-state or in terms of AUC. Having obtained expressions for these parameters the authors performed various investigations for an average 70kg man using these expressions for the case of an ideal carrier (drug release confined to the response compartment only) by varying various parameters in turn. The major assumptions the authors made were; that all metabolites are inactive; the effective concentration at the action site is a function of the measurable concentration in the venous blood leaving the tissue; as long as drug remains associated with carrier it is inactive; the carrier without drug attached has no significant pharmacological or toxic properties of its own and is pharmacologically inert; and the species of interest is man.

The main results from the investigations of these authors are that drugs with high total-body clearance, that are known to act at target tissues having effective blood flows that are small relative to the blood flow to the normal eliminating organs, will benefit most from combination with an efficient, targeted carrier. Direct elimination of the drug at the target site or at the tissues where toxicity originates dramatically improves the DTI. Also, the fraction of the drug actually released from the carrier at both target and non-target sites can radically affect index values (a 1% change in the fraction of the dose delivered to the target can result in a 50% change in DTI).

In the second of the two major drug-targeting models in the literature, the model by Boddy et al. [255], a similar physiologically based blood flow rate-limited pharmacokinetic model is presented to investigate some aspects of drug targeting, including the pharmacodynamics of therapeutic and toxic effects. The authors compared conventional administration and drug targeting at steady state for the same degree of therapeutic effect in man. The model consisted of three compartments: central, response, and toxicity, each with their own volumes. Blood flow was represented as occurring between the central and response compartments, and the central and toxicity compartments. Free drug elimination was represented as occurring

from any of the compartments by first-order processes, whilst the drug-carrier on the other hand was represented as being eliminated from the central compartment only, also by a first-order rate process. Either free drug or drug-carrier was administered into the central compartment at a constant rate. The rate of free drug release in each of the three compartments was assumed to be a first-order rate process. Rates of elimination and of release of free drug depended on the product of the rate constant and the volume of the compartment. (The carrier without drug attached, and the drug-carrier conjugate are assumed to be pharmacologically inert). The authors then solved analytically at steady-state the differential mass balance equations describing the concentrations of both free drug and drug-carrier in the model to produce steady-state concentration expressions of free drug, drug-carrier, and free drug released from drug-carrier, for each of the three compartments. Two simple pharmacodynamic model equations [453], which relate therapeutic effect or toxic effect caused by free drug to concentrations in the response or toxicity compartments, were then introduced into some of these expressions, as appropriate, to produce alternative expressions for the parameters TA and TI. TA was defined as the ratio of the rate of input of free drug to that of drug-carrier for the same degree of maximal therapeutic effect. Also, using the definition for DTI given in the previous model, when the concentrations in the response compartment are identical, DTI was found to be equal to the ratio of concentration in the toxicity compartment. Hence, the authors of this model defined a similar targeting index (TI) by substituting toxic effect for concentrations in the toxicity compartment. Having obtained the alternative expressions for these parameters the authors then performed various simulations using these expressions for the ideal case (release of free drug confined to response compartment) for an average 70kg man, by changing parameters in turn, to compare conventional administration and drug targeting at different fractions of the maximum therapeutic response.

The main conclusions from the second of these two general drug-targeting models were that TI and DTI are maximized by a drug which is rapidly eliminated from the central

compartment and targeted to a site with low blood flow. Both TI and DTI increase as the rate of elimination from the target site increases. The influence of these characteristics on the advantage of drug-targeting, prodrugs, or regional administration over conventional administration has also been noted previously [243, 254, 453, 454]. The effect of increasing the rate of elimination from the response and central compartments on DTI and TI changes if free drug is released from the drug-carrier outside of the response compartment. The kinetic characteristics of the drug-carrier complex, rate of elimination, and rate of free drug release, influence TA but not DTI or TI. The pharmacodynamics of the free drug in both the target and toxicity compartments have an important influence on TI but not on TA or DTI. As the pharmacological selectivity of the drug increases, so does TI, although a drug with good pharmacological selectivity may not gain an advantage from drug targeting. TI is very dependent on the shape of the effect-concentration curves, particularly that for toxicity. Also, while TA increases as the rate of elimination of free drug from either central or target compartments increases, TI may actually be reduced if release of free drug is not confined to the target compartment.

These two general drug-targeting models described above [254, 255] have several important disadvantages compared with the model presented in this study: The two general drug-targeting models [254, 255] do not consider the effect of molecular size or any other important physicochemical properties such as charge on distribution, since there are no parameters or expressions built into their structure to do this. Consequently they do not take into account any physiological membranes or account for different regional capillary permeabilities to different size molecules, and hence assume rapid (free) distribution for all molecules, which although may be true for very small molecules such as the free-drug, is certainly not the case for larger molecules such as the macromolecular carrier or drug-carrier system. Thus these models are valuable to the understanding of low molecular weight prodrug action. Macromolecular drug-carrier systems are inappropriately assumed to move within each compartment of

each model as easily and freely as the free-drug. First order release rates and the blood flow rates (which can only be assigned general values), are the only factors controlling how much drug is presented to and released from the drug-carrier into each compartment. The compartments of both the models [254, 255] do not represent specific organs or tissues such as the blood, lymph or liver, but instead represent general central, response, toxicity and elimination compartments (as appropriate), each with their own volumes, blood flow rates, and where appropriate first-order elimination rates. The values assigned to these parameters represent values which are not really appropriate to macromolecules. Also, the two major elimination processes, renal excretion and hepatic metabolism, are not specifically modelled for, since there is nothing in these two models [254, 255] which distinguishes renal excretion from hepatic metabolism, and no consideration is given to different rates of glomerular filtration (or liver sinusoidal extravasation) to different size molecules. There are no parameters or expressions built into these two models to take these processes into account. Additionally, the sets of differential mass balance equations describing both free-drug and drug-carrier in these two general models [254, 255] are solved at steady-state which means that equations to describe the concentration, mass, or fraction of drug in each compartment as a function of time are not obtainable, and consequently predictions as a function of time are not possible. The models can not therefore be used for any fitting purposes. Numerical methods would have been necessary if the models, certainly the four-compartment model [254], had been solved at non steady-state, and hence equations as a function of time for each compartment would still be unobtainable. This method of solution at steady-state is perhaps only really appropriate for low molecular weight prodrugs, since it is relatively easy to achieve infused steady-state for small rapidly distributing molecules, whereas for macromolecules this is much more difficult to achieve since their distribution will be much slower.

As a consequence of these points, and since the spirit behind the development of the above general drug-targeting models [254, 255] was geared towards aiding prediction

of the pharmacological benefits to be derived from the administration of a drug as a targeted drug-carrier combination, these two models tend to represent a more general (non-specific) and simplified situation which although may be true for small molecules such as the free-drug, is certainly not the case for large molecules such as the carrier or drug-carrier conjugate. They are therefore both essentially concerned with small molecules such as the free-drug, and are generally inappropriate for macromolecules.

The main advantage of these two general drug-targeting models [254, 255] compared with the model presented in this study is that they allow prediction of the pharmacological benefits to be derived from the administration of a drug-carrier combination, by presenting, and solving at steady-state, differential mass balance equations describing the concentrations of drug provided from a carrier. However, for the reasons already outlined, these models [254, 255], their method of solution, and predictions, may indeed be appropriate to low molecular weight prodrugs or indeed any drug with a molecular radius less than about 13 Å say in this more general situation, but are however generally inappropriate for macromolecular drug disposition and the targeting of macromolecular prodrugs to the lymph, or indeed for any molecules larger than the size at which free extravasation no longer occurs (i.e. greater than about 13 Å radius).

A general transport limitation model

The model presented in this study differs in several important respects from the set of general models presented in a recent publication by Aubrée-Lecat et al. [256], to investigate the influence of transport limitation on the amount of macromolecular drug taken up by a general target. These differences are discussed below.

To demonstrate the influence of transport limitation on the amount of macromolecular drug taken up by a target, four general compartmental pharmacokinetic models have been discussed [256]. Two of these models were one compartment models, whilst the other two consisted of a central and a peripheral compartment. In the latter cases the

two compartments modelled the transport limitation due to the presence of two intercompartmental transfer rate constants in both models. Two uptakes, one undesired, i.e. elimination, and one desired, i.e. representing uptake by a target, were also included in each model. These uptakes were represented by two general exiting parameters and were designated to be either both linear or both saturable. The first model therefore consisted of two linear elimination processes acting from a central compartment (the site where the initial drug dose is introduced). The second model consisted of two linear elimination pathways, each of them working from different compartments, i.e. central and peripheral. The third model consisted of a central compartment (with the same general volume as the first model) and two saturable uptake mechanisms. Finally the fourth model consisted of a central and peripheral compartment (each with the same respective general volume as those in the second model) with one nonlinear elimination mechanism in each. For each individual model the authors then solved the respective differential equation(s) for the concentration of drug in each compartment with respect to time and put these solutions into respective differential expressions for the amount of undesired (elimination) and desired (uptake by target) uptake in each model. These differential uptake equations for each individual model were then integrated to give the amount of desired and undesired uptake for each model. This was done algebraically for the first three models and numerically for the fourth. Having obtained equations for the amount of desired and undesired uptake for each model, each of these equations was then converted to infinite time. Having obtained these infinite time equations for each model the authors then investigated via simulations and plots, the fraction of the injected dose taken up by a general target at infinite time after injection as a function of different parameters of interest. The authors first compared the behaviour of the two models whose uptakes were both linear, i.e. the first two models, by investigating the fraction of the injected dose taken up by the target at an infinite time after injection as a function of: (a) the uptake rate by the target for different values of the rate constant of undesired elimination, (b) the ratio of the volume of the peripheral compartment over the volume of the central

compartment, and (c) the transfer rate from the first to the second compartment. The authors then compared the effect of transport limitations on the fraction of the injected dose taken up by the target at infinite time after injection when both uptakes were nonlinear, i.e. comparing the third and fourth models, investigating this as a function of: (a) the normalised maximum velocity of the undesired elimination, (b) the rate constant of the transfer from the first to the second compartment, and (c) the normalised uptake of the undesired elimination. In each case the numerical values used for these investigations were taken from the literature, and in general were for mice.

The main results from these general investigations by Aubrée-Lecat et al. [256], include the following somewhat obvious conclusions: (a) it is of little use to increase the affinity of a macromolecular drug for its target when a transport limitation and an undesired elimination from the plasma are both present, (b) an increase of the uptake (rate of uptake or maximal velocity) by the target is not very productive because permeability of the capillary wall is the factor limiting access of macromolecules to tissues, and (c) maximal efficiency of therapeutic macromolecules could be achieved by increasing, where feasible, the transport across the barrier between the plasma and the target, and by preventing the undesired elimination as much as possible.

As with the two drug-targeting models [254, 255] described earlier, these general transport limitation models [256], also have several important disadvantages compared with the model presented in this study. They do not consider the effect of molecular size or indeed charge on distribution since each of the models parameters are assigned only general values from the literature, with the two transfer rates between the compartments taking values appropriate for macromolecules the size of 150kDa and 420kDa only, and the two uptake rates being varied to cover a range of general values. The models therefore do not really take into account any physiological membranes or account for any different regional capillary permeabilities to different size macromolecules, since there are no parameters or expressions built into their structure to model or control this, and are subsequently therefore only really appropriate for

macromolecules the size of either 150kDa or 420kDa. A macromolecule of 420kDa is probably too big to be of much use in drug-targeting anyway. Similarly the compartments of each model do not represent specific key tissues (i.e. blood, lymph and liver), but instead represent general central or central and peripheral compartments. Likewise, when the term uptake by its target is used in each of these models, it is used only in a general sense to refer to some general values assigned to a unidirectional exiting parameter from the model, rather than actually modelling the movement between the blood and a specific key target such as the lymph. The two major elimination processes, renal excretion and hepatic metabolism, are not specifically modelled for, but are instead inappropriately combined together as one general elimination process from the central compartment, which is assigned values appropriate for only two macromolecule sizes (150 kDa and 420kDa). The investigations performed with these models are done so at infinite time which means that the equation(s) for the amount of drug with respect to time are not used for any other purpose than obtaining these infinite time equation(s). Investigations at infinite time may only be appropriate for extremely large, inert macromolecules such as 420kDa, since this size macromolecule may perhaps still be within the body after long periods of time, whereas smaller macromolecules, even the size of 150kDa, would almost certainly have been distributed around the body and been either partially or entirely eliminated by then.

As a consequence of the above points, the four general models presented in this recent publication [256], do not possess any major advantages over the model presented in this study.

Models concerned with antibody distribution and uptake into solid tumours.

Evidence in the literature indicates that monoclonal antibodies (MAbs) and their fragments do not distribute homogeneously and in adequate quantities in tumours [81-102]. Indeed, it had become apparent that pharmacokinetic issues at the whole-body (global) and microscopic levels must be considered to analyse the distribution of MAbs (and immunotoxins) in tumours [47, 57, 59, 70-72, 86, 96, 99, 245, 252, 253, 391]. Consequently several physiological pharmacokinetic models have been developed that integrate or involve various aspects of these global and microscopic issues [86, 87, 89-98, 252, 253, 262]. Although the assumptions made in each of these models varies, they can however typically be categorised either geometrically as follows:

(a) General cases of planar (cartesian) geometry [86, 96];

(b) A cylindrical geometry in which the centre of the cylinder is a tumour capillary which is surrounded by tumour interstitium [90, 95, 98];

(c) Varying cases of spherical geometries: (i) a tumour nodule uniformly surrounded by identical capillaries [91]; (ii) small avascular tumours surrounded by a fluid medium [262]; (iii) a macroscopic tumour nodule of densely packed tumour cells [87]; (iv) a prevascular tumour nodule embedded in normal tissue treated as a well-mixed compartment with the surrounding one blood and one lymphatic capillaries [97]; and (v) a homogeneously [89, 92] or nonuniformly [93, 94] perfused tumour surrounded by normal tissue;

or,

as compartmental models [252, 253].

Each of the geometrical models uses input parameters from a variety of sources (experimental studies in vitro, in animals, and occasionally clinical trials) and explores the sensitivity of MAb localisation in a tumour to variations in parameters the authors consider to be important. These parameters typically being any of either plasma

pharmacokinetics [86, 87, 90, 91, 96-98], vascular permeability [94, 98], transcapillary transport influx [87, 89-91, 97] and lymphatic efflux [93, 97] rates, diffusion coefficient [86, 87, 89-98, 262], convective transport [89, 90, 92-95], antibody dose [90, 93, 94], antibody binding affinity [86, 87, 90, 91, 94-98, 262], antigen density [94, 97], MAb size [90, 91, 94, 98], antibody metabolism [90, 94, 95, 98], necrosis [93, 94], or tumour interstitial pressure and fluid velocity [89, 92, 93, 95]. Each geometric model essentially consists of either one, two, or all three of the following major aspects, ((I), (II), (III)), each of which is embodied in one or more equations. The systems of equations in each model are solved numerically, often on very powerful computers such as a Cray supercomputer, and simulations are then performed to test the sensitivity of those parameters which the authors consider to be most influential in determining MAb distribution in tumours as a function of position and time (the simulations are also performed on very powerful computers). The major aspects of each of these geometrical models are as follows:

(I) The authors of several of the models, [86, 87, 90, 91, 96-98], incorporate an equation for the global plasma kinetics by presenting a biexponential or triexponential expression based upon experimental data (e.g. typically [251, 455, 456] in the former case and [457, 458] in the latter) to describe the time (temporal) decay of MAbs and their fragments in the plasma.

(II) In some of the models, [89-91, 97], movement of MAbs and their fragments across capillary membranes into the interstitium (normal tissue interstitium or tumour interstitium, as appropriate, depending upon the particular geometry of the model) is also represented. This movement is generally represented by the Kedem and Katchalsky flux equations [264, 265] either in their original form or an adapted form, or similar flux equations for the diffusive and convective transport of molecules across membranes. These flux equations are adapted in various ways, usually by balancing the mass transported across the interface between a capillary (blood, or where appropriate, lymphatic) and the interstitial space (tumour or normal interstitial space, depending

upon the geometry of the model), to give a first-order differential equation. The particular adaptations the authors make depends upon whether they are considering diffusion, convection, or both, to be the dominant transport mode (despite a very large literature on the subject it is still unclear how macromolecules cross capillary walls, although convection is commonly believed to account for most movement [460]). In some of these models both diffusive and convective flux of MAb through the capillary wall is assumed [89, 90], whereas in the others it is assumed to be either by diffusion only [91], or by convection only [97].

(III) In each of the models, [86, 87, 89-98, 262], a convection-diffusion-reaction partial differential equation (the general form of which depends upon the type of geometry being considered), and where appropriate (if binding of MAb to tumour antigen molecules, e.g. [86, 87, 90, 91, 94-98, 262], or MAb metabolism, e.g. [90, 94, 95, 98], is also being considered) a first order rate equation, are used to describe the spatial and temporal movement and distribution of free MAb and MAb-antigen bound concentration respectively in the tumour interstitium. Each convection-diffusion-reaction equation appears with a diffusion term, and either with [89, 90, 92-95] or without [86, 87, 91, 96-98, 262] a convection term, with [89, 92-95] or without [86, 87, 90, 91, 96-98, 262] a distributed solute source term (which when present is represented by the classical pore model for transcapillary exchange [461]), with [86, 87, 90, 91, 94-98, 262] or without [89, 92, 93] an extravascular binding term, and with [90, 94, 95, 98] or without [86, 87, 89, 91-93, 96, 97, 262] a metabolism term, as appropriate, depending upon the authors assumptions, i.e. whether these processes are being represented as occurring or not occurring. When MAb metabolism is being considered, [90, 94, 95, 98], it is assumed to occur only when MAb is bound to tumour antigen, and is usually represented in the accompanying first-order rate equation. Each convection-diffusion-reaction equation focuses on radial diffusion only, and has initial and boundary conditions defined when they are appropriate, i.e. either at the interface between the tumour and the surrounding normal tissue in which it is embedded in [89,

92-94, 97, 262], or at the interface between the tumour and the blood capillary wall [86, 87, 90, 91, 95, 96, 98]. The authors concentrate on either diffusive or convective transport, or both, for the percolation of MAb and MAb fragments through the tumour because as in the case of movement across capillaries, it is uncertain which is the dominant process (convection has also been considered the most important process in transport of macromolecules over macroscopic distances in tumours [462], although the basis for movement across microscopic distances into densely packed cellular areas is not at all clear, the pattern of penetration suggests diffusion [86, 96]).

To date, probably the most interesting and important result from these predictive geometrical models has been the concept of a "binding site barrier" to antibody percolation [86, 87, 90, 91, 94-98, 262], where the very fact of antibody binding to the tumour cell surface antigen inhibits the uniform distribution of antibody throughout the tumour. This is because percolating antibody tends to bind to tissue in the vicinity of the capillaries from which it extravasates. The binding site barrier is a function of binding affinity, antigen concentration, and the antibody transport coefficients, although these parameters can play a double-edged role [86, 87, 90, 91, 94-98, 262]. For example, increasing the diffusion coefficient of the antibody enhances its penetration of the tumour at early times and more antibody is bound more uniformly throughout the tumour, however, at longer times a higher diffusion coefficient also accelerates the loss of antibody from the tumour. Also, although increasing the binding affinity results at early times in a more heterogeneous distribution of antibody (more antibody is bound in the outer regions of the tumour, but far less penetrates to the tumour centre), at later times the distribution is less heterogeneous and more antibody is retained throughout the tumour. The implications of the binding site barrier have important implications for tumour therapy since depending upon the purpose one may often want to maximize particular characteristics of the antibody distribution. For diagnostic imaging for example, highly specific binding of antibody to antigen may be optimal, and microscopic homogeneity of the binding throughout the tumour is not

important. Alternatively if the aim of therapy is to incapacitate the tumour vasculature, then poor antibody percolation may be advantageous. However, if it is necessary to reach all viable cells within the tumour, good percolation may be essential. Other results from these predictive geometrical models can generally be summarised as showing that the poor penetration and heterogeneous distribution of MAb in tumours may result from high antibody affinity [86, 90, 96], high MAb molecular weight [90, 98], increased rates of antibody metabolism [90, 94, 98], slow rates of transcapillary influx [89-91, 97] and/or fast rates of lymphatic efflux [93, 97], high antigen concentration [97], and the elevated tumour interstitial pressure [89, 92, 93, 95]. Each of these factors therefore also plays an influential role.

These geometrical models [86, 87, 89-98, 262] have several important disadvantages compared with the physiological pharmacokinetic model presented in this study. The geometrical models are essentially concerned with exploring the sensitivity of MAb or MAb fragments (or immunotoxin) distribution and uptake in solid tumours and are consequently generally primarily concerned with issues at the local microscopic level in solid tumours (which as outlined in Chapter 1 are known to possess their own peculiar vascular properties) rather than specifically addressing the more regional problem of modelling (under normal vascular conditions) the movement of macromolecular drugs between the three major compartments of the body (blood, lymph, and liver), and the two major elimination processes (renal excretion and hepatic metabolism), which are important in macromolecular drug distribution and the targeting of anticancer agents to the lymph, and hence to any cancer micrometastases located there. Indeed, only one of the geometrical models considers the case of a prevascular tumour nodule, i.e. one of the models presented by Weinstein and co-workers [97], and only a few of the models also incorporate other important aspects of MAb pharmacology such as issues at the global (whole body) pharmacokinetic level [86, 87, 90, 91, 96-98]. Consequently, apart from one of the models, [97], no allowance is made for an interstitial fluid or lymph compartment, although some of the models, [93, 97], do incorporate lymphatic

efflux parameters. The two main elimination processes, renal excretion and hepatic metabolism are also not represented. Also, any transcapillary transport, is where given, generally represented in the form of flux equations, which are only really relevant for the particular MAb being studied, as indeed are any global pharmacokinetic issues or lymphatic efflux parameters where given. This is because many of the parameters used in each of the respective model equations (bi- or tri-exponential expression, first-order differential equation, convection-diffusion-reaction partial differential equation, and first-order rate equation, as appropriate, depending upon the particular geometrical situation being considered and the authors assumptions) are only appropriate for that particular size MAb or MAb fragment being considered (typically IgG (mw 150kD) [87, 89-95, 97, 262], $F(ab')_2$ (mw 100kD) [89, 90, 92, 98], or Fab (mw 50kD) [86, 89, 90, 92-96]) and not any other. Hence, if any other size macromolecule was to be considered, many new values for these parameters (typically these include as appropriate, the plasma concentration bi- or tri-exponential temporal decay parameters, the plasma-to-tissue transport coefficient, the lymphatic efflux parameter, the diffusion constant, convective transport terms, rate constants associated with binding and metabolism, and various parameters associated with distributed solute source terms) or indeed entirely different parameters, would be needed for each different size macromolecule. This data either does not exist (for either animals or man), or is extremely difficult to calculate experimentally. The fact that these authors use common diffusion and convection terms, parameters or expressions to describe any movement is perhaps a disadvantage in itself, because not only is it still not entirely clear which is the dominant process for either transcapillary transport, movement through the interstitium, or percolation into and through tumours, but also the inclusion of these processes means that the models require such a large number of input parameters that the equations correspondingly become extremely bulky and complex. A model which is based upon or incorporates extravasation data, blood-tissue/tissue-blood flow rates and organ volumes, as the model presented in this study does, overcomes these problems since it will automatically be representing any diffusion or convection as well, as it is real data

(extravasation data). The geometrical models therefore do not consider the effect of molecular size or indeed charge on distribution in the body, nor do they take account for any different regional capillary permeabilities to different size macromolecules since there are no parameters or expressions within the various models equations to model or control these processes. The only effects of molecular size or charge considered by these models are therefore those for the particular MAb or MAb fragment being studied, and are for the distribution either inside a solid tumour, or in one case only [97], a prevascular tumour nodule, and are therefore generally at a microscopic level only. Another important disadvantage with the geometrical models is that due to the large number of parameters required, most of the resulting complex and bulky equations describing the models, and indeed the subsequent simulations, can generally only be solved and performed respectively on powerful mainframe computers such as a Cray super-computer. This numerical method of solution usually involves the use of very powerful specifically written computer programme packages or algorithms, and often incorporates collocation finite element processes. Consequently exact analytical solutions as a function of time for these models are not usually obtainable and the models become so complex that they can not really be used for fitting purposes of any kind. They are also extremely difficult to validate either analytically, numerically, or experimentally. In brief, as a consequence of these points, these geometrical models therefore do not specifically model or allow prediction of, as a function of size or time, the movement of macromolecules (either proteins or uncharged polymers) in man.

The main advantage of these geometrical models [86, 87, 89-98, 262] compared with the model presented in this study is that they do allow insight at a microscopic level into the sensitivity of MAb or MAb fragment distribution and uptake in solid tumours, or in one case [97], a prevascular tumour nodule. This is desirable from a predictive point of view and it would be interesting to extend the studies presented here to include models of tumour uptake. Never the less it was felt that the emphasis placed by the above models on vascular tumours was not the prime concern and that attention

should be focused on delivery to the lymph compartment and hence to any cancer micrometastases located there, so that they can destroy or neutralize these malignant cells before they have a chance to become vascularized or spread. For the model presented in this study it was decided not to have an additional compartment, i.e. a fourth compartment, representing a cancer micrometastases cell. There were several reasons for this: Firstly, the inclusion of such an additional compartment and any associated input parameters or expressions would result in a model of such complexity that one would then be faced with many of the disadvantages of the geometrical models outlined above, i.e. they have too many parameters, are only solvable numerically on powerful mainframe computers etc. Such a model could not be solved to give exact analytical solutions and specific equations for each compartment and hence could not practically be used for fitting purposes. Also the complexity and amount of work required to do this as well would perhaps be beyond the time and facilities of a single Ph.D. study. Secondly, assigning appropriate realistic values to this additional compartment or any associated or additional parameters would be very difficult, particularly if the movement between the lymph compartment and the cancer micrometastases cell was represented by anything other than a first-order rate process. Thirdly, the interstitial fluid or lymph compartment is in any case the target tissue/site the macromolecular drug system must reach in order to deliver the therapeutic anticancer agent to the cancer micrometastases cells, and once in this compartment, it is reasonable to assume the various specifically engineered built-in processes found in most macromolecular drug conjugate systems will allow the movement, uptake, or release of a proportion of the dose of attached therapeutic agent into cancer micrometastases cells located there at the appropriate time. Finally, and perhaps most importantly of all, this study was primarily concerned with the somewhat different problem of modelling the movement of macromolecules (either proteins or uncharged polymers) under normal vascular conditions between the blood circulation and tissues and modelling the two major elimination processes (renal excretion and hepatic metabolism). The study was not immediately concerned with either solid tumours or

indeed any uptake, binding and distribution in solid tumours or prevascular tumour (cancer micromestastases) cells. Rather the objective was to develop models of the movement of macromolecules between the blood, lymph and liver, and to model the two major elimination processes, in order to obtain the optimum size candidate macromolecule for distribution to tissues.

Some authors have provided a simpler approach, compared to the geometrical models, of exploring MAb (or immunotoxin) uptake and distribution in tumours by considering a compartmental model, although there are comparatively few examples of these models in the literature. Typically the best of these compartmental models are the models presented by Sung et al [252, 253] since they can be regarded as representing simplified versions of the earlier compartmental models [244-250]. The models of Sung et all [252, 253] avoid the use of a large number of adjustable parameters, and hence they avoid the complexity of the equations used in earlier models which has made earlier models too cumbersome for data analysis. The simplified models [252, 253] consist of a plasma compartment and tumour tissue interstitium compartment, both of uniform concentration, with the latter compartment being further divided into two compartments containing cell-bound and free interstitial MAb [253] or immunotoxin [252]. In these models it is assumed that: (a) after a bolus i.v. injection the plasma MAb [253] or immunotoxin [252] concentration decreases biexponentially; (b) MAb [253] or immunotoxin [252] is transported from the plasma into the tumour unidirectionally at a rate equal to the product of the plasma-to-tissue transport constant (a first-order rate constant) and the plasma concentration; (c) MAb [253] or immunotoxin [252] in the tumour interstitium rapidly equilibrates between free and bound forms according to either the Langmuir adsorption isotherm [253], an equation where the binding affinity constant and the interstitial concentration of binding sites can be treated as separate parameters [253], or as a single constant [252], equal to the product of these two parameters; and (d) loss of free MAb [253] or immunotoxin [252] from the tumour occurs at a rate equal to the convective flow of interstitial fluid in

tumours, multiplied by the coexisting interstitial unbound MAb [253] or immunotoxin [252] concentration. The equations used to describe these two models, and which are necessarily solved either partially [252] or entirely [253] numerically, are therefore a biexponential expression for assumption (a), the appropriate respective Langmuir or single constant (as described above) for the rapid equilibration between free and bound forms in the tumour interstitium for assumption (c), a mass balance equation which states that the sum of the bound and free tumour interstitial concentrations is equal to the total tumour interstitial concentration, and finally a first-order differential equation which is for assumptions (b) and (d) combined and describes the overall rate of change of MAb [253] or immunotoxin [252] concentration in the tumour interstitium.

The strategy behind the development of these two compartmental models presented by Sung et al [252, 253] was to develop a simpler model of macromolecular transport, employing parameters that correlate with physiological processes, which could capture the predominant features of transport events, yet be parsimonious enough to be amenable to data fitting. Hence their purposes of development was 2-fold; (a) to examine theoretically via simulations (using appropriate model parameter estimates from the tumour physiology literature) the effects on MAb [253] or immunotoxin [252] uptake in solid tumours produced by changing the value of the parameters believed by the authors to play an important role in transport and binding (these model-predictions are then tested experimentally); and (b) to be capable of being applied to the analysis of animal experimental data in order to obtain quantitative estimates of MAb [253] or immunotoxin [252] transport and binding constants in in-vivo systems. The earlier of the two models [252] was used to describe the special case of doses being low enough so that binding sites in a tumour are far from being saturated (the low dose allowing the ratio of free and bound drug in the interstitium to be represented as a constant). In contrast, the later of the two models [253] was used to describe the more common case of doses being sufficiently high so that binding sites approach saturation. The latter of the two models was hence used to extend the work of the earlier model over a wider

dose range (by representing binding with the Langmuir adsorption isotherm for reversible, saturable binding). The main results from these two compartmental models are; (a) at low doses an increase in binding affinity may lead to an increase in MAb uptake [252, 253]; (b) at doses approaching saturation of antigen or when uptake is permeation limited an increase in the binding affinity from moderate to high affinity will have only a small effect on increasing MAb uptake [253]; (c) an increase in antigen density will greatly increase MAb uptake when uptake is not permeation limited [253], and (d) for high dose applications, efforts to increase MAb uptake in a tumour should emphasise the identification of an abundantly expressed antigen on tumour cells more than the selection of a very high affinity MAb [253]. These simulations will clearly be useful in design of antibody-based delivery systems, though they do not consider the intracellular fate of the molecules following binding.

As with the geometrical models, these two compartmental models development by Sung et al [252, 253], also have several restrictions compared with the model presented in this study, and these are as follows: They are both concerned with the uptake and binding of MAbs or immunotoxins in solid tumours and were consequently developed to be used solely in both the description of this process and in the analysis of associated tumour experimental data, rather than being developed to address the general issue of modelling the movement of macromolecular drugs (under normal vascular conditions) between the major compartments of the body. They are consequently both concerned with issues in solid tumours (which are known to posses their own peculiar vascular properties) rather than the extravasation of macromolecular drug systems under normal vascular conditions. They do not have any compartments representing the liver or the normal total interstitial fluid (lymph), nor do they model or represent the two main elimination processes (renal excretion and hepatic metabolism). The only elimination catered for in these two models [252, 253] is that which occurs either via interstitial fluid flow from the tumour or that which occurs with the temporal decay of the biexponential plasma concentration equation, both of which, for the

reasons explained later, are only appropriate for the particular MAb or immunotoxin being studied. They do not consider the effect of molecular size or any other important physicochemical properties such as charge on distribution, nor do they take into account the different regional capillary permeabilities or extravasation rates to different size molecules. Indeed, the only transcapillary movement represented in these two models [252, 253] is a first-order unidirectional process from the plasma to the tumour tissue which is governed by the product of a plasma-to-tissue transport constant and the coexisting plasma concentration, and which is also only relevant for the particular MAb or immunotoxin being studied. Macromolecules the size of the particular MAb or immunotoxin were considered by the authors (these being toxins of molecular weight 60KD and 210KD in one case [252], and an IgG monoclonal antibody of approximate molecular weight 150KD in the other [253]). The parameters used in each of the respective equations to describe each model are appropriate for that particular size MAb or immunotoxin macromolecule only, and are generally inappropriate for macromolecules of any other size. Hence, if any other size macromolecule was to be considered, many new values for these parameters (these parameters mainly being the plasma concentration biexponential temporal decay parameters, the plasma-to-tissue transport constant, the convective flow of interstitial fluid in tumours, the fractional interstitial volume of the tumour, the MAb binding affinity constant and the interstitial concentration binding sites), would need to be determined for each different size macromolecule. This datum either does not exist for animals or man, or is extremely difficult to determine experimentally. The later of these two compartmental models [253], also has the added important disadvantage in that the system of equations describing the model does not have an exact analytical solution, but must be solved entirely numerically using a complex algorithm (in this case a fourth-order Runge-Kutta algorithm from Mathematica) which can only be run on a powerful computer. Consequently any fitting of experimental data to these compartmental models [252, 253] can only be carried out using finite difference processes via computer programmes constructed from subroutines or algorithms from various statistical and

mathematical libraries. This is a disadvantage due to both the difficulty in constructing such a 'hybrid' programme and the requirement of a powerful computer to perform this operation on, and of course also the sheer complexity of the process itself by using such finite element processes. The main advantage with these two compartmental models [252, 253] is that they allow both a description and investigation of the uptake and binding of Mabs and immunotoxins in solid tumours, since they were developed for that purpose.

The afore mentioned theoretical/predictive pharmacokinetic models [86, 87, 89-98, 252-256, 262] are of considerable interest in relation to the work presented here but do not address the main objectives of this study. The model presented in this study models and allows prediction of, as a function of size and time, the movement of macromolecules (either protein or uncharged polymers) under normal vascular conditions between three important compartments of the body (blood, lymph, and liver), and models the two major elimination processes (renal excretion and hepatic metabolism). The model presented here takes account of varying molecular radius size and charge, and enables renal excretion and hepatic metabolism to occur from separate compartments. It is also able to some extent to take account of the different regional capillary permeabilities to different size macromolecules and the different physiology and flow rates within each compartment (tissue). The model and accompanying computer programme presented in this study is able to predict for any desired molecular radius within the 20 - 70 Å radius range and for any desired interval of time, the fraction of an intravenously administered macromolecular drug dose that is present in the blood, the lymph and the liver, and also the fractions of the dose which have been excreted by the kidney and hepatically cleared by the liver (the total fraction of the dose eliminated is also given). This is a vitally important issue, since from a drug-targeting point of view it is extremely important to know and be able to predict, the fate of a macromolecular drug in the body for each of these key tissues and elimination processes, and which macromolecule or macromolecular carrier or drug conjugate

system is most likely to produce the greatest fraction of the dose in the tissue fluids and lymph. Each of these issues is essentially determined by molecular size and charge, which the model presented in this study directly considers and the other theoretical/predictive models in the literature do not. The existing models in the literature are either inappropriate for macromolecules since they assume rapid biodistribution or are appropriate for one size of macromolecule only but are too theoretical and are mainly concerned with issues in solid tumours.

In addition to the above outlined advantages and strengths, the model presented in this study can also, as has already been described and discussed, be solved to give exact analytical equations and solutions for each compartment, and can be used to generate macromolecule distribution data following the fitting of the models equation describing plasma concentration versus time to plasma concentration versus time data by finding the appropriate k_m rate. Indeed, the modelling process presented in this study was developed so that these important criteria were satisfied. This was achieved by restricting the model to only the three compartments of the body (blood, lymph, and liver), the two major elimination processes (renal excretion, i.e. k_{excr}, and hepatic metabolism, i.e. k_m), and the other key inter-compartmental processes (k_{12}, k_{21}, k_{13}, k_{31}). Additional compartments, namely a compartment representing a cancer micrometastases cell, and/or additional tissue compartments could have been added to the model, but then the mathematical equations describing the model would then have become too complicated and complex to be solved analytically and would therefore have had to be solved entirely by numerical methods (probably on a very powerful computer and using various subroutines and algorithms imported from a variety of sources). This in turn would have meant that specific equations for each compartment as a function of time would not have been obtainable, and the model could not easily be used for a fitting purpose of any kind, without employing more cumbersome numerical methods, such as finite-difference algorithms. Any simulations or fits of the model presented in this study were therefore by comparison much easier to perform.

The fitting of experimental protein and BSA - methotrexate data described in chapter 4 illustrated the usefulness of the model. In this case it was possible to vary the k_m parameter whilst keeping all the other parameters fixed until the clearance fitted the selected plasma concentration versus time data. Having obtained the appropriate k_m rate, it was then possible to use MACROHOURS to calculate the fractions of the dose expected to be found in each of the blood, lymph, and liver, and also the fractions of the dose which would be expected to be excreted and hepatically cleared over the desired time interval.

Another key advantage of the model presented here which should also be emphasised, is the separation of the elimination process renal excretion and hepatic metabolism, so that they each can occur as individual processes in their own right from the appropriate compartment (i.e. renal excretion from the blood compartment and hepatic metabolism from the liver compartment). The model was indeed developed so that this important criterion was satisfied as there is a need to use this information in the design of macromolecular prodrugs. In each of the key theoretical/predictive macromolecular anticancer drug and drug-targeting models in the literature these processes are, as has already been outlined, either not represented at all, or are combined together as a single elimination process occurring from the plasma, often in the form of biexponential or occasionally a triexponential temporal decay equation, and appropriate only to the particular size macromolecule being considered by the author (usually IgG).

Since the model presented here is based on physiological parameters, by altering the value of the appropriate parameter(s), it can be used to make predictions for other animal species (e.g. as in chapter 4) and for different disease states (e.g. decreasing or increasing the value of GFR to investigate renal disease in man whilst keeping all the other parameter at their human values).

The major weakness of the model used in this study is the need to specify the nature of the capillary endothelium as a single model for the whole body. Thus, data for

continuous endothelia, which are present in the bulk of tissues, were used. However, clearly in practice there would be a different uptake into tissue, with fenestrated capillaries. The number of tissue compartments could have been increased to allow simultaneous modelling of various endothelia but at present there is not enough physiological data to make this worthwhile. Indeed a weakness of the modelling study presented here lies in the lack of useful human F/P ratio and L/P ratio data available from the experimental literature, and in the lack of abundant F/P ratio and L/P ratio data available for the same animal species. The lack of any reliable F/P ratio and L/P ratio data beyond a molecular radius of 70 Å was one of the principal reasons why the model was not used for predictions for any macromolecules with a molecular radius greater than 70 Å. However, as already discussed in chapter 2 the F/P ratio and L/P ratio data used in this modelling study was probably a good representation of the likely situation for man with respect to tissues with continuous endothelia. Ideally extravasation concentration ratio data regarding the movement of macromolecules from the sinusoidal blood capillaries into the extravascular spaces of the liver (i.e. the liver/plasma ratio), the corresponding concentration ratio of the movement back again (i.e. the plasma/liver ratio), and the movement of macromolecules from the lymph to the blood (i.e. plasma/lymph ratio), would have been available to confirm the assumptions made in this modelling study that these ratios, particularly the liver/plasma ratio, are close to unity. As discussed in the appropriate subsection of chapter 2, the evidence in the literature, and indeed the absence of this datum itself, suggests that this is indeed generally the case for all macromolecules, except possibly the extremely large macromolecules or particles with which this study is not concerned. In the cases of the liver/plasma and plasma/liver ratios there might possibly be some constraints on movement which may lead to concentration ratios very slightly, and hence probably insignificantly less than unity, but there is insufficient data available at present to illustrate this. However, the model was designed to allow estimates of these ratios to be built into the model should reliable data become available in the future.

There are also no anionic or cationic L/P ratio data available to go with the selected anionic and cationic F/P ratio data. This meant that any simulations could not be performed for either anionic or cationic macromolecules. However, protein and uncharged macromolecules are the two main types of macromolecule used in drug targeting and these are modelled for by the model. The anionic results would be very similar to the protein simulations in any case, as illustrated by the F/P ratio fits and parameters of best-fit described in chapter 2. The model is however also designed to allow estimates of these anionic or cationic ratios or indeed similar mathematical models to those developed to model the selected F/P ratio and L/P ratio data, to be built into the model should these data become available in the future (an additional advantage of the model).

Some of the other parameters used in the model did not have well quoted values in the literature. These were principally the BLFR and the total blood flow rate from the liver. The reasoning behind the choice of values assigned to each of these parameters has already been discussed in the appropriate subsection of chapter 2. In each case the most appropriate, logical and sensible choices of value were made in light of all the information available, i.e. in man 2ml/min for BLFR and 1440ml/min for the total blood flow rate from the liver. However, as with any parameters in the model, the model is designed to allow the values of these parameters to be adjusted should better data become available in the future. A lack of known or well quoted values in the literature for some model parameters is a common weakness which befalls almost all physiological pharmacokinetic models. Often, this is because the experiments required to establish values for these parameters are extremely difficult or sometimes even impossible to perform. The BLFR parameter is probably such a parameter.

The rates of metabolism used in this study refer to first-order rates of loss from the macromolecules within the liver and hence from the system altogether. In reality some macromolecules will in fact be converted to other active moieties during hepatic metabolism and not lost from the system, though to try and model this would be

inappropriate as it will be a unique property of each macromolecule. Ideally more information would have been available in the literature to confirm that the three selected rates of metabolism (hepatic clearance) used in this study were reasonable choices for macromolecules. For the reasons discussed in chapter 3 they do appear to be good choices, although all the general trends described in that chapter would still be the same even if they were slightly too fast or too slow.

It was hoped that the fits of the model to the selected macromolecular animal plasma concentration versus time data described in chapter 4 would have been more successful. This exercise emphasised that proteins do not behave as inert, non interacting species in the blood circulation. Where some of the fits described in that chapter were not so successful as the others, it may have reflected both the difficulty in scaling between species (a common feature of almost all physiological pharmacokinetic models) and the unpredictability of some of the experimental data (some of the selected protein macromolecule plasma data from the literature showed anomalies in it before any fitting was even attempted). Indeed, in this respect the fits of the model to the plasma concentration versus time data of the selected BSA-methotrexate conjugates from the literature were relatively good, whilst the fits to the plasma concentration versus time data of the selected protein macromolecules from the literature were not quite so successful. Possible reasons for this have already been discussed in chapter 4. Also as discussed in chapter 4, it was not possible to use nonlinear regression directly for fitting data. This was due to the form of the model, i.e. the number of compartments and the number of compartmental processes, and also because the roots γ, α, β depend upon the relationships between k_{12}, k_{21}, k_{13}, k_{31}, k_{excr} and k_m, with each of these in turn depending upon their assigned baseline values, with k_{12} and k_{excr} also depending upon the particular molecular radius of the macromolecule as well. The best and most logical way of trying to fit the model to the macromolecular plasma clearance data was to vary k_m whilst keeping all the other parameters fixed, so that the most appropriate rate of hepatic clearance is established. However, to use Miniq [441] with

only k_m entered as a varying parameter would be inappropriate because then γ, α and β would take independent values instead of each being dependent upon the relationship between k_{12}, k_{21}, k_{13}, k_{31}, k_{excr} and k_m. The way forward was therefore to simulate MACROHOURS for different k_m rates whilst keeping all other baseline parameters fixed, to establish the best choice of k_m. Once this had been established, this k_m rate was re-entered into MACROHOURS and simulations performed over the desired time interval to predict the fraction of the dose expected to be found in each of the blood, lymph, and liver, and also the fractions of the dose renally excreted and hepatically cleared (and the total fraction of the dose eliminated).

Another weakness of the model is the assumption that each drug molecule is uniformly spherical. To have assumed otherwise would have meant that the structure of each macromolecule would have had to be considered individually, and this would have been extremely unpractical and virtually impossible to do.

For simplicity the model does not consider the fate of the free-drug/therapeutic agent once it has been released from the carrier macromolecule, since this was not the prime objective of this study. To have included any additional compartments or compartmental processes would only have distracted from this objective. For similar reasons the model also does not consider any binding of macromolecules to plasma proteins whilst in the blood since this is generally an unpredictable process anyway and is therefore very difficult to model, and generally , if at all, occurs with the small macromolecules which are not so important to this study.

The value of the work presented in this study may only be known when more human data are available. A lack of useful human (and indeed animal) macromolecular drug disposition data currently available from pharmacokinetic studies involving targeted macromolecular systems in the field of cancer chemotherapy (due to the relative newness of this approach), or indeed from the non-chemotherapy macromolecular drug pharmacokinetic literature as well, for key compartments of the body (blood, lymph,

liver) and two major elimination processes (renal excretion and hepatic clearance) makes it difficult to conclude whether the model and modelling study presented in this thesis is an accurate representation of what is actually happening in vivo, or if the problem has been oversimplified. Most of the tissue distribution data which is currently available in the literature is for animals rather than humans, often consists of only a few data points or plots without any published data, and is usually clearance data or tumour accumulation data rather than distribution data for other important tissues. However, as with any predictive model, the model presented here proposes what is believed to be a likely situation and can be used as a guidance for the direction of future investigations and experiments. In this respect it is hoped that this work will be of some value to the high degree of interest which is currently being shown towards drug-targeting in the field of cancer chemotherapy, particularly the use of passively targeted macromolecular conjugate systems, or indeed to the field of macromolecular drug disposition in general. To date, it is not clear where macromolecules are going once they have been administered into the body, be it humans or animals (the fits of the model to the animal data presented in chapter 4 illustrated the latter). The key macromolecular anticancer drug system and drug-targeting theoretical/predictive pharmacokinetic models currently available in the literature are either inappropriate for any size of macromolecule since they assume rapid biodistribution, or are appropriate for one size of macromolecule only but are mainly concerned with issues in solid tumours and are too theoretical. The aim of this study was therefore to try and throw some light on the subject of macromolecule biodistribution by investigating the effect of molecular radius on distribution by developing a model which would try to predict the fate of either protein or uncharged macromolecular drugs in the body as a function of time (under normal vascular conditions) for the key compartments of the body (blood, lymph, and liver) and the two main elimination processes (renal excretion and hepatic metabolism) which are important to both macromolecular drug distribution and the targeting of anticancer agents to the lymph and hence to any cancer micrometastases located there (and which can also be used for fitting purposes if

desired as well). The success of any macromolecular drug system depends upon such predictive models as the one presented in this study.

Suggestions for Future Work

1. To perform more simulations should better animal or any human F/P ratio and L/P ratio data become available in the future.

2. To perform more simulations should any data become available in the future which differs significantly from any of the values assigned to the unknown parameters.

3. To fit the model to more data should better or more useful animal or any human macromolecular drug disposition data from pharmacokinetic studies involving targeted macromolecular anticancer drug conjugate systems become available in the future.

4. Use a specific animal model to determine physiological parameters i.e. rat (mouse).

5. This study showed that the best choice of size macromolecule, macromolecular carrier or macromolecular drug conjugate system to produce the greatest fraction of a macromolecular drug dose in the lymph following an intravenous bolus dose are macromolecules within the intermediate radii range of 40/45 - 50/55 Å, with the lower intermediate sizes being the more successful over earlier times and at faster rates of hepatic metabolism (hepatic clearance), and the upper intermediate sizes being the more successful over later times and at slower rates of hepatic metabolism (hepatic clearance). It was shown that for a macromolecular drug or macromolecular drug conjugate system which in hepatically metabolised (hepatically cleared) very quickly, then even molecular

radii as small as 35Å can also be relatively effective at early times in getting a significant fraction of the does into the lymph. Protein macromolecules were found to be better candidates than uncharged macromolecules for delivering the greatest fraction of the dose of the target, the lymph, and hence to any cancer micrometastases located there. In the case of the protein macromolecules in the absence of hepatic metabolism (hepatic clearance), the upper intermediate size range could in fact be extended to 65Å radius over very long time periods. Experiments should therefore be performed in man using different size macromolecular drug systems (preferably for each size macromolecule within 35 - 65Å range) and measuring at appropriate time intervals (e.g. 240 hours at 4 hour intervals) the fractions of the dose in the blood, the lymph, and the liver, and also the fractions which have been renally excreted and hepatically cleared, to test these findings, although this is of course very difficult to do (other animals e.g. rats or mice could alternatively be used but then other problems such as inter-species variations in addition to the difficulty in performing the experiments themselves in animals as well also come into operation).

6. Any experiments in the field of cancer chemotherapy involving the targeting of macromolecular anticancer drug systems to the lymph and hence to any cancer micrometastases located there should be performed using a macromolecular carrier or macromolecular drug conjugate system (preferably proteins) within the intermediate 40/45 - 50/55Å size ranges (with macromolecular drugs with radii as small as 35Å radius or as large as 65Å radius also being useful in certain situations). If the rate at which the particular macromolecular drug system is hepatically metabolised (hepatically cleared) is known, then the choice of size will depend upon the desired onset and duration of tissue distribution of the macromolecular prodrug.

References

1. Schirrmacher, V. *Cancer metastasis: Experimental approaches, theoretical concepts, and impacts for treatment strategies.* Adv.Cancer Res., 43, 1-73, 1985.

2. Maeda, H. and Matsumura, Y. *Tumouritropic and lymphotropic principles of macromolecular drugs.* Crit.Rev.Ther.Drug Carrier Syst., 6, 193-210, 1989.

3. Fidler, I.J., Gersten, D.M. and Hart, I.R. *The biology of cancer invasion and metastasis.* Adv.Cancer Res., 28, 149-250, 1978.

4. Nicolson, G.L. *Cancer metastasis: Tumour cell and host organ properties important in metastasis to specific secondary sites.* Biochim.Biophys.Acta, 948, 175-224, 1988.

5. Weiss, L. *Principles of metastasis.* Academic Press, Orlando, 1985.

6. Hart, I.R., Goode, N.T. and Wilson, R.E. *Molecular aspects of the metastatic cascade.* Biochim.Biophys.Acta, 989, 65-84, 1989.

7. Nicolson, G.L. *Cancer metastasis: Organ colonization and the cell-surface properties of malignant cells.* Biochim.Biophys.Acta, 695, 113-176, 1982.

8. Blood, C.H. and Zetter, B.R. *Tumour interactions with the vasculature: angiogeneois and tumour metastasis;* Biochim.Biophys.Acta, 1032, 89, 1990.

9. Folkman, J. *Tumour angiogenesis.* Adv.Cancer Res., 43, 175-203, 1985.

10. Ausprunk, D.H. and Folkman, J. *Migration and proliferation of endothelial cells in preformed and newly formed blood vessels during tumour angiogenesis.* Microvasc.Res., 14, 53-65, 1977.

11. Dvorak, H.F., Nagy, J.A. and Dvorak, A.M. *Structure of solid tumours and their vasculature - implications for therapy with monoclonal antibodies.* Cancer Cells - a monthly review, 3, 77, 1991.

12. Nagy, J.A., Brown, L.F., Senger, D.R., Lanir, N., Van de Water, L., Dvorak, A.M. and Dvorak, H.F. *Pathogenesis of tumour stroma generation: a critical role for leaky blood vessels and fibrin deposition.* Biochim.Biophys.Acta, 948, 305-326, 1988.

13. Dvorak, H.F., Nagy J., Dvorak, J.T. and Dvorak, A.M. *Leaky vessels and extravascular coagulation in tumours.* FASEB, 2, A1410, 1988.

14. Dvorak, H.F., Nagy, J.A., Dvorak, J.T. and Dvorak, A.M. *Identification and characterization of the blood vessels of solid tumours that are leaky to circulating macromolecules.* Am.J.Pathol., 133, 95-109, 1988.

15. Jain, R.K. *Transport of molecules across tumour vasculature.* Cancer Metastasis Rev., 6, 559-593, 1987.

16. Brown, L.F., Dvorak, A.M. and Dvorak, H.F. *Leaky vessels, fibrin deposition and fibrosis - a sequence of events common to solid tumours and to many other types of disease.* Am.J.Respir.Dis., 140, 1104, 1989.

17. Dvorak, H.F., Dvorak, A.M., Manseau, E.J., Wiberg, L. and Churchill, W.H., *Fibrin gel investment associated with line 1 and line 10 tumour growth, angiogenesis and fibro plasma in guinea pigs. Role of cellular immunity, myofibroblasts, microvascular damage and infarction in Line 1 tumour regression.* J.Natl.Cancer Inst., 62, 1459, 1979.

18. Senger, D.R., Perruzzi, C.A., Feder, J. and Dvorak, H.F. *A highly conserved vascular permeability factor secreted by a variety of human and rodent tumour cells.* Cancer Res., 46, 5629-5632, 1986.

19. Senger, D.R., Galli, S.J., Dvorak, A.M., Perruzzi, C.A., Harrey, V.S. and Dvorak, H.F. *Tumour cells secrete a vascular permeability factor that promotes accumulation of ascitic fluid.* Science, 219, 983-985, 1983.

20. Connolly, D.T., Heuvalman, D.M., Nelson, R., Olander, J.V., Eppley, B.L., Delfino, J.J., Siegel, N.R., Leimgruber, R.M. and Feder, J. *Tumour vascular permeability factor stimulates endothelial cell growth and angiogenesis.* J.Clin.Invest., 84, 1470-1478, 1989.

21. Leung, D.W., Cachianes, G., Kuang, W-J., Goeddel, D.V. and Ferrara, N. *Vascular endothelial growth factor is a secreted angiogenic mitogen.* Science, 246, 1306-1309, 1989.

22. Keck, P.J., Hauser, S.D., Krivi, G., Sanzo, K., Warren, T., Feder, J. and Connolly, D.T. *Vascular permeability factor and endothelial cell mitogen related to PDGF.* Science, 246, 1309-1312, 1989.

23. Matsumura, Y., Kimura, M., Yamamoto, T., and Maeda, H. *Involvement of kinin-generating cascade in enhanced vascular permeability in tumour tissue.* Jpn.J.Cancer Res., 79, 1327-1334, 1988.

24. Maeda, H. *SMANCS and polymer-conjugated macromolecular drugs: advantages in cancer chemotherapy..* Adv.Drug Delivery Rev., 6, 181-202, 1991.

25. Matsumura, Y. and Maeda, H. *A new concept for macromolecular therapeutics in cancer chemotherapy: Mechanism of tumoritropic accumulation of proteins and antitumour agent smancs.* Cancer Res., 46, 6387-6392, 1986.

26. Simionescu, N. *Cellular aspects of transcapillary exchange.* Physiol.Rev., 63, 1536, 1983.

27. Jain, R.K. *Delivery of novel therapeutic agents in tumours: physiological barriers and strategies.* J.Natl.Cancer Inst., 81, 570, 1989.

28. Maeda, H., Matsumoto, T., Konno, T., Iwai, K. and Ueda, M. *Tailor-making of protein drugs by polymer conjugation for tumour targeting. A brief review on smancs.* J.Protein Chem., 3, 181-193, 1984.

29. Suzuki, M., Takahashi, T. and Sato, T. *Medical regression and its functional significance in tumour-supplying host arteries.* Cancer, 59, 444, 1987.

30. Douglas, S.J., Davis, S.S. and Illum L. *Nanoparticles in drug delivery.* Crit.Rev.Ther.Drug Carrier Syst., 3, 233, 1987.

31. Tomlinson, E. *Passive and active vectoring with microparticles: localisation and drug release.* J.Cont.Rel., 2, 385-391, 1985.

32. Tomlinson, E. *Theory and practice of site-specific drug delivery.* Adv.Drug Delivery Rev., 1, 127-131, 1987.

33. Colcher, D., Esteban, J.M., Carrasquillo, J.A., Sugarbaker, P., Reynolds, J.C., Bryant, G., Larson, S.M. and Schlom, J. *Quantitative analysis of selective radiolabelled monoclonal antibody localisation in metastatic lesions of colorectal cancer patients.* Cancer Res., 47, 1185-1189, 1987.

34. Halsall, A.K., Fairweather, D.S., Bradwell, A.R., Blackburn, J.C., Dykes, P.W., Howell, A., Reeder, A and Hine, K.R. *Localisation of malignant germ cell tumours by external scanning after injection of radiolabelled anti-alpha-fetoprotein.* Br.Med.J., 283, 942-944, 1981.

35. Longley, C., Furmanski, P., Dienhart, D.G., Lear, J., Bloedow, D., Kasliwal, R. and Bunn, Jr., P.A., *Pharmacokinetics, biodistribution, and gamma camera imaging of ^{111}In-KC-4G3 murine monoclonal antibody in athymic nude mice with or without human tumour xenografts.* Cancer Res., 50, 5954-5961, 1990.

36. Holton, III, O.D., Black, C.D.V., Parker, R.J., Covell, D.G., Barbet, J., Sieber, S.M., Talley, M.J. and Weinstein, J.N. *Biodistribution of monoclonal antibody IgG1, $F(ab')_2$, and Fab' in mice after intravenous injection.* J.Immunol., 139, 3041-3049, 1987.

37. Trang, J.M., LoBuglio, A.F., Wheeler, R.H., Harvey, E.B., Sun, L., Ghrayeb, J. and Khazaeli, M.B. *Pharmacokinetics of a mouse/human chimeric monoclonal antibody (C-17-1A) in metastatic adenocarcinoma patients.* Pharm.Res., 7, 587-592, 1990.

38. Khazaeli, M.B., Saleh, M.N., Liu, T.P., Meredith, R.F., Wheeler, R.H., Baker, T.S., King, D., Secher, D., Allen, L., Rogers, K., Colcher, D., Schlom, J., Shochat, D. and LoBuglio, A.F. *Pharmacokinetics and immune response of ^{131}I-chimeric mouse/human B72.3 (human γ4) monoclonal antibody in humans.* Cancer Res., 51, 5461-5466, 1991.

39. Frodin, J-E., Lefvert, A-K. and Mellstedt, H. *Pharmacokinetics of the mouse monoclonal antibody 17-1A in cancer patients receiving various treatment schedules.* Cancer Res., 50, 4866-4871, 1990.

40. Rosenblum, M.G., Murray, J.L., Haynie, T.P., Glenn, H.J., Jahns, M.F., Benjamin, R.S., Frincke, J.M., Carlo, D.J. and Hersh, E.M. *Pharmacokinetics of ^{111}In-labelled anti-p97 monoclonal antibody in patients with metastatic malignant melanoma.* Cancer Res., 45, 2382-2386, 1985.

41. Pentel, P.R., Keyler, D.E., Gilbertson, D.G., Ruth, G. and Pond, S.M. *Pharmacokinetics and toxicity of high doses of antibody Fab fragments in rats.* Drug Metab.Dispos. 16, 141-145, 1988.

42. Kiozumi, M., Endo, K., Watanabe, Y., Saga, T., Sakahara, H., Konishi, J., Arano, Y., Miyachi, Y., Kashihara-Sawami, M. and Imamura, S. *Immunoscintigraphy and pharmacokinetics of indium-111-labelled ZME-018 monoclonal antibody in patients with malignant melanoma.* Jpn.J.Cancer Res. (Gann), 79, 973-981, 1988.

43. Haisma, H.J., Kessel, M.A.P., Silva, C., van Muijen, M., Roos, J-C., Bril, H., Martens, H.J.M., McCabe, R. and Boven, E. *Human IgM monoclonal antibody 16.88: pharmacokinetics and distribution in mouse and man.* Br.J.Cancer, 62, 40-43, 1990.

44. Stewart, J.S.W., Sivolapenko, G.B., Hird, V., Davies, K.A.A., Walport, M., Ritter, M.A. and Epenetos, A.A. *Clearance of ^{131}I-labelled murine monoclonal antibody from patients blood by intravenous human anti-murine immunoglobulin antibody.* Cancer Res., 50, 563-567, 1990.

45. Zalutsky, M.R., Moseley, R.P., Coakham, H.B., Coleman, R.E. and Bigner, D.D. *Pharmacokinetics and tumour localization of ^{131}I-labelled anti-tenascin monoclonal antibody 81C6 in patients with gliomas and other intracranial malignancies.* Cancer Res., 49, 2807-2813, 1989.

46. Hnatowich, D.J., Gionet, M., Rusckowski, M., Siebecker, D.A., Roche, J., Shealy, D., Mattis, J.A., Wilson, J., McGann, J., Hunter, R.E., Griffin, T. and Doherty, P.W. *Pharmacokinetics of ^{111}In-labelled OC-125 antibody in cancer patients compared with the 19-9 antibody.* Cancer Res., 47, 6111-6117, 1987.

47. Hayes, D.F., Zalutsky, M.R., Kaplan, W., Noska, M., Thor, A., Colcher, D. and Kufe, D.W. *Pharmacokinetics of radiolabelled monoclonal antibody B6.2 in patients with metastatic breast cancer.* Cancer Res., 46, 3157-3163, 1986.

48. Hnatowich, D.J. Rusckowski, M., Brill, A.B., Seibecker, D.A., Misra, H., Mardirossian, G., Bushe, H., Rescigno, A., Stevens, S., Johnson, D.K. and Griffin, T.W. *Pharmacokinetics in patients of an anti-carcinoembryonic antigen antibody radiolabelled with Indium-111 using a novel diethylenetriamine pentaacetic acid chelator.* Cancer Res., 50, 7272-7278, 1990.

49. Svec, J., Veselovska, Z., Keszeghova, V., Reinerova, M. and Makaiova, I. *Radioimmunoscintigraphy of human malignant melanoma. I. Pharmacokinetics and localization of ^{125}I-labelled monoclonal antibody RG-12 in thymectomized mice bearing renal melanoma xenotransplants.* Neoplasma, 36, 505-511, 1989.

50. Palme II, D.F., Berkopec, J.M., Wessels, B.W., Elson, M.K., Lange, P.H. and Vessella, R.L. *Dosimetry and pharmacokinetics of monoclonal antibody A6H with human renal cell carcinoma xenografts: single dose study.* Nucl.Med.Biol., 18, 527-537, 1991.

51. Zimmer, A.M., Kazikiewicz, J.M. Rosen, S.T. and Spies, S.M. *Pharmacokinetics of $^{99m}Tc(Sn)$- and ^{131}I-labelled anti-carcinoembryonic antigen monoclonal antibody fragments in nude mice.* Cancer Res., 47, 1691-1694, 1987.

52. Brown, B.A., Comeau, R.D., Jones, P.L., Liberatore, F.A., Neacy, W.P., Sands, H. and Gallagher, B.M. *Pharmacokinetics of the monoclonal antibody B72.3 and its fragments labelled with either ^{125}I or ^{111}In.* Cancer Res., 47, 1149-1154, 1987.

53. Barrett, J.S., Wagner, J.G., Fisher, S.J. and Wahl, R.L. *Effect of intraperitoneal injection volume and antibody protein dose on the pharmacokinetics of intraperitoneally administered IgG2ak murine monoclonal antibody in the rat.* Cancer Res., 51, 3434-3444, 1991.

54. Reilly, R.M. et al. *Compartmental analysis of the pharmacokinetics of radioiodinated monoclonal antibody B72.3 in colon cancer patients.* Nucl.Med.Biol., 20, 57-64, 1993.

55. Buist, M.R., Kenemans, P., van Hollander, W., Vermorken, J.B., Molthoff, C.J.M., Burger, C.W., Helmerhorst, T.J.M., Baak, J.P.A. and Roos, J.C. *Kinetics and tissue distribution of the radiolabeled chimeric monoclonal antibody mov18 IgG and $F(ab')_2$ fragments in ovarian carcinoma patients.* Cancer Res., 53, 5413-5418, 1993.

56. Yang, H.M. and Reisfeld, R.A. *Pharmacokinetics and mechanism of action of a doxorubicin-monoclonal antibody 9.,2.27 conjugate directed to a human melanoma proteoglycan.* J.Natl.Cancer Inst., 80, 1154-1159, 1988.

57. Goodwin, D.A. *Pharmacokinetics and antibodies..* J.Nucl.Med., 28, 1358-1362, 1987.

58. Lindstrom, T.D., Althaus, W.A., Ruterbories, K.J., and Kau, D. *Pharmacokinetics and disposition of the KS1/4 monoclonal antibody-desacetylvinblastine hydrazide conjugate LY203725 in rats and monkeys.* J.Pharmacol.Exp.Ther., 252, 1117-1124, 1990.

59. Hnatowich, D.J., Griffin, T.W., Kosciuczyk, C., et al. *Pharmacokinetics of an In-111-labelled monoclonal antibody in cancer patients.* J.Nucl.Med. 26, 849-858, 1985.

60. Begent, R.H.J., Ledermann, J.A., Green, A.J., Bagshawe, K.D., Riggs, S.J, et al. *Antibody distribution and dosimetry in patients receiving radiolabelled therapy for colorectal cancer.* Br.J.Cancer, 60, 406-412, 1989.

61. LoBuglio, A., Wheeler, R.H. and Trang, J. *Mouse/human chimeric monoclonal antibody in man: kinetics and immune response.* Proc.Natl.Acad.Sci.USA., 86, 4220-4224, 1989.

62. Molthoff, C.F.M., Pinedo, H.M., Schluper, H.M.M., Nijman, H.W. and Boven, E. *Comparison of the pharmacokinetics, biodistribution and dosimetry of monoclonal antibodies OC 125, OV-TL 3, and 139H2 as IgG and F(ab')$_2$ fragments in experimental ovarian cancer.* Br.J.Cancer, 65, 677-683, 1992.

63. Chatal, J-F., Saccavini, J-C., Gestin, J-F., Thedrez, P., Curtet, C., Kremer, M., Guerreau, D., Nolibe, D., Fumoleau, P. and Guillard, Y. *Biodistribution of indium 111-labelled OC 125 monoclonal antibody intraperitoneally injected into patients operated on for ovarian carcinomas.* Cancer Res., 49, 3087, 1989.

64. Fenwick, J.R., Philpott, G.W. and Connett, J.M. *Biodistribution and histological localization of anti-human colon cancer monoclonal antibody (MAb) 1A3: the influence of administered MAb dose on tumour uptake.* Int.J.Cancer, 44, 1017-1027, 1989.

65. Laborda, J., Douillard, J-Y., Lizzio, E.F. and Hoffman, T. *Comparative pharmacokinetics of a murine monoclonal antibody to a rat colon tumour in rats and nude mice.* Cancer Res., 50, 873-876, 1990.

66. Meredith, R.F., LoBuglio, A.F., Plott, W.E., Orr, R.A., Brezovich, I.A., Russell, C.D., Harvey, E.B., Yester, M.V., Wagner, A.J., Spencer, S.A., Wheeler, R.H., Saleh, M.N., Rogers, K.J., Polansky, A., Salter, M.N. and Khazaeli, M.B. *Pharmacokinetics, immune response, and biodistribution of iodine-131-labelled chimeric mouse/human IgG, K17-1A monoclonal antibody.* J.Nucl.Med., 32, 1162-1168, 1991.

67. Massuger, L.F.A.G., Claessens, R.A.M.J., Kenemans, P. Verheijne, R.H.M., Boerman, O.C., Meeuwis, A.P.W., Schijf, C.P.T., Buijs, C.A.M., Hanselaar, T.G.J.M. and Corstens, F.H.M. *Kinetics and biodistribution in relation to tumour detection with indium-111-labelled OV-TL3 (Fab')$_2$ in patients with ovarian cancer.* Nucl.Med.Commun., 12, 593-609, 1991.

68. Buist, M.R., Kenemans, P., Vermorken, J.B., Golding, R.P., Burger, C.W., den Hollander, W., van Kamp, G.J., van Lingen, A., Teule, J.J., Baak, J.P.A. and Roos, J.C. *Radioimmunotargeting in ovarian carcinoma patients with indium-111-labelled monoclonal antibody OV-TL3 F(ab')$_2$: pharmacokinetics, tissue distribution, and tumour imaging.* Int.J.Gynecol. Cancer, 2, 23-34, 1992.

69. Doherty, P.W. *Biodistribution and pharmacokinetics of In-111 labelled monoclonal-antibody F(ab')$_2$ fragments in patients.* Br.J.Cancer, 52, 646-647, 1985.

70. Hagan, P.L., Halpern, S.E., Chen, A., Krishnan, L., Frincke, J., Bartholomew, R.M., David, G.S. and Carlo, D. *In vivo kinetics of radiolabelled monoclonal anti-CEA antibodies in animal models.* J.Nucl.Med., 26, 1418-1422, 1985.

71. Douillard, J.Y., Chatal, J.F., Saccavini, J.C. et al. *Pharmacokinetic study of radiolabelled anti-colorectal carcinoma monoclonal antibody in tumour-bearing nude mice.* Eur.J.Nucl.Med., 11, 107-113, 1985.

72. Epenetos, A.A., Snook, D., Durban, H., Johnson, P.M. and Taylor-Papadimitriou, J. *Limitations of radiolabelled monoclonal antibodies for localization of human neoplasms.* Cancer Res., 46, 3183-3191, 1986.

73. Henry, R., Begent, J. and Pedley, R.B. *Monoclonal antibody administration: current clinical pharmacokinetic status and future trends.* Clin.Pharmacokinet. 23, 85-89, 1992.

74. Bagshawe, K.D. *Towards generating cytotoxic agents at cancer sites.* Br.J.Cancer, 60, 275-281, 1989.

75. Pimm, M.V. *Drug-monoclonal antibody conjugates for cancer therapy: potentials and limitations.* Crit.Rev.Ther.Drug Carrier Syst., 5, 189-227, 1988.

76. Blumenthal, R.D., Sharkey, R.D. and Goldenberg, D.M. *Current perspectives and challenges in the use of monoclonal antibodies as imaging and therapeutic agents.* Adv.Drug Deliv.Rev., 4, 279-318, 1990.

77. Larrick, J.W. *Potential of monoclonal antibodies as pharmacological agents.* Pharmacol.Rev., 41, 539-557, 1989.

78. Embleton, M.J. *Targeting of anticancer therapeutic agents by monoclonal antibodies.* Biochem.Soc.Trans., 14, 393-395, 1986.

79. Schlom et al. *Concepts in the delivery of monoclonal antibodies in the targeting of human carcinomas.* Adv.Drug Deliv.Rev., 2. 229-251. 1988.

80. Waldman, T.A. *Monoclonal antibodies in diagnosis and therapy.* Science, 252, 1657, 1991.

81. Jones, P.L., Gallagher, B.M. and Sands, H. *Autoradiographic analysis of monoclonal antibody distribution in human colon and breast tumour xenografts.* Cancer Immunol.Immunother., 22, 139-143, 1986.

82. Blasberg, R.G., Nakagawa, H., Bourdon, M.A., Groothuis, D.R., Patlak, C.S. and Binger, D.D. *Regional localization of a glioma-associated antigen defined by monoclonal antibody 81C6 in vivo: kinetics and implications for diagnosis and therapy.* Cancer Res., 47, 4432-4443, 1987.

83. Sands, H., Jones, P.L., Shah, S.A., Palme, D., Vessella, R.L. and Gallagher, B.M. *Correlation of vascular permeability and blood flow with monoclonal antibody uptake by human clouser and renal xenografts.* Cancer Res., 48, 188-193, 1988.

84. Del Vecchio, S., Reynolds, J.C., Blasberg, R.G., Neumann, R.D., Carrasquillo, J.A., Hellstrom, I. and Larson, S.M. *Measurement of local M_r 97,000 and 250,000 protein antigen concentration in sections of human melanoma tumour using in vitro quantitative autoradiography.* Cancer Res., 48, 5475-5481, 1988.

85. Del Vecchio, S., Reynolds, J.C., Carrasquillo, J.A., Blasberg, R.G., Neumann, R.D., Lotze, M.T., Bryant, G.J., Farkas, R.J. and Larson, S.M. *Local distribution and concentration of intravenously injected ^{131}I-9.2.27 monoclonal antibody in human malignant melanoma.* Cancer Res., 49, 2783-2789, 1989.

86. Weinstein, J.N., Eger, R.R., Covell, D.G., Black, C.D.V., Mulshine, J., Carrasquillo, J.A., Larson, S.M. and Keenan A.M. *The pharmacology of monoclonal antibodies.* Ann.NY Acad.Sci., 507, 199-210, 1987.

87. Fujimori, K., Fisher, D.R. and Weinstein, J.N. *Integrated microscopic-macroscopic pharmacology of monoclonal antibody radioconjugates: the radiation dose distribution.* Cancer Res., 51, 4821-4827, 1991.

88. Ong, G.L. and Mattes, M.J. *Penetration and binding of antibodies in experimental human solid tumours grown in mice.* Cancer Res., 49, 4264-4273, 1989.

89. Jain, R.K. and Baxter, L.T. *Mechanisms of heterogeneous distribution of monoclonal antibodies and other macromolecules in tumours: significance of elevated interstitial pressure.* Cancer Res., 48, 7022-7032, 1988.

90. Fujimori, K., Covell, D.C., Fletcher J.E. and Weinstein, J.N. *Modelling analysis of the global and microscopic distribution of IgG, $F(ab')_2$, and Fab in tumours.* Cancer Res., 49, 5656-5663, 1989.

91. Fujimori, K., Covell, D.G., Fletcher, J.E. and Weinstein, J.N. *A modelling analysis of monoclonal antibody percolation through tumours: a binding site barrier.* J.Nucl.Med., 31, 1191-1198, 1990.

92. Baxter, L.T. and Jain, R.K. *Transport of fluid and macromolecules in tumours. I. Role of interstitial pressure and convection.* Microvasc.Res., 37, 77-104, 1989.

93. Baxter, L.T. and Jain, R.K. *Transport of fluid and macromolecules in tumours. II. Role of heterogeneous perfusion and lymphatics.* Microvasc.Res., 40, 246-263, 1990.

94. Baxter, L.T. and Jain, R.K. *Transport of fluid and macromolecules in tumours. III. Role of binding and metabolism.* Microvasc.Res., 41, 5-23, 1991.

95. Baxter, L.T. and Jain, R.K. *Transport of fluid and macromolecules in tumours. IV. A microscopic model of the perivascular distribution.* Microvasc.Res., 41, 252-272, 1991.

96. Weinstein, J.N., Black, C.D.V., Barbet, J., Eger, R.R., Parker, R.J., Holton, O.D., III, Mulshine, J.L., Keenan, A.M., Larson S.M., Carrasquillo, J.A., Sieber, S.M. and Covell, D.G. *Selected issues in the pharmacology of monoclonal antibodies.* In: E. Tomlinson and S.S. Davis (eds.), Site-Specific Drug Delivery, pp 81-91. New York: John Wiley and Sons, 1986.

97. van Osdol, W., Fujimori, K. and Weinstein, J.N. *An analysis of monoclonal antibody distribution in microscopic tumour models: consequences of a 'binding-site barrier'.* Cancer Res., 51, 4776-4784, 1991.

98. Baxter, L.T., Yuan, F. and Jain, R.K. *Pharmacokinetic analysis of the perivascular distribution of bifunctional antibodies and haptens: comparison with experimental data.* Cancer Res., 52, 5838-5844, 1992.

99. Kwok, C.S., Cole, S.E. and Liao, S.K. *Uptake kinetics of monoclonal antibody by human malignant melanoma multicell spheroids.* Cancer Res., 48, 1856-1863, 1988.

100. van Osdol, W.W., Sung, C., Dedrick, R.L. and Weinstein., J.N. *A distributed pharmacokinetic model of two-step imaging and treatment protocols: application to streptavidin-conjugated monoclonal antibodies and radiolabelled biotin.* J.Nucl.Med., 34, 1552-1564, 1993.

101. Meeker, T.C., Lowder, J., Maloney, D.G., Miller, R.A., Thielemans, K., Warnke, R. and Levy R.A. *A clinical trial of anti-idiotype therapy for B cell malignancy.* Blood, 65, 1349-1363, 1985.

102. Pervez, S., Epenetos, A.A., Mool, W.J., Evans, D.J., Rowlinson, G., Dhokia, B. and Krausz, T. *Localisation of monoclonal antibody AVAI and its F(ab')$_2$ fragments in human tumour xenografts: an autoradiographic and immunohistochemical study.* Int.J. Cancer, 3, 23-29, 1988.

103. Juweid, M., Neumann, R., Paik, C., Perez-Bacete, M.J., Sato, J., van Osdol, W. and Weinstein, J.N. *Micropharmacology of monoclonal antibodies in solid tumours: direct experimental evidence for a binding site barrier.* Cancer Res., 52, 5144-5153, 1992.

104. Sutherland, R., Buchegger, F., Schreyer, M., Vacca, A.. and Mach, J.P. *Penetration and binding of radiolabelled anti-carcinoembrionic antigen monoclonal antibodies and their antigen binding fragments in human colon multicellular tumour spheroids.* Cancer Res., 47, 1627-1633, 1987.

105. Langmuir, V.K., McGann, J.K., Buchegger, F. and Sutherland, R.M. *^{131}I-Anticarcinoembryonic antigen therapy of LS174T human colon adenocarcinoma spheroids.* Cancer Res., 49, 3401-3406, 1989.

106. Shockley, T.R., Lin, K., Sung, C., Nagy, J.A., Tompkins, R.G., Dedrick, R.L., Dvorak, H.F. and Yarmush, M.L. *A quantitative analysis of tumour specific monoclonal antibody uptake by human melanoma xenografts: effects of antibody immunological properties and tumour antigen expression levels.* Cancer Res., 52, 357-366, 1992.

107. Kennel, S.J. *Effects of target antigen competition on distribution of monoclonal antibody to solid tumours.* Cancer Res., 52, 1284-1290, 1992.

108. Fiume, L., Bassi, B., Busi, C., Mattioli, A. and Spinosa, G. *Drug targeting in antiviral chemotherapy. A chemically stable conjugate of 9-β-D-arabinofuranosyl-adenine 5′-monophosphate with lactosaminated albumin accomplishes a selective delivery of the drug to liver cells.* Biochem.Pharmacol., 35, 967-972, 1986.

109. Chaudhuri, G., Mukhopadhyay, A. and Basu, S.K. *Selective delivery of drugs to macrophages through a highly specific receptor. An efficient chemotherapeutic approach against leishmaniasis.* Biochem.Pharmacol., 38, 2995-3002, 1989.

110. Fiume, L., Bassi, B., Busi, C., Mattioli, A., Spinosa, G. and Faulstich, H. *Galactosylated poly(L-lysine) as a hepatotropic carrier of 9-β-D-arabinofuranosyl-adenine 5′-monophosphate.* FEBS Lett., 203, 203-206, 1986.

111. Nishikawa, M., Ohtsubo, Y., Ohno, J., Fujita, T., Koyama, Y., Yamashita, F., Hashida, M. and Sezaki, H. *Pharmacokinetics of receptor-mediated hepatic uptake of glycosylated albumin in mice.* Int.J.Pharm., 85, 75-85, 1992.

112. Fujita, T., Nishikawa, M., Tamaki, C., Takakura, Y., Hashida, M. and Sezaki, H. *Targeted delivery of human recombinant super-oxide dismutase by chemical modification with mono- and poly-saccharide derivatives.* J.Pharmacol.Exp.Ther., 263, 971-978, 1992.

113. Nishikawa, M., Kamijo, A., Fujita, T., Takakura, Y., Sezaki, H. and Hashida, M. *Synthesis and pharmacokinetics of a new liver-specific carrier, glycosylated carboxymethyl-dextran, and its application to drug targeting.* Pharm.Res., 10, 1253-1261, 1993.

114. Ashwell, G. and Harford, J. *Carbohydrate-specific receptors of the liver.* Annu.Rev.Biochem., 51, 531-554, 1982.

115. Fallon, R.J. and Schwartz, A.L. *Receptor-mediated delivery of drugs to hepatocytes.* Adv.Drug Deliv.Rev., 4, 49-63, 1989.

116. Gordon, S. and Rabinowitz, S. *Macrophages as targets for drug delivery.* Adv.Drug Deliv.Rev., 4, 27-47, 1989.

117. Meijer, D.F.K. and van der Sluijs, P. *Covalent and noncovalent protein binding of drugs: Implications for hepatic clearance, storage, and cell-specific drug delivery.* Pharm.Res., 6, 105-118, 1989.

118. Worrell, N.R., Cumber, A.J., Parnell, G.D., Mirza, A., Forrester, J.A. and Ross, W.C.J. *Effect of linkage variation on pharmacokinetics of ricin A chain-antibody conjugates in normal rats.* Anti-Cancer Drug Design, 1, 179-188, 1986.

119. Fulton, R.J., Tucker, T.F., Vitetta, E.S. and Uhr, J.W. *Pharmacokinetics of tumour-reactive immunotoxins in tumour-bearing mice: Effect of antibody valency and deglycosylation of the ricin A chain on clearance and tumour localization.* Cancer Res., 48, 2618-2625, 1988.

120. Byers, V., Pimm, M., Pawluczyk, I., Lee, H., Scannon, P. and Baldwin, R. *Biodistribution of ricin toxin A chain-monoclonal antibody 791T/36 immunotoxin and influence of hepatic blocking agents.* Cancer Res., 47, 5277-5283, 1987.

121. Seymour, L. *Passive tumour-targeting of soluble macromolecules and drug conjugates.* Crit.Rev.Ther.Drug Carrier Syst., 9, 135-137, 1992.

122. Duncan, R. *Drug-polymer conjugates: potential for improved chemotherapy.* Anti-Cancer Drugs, 1992.

123. Maeda, H., Seymour, L.W. and Miyamoto, Y. *Conjugates of anticancer agents and polymers: advantage of macromolecular therapeutics in vivo.* Bioconjugate Chemistry, 3, 351-362, 1992.

124. Hashida, M., Kato, A., Takakura, Y and Sezaki, H. *Disposition and pharmacokinetics of a polymeric prodrug of mitomycin C, mitomycin C-dextran conjugate, in the rat.* Drug Metab.Dispos., 12, 492-499, 1984.

125. Hashida, M., Atsumi, R., Nishida, K., Nakane, S., Takakura, Y. and Sezaki, H. *Bilary excretion of mitomycin c-dextran conjugates in relation to physicochemical characteristics of carrier dextran.* J.Pharmacobio-Dyn., 13, 441-447, 1990.

126. Sato, K., Itakura, K., Nishida, K., Takakura, Y., Hashida, M. and Sezaki, H. *Disposition of a polymeric prodrug of mitomycin C, mitomycin C-dextran conjugate, in the perfused rat liver.* J.Pharm.Sci., 78, 11-16, 1989.

127. Takakura, Y., Kitajima, M., Matsumoto, S., Hashida, M. and Sezaki, H. *Development of a novel polymeric prodrug of mitomycin C, mitomycin C-dextran conjugate with anionic charge. I.Physicochemical characteristics and in vivo and in vitro antitumour activities.* Int.J.Pharm., 37, 135-143, 1987.

128. Takakura, Y., Atsumi, R., Hashida, M. and Sezaki, H. *Development of a novel polymeric prodrug of mitomycin C, mitomycin C-dextran conjugate with anionic charge.*

II. Disposition and pharmacokinetics following intravenous and intramuscular administration. Int.J.Pharm., 37, 145-154, 1987.

129. Takakura, Y., Takagi, A., Hashida, M. and Sezaki, H. *Disposition and tumour localization of mitomycin C-dextran conjugates in mice.* Pharm.Res., 4, 293-300, 1987.

130. Nishida, K., Mihara, K., Takino, T., Nakane, S., Takakura, Y., Hashida, M. and Sezaki, H. *Hepatic disposition characteristics of electrically charged macromolecules in rat in vivo and in the perfused liver.* Pharm.Res., 8, 437-444, 1991.

131. Atsumi, R., Endo, K., Kakutani, T., Takakura, Y., Hashida, M. and Sezaki, H. *Disposition characteristics of mitomycin C-dextran conjugates in normal and tumour-bearing muscles of rabbits.* Cancer Res., 47, 5536-5546, 1987.

132. Meyers, F.J., Paradise, C., Scudder, S.A., Goodman, G. and Konrad, M. *A phase I study including pharmacokinetics of polyethylene glycol conjugated interleukin-2.* Clin.Pharmacol.Ther., 49, 307-313, 1991.

133. Knauf, M.J., Bell, D.P., Hirtzer, P, Luo, Z-P, Young, J.D. and Katre, N.V. *Relationship of effective molecular size to systemic clearance in rats of recombinant interleukin-2 chemically modified with water-soluble polymers.* J.Biol.Chem., 263, 15064-15070, 1988.

134. Meyers, F.J., Paradise, C., Tanaka, L., Turrell, C., Scudder, S. and Konrad, M. *A phase I study including pharmacokinetics of PEG-IL-2 in patients with advanced cancer.* Clin.Res., 37, 163A, 1989.

135. Yoon, E.J., Chang, H.W., Lee, M.G., Lee, H., Park, M.K. and Kim, C.K. *Pharmacokinetics of methotrexate after intravenous infusion of methotrexate-rabbit serum albumin conjugate to rabbits.* Int.J.Pharm., 67, 177-184, 1991.

136. Chung, S.M., Yoon, E.J., Kim, S.H., Lee, M.G., Lee, H., Park, M.K. and Kim, C-K. *Pharmacokinetics of 5-fluorouracil after intravenous infusion of 5-fluorouracil-acetic acid-human serum albumin conjugates to rabbits.* Int.J.Pharm., 68, 61-68, 1991.

137. Melton, R.G., Wiblin, C.N., Foster, R.L. and Sherwood, R.F. *Covalent linkage of carboxypeptidase G_2 to soluble dextrans. I. Properties of conjugates and effects on plasma persistence in mice.* Biochem.Pharmacol., 36, 105-112, 1987.

138. Melton, R.G., Wiblin, C.N., Baskerville, A., Foster, R.L. and Sherwood, R.F. *Covalent linkage of carboxypeptidase G_2 to soluble dextrans. II. In vivo distribution and fate of conjugates.* Biochem.Pharmacol., 36, 113-121, 1987.

139. Takakura, Y., Kaneko, Y., Fujita, T., Hashida, M., Maeda, H. and Sezaki, H. *Control of the pharmaceutical properties of soybean trypsin inhibitor by conjugation with dextran. (i) Synthesis and characterization.* J.Pharm.Sci, 78, 117-121, 1989.

140. Wileman, T.E., Foster, R.L. and Elliott, P.N.C. *Soluble asparaginase-dextran conjugates show increased circulatory persistence and lowered antigen reactivity.* J.Pharm.Pharmacol., 38, 264-271, 1986.

141. Noguchi, A., Takahashi, T., Yamaguchi, T., Kitamura, K., Takakura, Y., Hashida, M. and Sezaki, H. *Tumour localization and in vivo antitumour activity of the immunoconjugate composed of anti-human colon cancer monoclonal antibody and mitomycin C-dextran conjugate.* Jpn.J.Cancer Res., 82, 219-226, 1991.

142. Takashina, K-I., Kitamura, K., Yamaguchi, T., Noguchi, A., Noguchi, A., Tsurumi, H. and Takahasi, T. *Comparative pharmacokinetic properties of murine monoclonal antibody A7 modified with neocarzinostatin, dextran and polyethylene glycol.* Jpn.J.Cancer Res., 82, 1145-1150, 1991.

143. Khaw, B-A., Klibanov, A., O'Donnell, S.M., Saito, T., Nossiff, N., Slinkin, M.A., Newell, J.B., Strauss, H.W. and Torchilin, V.P. *Gamma imaging with negatively charge-modified monoclonal antibody: Modification with synthetic polymers.* J.Nucl.Med., 32, 1742-1751, 1991.

144. Seymour, L.W., Ulbrich, K., Strohalm, J., Kopecek, J. and Duncan, R. *The pharmacokinetics of polymer-bound adriamycin.* Biochem.Pharmacol., 39, 1125-1131, 1990.

145. Duncan, R., Seymour, L.W., Scarlett, L., Lloyd, J.B., Rajmanova, P. and Kopecek, J. *Fate of HPMA copolymers with pendent galactosamine residues after intravenous administration to rats.* Biochim.Biophys.Acta, 880, 62, 1986.

146. Seymour, L.W., Ulbrich, K., Wedge, S.R., Hume, I.C., Strohalm, J. and Duncan, R. *HPMA copolymers targeted to the hepatocyte galactose-receptor: pharmacokinetics in DBA_2 mice.* Br.J.Cancer, 63, 859-866, 1991.

147. Rihova, B., Veres, K., Fornusek, L., Ulbrich, K., Strohalm, J., Vetvicka, V., Bilej, M. and Kopecek, J. *Action of polymeric prodrugs based on HPMA copolymers. II. Body distribution and T-cell accumulation of free and polymer-bound ^{125}I-daunomycin.* J.Cont.Rel., 10, 37-49, 1989.

148. Flanagan, P.A., Duncan, R., Subr, V., Ulbrich, K., Kopeckova, P. and Kopecek, J. *Evaluation of protein-HPMA copolymer conjugates as targetable drug-carriers. 2. Body distribution of conjugates containing transferrin, anti-transferrin receptor antibody or*

anti-Thy 1.2 antibody and effectiveness of transferrin-containing daunomycin conjugates against mouse L1210 leukaemia in vivo. J.Cont.Rel., 18, 25-38, 1992.

149. Sezaki, H. and Hashida, M. *Macromolecular drug conjugates in cancer chemotherapy.* Crit.Rev.Ther.Drug Carrier Syst., 1, 1-38, 1984.

150. Maeda, H., Oda, T., Matsumura, Y. and Kimura, M. *Improvement of pharmacological properties of protein drug by tailoring with synthetic polymers.* J.Bioact.Compat.Polym., 3, 27-43, 1988.

151. Suzuki, M., Hori, K., Abe, I., Saito, S., and Sato, H. *A new approach to cancer chemotherapy: Selective enhancement of tumour blood flow with angiotensin II.* J.Natl.Cancer Inst., 67, 663-669, 1981.

152. Hori, K., Suzuki, M., Abe, I., Saito, S. and Sato, H. *Increase in tumour vascular area due to increased blood flow by angiotensin II in rats.* J.Natl.Cancer Inst., 74, 453-459, 1985..

153. Matsumura, Y., Maeda, H. and Kato, H. *Degradation pathway of kinins in tumour ascites and inhibition by kininase inhibitors: Analysis by HPLC.* Agents Actions, 29, 172-180, 1990.

154. Noguchi, A., Takahashi, T., Yamaguchi, T., Kitamura, K., Noguchi, A., Tsurumi, H., Takashima, K. and Maeda, H. *Enhanced tumour localisation of monoclonal antibody by treatment with kininase II inhibitor and agiotensin II.* Jpn.J. Cancer Res., 83, 240-243, 1992.

155. Bocci, V. *Metabolism of protein anticancer agents.* Pharmacol.Ther., 34, 1, 1987.

156. Evans, W.E. and Relling, M.V. *Clinical pharmacokinetics-pharmacodynamics of anticancer drugs.* Clin.Pharmacokinet., 16, 327-336, 1989.

157. Liliemark, J. and Peterson, C. *Pharmacokinetic optimisation of anticancer therapy.* Clin.Pharmacokinet., 21, 213-231, 1991.

158. Balis, F.M., Holcenberg, J.S., and Bleyer, W.A. *Clinical pharmacokinetics of commonly used anticancer drugs.* Clin.Pharmacokinet., 8, 202-232, 1983.

159. Balis, F.M. *Pharmacokinetic drug interactions of commonly used anticancer drugs.* Clin.Pharmacokinet., 11, 223-235, 1986.

160. Friend, D.R. and Pangburn, S. *Site specific drug delivery.* Med.Res.Rev., 7, 53-106, 1987.

161. Kobayashi, A., Oda, T. and Maeda, H. *Protein binding of macromolecular anticancer agent SMANCS: characterization of poly(styrene-comaleic acid) derivatives as an albumin binding ligand.* J.Bioact.Compat.Polym., 33, 19-328, 1988

162. Sezaki, H., Takakura, Y. and Hashida, M. *Soluble macromolecular carriers for the delivery of antitumour drugs.* Adv.Drug Deliv.Rev., 3, 247-266, 1989.

163. Takakura, Y., Fujita, T., Hashida, M. and Sezaki, H. *Disposition characteristics of macromolecules in tumour-bearing mice.* Pharm.Res., 7, 339-346, 1990.

164. Seymour, L.W., Duncan, R., Strohalm, J. and Kopecek, J. *Effect of molecular weight (Mw) of HPMA copolymers on body distribution and rate of excretion after subcutaneous, intraperitoneal and intravenous administration to rats.* J.Biomed.Mater.Res., 21, 1341-1358, 1987.

165. Subr, V., Kopecek, J. and Duncan, R. *Degradation of oligopeptide sequences connecting poly [N-(2-hydroxypropyl) methacrylamide] chains by lysosomal cysteine proteinases.* J.Bioact.Compat.Polym., 1, 133-146, 1986.

166. Kopecek, J. *The potential of water soluble polymeric carriers in targeted and site-specific drug delivery.* J.Cont.Rel., 11, 279-290, 1990.

167. Lloyd, J.B. *Targeting with synthetic polymers: A realistic goal.* In: Targeting of drugs with synthetic systems, G. Gregoriadis, J. Senior and G. Poste. Eds.,Plenum Press, New York, London, 1986.

168. Drobnik, J. *Biodegradable soluble macromolecules as drug carriers.* Adv.Drug Deliv.Rev., 3, 229-245, 1989.

169. Seymour, L.W., Ulbrich, K., Strohalm, J. and Duncan R. *Pharmacokinetics of a polymeric drug carrier targeted to the hepatocyte galactose receptor.* Br.J.Cancer, 63, 859, 1991.

170. Joyce, D.A., Day, R.O. and Murphy, B.R. *The pharmacokinetics of albumin conjugates of D-penicillamine in humans.* Drug.Metab.Dispos., 19, 309-311, 1991.

171. Fiume, L., Bassi, B., Busi, C., Mattioli, A. and Wieland, T. *A study on the pharmacokinetics in mouse of adenine-9-β-D-arabinofuranoside 5-monophosphate conjugated with lactosaminated albumin.* Experientia, 41, 1326-1328, 1985.

172. Schulz, B., Stowhas, H., Becker, R., Steinicke, A. and Besch, W. *Semisynthetic human insulin: Pharmacokinetics and biological potency in healthy subjects in comparison with highly purified porcine insulin.* Exp.Clin.Endocrinol, 92, 307-313, 1988.

173. Braslis, K.G., Shulkes, A., Fletcher, D.R. and Hardy, K.J. *Pharmacokinetics and organ-specific metabolism of calcitonin gene-related peptide in sheep.* J.Endocr., 118, 25-31, 1988.

174. Girard, P. Cohhen, R., Sassolas, G., Harthe, C., Cabrera, P. and Boissel, J.P. *Pharmacokinetics of human growth hormone releasing factor (hGRF-44 NH2) in normal man after intravenous administration of a large range of doses.* Eur.J.Clin.Pharmacol., 32, 507-513, 1987.

175. Grierson, D.S. and Bjornsson, T.D. *Pharmacokinetics of streptokinase in patients based on amidolytic activator complex activity.* Clin.Pharmacol.Ther., 41, 304-313, 1987.

176. Stump, D.C., Kieckens, L., De Cock, F. and Collen, D. *Pharmacokinetics of single chain forms of urokinase-type plasminogen activator.* J.Pharmacol.Exp.Ther., 242, 245-250, 1987.

177. Berger, J., Heinrich, N., Schafer, J., Baeger, I. and Mehlis, B. *Gonadotropin-releasing hormone (GnRH) pharmacokinetics: peptide hormone pharmacokinetics needs clarification.* Life Sci., 42, 985-991, 1988.

178. Zilker, T.R., Gray, I.P., Hales, C.N., Wahl, K., Ermler, R., Lebender, A., Heinzel, G. and Bottermann. *Pharmacokinetics of biosynthetic human proinsulin following*

intravenous and subcutaneous administration in metabolically healthy volunteers. Horm.Metab.Res.Proinsulin., 18, 37-43, 1988.

179. Muhlhauser, I., Koch, J. and Berger, M. *Pharmacokinetics and bioavailability of injected glucagon: Differences between intramuscular, subcutaneous and intravenous administration.* Diabetes Care, 8, 39-42., 1985.

180. Lundin, S., Akerlund, M., Fagerstrom, P-O., Hauksson, A. and Melin, P. *Pharmacokinetics in the human of a new synthetic vasopressin and oxytocin uterine antagonist.* Acta Endocrinologica, 112, 465-472, 1986.

181. Gottesman, I., Tobert, J., Vandlen, R. and Gerich, J. *Efficacy, pharmacokinetics and tolerability of a somatostatin analogue (L-363,586) in insulin-dependent diabetes mellitus.* Life Sci., 38, 2211-2219, 1986.

182. Sweeney, G., Holbrook, A.M., Levine, M., Yip, M., Atredsson, K., Cappi, S., Ohlin, M., Schulz, P. and Wassenaar. *Pharmacokinetics of carbetocin, a long-acting oxytocin analog, in non-pregnant women.* Current Therapeutic Research-Clinical and Experimental, 47, 528-540, 1990.

183. Nicholls, J., Wynick, D., Domin, J., Sandler, C.M. and Bloom, S.R. *Pharmacokinetics of the long-acting somatostatin analog octreotide (SMS 201-995) in acromegaly.* Clinical endocrinology, 32, 545-550, 1990.

184. Miyashita, C., Sen, S., Kohler, M., Pindur, G. and Heiden, M. *Pharmacokinetics of urokinase (UK) and pro-urokinase (PUK) in patients with acute myocardial-infarction (AMI).* Thrombosis and Haemostasis, 62, 539, 1989.

185. Morfini, M., Messori, A., Longo, G., White, G.C., Comperts, E. and Mannucci, P.M. *Pharmacokinetics of recombinant FVIII compared with monoclonal-antibody purified, plasma derived FVIII.* Thrombosis and Haemostasis, 62, 198, 1989.

186. Ravis, W.R., Comerci, C., and Ganjam, V.K. *Pharmacokinetics of insulin following intravenous and subcutaneous administration in canines.* Biopharm.Drug Dispos., 7, 407-420, 1986.

187. Maizel, A.S. and Bookstein, J.. *Streptokinase, urokinase and tissue plasminogen activator: pharmacokinetics, relative advantages and methods for maximising rates and consistency of lysis.* Cardiovasc.Intervent.Radiol., 9, 236-244, 1986.

188. Fong, K.L., Crysler, C.S., Mico, B.A., Boyle, K.E., Kopia, .G., Kopaciewicz, L. and Lynn, R.K. *Dose-dependent pharmacokinetics of recombinant tissue-type plasminogen activator in anaesthetized dogs following intravenous infusion.* Drug Metab.Dispos., 16, 201-206, 1988.

189. Tanaka, H., Satake-Ishikawa, R., Ishikawa, M., Matsuki, S. and Asano, K. *Pharmacokinetics of recombinant human granulocyte colony-stimulating factor conjugated to polyethylene glycol in rats.* Cancer Res., 51, 3710-3714, 1991.

190. Gural, R., Abuchowski, A., Scudiery, D., Herron, J. and Zabronsky, A. *Clinical pharmacokinetics of PEG-superoxide dismutase.* Clin.Pharmacol.Ther., 43, 136, 1988.

191. Mehvar, R. and Reynolds. J.M. *Pharmacokinetics of 70-kilodalton fluoresciein-dextran in experimental diabetes mellitus.* J.Pharmacol.Exp.Ther., 264, 662-669, 1993.

192. Mehvar, R. and Shepard, T.L. *Molecular weight-dependent pharmacokinetics of fluorescien-labelled dextrans in rats.* J.Pharm.Sci., 81, 908-912, 1992.

193. Thanh-Barthet, C.V. Urtizberea, M., Sabouraud, A.E., Cano, N.J. and Scherrmann, J.M. *Development of a sensitive radioimmunoassay for Fab fragments: application to Fab pharmacokinetics in humans.* Pharm.Res., 10, 692-696, 1993.

194. Ferraiolo, B.L., McCabe, J., Hollenbach, S., Hultgren, B., Pilte, R. et al. *Pharmacokinetics of recombinant human tumour necrosis factor-αin rats: effects of size and number of doses and nephrectomy.* Drug Metab.dispos., 17, 369-372, 1989.

195. Bocci, V. *Interleukins: Clinical pharmacokinetics and practical implications.* Clin.Pharmacokinet., 21, 274, 1991.

196. Konrad, M.W., Hamstreet, G., Hersh, E.M., Mansell, P.W.A., Mertelsmann, R., Kolitz, J.E. and Bradley, E.C. *Pharmacokinetics of recombinant interleukin-2 in humans.* Cancer Res., 50, 2009-2017, 1990.

197. Thompson, J.A., Lee, D.J., Cox, W.W., Lindgren, C.G., Collins, C., Neraas, K.A., Dennin, R.A. and Fefer, A. *Recombinant interleukin 2 toxicity, pharmacokinetics, and immunomodulatory effects in phase I trial.* Cancer Res., 47, 4202-4207, 1987.

198. Sands, H. and Loveless, S.E. *Biodistribution and pharmacokinetics of recombinant human ^{125}I-interleukin-2 in mice.* Int.J. Immunopharmac., 11, 411-416, 1989.

199. Gustavson, L.E., Nadeau, R.W. and Oldfield, N.F. *Pharmacokinetics of Teceleukin (Recombinant Human Interleukin-2) after intravenous or subcutaneous administration to patients with cancer.* J.Biol.Response Mod., 8, 440-449, 1989.

200. Sculier, J.P., Body, J.J., Donnadieu, N., Nejai, S., Gilbert, F., Raymakers, N. and Paesmans, M. *Pharmacokinetics of repeated i.v. bolus administration of high doses of r-met-Hu interleukin-2 in advanced cancer patients.* Cancer Chemother.Pharmacol., 26, 355-358, 1990.

201. Biesma, B., Pokorny, R., Kovarik, J.M., Duffy, F.A., Willemse, P.H.B., Mulder, N.H. and de Vries, E.G.E. *Pharmacokinetics of recombinant human interleukin-3 administered subcutaneously and by continuous iv infusion in patients after chemotherapy for ovarian cancer.* Cancer Res., 53, 5915-5919, 1993.

202. Wills, R.J. *Clinical pharmacokinetics of interferons.* Clin.Pharmacokinet., 19, 390-399, 1990.

203. Kurzrock, R., Rosenblum, M.G., Sherwin, S.A., Rios, A., Talpaz, M. Quesada, J.R. and Gutterman, J.U. *Pharmacokinetics, single-dose tolerance, and biological activity of recombinant γinterferon in cancer patients.* Cancer Res., 45, 2866-2872, 1985.

204. Radwanski, E., Perentesis, G., Jacobs, S., Oden, E., Affrime, M., Symchowicz, S. and Zampaglione, N. *Pharmacokinetics of interferon α2b in healthy volunteers.* J.Clin.Pharmacol., 27, 432-435, 1987.

205. Rutenfranz, I. and Kirchner, H. *Pharmacokinetics of recombinant murine interferon-γ in mice.* J.Interferon Res., 8, 573-580, 1988.

206. Bornemann, L.D., Spiegel, H.E., Dziewanowska, Z.E., Krown, S.E. and Colburn, W.A. *Intravenous and intramuscular pharmacokinetics of recombinant leukocyte A interferon.* Eur.J.Clin.Pharmacol., 28, 469-471, 1985.

207. Wills, R.J. and Spiegel, H.E. *Continuous intravenous infusion pharmacokinetics of interferon to patients with leukaemia.* J.Clin.Pharmacol., 25, 616-619, 1985.

208. Greig, N.H., Soncrant, T.T., Wozniak, K.M. and Rapoport, S.I. *Plasma and tissue pharmacokinetics of human interferon-alpha in the rat after its intravenous administration.* J.Pharmacol.Exp.Ther., 245, 574-580, 1988.

209. Merimsky, O., Rubinstein, M., Fischer, D., Danon, A. and Chaitchik, S. *Pharmacokinetics of recombinant interferon alpha-C.* Cancer Chemother.Pharmacol., 27, 406-408, 1991.

210. Bohoslawec, O., Trown, P.W. and Willis, R.J. *Pharmacokinetics and tissue distribution of recombinant human alpha A, D, A/D(Bgl) and I interferons and mouse-alpha interferon in mice.* J.Interferon.Res., 6, 207-213, 1986.

211. Teorell, T. *Kinetics of distribution of substances administered to the body. I. The extravascular modes of administration.* Arch.Int.Pharmacodyn., 57, 205, 1937.

212. Teorell, T. *Kinetics of distribution of substances administered to the body. II. The intravascular modes of administration.* Arch.Int.,Pharmacodyn., 57, 226, 1937.

213. Benet, L.Z. *General treatment of linear mammillary models with elimination from any compartment as used in pharmacokinetics.* J.Pharm.Sci., 61, 536-541, 1972.

214. Benet, L.Z. and Turi, J.S. *Use of a general partial fraction theorem for obtaining inverse haplace transforms in pharmacokinetic analysis.* J.Pharm.Sci., 60, 1593-1594, 1971.

215. Wagner, J.G. *Biopharmaceutics and Relevant Pharmacokinetics.* Drug Intelligence Publications, Hamilton, Illinois, 1971.

216. Wagner, J.G. *Fundamentals of Clinical Pharmacokinetics.* Drug Intelligence Publications, Hamilton, Illinois, 1975.

217. Gibaldi, M. and Perrier, D. *Pharmacokinetics.* Marcel Dekker, New York, 1975.

218. Welling, P.G., *Pharmacokinetics: Processes and Mathematics.* American Chemical Society, Washington D.C., 1986.

219. Lutz, R.J., Dedrick, R.L., Straw, J.A., Hart, M.M., Klubes, P. and Zaharko, D.S. *The kinetics of methotrexate distribution in spontaneous canine lymphosarcoma.* J.Pharmacokin.Biopharm, 3, 77-97, 1975.

220. Lutz, R.J. Galbraith, W.M., Dedrick, R.L., Shrager, R. and Mellett, L.B. *A model for the kinetics of distribution of actinomycin-D in the beagle dog.* J.Pharmacol.Exp.Ther., 200, 469-478, 1977.

221. Bischoff, K.B. and Dedrick, R.L. *Thiopental pharmacokinetics.* J.Pharm.Sci., 57, 1347-1357, 1968.

222. Bischoff, K.B., Dedrick, R.L. and Zaharko, D.S. *Preliminary model for methotrexate pharmacokinetics.* J.Pharm.Sci, 59, 149-154, 1970.

223. Dedrick, R.L., Forrester, D.D. and Ho, D.H.W. *In-vitro-in-vivo correlation of drug metabolism - determination of 1-β-D-arabinsfurenosylcytosine.* Biochem.Pharmacol., 21, 1-16, 1972.

224. Benowitz, N., Forsyth, R.P., Melman, K.L. and Rowland, M. *Lidocaine disposition kinetics in monkey and man. I. Predicted by a perfusion model.* Clin.Pharmacol.Ther., 16, 87-98, 1974.

225. Benowitz, N., Forsyth, R.P., Melman K.L. and Rowland M. *Lidocaine disposition kinetics in monkey and man. II. Effects of haemorrhage and sympathomimetic drug administration.* Clin.Pharmacol.Ther., 16, 99-109, 1974.

226. Montandon, B., Roberts, R.J., Fisher, L.J. *Computer simulation of sulfobromophthalein kinetics in the rat using flow-limited models with extrapolation to man.* J.Pharmacokin.Biopharm., 3, 277-290, 1975.

227. Harris, P.A. and Gross, J.F. *Preliminary pharmacokinetic model for adriamycin (NSC-123127).* Cancer Chemother.Rep.Part I., 59, 819-825, 1975.

228. Harrison, L.I. and Gibaldi, M. *Physiologically based pharmacokinetic model for digoxin distribution and elimination in the rat.* J.Pharm.Sci., 66, 1138-1142, 1977.

229. Harrison, L.I. and Gibaldi, M. *Physiologically based pharmacokinetic model for digoxin distribution in dogs and its preliminary application to humans.* J.Pharm.Sci., 66, 1679-1683, 1977.

230. Himmelstein, K.J. and Gross, J.F. *Mathematical model for cyclocytidine pharmacokinetics.* J.Pharm.Sci., 66, 1441-1444, 1977.

231. Chen, C.N., Coleman, D.L., Andrade, J.D. and Temple, A.R. *Pharmacokinetic model for salicylate in cerebrospinal fluid, blood, organs and tissues.* J.Pharm.Sci., 67, 38-45, 1978.

232. Bischoff, K.B., Dedrick, R.L., Zaharko, D.S. and Longstreth, J.A. *Methotrexate pharmacokinetics.* J.Pharm.Sci., 60, 1128-1133, 1971.

233. Dedrick, R.L., Forrester, D.D., Cannon, J.N., El Dareer, S.M. and Mellett, L.B. *Pharmacokinetics of 1-β-D-arabinofuranosylcytosine (Ara-C) deamination in several species.* Biochem.Pharmacol., 22, 2405-2417, 1973.

234. Tterlikkis, L., Ortega, E., Solomon, R. and Day, J.L. *Pharmacokinetics of mercaptopurine.* J.Pharm.Sci., 66, 1454-1457, 1977.

235. Greene, D.S., Quintiliani, R. and Nightingale, C.H. *Physiological perfusion model for cephalosporin antibiotics. I. Model selection based on blood drug concentrations.* J.Pharm.Sci., 67, 191-196, 1978.

236. King, F.G. and Dedrick, R.L. *Physiologic model for the pharmacokinetics of 2'deoxycotormycin in normal and leukaemic mice.* J.Pharmacokin.Biopharm., 9, 519-534, 1981.

237. Collins, J.M., Dedrick, R.L., King, F.G., Speyer, J.L. and Meyers, C.E. *Nonlinear pharmacokinetic models for 5-fluorouracil in man: intravenous and intraperitoneal routes.* Clin.Pharmacol.Ther., 28, 235-246, 1980.

238. Zaharko, D.S., Dedrick, R.L., Peal, A.L., Drake, J.C. and Lutz, R.J. *Relative toxicity of methotrexate in several tissues of mice bearing lewis lung carcinoma* J.Pharmacol.Exp.Ther., 189, 585-592, 1974.

239. Jain, R.K., Wei, J. and Gullino, P.M. *Pharmacokinetics of methotrexate in solid tumours.* J.Pharmacokin.Biopharm., 7, 181-194, 1979.

240. Bellman, R., Jacquez, J.A. and Kalaba, R. *Some mathematical aspects of chemotherapy. I. One-organ models.* Bull.Math.Biophys., 22, 181-190, 1960.

241. Jacquez, J.A., Bellman, R. and Kalaba, R. *Some mathematical aspects of chemotherapy. II. The distribution of a drug in the body.* Bull.Math.Biophys., 22, 309-322, 1960.

242. Bischoff, K.B. *Pharmacokinetic modelling of anticancer drugs: Some fundamental considerations of the applications of pharmacokinetics to cancer chemotherapy.* Cancer Chemother.Rep., 59, 772-793, 1975.

243. Oie, S. and Huang, J.D. *Influence of administration route on drug delivery to a target organ.* J.Pharm.Sci., 70, 1344-1347.

244. Yuan, F., Baxter, L.T. and Jain R.K. *Pharmacokinetic analysis of two-step approaches using bifunctional and enzyme-conjugated antibodies.* Cancer Res., 51, 3119-3130, 1991.

245. Covell, D.G., Barbet, J., Holton, O.D., Black, C.D.V., Parker, R.J. and Weinstein, J.N. *Pharmacokinetics of monoclonal immunoglobulin G_1, $F(ab')_2$ and Fab' in mice.* Cancer Res., 46, 3969-3978, 1986.

246. Blasberg, R.G., Nakagawa, H., Bourdon, M.A., Groothuis, D.R., Patlak, C.S. and Bigner, D.D. *Regional localization of a glioma-associated antigen defined by monoclonal antibody 81C6 in vivo: kinetics and implications for diagnosis and therapy.* Cancer Res., 47, 4432-4443, 1987.

247. Thomas, G.D., Chappell, M.J., Dykes, P.W. Ramsden, D.B., Godfrey, K.R., Ellis, J.R.M. and Bradwell, A.R. *Effect of dose, molecular size, affinity and protein binding on tumour uptake of antibody or ligand: A biomathematical model.* Cancer Res., 49, 3290-3296, 1989.

248. Rescigno, A., Bushe, H., Brill, A.B., Rusckowski, M., Griffin, T.W. and Hnatowich, D.J. *Pharmacokinetic modelling of radiolabelled antibody distribution in man.* Am.J.Physiologic Imaging, 5, 141-150, 1990.

249. Imoto, H., Sakamura, Y., Ohkouchi, K., Atsumi, R., Takakura, Y., Sezaki, H. and Hashida, M. *Disposition characteristics of macromolecules in the perfused tissue-isolated tumour preparation.* Cancer Res., 52, 4396-4401, 1992.

250. Chappell, M.J., Thomas, G.D., Godfrey, K.R. and Bradwell, A.F. *Optimal tumour targeting by antibodies: development of a mathematical model.* J.Pharmacokin.Biopharm., 19, 227-260, 1991.

251. Eger, R.R., Covell, D.G., Carrsquillo, J.A., Abrams, P.G., Foon, K.A., Reynolds, J.C., Schroff, R.W., Morgan, A.C., Larson, S.M. and Weinstein, J.N. *Kinetic model for the biodistribution of an ^{111}In-labelled monoclonal antibody in humans.* Cancer Res., 47, 3328-3336, 1987.

252. Sung, C., Youle, R.J. and Dedrick, R.L. *Pharmacokinetic analysis of immunotoxin uptake in solid tumours: Role of plasma kinetics, capillary permeability, and binding.* Cancer Res., 50, 7382-7392, 1990.

253. Sung, C., Shockley, T.R., Morrison, P.F., Dvorak, H.F., Yarmush, M.L. and Dedrick, R.L. *Predicted and observed effects of antibody affinity and antigen density on monoclonal antibody uptake in solid tumours.* Cancer Res., 52, 377-384, 1992.

254. Hunt, C.A., MacGregor, R.D. and Siegel, R.A. *Engineering targeted in vivo drug delivery. I. The physiological and physicochemical principles governing opportunities and limitations.* Pharm.Res., 3, 333-344, 1986.

255. Boddy, A., Aarons, L. and Petrak, K. *Efficiency of drug targeting: steady-state considerations using a three-compartment model.* Pharm.Res., 6, 367-372, 1989.

256. Aubrée-Lecat, A., Duban, M-C., Demignot, S., Domurado, M., Fournié, P. and Domurado, D. *Influence of barrier-crossing limitations on the amount of macromolecular drug taken up by its target.* J.Pharmacokin.Biopharm., 21, 75-98, 1993.

257. Dedrick, R.L., Zaharko, D.S. and Lutz, R.J. *Transport and binding of methotrexate in vivo.* J.Pharm.Sci., 62, 882-890, 1973.

258. Mintun, M., Himmelstein, K.J., Schroder, R.L., Gibaldi, M. and Shen, D.D. *Tissue distribution kinetics of tetraethylammonium ion in the rat.* J.Pharmacokin.Biopharm., 8, 373-409, 1980.

259. Weissbrod, J.M. and Jain, R.K. *Preliminary model for streptozocin metabolism in mice.* J.Pharm.Sci., 69, 691-694, 1980.

260. Yang, K.H., Fung, W.P., Lutz, R.J., Dedrick, R.L. and Zaharko, D.S. *In vivo methotrexate transport in murine lewis lung tumour.* J.Pharm.Sci., 68, 941-945, 1979.

261. Weissbrod, J.M., Jain R.K. and Sirotnak. *Pharmacokinetics of methotrexate in leukaemia cells: effect of dose and mode of injection.* J.Pharmacokin.Biopharm., 6, 487-503, 1978.

262. McFadden, R. and Kwok, C.S. *Mathematical model of simultaneous diffusion and binding of antitumour antibodies in multicellular human tumour spheroids.* Cancer Res., 48, 4032-4037, 1988.

263. Jain, R.K. and Wei, J. *Dynamics of drug transport in solid tumours: Distributed parameter model.* J. Bioeng., 1, 313-330, 1977.

264. Kedem, O. and Katchalsky, A. *Thermodynamic analysis of the permeability of biological membranes to non-electrolytes.* Biochim.Biophys.Acta., 27, 229-246, 1958.

265. Kedem, O. and Katchalsky, A. *A physical interpretation of the phenomenological coefficients of membrane permeability.* J.Gen.Physiol., 45, 143-179, 1961.

266. Himmelstein, K.J. and Lutz, R.J. *A review of the applications of physiologically based pharmacokinetic modelling.* J.Pharmacokin.Biopharm., 7, 127-145, 1979.

267. Gerlowski, L.E. and Jain, R.K. *Physiologically based pharmacokinetic modelling: principles and applications.* J.Pharm.Sci., 72, 1103-1127, 1983.

268. Chen, H-S.G. and Gross, J.F. *Estimation of tissue-to-plasma partition coefficients used in physiological pharmacokinetic models.* J.Pharmacokin.Biopharm., 7, 117-125, 1979.

269. Wagner, J.G. *Blood flow rate-limited models,* In: Chapter 1, Fundamentals of clinical pharmacokinetics. (J.G. Wagner Ed.), Drug Intelligence Publications, Hamilton, Illinois, 1975, pp124-126.

270. Welling, P.G. *Physiological pharmacokinetic models,* In: Pharmacokinetics: Processes and Mathematics, Chapter 15. (P.G. Welling Ed.), American Chemical Society, Washington D.C., 1986, pp241-254.

271. Wagner, J.G. *Nonlinear pharmacokinetics,* In: Fundamentals of clinical pharmacokinetics, Chapter 7. (J.G. Wagner Ed), Drug Intelligence Publications, Hamilton, Illinois, 1975 pp247-284.

272. Welling, P.G. *Nonlinear pharmacokinetics,* In: Pharmacokinetics: Processes and Mathematics, Chapter 16. (P.G. Welling Ed.), American Chemical Society, Washington D.C., 1986, pp255-268.

273. Gibaldi, M. and Perrier, D. *Nonlinear pharmacokinetics,* In: Pharmacokinetics, Chapter 7. (M. Gibaldi and D Perrier Ed.). Marcel Dekker, New York, 1975, pp215-228.

274. Wagner, J.G. *A new generalized nonlinear pharmacokinetic model and its implications,* In: Biopharmaceutics and Relevant Pharmacokinetics, Section Two. (J.G. Wagner Ed.), Drug Intelligence Publications, Hamilton, Illinois, 1971, pp302-317.

275. Ludden, T.M. *Nonlinear pharmacokinetics.* Clin.Pharmacokinet., 20, 429-446, 1991.

276. Welling, P.G. *Pharmacokinetics: Processes and Mathematics.* (P.G. Welling Ed), American Chemical Society, Washington D.C., pp237-238, 1986.

277. Wagner, J.G. *Scientific commentary: Linear pharmacokinetic equations allowing direct calculation of many needed pharmacokinetic parameters from the coefficients and*

exponents of polyexponential equations which have been fitted to data. J.Pharmacokin.Biopharm., 4, 443-467, 1976.

278. Benet, L.Z. and Galeazzi, R.L. *Noncompartmental determination of the steady-state volume of distribution.* J.Pharm.Sci., 68, 1071-1074, 1979.

279. Cutler, D.J. *Theory of the mean absorption time, and adjunct to conventional bioavailabilty studies.* J.Pharm.Pharmacol., 30, 476-478, 1978.

280. Yamaoka, K., Nakagawa, T. and Uno, T. *Statistical moments in pharmacokinetics.* J.Pharmacokin.Biopharm., 6, 547-558, 1978.

281. Veng-Pedersen, P. *Meantime parameters in pharmacokinetics: definition, computation and clinical implications (parts I and II).* Clin.Pharmacokinet., 17, 345-366, 424-440, 1989.

282. Cutler, D.J. *Definition of mean residence times in pharmacokinetics.* Biopharm.Drug Dispos., 8, 87-97, 1987.

283. Veng-Pedersen, P. *Theorems and implications of a model independent elimination/distribution function decomposition of linear and some nonlinear drug disposition I. Derivation and theoretical analysis.* J.Pharmacokin.Biopharm., 12, 627-647, 1984.

284. Cheng, H. and Jusko, W.J. *Mean residence times and distribution volumes for drugs undergoing linear reversible metabolism and tissue distribution and linear or nonlinear elimination from the central compartments.* Pharm.Res., 8, 508-511, 1991.

285. Gillespie, W.R. *Noncompartmental versus compartmental modelling in clinical pharmacokinetics.* Clin.Pharmacokinet., 20, 253-262, 1991.

286. Powers, J.D. *Statistical considerations in pharmacokinetic study design.* Clin.Pharmacokinet., 24, 380-387, 1993.

287. Gibaldi, M. *Compartmental and noncompartmental pharmacokinetics* In: Biopharmaceutics and Clinical Pharmacokinetics. 4th Ed., Lea and Febiger, Philadelphia, London, 1991, pp14-23.

288. Sheiner, L.B., Beal, S.L., Rosenberg, B and Marathe, V.V. *Forecasting individual pharmacokinetics.* Clin.Pharmacol.Therap., 26, 294-305, 1979.

289. Whiting, B., Kelman, A.W. and Grevel, J. *Population pharmacokinetics: Theory and clinical application.* Clin.Pharmacokinet., 11, 387-401, 1986.

290. Thomson, A.H. and Whiting, B. *Bayesian parameter estimation and population pharmacokinetics.* Clin.Pharmacokinet., 22, 447-467, 1992.

291. Vozeh, S. and Steimer, J-L. *Feedback control mechanisms for drug dosage optimisation: concepts, classification and clinical applications.* Clin.Pharmacokinet., 10, 457-476, 1985.

292. Whiting, B., Kelman, A.W. and Grevel, J.G. *Population pharmacokinetics: In Hansch et al.* (Eds.), Comprehensive medicinal chemistry, volume 5: Biopharmaceutics, Pergamon Press, pp297-304, 1990.

293. Taylor, A.E. and Granger, D.N. *Exchange of macromolecules across the microcirculation.* In: Handbook Physiol., 6, (Microcirculation Part 1, Chapter 11). E.M. Renkin and C.C. Michel, Eds., Am.Physiol.Soc., Washington D.C., pp467-520, 1984.

294. Petrak, K. and Goddard, P. *Transport of macromolecules across the capillary walls.* Adv.Drug Deliv.Rev., 3, 191-214, 1989.

295. Joyner, W.L. and Kern, D.F. *Microvascular permeability to macromolecules and its dynamic modulation.* Adv.Drug Deliv.Rev., 4, 319-342, 1990.

296. Renkin, E. *Transport pathways and processes.* In: Endothelial Cell Biology in Health and Disease, Chap. 3. N. Simionescu and M. Simionescu, Eds., Plenum press, pp51-68, 1988.

297. Artursson, P. and O'Mullane, J. *Cellular and biochemical interactions of macromolecular drug delivery systems.* Adv.Drug Deliv.Rev., 3, 165-189, 1989.

298. Drobnik, J. and Rypacek, F. *Soluble synthetic polymers in biological systems.* Adv.Polym.Sci., 57, 2, 1984.

299. Kopecek, J. and Duncan, R. *Targetable polymeric prodrugs.* J.Cont.Rel., 6, 315, 1987.

300. Bundgaard, M. *Transport pathways in capillaries - in search of pores.* Ann.Rev.Physiol., 42, 325-336, 1980.

301. Mayerson, H.S., Wolfram, C.G., Shirley, H.H. and Wasserman, K. *Regional differences in capillary permeability.* Am.J.Physiol., 198, 155-160, 1960.

302. Simionescu, M. and Simionescu, N. *Ultrastructure of the microvascular wall: functional correlations.* In: Handbook of Physiol.6., (Microcirulation Part 1, Chap. 3). E.M. Renkin and C.C. Michel, Eds., Am.Physiol.Soc., Washington D.C., pp41-101, 1984.

303. Bennet, H.S., Luft, J.H. and Hampton, J.C. *Morphological classification of vertebrate blood capillaries.* Am.J.Physiol., 196, 381-390, 1959.

304. Karnovsky, M.J. *The ultrastructural basis of transcapillary exchanges.* J.Gen.Physiol., 52, 641-696, 1968.

305. Kardon, R.H. and Kessel, R.G. *Three-dimensional organization of the hepatic microcirculation in the rodent as observed by scanning electron microscopy of corrosion casts.* Gastroenterology, 79, 72-81, 1980.

306. Poulsen, H.L. *Interstitial fluid concentrations of albumin and immunoglobulin G in normal men.* Scand.J.Clin.Lab.Invest., 34, 119-122, 1974.

307. Palade, G.E., Simionescu, M.A. and Simionescu, N. *Structural aspects of the permeability of the microvascular endothelium.* Acta Physiol.Scand., 463, 11-32, 1979.

308. Patlak, C.S., Goldstein, D.A. and Hoffman, J.F. *The flow of solute and solvent across a two-membrane system.* J.Theor.Biol., 5, 425-442, 1963.

309. Renkin, E.M. *Multiple pathways of capillary permeability.* Circ.Res., 41, 735, 1978.

310. Simionescu, N. *Cellular aspects of transcapillary exchange.* Phys.Rev., 63, 1536-1579, 1983.

311. Firrell, J.C., Lewis, G.P. and Youlten, L.J.F. *Vascular permeability to macromolecules in rabbit paw and skeletal muscle: a study with a mathematical interpretation of transport processes.* Microvasc.Res., 23, 294, 1982.

312. Simionescu, N., Simionescu, M.A. and Palade, G.E. *Open junctions in the endothelium of postcapillary venules of the diaphragm.* J.Cell Biol., 79, 27-44, 1978.

313. Reese, T.S. and Karnovsky, M.J. *Fine structural localization of a blood-brain barrier to exogenous peroxidase.* J.Cell Biol., 34, 207-217, 1969.

314. Simionescu, M., Simionescu, N. and Palade, G.E. *Morphometric data on the endothelium of blood capillaries.* J.Cell Biol., 60, 128-137, 1974.

315. Simionescu, M., Simionescu, N. and Palade, G.E. *Segmental differentiations of cell junctions in the vascular endothelium. The microvasculature.* J.Cell Biol., 67, 863-885, 1975.

316. Bruns, R.R. and Palade, G.E. *Studies on blood capillaries. II. Transport of ferritin molecules across the wall of muscle capillaries.* J.Cell Biol., 37, 277-299, 1968.

317. Simionescu, N., Simionescu, M. and Palade, G.E. *Structural basis of permeability in sequential segments of the microvasculature. II. Pathways followed by microperoxidase across the endothelium.* Microvasc.Res., 15, 17-36, 1978.

318. Palade, G.E. *Blood capillaries of the heart and other organs.* Circulation, 24, 368, 1961.

319. Palade, G.E. and Bruns, R.R. *Structural modulations of plasmalemmal vesicles.* J.Cell Biol., 37, 633-649, 1968.

320. Simionescu, N., Simionescu, M. and Palade, G.E. *Structural-functional correlates in the transendothelial exchange of water soluble macromolecules.* Thromb.Res., 8, 257-269, 1976.

321. Wagner, R.C. and Casley-Smith, J.R. *Endothelial vesicles.* Microvasc.Res., 21, 267, 1981.

322. Renkin, E.M., Carter, R.D. and Joyner, W.L. *Mechanism of the sustained action of histamine and bradykinin on transport of large molecules across capillary walls in the dog paw.* Microvasc.Res., 7, 49, 1976.

323. Rippe, B., Kamiya, A. and Folkow, B. *Transcapillary passage of albumin, effects of tissue cooling and increase in filtration and plasma colloid osmotic pressure.* Acta Physiol.Scand., 105, 171-187, 1979.

324. Crone, C. *Ariadne's thread - an autobiographical essay on capillary permeability.* Microvasc.Res., 20, 133-149, 1980.

325. Renkin, E.M., Watson, P.D., Sloop, C.H., Joyner, W.L. and Curry, F.E. *Transport pathways for fluid and large molecules in microvascular endothelium of the dog's paw.* Microvasc.Res., 14, 205-214, 1977.

326. Renkin, E.M. and Gilmore, J.P. *Glomerular filtration.* In: Handbook of Physiology, Section 8, Renal Physiology, (Chapter 9), edited by J. Orloff, R.W. Berliner, Washington D.C., American Physiological Society, pp185-248, 1973.

327. Brenner, B.M., Deen, W.M. and Robertson, C.R. *Glomerular filtration.* Chapter 6, In: The Kidney, Vol.1, B.M. Brenner and F.C. Rector, Eds., W.B. Saunders Company, Philadelphia, pp251-271, 1976.

328. Latta, H., Johnston, W.H. and Stanley, T.M. *Sialoglycoproteins and filtration barriers in the glomerular capillary wall.* J.Ultrastruct.Res., 51, 354-376, 1975.

329. Latta, H. *The glomerular capillary wall.* J.Ultrastruct.Res., 32, 526, 1970.

330. Simionescu, M., Simionescu, N. and Palade, G.E. *Preferential distribution of anionic sites on the basement membrane and the abluminal aspect of the endothelium in fenestrated capillaries.* J.Cell Biol., 95, 425-434, 1982.

331. Venkatachalam, M.A. and Rennke, H.G. *The structural and molecular basis of glomerular filtration.* Circulation Res., 43, 337-347, 1978.

332. Solez, K. and Heptinstall, R.H. *The anatomy of the renal circulation.* In: Structure and function of the circulation, Vol.1., C.J. Schwartz, N.T. Werthessen and S., Wolf, Eds., Plenum Press, New York, London, pp631-660, 1980.

333. Guyton, A.C. *Formation of urine by the kidney: glomerular filtration, tubular function, and plasma clearance.* In: Textbook of Medical Physiology (Sixth edition), Chapter 34, A.C. Guyton, Ed., W.B. Saunders Company, Philadelphia, London, Toronto, pp403-419, 1981.

334. West, J.B. *Filtration and blood flow.* In: Best and Taylor's physiological basis of medical practice, (twelfth edition), Chapter 27, J.B. West, Ed., Williams and Wilkins, Baltimore, Hong Kong, London, Sydney, pp429-439, 1991.

335. Keele, C.A., Neil, E. and Joels, N. *Functions of the kidney: glomerular filtration.* In: Samson Wright's applied physiology, (thirteenth edition), Part IV, The kidney and the regulation of body fluids: Structure and function of the kidney, C.A. Keele, E. Neil and N. Joels, Eds., Oxford University Press, Oxford, pp218-224, 1982.

336. Ganong, W.F. *Formation and excretion of urine: renal function and micturition.* In: Review of Medical Physiology, (fifteenth edition), Section VIII, Chapter 38, W.F. Ganong, Ed., Prentice-Hall International Inc., U.S.A., pp649-678, 1991.

337. Hamburger, J., Richet, G. and Grunfeld, J.P. *Physiology.* In: Organ physiology: structure and function of the kidney, Chapter 2, J. Hamburger, G. Richet, and J.P. Grunfeld, Eds., W.B. Saunders Company, Philadelphia, London, Toronto, pp50-103, 1971.

338. Vender, A.J. *Glomerular filtration.* In: Renal physiology, (third edition), Chapter 2, A.J. Vender, Ed., McGraw-Hill Book Company, New York, London, pp19-45, 1985.

339. Lote, C.J. *Glomerular filtration.* In: Principles of renal physiology, Chapter 3, C.J. Lote, Ed., Croom Helm, London, Canberra, pp40-50, 1982.

340. Rennke, H.G. and Venkatachalam, M.A. *Structural determinants of glomerular permselectivity.* Federation Proc., 36, 2619-2626, 1977.

341. Latta, H. *Ultrastructure of the glomerulus and juxtaglomerular apparatus.* In: Handbook of Physiology. Renal Physiology, edited by J. Orloff and R.W. Berliner. Washington D.C., Am.Physiol.Soc., Chapter 1, Sect.8., pp1-29, 1973.

342. Tisher, C.C. *Anatomy of the Kidney.* In: The Kidney, Vol.1., B.M. Brenner and F.C. Rector, Eds., W.B. Saunders Company, Philadelphia, London, Toronto, 1976, pp3-64.

343. Farquhar, M.G. *The primary glomerular filtration barrier - basement membrane or epithelial slits.* Kidney Int., 8, 197-211, 1975.

344. Karnovsky, M.J. *The structural basis for glomerular filtration.* In: Kidney Disease: Present status, J. Chung, Ed., Williams and Wilkins, Baltimore, M.D., p1-41, 1979.

345. Ryan, G.B. *The glomerular filtration barrier.* In: Advances in renal physiology, C.J. Lote, Ed., Chapter 1, Croom Helm, London, Sydney, pp1-32, 1986.

346. Simionescu, N., Simionescu, M. and Palade, G.E. *Permeability of intestinal capillaries. Pathway followed by dextrans and glycogens.* J.Cell Biol., 53, 365-392, 1972.

347. Clementi, F. and Palade, G.E. *Intestinal capillaries. I. Permeability to peroxidase and ferritin.* J.Cell Biol., 41, 33-58, 1969.

348. Bohrer, M.P., Deen, W.M., Robertson, C.R. and Brenner, B.M. *Mechanism of angiotensin II-induced proteinuria in the rat.* Am.J.Physiol., 233, F13-F21, 1977.

349. Bohrer, M.P., Baylis, C., Humes, H.D. Glassock, R.J., Robertson, C.R. and Brenner, B.M. *Permselectivity of the glomerular capillary wall: facilitated filtration of circulating polycations.* J.Clin.Invest., 61, 72-78, 1978.

350. Brenner, B.M., Hostetter, T.H. and Humes, H.D. *Glomerular permselectivity: barrier function based on discrimination of molecular size and charge.* Am.J.Physiol., 234, F455-F460, 1978.

351. Rennke, H.G., Cotran, R.S. and Venkatachalam, M.A. *Role of molecular charge in glomerular permeability.* J.Cell Biol., 67, 638-646, 1975.

352. Rennke, H.G., Patel, Y. and Venkatachalam, M.A. *Effect of molecular charge in glomerular permeability. Clearance studies using neutral, anionic and cationic horseradish peroxidase.* Kidney Int., 13, 278-288, 1978.

353. Chang, R.L.S., Veki, I.F., Troy, J.L., Deen, W.M., Robertson, C.R. and Brenner, B.M. *Permselectivity of the glomerular capillary wall to macromolecules. II. Experimental studies in rats using neutral dextran.* Biophys.J., 15, 887-906, 1975.

354. Mihara, K., Hojo, T., Fujikawa, M., Takakura, Y., Sezaki, H. and Hashida, M. *Disposition characteristics of protein drugs in the perfused rat kidney.* Pharm.Res., 10, 823-827, 1993.

355. Ulbrich, K., Konak, C., Tuzar, Z. and Kopecek, K. *Solution properties of drug carriers based on poly (N-(2-hydroxypropyl)methacrylamide) containing biodegradable bonds.* Macromol.Chemie, 188, 1261, 1987.

356. Rennke, H.G. and Venkatachalam, M.A. *Glomerular permeability of macromolecules. Effect of molecular configuration on the fractional clearance of*

uncharged dextrans and neutral horseradish peroxidase in the rat. J.Clin.Invest., 63, 713-717, 1979.

357. Bohrer, M.P., Deen, W.M., Robertson, D.R., Troy, J.L. and Brenner, B.M. *Influence of molecular configuration on the passage of macromolecules across the glomerular capillary wall.* J.Gen.Physiol., 74, 583-593, 1979.

358. De Gennes, P.L. *Reptilation of a polymer chain in the presence of fixed obstacles.* J.Chem.Phys., 55, 572, 1971.

359. Hardwicke, J., Hulme, B., Henry Jones, J. and Ricketts, C.R. *Measurement of glomerular permeability to polydisperse radioactively-labelled macromolecules in normal rabbits.* Clin.Sci., 34, 505, 1968.

360. Jorgensen, K.E. and Moller J.V. *Use of flexible polymers as probes of glomerular size.* Am.J.Physiol., 236, F103, 1979.

361. Granger, D.N., Miller, T., Allen, R., Parker, R.E., Parker, J.C. and Taylor, A.E. *Permselectivity of the liver blood-lymph barrier to endogenous macromolecules.* Gastroenterology, 77, 103-109, 1979.

362. Dumont, A.E., Witte, C.L. and Witte, M.H. *Protein content of liver lymph in patients with portal hypertension secondary to hepatic cirrhosis.* Lymphology, 8, 111-113, 1975.

363. Roberts, S.H., Kepkay, D.L. and Barrowman, J.A. *Proteins of ascitic fluid in constrictive pericarditis.* Am.J.Dig.Dis., 23, 844, 848, 1978.

364. Goresky, C.A. *The nature of transcapillary exchange in the liver.* Can.Med.Assoc.J., 92, 519-522, 1965.

365. Perry, M.A., Barrowman, J.A., Kvietys, P.R. and Granger, D.N. *The exclusion phenomenon in the liver interstitium.* Gastroenterology, 80, 1251, 1981.

366. Rouiller, C.H. *The Liver: Morphology, Biochemistry, Physiology; A treatise in two volumes* C.H. Rouiller, Chief Ed., Academic Press, New York, London, Vol.I 1963, Vol. II 1964.

367. Hargreves, T. *The liver and bile metabolism.* North-Holland Publishing Company, Amsterdam, 1968.

368. Guyton, A.C. *Cerebral, splanchnic and skin blood flows.* In: Textbook of Medical Physiology, (sixth edition) Chapter 29, A.C. Guyton, Ed., W.B. Saunders Company, Philadelphia, London, Toronto, pp-344-356, 1981.

369. Gibaldi, M. *Bioavailability.* In: Biopharmaceutics and Clinical Pharmacokinetics, (Chapter 8), M. Gibaldi, Ed., Lea and Febiger, Philadelphia, London, pp155, 1991.

370. Ganong, W.F. *The general and cellular basis of medical physiology,* In: Review of Medical Physiology (fifteenth edition), Section 1, Chapter 1, W.F. Ganong, Ed., Prentice-Hall International Inc., U.S.A., pp1-41, 1991.

371. Russnyak, I., Foldi, M. and Szabo, G. (Eds.), In: Lymphatics and Lymph Circulation: Physiology and Pathology (second edition), Pergamon, Oxford, U.K., pp971, 1967.

372. Garlick, D.G. and Renkin, E.M. *Transport of large molecules from plasma to interstitial fluid and lymph in dogs.* Am.J.Physiol., 219, 1595-1605, 1970.

373. Rutili, G. and Arfors, K.E. *Protein concentration in interstitial and lymphatic fluids from the subcutaneous tissue.* Acta Physiol.Scand., 99, 1-8, 1977.

374. Renkin, E.M. *Lymph as a measure of the composition of interstitial fluid.* In: Pulmonary Edema, A.P. Fishman and E.M. Renkin, Eds. Am.Physiol.Soc., Bethesda, MD, pp145-159, 1979.

375. Grotte, G. *Passage of dextran molecules across the blood-lymph barrier.* Acta Chir.Scand.Suppl., 211, 1-84, 1956.

376. Yoffey, J.M. and Courtice, F.C. *Lymphatics, Lymph and the Lymphomyeloid Complex.* Academic Press, London, 1970.

377. Leak, L.V. *Studies on the permeability of lymphatic capillaries.* J.Cell Biol., 50, 300-323, 1971.

378. Weinstein, J.N., Stellar, M.A., Covell, D.G., Holton, O.D., Keenan, A.N., Sieber, S.M. and Parker, R.J. *Monoclonal antitumour antibodies in the lymphatics.* Cancer Treat.Rep., 68, 257-264, 1984.

379. Supersaxo, A., Hein, W.R., Gallati, H. and Steffen, H. *Recombinant human interferon alpha-2a: Delivery to lymphoid tissue by selected modes of application.* Pharm.Res., 5, 472-478, 1988.

380. Supersaxo, A., Hein, W.R. and Steffen, H. *Effect of molecular weight on the lymphatic absorption of water-soluble compounds following subcutaneous administration.* Pharm.Res., 7, 167-169, 1990.

381. Weinstein, J.N., Parker, R.J., Keenan, A.M., Dower, S.K., Morse, H.C. III and Sieber, S.M. *Monoclonal antibodies in the lymphatics: toward the diagnosis and therapy of tumour metastases.* Science, 218, 1334-1337, 1982.

382. Zweifach, B.W. and Lipowsky, H.H. *Pressure-flow relations in blood and lymph microcirculation.* In: E.M. Renkin and C.C. Michel (Eds)., Handbook of Physiology, American Physiological Society, Bethesda, pp295-299, 1984.

383. Keenan, A.M., Weinstein, J.N. and Mulshine, J.L. *Immunolymphoscintigraphy in patients with lymphoma after subcutaneous injection of In-^{111}-labelled T101 monoclonal antibody.* J.Nucl.Med., 28, 42-46, 1987.

384. Mayerson, H.S. *The physiologic importance of lymph.* In: Handbook of Physiology, Section 2, Circulation Vol.II, W.F. Hamilton, Section Ed., P. Dow, Exec.Ed., American Physiological Society, Washington D.C., pp1035-1074, 1963.

385. Clauss, M.A. and Jain, R.K. *Interstitial transport of rabbit and sheep antibodies in normal and neoplastic tissue.* Cancer Res., 50, 3487, 1990.

386. Nugent, L.J. and Jain, R.K. *Extravascular diffusion in normal and neoplastic tissue.* Cancer Res., 44, 238, 1984.

387. Gerlowski, L.E. and Jain, R.K. *Microvascular permeability of normal and neoplastic tissues.* Microvasc.Res., 31, 288, 1986.

388. Guyton, A.C. *The lymphatic system, interstitial fluid dynamics, edema, and pulmonary fluid.* In: Textbook of Medical Physiology, (sixth edition), Chapter 31, A.C. Guyton, Ed., W.B. Saunders Company, Philadelphia, London, Toronto, pp370-382, 1981.

389. Yoffey, J.M. and Courtice, F.C. *Flow and composition of lymph.* In: Lymphatics, Lymph and the Lymphomyeloid Complex, (Chapter 3), J.M. Yoffey and F.C. Courtice, Eds., London, Academic Press, pp160-205, 1970.

390. Rowland, M. and Tozer N. *Distribution.* In: Clinical Pharmacokinetics: Concepts and Applications, (Chapter 4), M. Rowland and N. Tozer, Eds., Lea and Febiger, Philadelphia, pp34-47, 1980.

391. Jain, R.K. *Transport of molecules in the tumour interstitium: a review.* Cancer Res., 47, 3039-3051, 1987.

392. Jain, R.K. *Determinants of tumour blood flow: a review* Cancer Res., 48, 2641-2658, 1988.

393. Jain, R.K. *Vascular and interstitial barriers to the delivery of therapeutic agents to tumours.* Cancer Metast.Rev., 9, 253, 1991.

394. Jain, R.K. *Haemodynamic and transport barriers to the treatment of solid tumours: a review.* Int.J.Radiat.Biol., 60, 85-100, 1991.

395. Brigham. K.L. and Owen, P.J. *Mechanism of the serotonin effect on lung transvascular fluid and protein movement in awake sheep.* Circ.Res., 36, 761-770, 1975.

396. Brigham, K.L. and Owen, P.J. *Increased sheep lung vascular permeability caused by histamine.* Circ.Res., 37, 647-657, 1975.

397. Parker, J.C., Parker, R.E., Granger, D.N. and Taylor, A.E. *Vascular permeability and transvascular fluid and protein transport in the dog lung.* Circ.Res., 48, 545-561, 1981.

398. Boyd, R.D.H., Hill, J.R., Humphreys, P.W., Normand, I.C.S., Reynolds, E.O.R. and Strang, L.B. *Permeability of lung capillaries to macromolecules in foetal and new-born lambs and sheep.* J.Physiol.London, 201, 567-588, 1969.

399. McNamee, J.E. and Staub, N.C. *Pore models of sheep lung microvascular barrier using new data on protein tracers.* Microvasc.Res., 18, 229-244, 1979.

400. Boonyaprakob, U., Taylor, P.M., Watson, D.W., Waterman, V. and Lopata, E. *Hypoxia and protein clearance from the pulmonary vascular beds of adult dogs and pups.* Am.J.Physiol., 216, 1013-1019, 1969.

401. Taylor, P.M., Boonyaprakob, U., Watson, D.W. and Fireman, P. *Relative efflux of native proteins from the canine pulmonary vascular bed.* Am.J.Physiol., 214, 1310-1314, 1968.

402. Erdmann, A.J., Vaughan, T.R., Brigham, K.L., Woolverton, W.C. and Staub, N.C. *Effect of increased vascular pressure on lung fluid balance in unanaesthetized sheep.* Circ.Res., 37, 271-284, 1975.

403. Binder, A.S., Nakahara, K., Ohkuda, K., Kageler, W. and Staub, N.C. *Effect of heparin or fibrinogen depletion on lung fluid balance in sheep after emboli.* J.Appl.Physiol.: Respirat.Environ.Exercise Physiol., 47, 213-219, 1979.

404. Bland, R.D., Demling, R.H., Selinger, S.L. and Staub, N.C. *Effects of alveolar hypoxia on lung fluid and protein transport in unanaesthetized sheep.* Circ.Res. 40, 269-273, 1977.

405. Bland, R.D. and McMillan, D.D. *Lung fluid dynamics in awake and new-born lambs.* J.Clin.Invest., 60, 1107-1115, 1977.

406. Anderson, R.W. and De Vries, W.C. *Transvascular fluid and protein dynamics in the lung following hemorrhagic shock.* J.Surg.Res., 20, 281-290, 1976.

407. Northrup, W.F. and Humphrey, E.W. *Pulmonary and systemic capillary permeability to protein following endotoxin.* Surg.Forum, 27, 65-57, 1976.

408. Northrup, W.F. and Humphrey, E.W. *Albumin permeability in the pulmonary capillaries.* Surg.Forum, 28, 224-226, 1978.

409. Zollinger, R.M. *Plasma volume and protein restoration after haemorrhage: role of the left thoracic duct versus transcapillary refilling.* J.Surg.Res., 151-160, 1972.

410. Arturson, G. *Microvascular permeability to macromolecules in thermal injury.* Acta Physiol.Scand.Suppl., 463, 111-122, 1979.

411. Carter, R.D., Joyner, W.L. and Renkin, E.M. *Effects of histamine and some other substances on molecular selectivity of the capillary wall to plasma proteins and dextran.* Microvasc.Res., 7, 31-48, 1974.

412. Bell, D.R., Watson, P.D. and Renkin, E.M. *Exclusion of plasma proteins in interstitium of tissues from the dog hind paw.* Am.J.Physiol., 239 (Heart Circ.Physiol.8): H532-H538, 1980.

413. Haljamae, H. and Freden, H. *Comparative analysis of the protein content of local subcutaneous tissue fluid and plasma.* Microvasc.Res., 2, 163-171, 1970.

414. Aukland, K. and Fadnes, H.O. *Protein concentration of interstitial fluid collected from rat skin by a wick method.* Acta Physiol.Scand., 88, 350-358, 1973.

415. Watson, P.D., Bell, D.R. and Renkin, E.M. *Early kinetics of large molecule transport between plasma and lymph in dogs.* Am.J.Physiol. 239 (Heart Circ.Physiol.8): H525-H531, 1980

416. Olszewski, W.L., Engeset, A. and Sokolowski, J. *Lymph flow and protein in the normal male leg during lying, getting up and walking.* Lymphology, 10, 178-183, 1977.

417. Olszewski, W.L. and Engeset, A. *Capillary transport of immunoglobulins and complement proteins to the interstitial fluid and lymph.* Arch.Immunol.Ther.Exp., 26, 57-65, 1978.

418. Reichel, A., Rother, V., Werner, J. and Reichel, F. *On the transport of various endogenous plasma proteins from blood to peripheral lymph in man.* Lymphology, 9, 118-121, 1976.

419. Ganrot, P.O., Laurell, C.B. and Ohlsson, K. *Concentration of trypsin inhibitors of different molecular size and of albumin and haptoglobin in blood and lymph of various organs in the dog.* Acta Physiol.Scand., 79, 280-286, 1970.

420. Courtice, F.C. and Sabine, M.S. *Effect of different degrees of thermal injury on the transfer of proteins and lipoproteins from plasma to lymph in the leg of the hypercholesterolaemic rabbit.* Aust.J.Exp.Biol.Med.Sci., 44, 37-44, 1966.

421. Aukland, K. and Johnsen, H.M. *Protein concentration and colloid osmotic pressure of rat skeletal muscle interstitial fluid.* Acta Physiol.Scand., 91, 354-364, 1974.

422. Appelgren, L.S., Jacobsson, S. and Kjellmer, I. *Estimation of the protein concentration of the capillary filtrate by an isotope technique.* Acta Physiol.Scand., 66, 353-361, 1966.

423. Lewis, G.P. and Winsey, N.J.P. *The action of pharmacologically active substances on the flow and composition of cat hind limb lymph.* Br.J.Pharmacol., 40, 446-460, 1970.

424. Amelang, E., Prasad, C.M., Raymond, R.M. and Grega, G.J. *Interactions among inflammatory mediators on edema formation in the canine forelimb.* Circ.Res., 49, 298-306, 1981.

425. Butler, K. and Lewis, G.P. *Effect of anti-inflammatory agents on the changes in local lymph after thermal injury.* Br.J.Pharmacol., 45, 644-650, 1972.

426. Youlten, L.J.F. *Permeability to human serum albumin (HSA) and polvinylpyrrolidone (PVP) of skeletal muscle (rat cremaster) blood vessel walls.* J.Physiol.London, 204: 112P-113P, 1969.

427. Shannon, A.D. and Lascelles, A.K. *A study of lipid absorption in young milk-fed calves with the use of a lymphatico-venous shunt for the collection of thoracic duct lymph.* Aust.J.Exp.Physiol., 20, 669-681, 1967.

428. Granger, D.N. and Taylor, A.E. *Permeability of intestinal capillaries to endogenous macromolecules.* Am.J.Physiol., 238 (Heart Circ.Physiol.7):H457-H464, 1980.

429. Bruggeman, T.M. *Plasma proteins in canine gastric lymph.* Gastroenterology, 68, 1204-1210, 1975.

430. Perry, M.A., Crook, W.J. and Granger, D.N. *Permeability of gastric capillaries to small and large molecules.* Am.J.Physiol. 241 (Gastrointest.Liver Physiol.4): G478-G486, 1981.

431. Richardson, P.D.I., Granger, D.N., Mailman, D. and Kvietys, P.R. *Permeability characteristics of colonic capillaries.* Am.J.Physiol. 239 (Gastrointest. Liver Physiol. 2): G300-G305, 1980.

432. Arturson, G. and Granath, K. *Dextrans as test molecules in studies of the functional ultrastructure of biological membranes.* Clin.Chim.Acta., 37, 309-322, 1972.

433. Witte, M.H., Witte, C.L. and Dumont, A.E. *Estimates of net transcapillary water and protein flux in the liver and intestine of patients with portal hypertension from hepatic cirrhosis.* Gastroenterology, 80, 265-272, 1981.

434. Vaerman, J-P. and Heremans, J.F. *Origin and molecular size of immunoglobulin-A in the mesenteric lymph of the dog.* Immunology, 18, 27-38, 1970.

435. Dive, C.C., Nadalini, A. and Heremans, J.F. *Origin and composition of hepatic lymph proteins in the dog.* Lymphology, 4, 133-139, 1979.

436. Friedman, M., Byers, S.O. and Omoto, C. *Some characteristics of hepatic lymph in the intact rat.* Am.J.Physiol., 184, 11-17, 1956.

437. Morris, B. *The hepatic and intestinal contributions to the thoracic duct lymph.* Q.J.Exp.Physiol., 41, 318-325, 1956.

438. Courtice, F.C. and Garlick., D.G. *The permeability of the capillary wall to the different plasma lipoproteins of the hypercholesterolaemic rabbit in relation to their size..* Q.J.Exp.Physiol., 47, 221-227, 1961.

439. Wolley, G. and Courtice, F.C. *The origin of albumin in hepatic lymph.* Aust.J.Exp.Biol.Med.Sci., 40, 121-128, 1962.

440. Witte, M.H., Witte, C.L. and Dumont, A.E. *Progress in liver disease: physiological factors involved in the causation of cirrhotic ascites.* Gastroenterology, 61, 742-750, 1971.

441. Minsq: *Nonlinear Parameter Estimation and Model Development.* MicroMath Scientific Software, Salt Lake City, Utah, 1988.

442. Pape, V. *Methotrexate-protein conjugates as soluble drug delivery systems.* Ph.D. thesis, Bath University, 1990.

443. Dedrick, R.L. and Bischoff, K.B. *Species similarities in pharmacokinetics.* Federation Proc., 39, 54-59, 1980.

444. Adolph, E.F. *Quantitative relations in the physiological constitutions of mammals.* Science, 109, 579-585, 1949.

445. Dedrick, R.L. *Animal scale-up.* J.Pharmacokin.Biopharm., 1, 435-461, 1973.

446. Williams, R.T. *Inter-species variations in the metabolism of xenobiotics.* Biochem.Soc.Trans., 2, 359-377, 1974.

447. Quin, G.P., Axelrod, J. and Brodie, B.B. *Species, strain and sex differences in metabolism of hexobarbitone, amidopyrine, antipyrine and aniline.* Bioichem.Pharmacol., 1, 152-159, 1958.

448. Krasovskii, G.N. *Extrapolation of experimental data from animals to man.* Environ.Health Persp., 13, 51-58, 1976.

449. Mordenti, J., Chen, S.A., Moore, J.A., Farraiolo, B.L. and Green, J.D. *Interspecies scaling of clearance and volume of distribution for five therapeutic proteins.* Pharm.Res., 8, 1351-1359, 1991.

450. Hamilton, W.F. In: Handbook of Physiology, Section 2: Circulation, Vol. I., Chapter 3, P. Dow, Exec.Ed., American Physiological Society, Washington D.C., pp52, 1962.

451. Knaak, J.B., Al-Bayati, M., Raabe, O.G. and Blancato, J.N. *In vivo percutaneous absorption studies in the rat: pharmacokinetics and modelling of isofenphos absorption.* In: Prediction of percutaneous penetration: Methods, Measurements, Modelling, R.C. Scott, R.H. Guy and J. Hadgraft Eds., (Preceedings of the conference held in April 1989; Session 1, in vivo methology), S.M. Tittensor, Assoc., Ed., IBC Technical Services Ltd., London, pp1-18, 1990.

452. Stella, V.J. and Himmelstein, K.J. *Prodrugs and site-specific drug delivery.* J.Med.Chem., 23, 1275-1282, 1980.

453. Dedrick, R.L. *Interspecies scaling of regional drug delivery.* J.Pharm.Sci., 75, 1047-1052, 1986.

454. Eckman, W.W., Patlak, C.S. and Fenstermacher, J.D. *A critical evaluation of the principles of governing the advantages of intra-arterial infusions.* J.Pharmacokin.Biopharm., 2, 257-285, 1974.

455. Buraggi, G.L., Callegaro, L., Mariani, G. et al. *Imaging with ^{131}I-labelled monoclonal antibodies to a high-molecular-weight melanoma-associated antigen in patients with melanoma: efficacy of whole immunoglobulin and its F(ab')$_2$ fragments.* Cancer Res., 45, 3378-3387, 1985.

456. Lotze, M.T., Carrasquillo, J.A., Weinstein, J.N. et al. *Monoclonal antibody imaging of human melanoma: radioimmunodetection by subcutaneous or systemic injection.* Ann.Surg., 204, 223-235, 1986.

457. Le Doussal, J.M., Gruaz-Guyon, A., Martin, M. et al. *Targeting of Indium ^{111}-labelled bivalent hapten to human melanoma mediated by bispecific monoclonal*

antibody conjugates: imaging of tumours hosted in nude mice. Cancer Res., 50, 3445-3452, 1990.

458. Stickney, D.R., Anderson, L.D., Slater, J.B. et al. *Bifunctional antibody: a binary radiopharmaceutical delivery system for imaging colorectal carcinoma.* Cancer Res., 51, 6650-6655, 1991.

459. Poznansky, M.J. and Juliano, R.L. *Biological approaches to the controlled delivery of drugs: A critical review.* Pharmacol.Rev., 36, 277-334, 1984.

460. Rippe, B. and Haraldsson, B. *Fluid and protein fluxes across small and large pores in the microvasculature. Application of two-pore equations.* Acta Physiol.Scand., 131, 411-428, 1987.

461. Curry, F.E. *Mechanisms and thermodynamics of transcapillary exchange.* In: Handbook of Physiology, Section 2: The Cardiovascular System. E.M. Renkin and C.C. Michel, Eds., Am.Physiol.Soc., Bethesda, M.D., pp309-374, 1984.

462. Swabb, E.A., Wei, J. and Gullino, M. *Diffusion and Convection in normal and neoplastic tissues.* Cancer Res., 34, 2814-2822, 1974.

Appendices A1 - A5

Appendix A1

Solution of the new physiological three compartment pharmacokinetic model

From 2.3.2.1 the set of differential equations which describe the new physiological three compartment pharmacokinetic model are:

$$\frac{dA_P}{dt} = -(k_{12} + k_{13} + k_{excr})A_P + k_{21}A_L + K_{31}A_H \qquad \text{A1.1}$$

$$\frac{dA_L}{dt} = k_{12}A_P - k_{21}A_L \qquad \text{A1.2}$$

$$\frac{dA_H}{dt} = -(k_{31} + k_m)A_H + k_{13}A_P \qquad \text{A1.3}$$

where all notation is as defined in section 2.3.2.

Using the Laplace transform rules for constants, linearity and first-derivatives (as defined in 2.3.2.3) the Laplace transforms of equations A1.1, A1.2 and A1.3 can be taken to give equations A1.4, A1.5, and A1.6 respectively as follows:-

For equation A1.1,

$$L\left[\frac{dA_P}{dt}\right] = L\left[-(k_{12} + k_{13} + k_{excr})A_P + k_{21}A_L + k_{31}A_H\right]$$

therefore,

$$sL[A_P] - A_P|_{t=0} = -(k_{12} + k_{13} + k_{excr})L[A_P] + k_{21}L[A_L] + k_{31}L[A_H]$$

hence,

$$sa_1 - D_0 = -(k_{12} + k_{13} + k_{excr})a_1 + k_{21}a_2 + k_{31}a_3 \qquad \text{A1.4}$$

Similarly for equation A1.2,

$$L\left[\frac{dA_L}{dt}\right] = L\left[k_{12}A_P - k_{21}A_L\right]$$

therefore,

$$sL[A_L] - A_L\big|_{t=0} = k_{12}L[A_P] - k_{21}L[A_L]$$

hence,

$$sa_2 - 0 = k_{12}a_1 - k_{21}a_2 \qquad \text{A1.5}$$

Similarly for equation A1.3,

$$L\left[\frac{dA_H}{dt}\right] = L\left[-(k_{31} + k_m)A_H + k_{13}A_P\right]$$

therefore,

$$sL[A_H] - A_H\big|_{t=0} = -(k_{31} + k_m)L[A_H] + k_{13}L[A_P]$$

hence,

$$sa_3 - 0 = -(k_{31} + k_m)a_3 + k_{13}a_1 \qquad \text{A1.6}$$

Re-arranging equations A1.4, A1.5 and A1.6 gives equations A1.7, A1.8 and A1.9 respectively as follows:-

(For equation A1.4) $\quad (s + k_{12} + k_{13} + k_{excr})a_1 - k_{21}a_2 - k_{31}a_3 = D_0 \qquad$ A1.7

(For equation A1.5) $\quad -k_{12}a_1 + (s + k_{21})a_2 = 0 \qquad$ A1.8

(For equation A1.6) $\quad -k_{13}a_1 + (s + k_{31} + k_m)a_3 = 0 \qquad$ A1.9

The determinant Δ of the system of equations A1.7, A1.8 and A1.9 is therefore,

$$\Delta = \begin{vmatrix} s + k_{12} + k_{13} + k_{excr} & -k_{21} & -k_{31} \\ -k_{12} & s + k_{21} & 0 \\ -k_{13} & 0 & s + k_{31} + k_m \end{vmatrix}$$

$$
\begin{aligned}
&=(s+k_{12}+k_{13}+k_{excr})\{(s+k_{21})(s+k_{31}+k_m)-(0)(0)\}-(-k_{21})\{(-k_{12})(s+k_{31}+k_m)-(0)(-k_{13})\}\\
&+(-k_{31})\{(-k_{12})(0)-(-k_{13})(s+k_{21})\}\\
&=(s+k_{12}+k_{13}+k_{excr})\left(s^2+k_{31}s+k_ms+k_{21}s+k_{21}k_{31}+k_{21}k_m\right)\\
&-(k_{12}k_{21}s+k_{12}k_{21}k_{31}+k_{12}k_{21}k_m)-(k_{13}k_{31}s+k_{13}k_{31}k_{21})
\end{aligned}
$$

$$
\begin{aligned}
&=s^3+k_{31}s^2+k_ms^2+k_{21}s^2+k_{21}k_{31}s+k_{21}k_ms\\
&+k_{12}s^2+k_{12}k_{31}s+k_{12}k_ms+k_{12}k_{21}s+k_{12}k_{21}k_{31}+k_{12}k_{21}k_m\\
&+k_{13}s^2+k_{13}k_{31}s+k_{13}k_ms+k_{13}k_{21}s+k_{13}k_{21}k_{31}+k_{13}k_{21}k_m\\
&+k_{excr}s^2+k_{excr}k_{31}s+k_{excr}k_ms+k_{excr}k_{21}s+k_{excr}k_{21}k_{31}+k_{excr}k_{21}k_m\\
&-k_{12}k_{21}s-k_{12}k_{21}k_{31}-k_{12}k_{21}k_m-k_{13}k_{31}s-k_{13}k_{31}k_{21}
\end{aligned}
$$

$$
\begin{aligned}
&=s^3+(k_{31}+k_m+k_{21}+k_{12}+k_{13}+k_{excr})s^2\\
&+(k_{21}k_{31}+k_{21}k_m+k_{12}k_{31}+k_{12}k_m+k_{13}k_m+k_{13}k_{21}+k_{excr}k_{31}+k_{excr}k_m+k_{excr}k_{21})s\\
&+(k_{13}k_{21}k_m+k_{excr}k_{21}k_{31}+k_{excr}k_{21}k_m)
\end{aligned}
$$

A1.10

Now equation A1.10 can be thought of as tracing the same general form as a cubic equation with roots γ , α and β say as follows,

$$(s+\gamma)(s+\alpha)(s+\beta) \qquad \text{A1.11}$$

which when expanded out gives,

$$s^3+s^2(\alpha+\beta+\gamma)+s(\alpha\beta+\alpha\gamma+\beta\gamma)+\alpha\beta\gamma \qquad \text{A1.12}$$

since a polynomial of degree n has n roots (i.e. $n = 3$ in this case).

Therefore by comparing the coefficients of the s^3 , s^2 , s and constant terms in equation A1.10 with the corresponding terms in equation A1.12, it is readily apparent that the roots of equation A1.10 can be expressed in terms of the inter-compartmental parameters (first order rate constants) as follows,

$$\alpha+\beta+\gamma = k_{31}+k_m+k_{21}+k_{12}+k_{13}+k_{excr} \qquad \text{A1.13}$$

$$
\begin{aligned}
\alpha\beta+\alpha\gamma+\beta\gamma = {} & k_{21}k_{31}+k_{21}k_m+k_{12}k_{31}+k_{12}k_m+k_{13}k_m\\
& +k_{13}k_{21}+k_{excr}k_{31}+k_{excr}k_m+k_{excr}k_{21}
\end{aligned} \qquad \text{A1.14}
$$

$$\alpha\beta\gamma = k_{13}k_{21}k_m+k_{excr}k_{21}k_{31}+k_{excr}k_{21}k_m \qquad \text{A1.15}$$

So defining the roots of equation A1.10 to be α, γ and β, the system of equations A1.13, A1.14 and A1.15 can therefore be solved for either γ, α or β to give the three roots of equation A1.10. In each case, and for the reasons explained below, this calculation produces another cubic equation in terms of whichever root γ, α or β is being solved for, and whose roots will actually represent the roots of equation A1.10. This is because regardless of whether γ, α or β is selected to perform this calculation, the coefficients of the resulting cubic equation in each case will be exactly the same for each of γ, α and β, hence the roots of each resulting cubic equation will be exactly the same in each case as well, and as shown below will actually represent the three roots of equation A1.10. This is illustrated as follows by obtaining the cubic equation in terms of γ,

Multiplying equation A1.14 by γ gives,

$$\alpha\beta\gamma + \beta\gamma^2 + \alpha\gamma^2 = \gamma\left(k_{21}k_{31} + k_{21}k_m + k_{12}k_{31} + k_{12}k_m + k_{13}k_m + k_{13}k_{21} + k_{excr}k_{31} + k_{excr}k_m + k_{excr}k_{21}\right) \quad \text{A1.16}$$

Now putting equation A1.15 into equation A1.16 gives,

$$k_{13}k_{21}k_m + k_{excr}k_{21}k_{31} + k_{excr}k_{21}k_m + \gamma^2(\alpha+\beta) = \gamma\left(k_{21}k_{31} + k_{21}k_m + k_{12}k_{31} + k_{12}k_m + k_{13}k_m + k_{13}k_{21} + k_{excr}k_{31} + k_{excr}k_m + k_{excr}k_{21}\right) \quad \text{A1.17}$$

But from equation A1.13 $$\alpha + \beta = \left(k_{12} + k_{21} + k_{13} + k_{31} + k_{excr} + k_m\right) - \gamma \quad \text{A1.18}$$

So putting equation A1.18 into equation A1.17 and re-arranging gives,

$$\gamma^3 - \gamma^2\left(k_{12} + k_{21} + k_{13} + k_{31} + k_{excr} + k_m\right) + \gamma\left(k_{21}k_{31} + k_{21}k_m + k_{12}k_{31} + k_{12}k_m + k_{13}k_m + k_{13}k_{21} + k_{excr}k_{31} + k_{excr}k_m + k_{excr}k_{21}\right) - \left(k_{13}k_{21}k_m + k_{excr}k_{21}k_{31} + k_{excr}k_{21}k_m\right) = 0 \quad \text{A1.19}$$

Equation A1.19 is therefore a cubic equation in terms of the root γ and the inter-compartmental parameters, with the inter-compartmental parameters representing the coefficients of the cubic. By Descartes rule of sign all three roots of equation A1.19 are positive, and by the nature of the inter-compartmental parameters and the fact that the physiological pharmacokinetic model consists of three compartments, these roots are

also obviously distinct and greater than zero. So for equation A1.19, letting the largest root be γ_3 say, the middle (next largest) root be γ_2 say, and the smallest root be γ_1 say, then $\gamma_3 > \gamma_2 > \gamma_1 > 0$. Similarly, if the system of equations A1.13, A1.14 and A1.15 were solved for either α or β as well, the resulting cubic equation in each case in terms of α or β would have exactly the same coefficients as those in equation A1.19, and due to Descartes rule and the reasons outlined above, the three roots of each of these equations would be real, distinct and greater than zero. Hence for the resulting cubic equation in terms of α, letting the largest root be α_3 say, the middle (next largest) root be α_2 say, and the smallest root be α_1 say, then $\alpha_3 > \alpha_2 > \alpha_1 > 0$. Likewise for the resulting cubic equation in terms of β, letting the largest root be β_3, say, the middle (next largest) root be β_2 say, and the smallest root be β_1 say, then $\beta_3 > \beta_2 > \beta_1 > 0$. However, because the coefficients of the resulting cubic equations are exactly the same in each case regardless of whether γ, α or β has been selected to solve the system of equations A1.13, A1.14 and A1.15, then this also means that the roots in each case will be exactly the same (having the same respective values) in each case as well,

hence $\gamma \equiv \gamma_3 = \alpha_3 = \beta_3$, $\alpha \equiv \gamma_2 = \alpha_2 = \beta_2$, and $\beta \equiv \gamma_1 = \alpha_1 = \beta_1$.

Therefore since a polynomial of degree *n* has *n* roots, then the cubic equation of general form given by *f(x)* say as follows,

$$f(x) = a_3 x^3 + a_2 x^2 + a_1 x + a_0 = 0 \qquad \text{A1.20}$$

with

$$a_3 = 1$$
$$a_2 = -\left(k_{12} + k_{21} + k_{13} + k_{31} + k_{excr} + k_m\right)$$
$$a_1 = \left(k_{21}k_{31} + k_{21}k_m + k_{12}k_{31} + k_{12}k_m + k_{13}k_m + k_{13}k_{21} + k_{excr}k_{31} + k_{excr}k_m + k_{excr}k_{21}\right)$$
$$a_0 = -\left(k_{13}k_{21}k_m + k_{excr}k_{21}k_{31} + k_{excr}k_{21}k_m\right)$$

gives the three roots γ, α and β with $\gamma > \alpha > \beta > 0$.

Equation A1.20 can then be solved numerically using the Newton-Raphson and synthetic division techniques described in subsection 2.3.2.3 to find the roots γ, α and β . (The root γ was selected purely arbitrarily to illustrate the calculation described above.) The roots γ, α and β therefore can be thought of also as being hybrid physiological parameters.

Before progressing to the next stage, it is important to note that if E_i is defined to be the sum of all exit inter-compartmental parameters (first-order rate constants) out of physiological compartment *i*, then for the sake of convenience of notation the bulky expressions above are simplified as follows,

Defining E_i = sum of all exit inter-compartmental parameters out of physiological compartment *i*

then,

$$E_1 = k_{12} + k_{13} + k_{excr} \qquad \text{A1.21}$$

$$E_2 = k_{21} \qquad \text{A1.22}$$

$$E_3 = k_{31} + k_m \qquad \text{A1.23}$$

and equations A1.7, A1.8 and A1.9 become equation A1.24, A1.25 and A1.26 respectively as follows:

(equation A1.7 becomes) $$(s+E_1)a_1 - E_2a_2 - k_{31}a_3 = D_0 \qquad \text{A1.24}$$

(equation A1.8 becomes) $$-k_{12}a_1 + (s+E_2)a_2 = 0 \qquad \text{A1.25}$$

(equation A1.9 becomes) $$-k_{13}a_1 + (s+E_3)a_3 = 0 \qquad \text{A1.26}$$

so the determinant Δ of the system of equations A1.24, A1.25 and A1.26 is,

$$\Delta = \begin{vmatrix} s+E_1 & -E_2 & -k_{31} \\ -k_{12} & s+E_2 & 0 \\ -k_{13} & 0 & s+E_3 \end{vmatrix}$$

$$= (s+E_1)\{(s+E_2)(s+E_3) - (0)(0)\} - (-E_2)\{(-k_{12})(s+E_3) - (0)(-k_{13})\}$$
$$+ (-k_{31})\{(-k_{12})(0) - (-k_{13})(s+E_2)\}$$

$$
\begin{aligned}
&= (s+E_1)(s+E_2)(s+E_3) - k_{12}E_2(s+E_3) - k_{31}k_{13}(s+E_2) \\
&= (s+E_1)(s^2 + E_2 s + E_3 s + E_2 E_3) - k_{12}E_2 s - k_{12}E_2E_3 - k_{31}k_{13}s - k_{31}k_{13}E_2 \\
&= s^3 + E_2 s^2 + E_3 s^2 + E_2E_3 s + E_1 s^2 + E_1E_2 s + E_1E_3 s + E_1E_2E_3 - k_{12}E_2 s \\
&\quad - k_{12}E_2E_3 - k_{31}k_{13}s - k_{31}k_{13}E_2 \\
&= s^3 + s^2(E_1 + E_2 + E_3) + s(E_1E_2 + E_2E_3 + E_1E_3 - k_{12}E_2 - k_{31}k_{13}) \\
&\quad + (E_1E_2E_3 - k_{12}E_2E_3 - k_{31}k_{13}E_2)
\end{aligned}
\qquad \text{A1.27}
$$

where equations A1.10 and A1.27 are identical.

Similarly, equations A1.13, A1.14 and A1.15 can also be expressed as equations A1.28, A1.29 and A1.30 respectively as follows,

(equation A1.13 becomes) $$\alpha + \beta + \gamma = E_1 + E_2 + E_3 \qquad \text{A1.28}$$

(equation A1.14 becomes) $$\alpha\beta + \alpha\gamma + \beta\gamma = E_1E_2 + E_2E_3 + E_1E_3 - k_{12}E_2 - k_{31}k_{13} \qquad \text{A1.29}$$

(equation A1.15 becomes) $$\alpha\beta\gamma = \mathrm{E}_1E_2E_3 - k_{12}E_2E_3 - k_{31}k_{13}E_2 \qquad \text{A1.30}$$

where equation A1.28 is identical to equation A1.13, equation A1.29 is identical to equation A1.14, and equation A1.30 is identical to equation A1.15.

For a_1:-

Applying Cramers rule gives,

$$
a_1 = \frac{\begin{vmatrix} D_0 & -E_2 & -k_{31} \\ 0 & s+E_2 & 0 \\ 0 & 0 & s+E_3 \end{vmatrix}}{\Delta}
$$

$$
= \frac{D_0\{(s+E_2)(s+E_3) - (0)(0)\} - (-E_2)\{(0)(s+E_3) - (0)(0)\} + (-k_{31})\{(0)(0) - (0)(s+E_2)\}}{(s+\gamma)(s+\alpha)(s+\beta)}
$$

$$
= \frac{D_0(s+E_2)(s+E_3)}{(s+\gamma)(s+\alpha)(s+\beta)} \qquad \text{A1.31}
$$

Therefore to get A_p the inverse Laplace transform of this function must be taken, but first the function must be separted by the method of partial fractions as follows,

let $$\frac{D_0(s+E_2)(s+E_3)}{(s+\gamma)(s+\alpha)(s+\beta)} = \frac{G}{(s+\gamma)} + \frac{H}{(s+\alpha)} + \frac{I}{(s+\beta)}$$

therefore, $$D_0(s+E_2)(s+E_3) = G(s+\alpha)(s+\beta) + H(s+\gamma)(s+\beta) + I(s+\gamma)(s+\alpha)$$

so when $s = -\gamma$,

$$D_0(E_2 - \gamma)(E_3 - \gamma) = G(\alpha - \gamma)(\beta - \gamma)$$

hence,

$$G = \frac{D_0(E_2 - \gamma)(E_3 - \gamma)}{(\alpha - \gamma)(\beta - \gamma)} = \frac{D_0(E_2 - \gamma)(E_3 - \gamma)}{(\gamma - \alpha)(\gamma - \beta)} \qquad \text{A1.32}$$

Similarly when $s = -\alpha$

$$D_0(E_2 - \alpha)(E_3 - \alpha) = H(\gamma - \alpha)(\beta - \alpha)$$

hence,

$$H = \frac{D_0(E_2 - \alpha)(E_3 - \alpha)}{(\gamma - \alpha)(\beta - \alpha)} = \frac{D_0(E_2 - \alpha)(\alpha - E_3)}{(\gamma - \alpha)(\alpha - \beta)} \qquad \text{A1.33}$$

Similarly when $s = -\beta$,

$$D_0(E_2 - \beta)(E_3 - \beta) = I(\gamma - \beta)(\alpha - \beta)$$

hence,

$$I = \frac{D_0(E_2 - \beta)(E_3 - \beta)}{(\gamma - \beta)(\alpha - \beta)} \qquad \text{A1.34}$$

Therefore,

$$a_1 = \frac{D_0(s + E_2)(s + E_3)}{(s+\gamma)(s+\alpha)(s+\beta)} = \frac{D_0(E_2 - \gamma)(E_3 - \gamma)}{(\gamma - \alpha)(\gamma - \beta)(s+\gamma)} + \frac{D_0(E_2 - \alpha)(\alpha - E_3)}{(\gamma - \alpha)(\alpha - \beta)(s+\alpha)} + \frac{D_0(E_2 - \beta)(E_3 - \beta)}{(\gamma - \beta)(\alpha - \beta)(s+\beta)}$$

so taking the inverse Laplace transform gives

$$L^{-1}[a_1] = L^{-1}\left[\frac{D_0(E_2-\gamma)(E_3-\gamma)}{(\gamma-\alpha)(\gamma-\beta)(s+\gamma)} + \frac{D_0(E_2-\alpha)(\alpha-E_3)}{(\gamma-\alpha)(\alpha-\beta)(s+\alpha)} + \frac{D_0(E_2-\beta)(E_3-\beta)}{(\gamma-\beta)(\alpha-\beta)(s+\beta)}\right]$$

$$= \frac{D_0(E_2-\gamma)(E_3-\gamma)}{(\gamma-\alpha)(\gamma-\beta)} L^{-1}\left[\frac{1}{s+\gamma}\right] + \frac{D_0(E_2-\alpha)(\alpha-E_3)}{(\gamma-\alpha)(\alpha-\beta)} L^{-1}\left[\frac{1}{s+\alpha}\right] + \frac{D_0(E_2-\beta)(E_3-\beta)}{(\gamma-\beta)(\alpha-\beta)}\left[\frac{1}{s+\beta}\right]$$

therefore,

$$A_P = \frac{D_0(E_2-\gamma)(E_3-\gamma)e^{-\gamma t}}{(\gamma-\alpha)(\gamma-\beta)} + \frac{D_0(E_2-\alpha)(\alpha-E_3)e^{-\alpha t}}{(\gamma-\alpha)(\alpha-\beta)} + \frac{D_0(E_2-\beta)(E_3-\beta)e^{-\beta t}}{(\gamma-\beta)(\alpha-\beta)} \qquad \text{A1.35}$$

i.e. $A_P = Ge^{-\gamma t} + He^{-\alpha t} + Ie^{-\beta t}$ A1.36

hence in terms of the original notation

$$A_P = \frac{D_0(k_{21}-\gamma)(k_{31}+k_m-\gamma)e^{-\gamma t}}{(\gamma-\alpha)(\gamma-\beta)} + \frac{D_0(k_{21}-\alpha)(\alpha-(k_{31}+k_m))e^{-\alpha t}}{(\gamma-\alpha)(\alpha-\beta)} + \frac{D_0(k_{21}-\beta)(k_{31}+k_m-\beta)e^{-\beta t}}{(\gamma-\beta)(\alpha-\beta)}$$

A1.37

Also, since at time t the concentration of the drug in the blood compartment is given by $C_P = \frac{A_P}{V_c}$, with $C_P|_{t=0} = C_0 = \frac{D_0}{V_c}$, then equation A1.35, A1.36, and A1.37 can also be

expressed in concentration terms as follows as well,

$$C_P = \frac{D_0(E_2-\gamma)(E_3-\gamma)e^{-\gamma t}}{V_c(\gamma-\alpha)(\gamma-\beta)} + \frac{D_o(E_2-\alpha)(\alpha-E_3)e^{-\alpha t}}{V_c(\gamma-\alpha)(\alpha-\beta)} + \frac{D_o(E_2-\beta)(E_3-\beta)e^{-\beta t}}{V_c(\gamma-\beta)(\alpha-\beta)} \qquad \text{A1.38}$$

i.e. $C_P = \frac{1}{V_c}\left(Ge^{-\gamma t} + He^{-\alpha t} + Ie^{-\beta t}\right) = G_1e^{-\gamma t} + H_1e^{-\alpha t} + I_1e^{-\beta t}$ A1.39

where $G_1 = \frac{G}{V_c}$ A1.40

$H_1 = \frac{H}{V_c}$ A1.41

$I_1 = \frac{I}{V_c}$ A1.42

hence in terms of the original notation,

$$C_P = \frac{D_0(k_{21}-\gamma)(k_{31}+k_m-\gamma)e^{-\gamma t}}{V_c(\gamma-\alpha)(\gamma-\beta)} + \frac{D_0(k_{21}-\alpha)(\alpha-(k_{31}+k_m))e^{-\alpha t}}{V_c(\gamma-\alpha)(\alpha-\beta)} + \frac{D_0(k_{21}-\beta)(k_{31}+k_m-\beta)e^{-\beta t}}{V_c(\gamma-\beta)(\alpha-\beta)}$$

A1.43

For a_2:-

Applying Cramers rule gives,

$$a_2 = \frac{\begin{vmatrix} s+E_1 & D_0 & -k_{31} \\ -k_{12} & 0 & 0 \\ -k_{13} & 0 & s+E_3 \end{vmatrix}}{\Delta}$$

$$= \frac{(s+E_1)\{(0)(s+E_3)-(0)(0)\} - D_0\{(-k_{12})(s+E_3)-(0)(-k_{13})\} + (-k_{31})\{(-k_{12})(0)-(0)(-k_{13})\}}{(s+\gamma)(s+\alpha)(s+\beta)}$$

$$= \frac{D_0 k_{12}(s+E_3)}{(s+\gamma)(s+\alpha)(s+\beta)} \qquad \text{A1.44}$$

Therefore to get A_L the inverse Laplace transform of this function must be taken, but first the function must be separated by the method of partial fractions as follows,

$$\frac{D_0 k_{12}(s+E_3)}{(s+\gamma)(s+\alpha)(s+\beta)} = \frac{A}{(s+\gamma)} + \frac{B}{(s+\alpha)} + \frac{C}{(s+\beta)}$$

therefore,

$$D_0 k_{12}(s+E_3) = A(s+\alpha)(s+\beta) + B(s+\gamma)(s+\beta) + C(s+\gamma)(s+\alpha)$$

so when $s = -\gamma$,

$$D_0 k_{12}(E_3 - \gamma) = A(\alpha - \gamma)(\beta - \gamma)$$

hence,

$$A = \frac{D_0 k_{12}(E_3 - \gamma)}{(\alpha - \gamma)(\beta - \gamma)} = \frac{D_0 k_{12}(E_3 - \gamma)}{(\gamma - \alpha)(\gamma - \beta)} \qquad \text{A1.45}$$

Similarly when $s = -\alpha$,

$$D_0 k_{12}(E_3 - \alpha) = B(\gamma - \alpha)(\beta - \alpha)$$

hence,

$$B = \frac{D_0 k_{12}(E_3 - \alpha)}{(\gamma - \alpha)(\beta - \alpha)} = \frac{D_0 k_{12}(\alpha - E_3)}{(\gamma - \alpha)(\alpha - \beta)} \qquad \text{A1.46}$$

Similarly when $s = -\beta$

$$D_0 k_{12}(E_3 - \beta) = C(\gamma - \beta)(\alpha - \beta)$$

hence,

$$C = \frac{D_0 k_{12}(E_3 - \beta)}{(\gamma - \beta)(\alpha - \beta)} \qquad \text{A1.47}$$

Therefore,

$$a_2 = \frac{D_0 k_{12}(s+E_3)}{(s+\gamma)(s+\alpha)(s+\beta)} = \frac{D_0 k_{12}(E_3 - \gamma)}{(\gamma-\alpha)(\gamma-\beta)(s+\gamma)} + \frac{D_0 k_{12}(\alpha - E_3)}{(\gamma-\alpha)(\alpha-\beta)(s+\alpha)} + \frac{D_0 k_{12}(E_3 - \beta)}{(\gamma-\beta)(\alpha-\beta)(s+\beta)}$$

so taking the inverse Laplace transform gives,

$$L^{-1}[a_2] = L^{-1}\left[\frac{D_0 k_{12}(E_3 - \gamma)}{(\gamma-\alpha)(\gamma-\beta)(s+\gamma)} + \frac{D_0 k_{12}(\alpha - E_3)}{(\gamma-\alpha)(\alpha-\beta)(s+\alpha)} + \frac{D_0 k_{12}(E_3 - \beta)}{(\gamma-\beta)(\alpha-\beta)(s+\beta)}\right]$$

$$= \frac{D_0 k_{12}}{(\gamma-\alpha)(\gamma-\beta)} L^{-1}\left[\frac{1}{s+\gamma}\right] + \frac{D_0 k_{12}}{(\gamma-\alpha)(\alpha-\beta)} L^{-1}\left[\frac{1}{s+\alpha}\right] + \frac{D_0 k_{12}}{(\gamma-\beta)(\alpha-\beta)} L^{-1}\left[\frac{1}{s+\beta}\right]$$

therefore,

$$A_L = \frac{D_0 k_{12}(E_3 - \gamma)e^{-\gamma t}}{(\gamma-\alpha)(\gamma-\beta)} + \frac{D_0 k_{12}(\alpha - E_3)e^{-\alpha t}}{(\gamma-\alpha)(\alpha-\beta)} + \frac{D_0 k_{12}(E_3 - \beta)e^{-\beta t}}{(\gamma-\beta)(\alpha-\beta)} \qquad \text{A1.48}$$

i.e. $A_L = Ae^{-\gamma t} + Be^{-\alpha t} + Ce^{-\beta t}$ A1.49

hence in terms of the original notation,

$$A_L = \frac{D_0 k_{12}(k_{31} + k_m - \gamma)e^{-\gamma t}}{(\gamma-\alpha)(\gamma-\beta)} + \frac{D_0 k_{12}(\alpha - (k_{31} + k_m))e^{-\alpha t}}{(\gamma-\alpha)(\alpha-\beta)} + \frac{D_0 k_{12}(k_{31} + k_m - \beta)e^{-\beta t}}{(\gamma-\beta)(\alpha-\beta)}$$

A1.50

For a_3 :-

Applying Cramers rule gives,

$$a_3 = \frac{\begin{vmatrix} s+E_1 & -E_2 & D_0 \\ -k_{12} & s+E_2 & 0 \\ -k_{13} & 0 & 0 \end{vmatrix}}{\Delta}$$

$$= \frac{(s+E_1)\{(s+E_2)(0)-(0)(0)\}-(-E_2)\{(-k_{12})(0)-(0)(-k_{13})\}+D_0\{(-k_{12})(0)-(-k_{13})(s+E_2)\}}{(s+\gamma)(s+\alpha)(s+\beta)}$$

$$= \frac{D_0 k_{13}(s+E_2)}{(s+\gamma)(s+\alpha)(s+\beta)} \qquad \text{A1.51}$$

Therefore to get A_H the inverse Laplace transform of this function must be taken, but first the function must be separated by the method of partial fractions as follows,

let $$\frac{D_0 k_{13}(s+E_2)}{(s+\gamma)(s+\alpha)(s+\beta)} = \frac{P}{(s+\gamma)} + \frac{Q}{(s+\alpha)} + \frac{R}{(s+\beta)}$$

therefore,

$$D_0 k_{13}(s+E_2) = P(s+\alpha)(s+\beta) + Q(s+\gamma)(s+\beta) + R(s+\gamma)(s+\alpha)$$

so when $s = -\gamma$,

$$D_o k_{13}(E_2 - \gamma) = P(\alpha - \gamma)(\beta - \gamma)$$

hence,

$$P = \frac{D_0 k_{13}(E_2 - \gamma)}{(\alpha - \gamma)(\beta - \gamma)} = \frac{D_0 k_{13}(E_2 - \gamma)}{(\gamma - \alpha)(\gamma - \beta)} \qquad \text{A1.52}$$

Similarly when $s = -\alpha$,

$$D_0 k_{13}(E_2 - \alpha) = Q(\gamma - \alpha)(\beta - \alpha)$$

hence,

$$Q = \frac{D_0 k_{13}(E_2 - \alpha)}{(\gamma - \alpha)(\beta - \alpha)} = \frac{D_0 k_{13}(\alpha - E_2)}{(\gamma - \alpha)(\alpha - \beta)} \qquad \text{A1.53}$$

Similarly when $s = -\beta$,

$$D_0 k_{13}(E_2 - \beta) = R(\gamma - \beta)(\alpha - \beta)$$

hence,

$$R = \frac{D_0 k_{13}(E_2 - \beta)}{(\gamma - \beta)(\alpha - \beta)} \qquad \text{A1.54}$$

Therefore,

$$a_3 = \frac{D_0 k_{13}(s + E_2)}{(s+\gamma)(s+\alpha)(s+\beta)} = \frac{D_0 k_{13}(E_2 - \gamma)}{(\gamma - \alpha)(\gamma - \beta)(s+\gamma)} + \frac{D_0 k_{13}(\alpha - E_2)}{(\gamma - \alpha)(\alpha - \beta)(s+\alpha)} + \frac{D_0 k_{13}(E_2 - \beta)}{(\gamma - \beta)(\alpha - \beta)(s+\beta)}$$

so taking the inverse Laplace transform gives,

$$L^{-1}[a_3] = L^{-1}\left[\frac{D_0 k_{13}(E_2 - \gamma)}{(\gamma - \alpha)(\gamma - \beta)(s+\gamma)} + \frac{D_0 k_{13}(\alpha - E_2)}{(\gamma - \alpha)(\alpha - \beta)(s+\alpha)} + \frac{D_0 k_{13}(E_2 - \beta)}{(\gamma - \beta)(\alpha - \beta)(s+\beta)}\right]$$

$$= \frac{D_0 k_{13}(E_2 - \gamma)}{(\gamma - \alpha)(\gamma - \beta)} L^{-1}\left[\frac{1}{s+\gamma}\right] + \frac{D_0 k_{13}(\alpha - E_2)}{(\gamma - \alpha)(\alpha - \beta)} L^{-1}\left[\frac{1}{s+\alpha}\right] + \frac{D_0 k_{13}(E_2 - \beta)}{(\gamma - \beta)(\alpha - \beta)} L^{-1}\left[\frac{1}{s+\beta}\right]$$

therefore,

$$A_H = \frac{D_0 k_{13}(E_2 - \gamma)e^{-\gamma t}}{(\gamma - \alpha)(\gamma - \beta)} + \frac{D_0 k_{13}(\alpha - E_2)e^{-\alpha t}}{(\gamma - \alpha)(\alpha - \beta)} + \frac{D_0 k_{13}(E_2 - \beta)e^{-\beta t}}{(\gamma - \beta)(\alpha - \beta)} \qquad \text{A1.55}$$

i.e. $$A_H = Pe^{-\gamma t} + Qe^{-\alpha t} + \mathrm{R}e^{-\beta t} \qquad \text{A1.56}$$

hence in terms of the original notation,

$$A_H = \frac{D_0 k_{13}(k_{21} - \gamma)e^{-\gamma t}}{(\gamma - \alpha)(\gamma - \beta)} + \frac{D_0 k_{13}(\alpha - k_{21})e^{-\alpha t}}{(\gamma - \alpha)(\alpha - \beta)} + \frac{D_0 k_{13}(k_{21} - \beta)e^{-\beta t}}{(\gamma - \beta)(\alpha - \beta)} \qquad \text{A1.57}$$

Appendix A2

Calculation of the equations for A_{EXCR} and A_M

In this appendix, calculation of the equations to describe the fractions of the dose which have been excreted by the kidneys and metabolised (hepatically cleared) by the liver with respect to time in the new physiological three-compartment pharmacokinetic model are presented:

From 2.3.2.3 the rate of change in the mass (amount) of drug excreted by the kidneys is represented by the equation,

$$\frac{dA_{EXCR}}{dt} = k_{excr} A_P \qquad \text{A2.1}$$

therefore,

$$dA_{EXCR} = k_{excr} A_p dt \qquad \text{A2.2}$$

hence,

$$A_{EXCR} = \int_{t=0}^{t=t} k_{excr} A_p dt = k_{excr} \int_{t=0}^{t=t} A_p dt \qquad \text{A2.3}$$

Now the equation for A_p has been calculated in part 2.3.2.3 and Appendix A1 to be,

$$A_p = \frac{D_0(k_{21}-\gamma)(k_{31}+k_m-\gamma)e^{-\gamma t}}{(\gamma-\alpha)(\gamma-\beta)} + \frac{D_0(k_{21}-\alpha)(\alpha-(k_{31}+k_m))e^{-\alpha t}}{(\gamma-\alpha)(\alpha-\beta)} + \frac{D_0(k_{21}-\beta)(k_{31}+k_m-\beta)e^{-\beta t}}{(\gamma-\beta)(\alpha-\beta)}$$

A2.4

hence,

$$A_{EXCR} = k_{excr}\int_{t=0}^{t=t}\left\{\frac{D_0(k_{21}-\gamma)(k_{31}+k_m-\gamma)e^{-\gamma t}}{(\gamma-\alpha)(\gamma-\beta)}+\frac{D_0(k_{21}-\alpha)(\alpha-(k_{31}+k_m))e^{-\alpha t}}{(\gamma-\alpha)(\alpha-\beta)}+\frac{D_0(k_{21}-\beta)(k_{31}+k_m-\beta)e^{-\beta t}}{(\gamma-\beta)(\alpha-\beta)}\right\}dt$$

$$= k_{excr}\left[\frac{D_0(k_{21}-\gamma)(k_{31}+k_m-\gamma)e^{-\gamma t}}{-\gamma(\gamma-\alpha)(\gamma-\beta)}+\frac{D_0(k_{21}-\alpha)(\alpha-(k_{31}+k_m))e^{-\alpha t}}{-\alpha(\gamma-\alpha)(\alpha-\beta)}+\frac{D_0(k_{21}-\beta)(k_{31}+k_m-\beta)e^{-\beta t}}{-\beta(\gamma-\beta)(\alpha-\beta)}\right]_{t=0}^{t=t}$$

$$= k_{excr}\left[\frac{D_0(k_{21}-\gamma)(k_{31}+k_m-\gamma)e^{-\gamma t}}{-\gamma(\gamma-\alpha)(\gamma-\beta)}+\frac{D_0(k_{21}-\alpha)(\alpha-(k_{31}+k_m))e^{-\alpha t}}{-\alpha(\gamma-\alpha)(\alpha-\beta)}+\frac{D_0(k_{21}-\beta)(k_{31}+k_m-\beta)e^{-\beta t}}{-\beta(\gamma-\beta)(\alpha-\beta)}\right.$$

$$\left.-\left\{\frac{D_0(k_{21}-\gamma)(k_{31}+k_m-\gamma)}{-\gamma(\gamma-\alpha)(\gamma-\beta)}+\frac{D_0(k_{21}-\alpha)(\alpha-(k_{31}+k_m))}{-\alpha(\gamma-\alpha)(\alpha-\beta)}+\frac{D_0(k_{21}-\beta)(k_{31}+k_m-\beta)}{-\beta(\gamma-\beta)(\alpha-\beta)}\right\}\right]$$

Therefore,

$$A_{EXCR} = k_{excr}D_0\left\{\frac{(k_{21}-\gamma)(k_{31}+k_m-\gamma)}{\gamma(\gamma-\alpha)(\gamma-\beta)}+\frac{(k_{21}-\alpha)(\alpha-(k_{31}+k_m))}{\alpha(\gamma-\alpha)(\alpha-\beta)}+\frac{(k_{21}-\beta)(k_{31}+k_m-\beta)}{\beta(\gamma-\beta)(\alpha-\beta)}\right.$$

$$\left.-\frac{(k_{21}-\gamma)(k_{31}+k_m-\gamma)e^{-\gamma t}}{\gamma(\gamma-\alpha)(\gamma-\beta)}-\frac{(k_{21}-\alpha)(\alpha-(k_{31}+k_m))e^{-\alpha t}}{\alpha(\gamma-\alpha)(\alpha-\beta)}-\frac{(k_{21}-\beta)(k_{31}+k_m-\beta)e^{-\beta t}}{\beta(\gamma-\beta)(\alpha-\beta)}\right\}$$

A2.5

i.e. $$A_{EXCR} = k_{excr}D_o\left\{X+Y+Z-Xe^{-\gamma t}-Ye^{-\alpha t}-Ze^{-\beta t}\right\} \qquad \text{A2.6}$$

where $$X = \frac{(k_{21}-\gamma)(k_{31}+k_m-\gamma)}{\gamma(\gamma-\alpha)(\gamma-\beta)} \qquad \text{A2.7}$$

$$Y = \frac{(k_{21}-\alpha)(\alpha-(k_{31}+k_m))}{\alpha(\gamma-\alpha)(\alpha-\beta)} \qquad \text{A2.8}$$

$$Z = \frac{(k_{21}-\beta)(k_{31}+k_m-\beta)}{\beta(\gamma-\beta)(\alpha-\beta)} \qquad \text{A2.9}$$

Similarly, from 2.3.2.3 the rate of change in the mass (amount) of drug metabolised (hepatically cleared) by the liver is represented by the equation,

$$\frac{dA_M}{dt} = k_m A_H \qquad \text{A2.10}$$

therefore,

$$dA_M = k_m A_H dt \qquad \text{A2.11}$$

hence,

$$A_M = \int_{t=0}^{t=t} k_m A_H dt = k_m \int_{t=o}^{t=t} A_H dt \qquad \text{A2.12}$$

Now the equation for A_H has been calculated in part 2.3.2.3 and Appendix A1 to be,

$$A_H = \frac{D_0 k_{13}(k_{21}-\gamma)e^{-\gamma t}}{(\gamma-\alpha)(\gamma-\beta)} + \frac{D_0 k_{13}(\alpha-k_{21})e^{-\alpha t}}{(\gamma-\alpha)(\alpha-\beta)} + \frac{D_0 k_{13}(k_{21}-\beta)e^{-\beta t}}{(\gamma-\beta)(\alpha-\beta)} \qquad \text{A2.13}$$

hence,

$$A_M = k_m \int_{t=0}^{t=t} \left\{ \frac{D_0 k_{13}(k_{21}-\gamma)e^{-\gamma t}}{(\gamma-\alpha)(\gamma-\beta)} + \frac{D_0 k_{13}(\alpha-k_{21})e^{-\alpha t}}{(\gamma-\alpha)(\alpha-\beta)} + \frac{D_0 k_{13}(k_{21}-\beta)e^{-\beta t}}{(\gamma-\beta)(\alpha-\beta)} \right\} dt$$

$$= k_m \left[\frac{D_0 k_{13}(k_{21}-\gamma)e^{-\gamma t}}{-\gamma(\gamma-\alpha)(\gamma-\beta)} + \frac{D_0 k_{13}(\alpha-k_{21})e^{-\alpha t}}{-\alpha(\gamma-\alpha)(\alpha-\beta)} + \frac{D_0 k_{13}(k_{21}-\beta)e^{-\beta t}}{-\beta(\gamma-\beta)(\alpha-\beta)} \right]_{t=0}^{t=t}$$

$$= k_m \left[-\frac{D_0 k_{13}(k_{21}-\gamma)e^{-\gamma t}}{\gamma(\gamma-\alpha)(\gamma-\beta)} - \frac{D_0 k_{13}(\alpha-k_{21})e^{-\alpha t}}{\alpha(\gamma-\alpha)(\alpha-\beta)} - \frac{D_0 k_{13}(k_{21}-\beta)e^{-\beta t}}{\beta(\gamma-\beta)(\alpha-\beta)} \right.$$

$$\left. - \left\{ -\frac{D_0 k_{13}(k_{21}-\gamma)}{\gamma(\gamma-\alpha)(\gamma-\beta)} - \frac{D_0 k_{13}(\alpha-k_{21})}{\alpha(\gamma-\alpha)(\alpha-\beta)} - \frac{D_0 k_{13}(k_{21}-\beta)}{\beta(\gamma-\beta)(\alpha-\beta)} \right\} \right]$$

Therefore,

$$A_M = k_m k_{13} D_0 \left\{ \frac{(k_{21}-\gamma)}{\gamma(\gamma-\alpha)(\gamma-\beta)} + \frac{(\alpha-k_{21})}{\alpha(\gamma-\alpha)(\alpha-\beta)} + \frac{(k_{21}-\beta)}{\beta(\gamma-\beta)(\alpha-\beta)} \right.$$

$$\left. - \frac{(k_{21}-\gamma)e^{-\gamma t}}{\gamma(\gamma-\alpha)(\gamma-\beta)} - \frac{(\alpha-k_{21})e^{-\alpha t}}{\alpha(\gamma-\alpha)(\alpha-\beta)} - \frac{(k_{21}-\beta)e^{-\beta t}}{\beta(\gamma-\beta)(\alpha-\beta)} \right\} \qquad \text{A2.14}$$

i.e. $$A_M = k_m k_{13} D_0 \{U + V + W - Ue^{-\gamma t} - Ve^{-\alpha t} - We^{-\beta t}\} \qquad \text{A2.15}$$

where $$U = \frac{(k_{21}-\gamma)}{\gamma(\gamma-\alpha)(\gamma-\beta)} \qquad \text{A2.16}$$

$$V = \frac{(\alpha - k_{21})}{\alpha(\gamma - \alpha)(\alpha - \beta)} \qquad \text{A2.17}$$

$$W = \frac{(k_{21} - \beta)}{\beta(\gamma - \beta)(\alpha - \beta)} \qquad \text{A2.18}$$

Appendix A3

BasicV algorithms run on Acorn Archimedes RISC processor for calculation of pharmacokinetic data

Program MACROHOURS

```
 10 REM PROGRAM FOR SIMULATION OF MACROMOLECULAR DISPOSITION
 20 REM ------------------------------------------------------
 30 REM C W POUTON and P R SNELL,   APRIL 1991
 40 REM ------------------------------------------------------
 50 REM
 60 REM >ADFS::0.$.MACRODISP
 70 ON ERROR PROCerror
 80 DIM A(1000,4),AA(20),B(20),XW(20)
 90 PROCoriginal
100 PROCparam
110 PROCsize
120 PROCcube
130 PROCassign
140 PROCtimes
150 PROCcalc
160 PRINT:
    PRINT:
    INPUT TAB(15)"DO YOU WISH TO PRINT TO DISC? (Y/N?)";PCHOICE$
170 IF PCHOICE$="Y" THEN 180 ELSE 210
180 PROCfilename
190 PROCdisc
200 PROCdiscgraph
210 PRINT:
    INPUT"DO YOU WISH TO ENTER NEW EXPERIMENTAL TIMES? (Y/N?)";TCHOICE$
220 IF TCHOICE$="Y" THEN 140 ELSE 230
230 PRINT:
    INPUT"DO YOU WISH TO ENTER A NEW MOLECULAR RADIUS? (Y/N?)";RCHOICE$
240 IF RCHOICE$="Y" THEN 110 ELSE 250
250 PRINT:
    INPUT"DO YOU WISH TO USE NEW PARAMETERS? (Y/N?)";PCHOICE$
260 IF PCHOICE$="Y" THEN 100 ELSE 270
270 PRINT:
    INPUT"ARE YOU SURE YOU WANT TO QUIT? (Y/N?)";FCHOICE$
280 IF FCHOICE$="Y"THEN 290 ELSE 210
290 END
300 :
    ------------------------------------------------------------------------
-
310 DEF PROCoriginal
320 DOSE=1
330 GFR=125
340 BLFR=2
350 VC=5600
360 HRADIUS=35.5
370 K21=1.78571E-4
380 K13=0.2571428
390 K31=2.5714286
400 KM=0
410 KFILT=0.007333
420 AFILT=17.612
430 NFILT=2
440 KLYMPH=0.019532
```

```
450 ALYMPH=14.711
460 NLYMPH=1
470 ENDPROC
480 :
    ------------------------------------------------------------------------
-
490 DEF PROCparam
500 REPEAT
510   CLS:
      @%=&0A
520   PRINT TAB(15,3)"CURRENT VALUES OF PARAMETERS ARE AS FOLLOWS"
530   PRINT
540   PRINT TAB(20)"B)     GFR = ";GFR;"  (ml/min)"
550   PRINT TAB(20)"C)     BLFR = ";BLFR;"  (ml/min)"
560   PRINT TAB(20)"D)     VC = ";VC;"  (ml)"
570   PRINT TAB(20)"E)     K21 = ";K21;"  (min^-1)"
580   PRINT TAB(20)"F)     K13 = ";K13;"  (min^-1)"
590   PRINT TAB(20)"G)     K31 = ";K31;"  (min^-1)"
600   PRINT TAB(20)"H)     KM = ";KM;"  (min^-1)"
610   PRINT TAB(20)"I)     KFILT = ";KFILT
620   PRINT TAB(20)"J)     AFILT = ";AFILT
630   PRINT TAB(20)"K)     NFILT = ";NFILT
640   PRINT TAB(20)"L)     KLYMPH = ";KLYMPH
650   PRINT TAB(20)"M)     ALYMPH = ";ALYMPH
660   PRINT TAB(20)"N)     NLYMPH = ";NLYMPH
670   PRINT:
      PRINT:
      PRINT:
      PRINT
680   INPUT TAB(15)"DO YOU WISH TO ALTER ANY PARAMETERS? (Y/N?)";CPARAM$
690   IF CPARAM$="Y" THEN 700 ELSE 1020
700   PRINT:
      PRINT
710   INPUT TAB(15)"TYPE THE RELEVANT LETTER AND PRESS RETURN";PARAM$
720   PRINT:
      PRINT
730   CASE PARAM$ OF
740     WHEN "B"
750     INPUT TAB(15)"TYPE NEW VALUE OF GFR (ml/min) ";GFR
760     WHEN "C"
770     INPUT TAB(15)"TYPE NEW VALUE OF BLFR (ml/min) ";BLFR
780     WHEN "D"
790     INPUT TAB(15)"TYPE NEW VALUE OF VC (ml) ";VC
800     WHEN "E"
810     INPUT TAB(15)"TYPE NEW VALUE OF K21 (min^-1) ";K21
820     WHEN "F"
830     INPUT TAB(15)"TYPE NEW VALUE OF K13 (min^-1) ";K13
840     WHEN "G"
850     INPUT TAB(15)"TYPE NEW VALUE OF K31 (min^-1) ";K31
860     WHEN "H"
870     INPUT TAB(15)"TYPE NEW VALUE OF KM (min^-1) ";KM
880     WHEN "I"
890     INPUT TAB(15)"TYPE NEW VALUE OF KFILT ";KFILT
900     WHEN "J"
910     INPUT TAB(15)"TYPE NEW VALUE OF AFILT ";AFILT
920     WHEN "K"
930     INPUT TAB(15)"TYPE NEW VALUE OF NFILT ";NFILT
940     WHEN "L"
950     INPUT TAB(15)"TYPE NEW VALUE OF KLYMPH ";KLYMPH
960     WHEN "M"
```

```
 970      INPUT TAB(15)"TYPE NEW VALUE OF ALYMPH ";ALYMPH
 980      WHEN "N"
 990      INPUT TAB(15)"TYPE NEW VALUE OF NLYMPH ";NLYMPH
1000    ENDCASE
1010 UNTIL CPARAM$="N"
1020 ENDPROC
1030 :
     ------------------------------------------------------------------------
-
1040 DEF PROCsize
1050 CLS:
     PRINT:
     PRINT
1060 INPUT"ENTER A VALUE FOR THE HYDRODYNAMIC RADIUS (Angstroms) ";HRADIUS
1070 K12=EXP(-KLYMPH*(HRADIUS-ALYMPH)^NLYMPH)*BLFR/VC
1080 KEXCR=EXP(-KFILT*(HRADIUS-AFILT)^NFILT)*GFR/VC
1090 PRINT:
     PRINT:
     PRINT TAB(20)"CALCULATED VALUE OF K12 = ";K12
1100 PRINT:
     PRINT TAB(20)"CALCULATED VALUE OF KEXCR = ";KEXCR
1110 AA(3)=1
1120 AA(2)=-(K12+K21+K13+K31+KEXCR+KM)
1130
AA(1)=(K21*K31)+(K21*KM)+(K12*K31)+(K12*KM)+(K13*KM)+(K13*K21)+(KEXCR*K31)+(KE
XCR*KM)+(KEXCR*K21)
1140 AA(0)=-((K13*K21*KM)+(KEXCR*K21*K31)+(KEXCR*K21*KM))
1150 PRINT:
     PRINT "THE COEFFICIENTS OF THE CUBIC EQUATION ARE:"
1160 FOR K = 3 TO 0 STEP -1
1170   PRINT:
       PRINT TAB(20) "A";K;" = ";AA(K)
1180 NEXT
1190 PRINT:
     PRINT:
     PRINT TAB(20)"PRESS ANY KEY TO CONTINUE":
     IFGET
1200 ENDPROC
1210 :
     ------------------------------------------------------------------------
-
1220 DEF PROCcube
1230 REM NEWTON RAPHSON ROUTINE WITH SYNTHETIC DIVISION
1240 REM FOR SOLUTION OF CUBIC EQUATIONS
1250 CLS
1260 N=3:
     NW=3
1270 PRINT:
     PRINT"THE RANGE OF SEARCH IS DEFINED AS -10 TO 10"
1280 MINX = -10
1290 MAXX = 10
1300 PRINT:
     PRINT"STARTING GUESS OF ROOT IS 0.5":
      X1 = 0.5
1310 PRINT:
     PRINT"THE CONVERGENCE VALUE OF F IS SET AT 1E-14":
     EPS = 1E-14
1320 REM CALCULATES THE FUNCTION IN THE RANGE OF SEARCH
1330 DX = (MAXX-MINX)/100
1340 FOR K = 0 TO 100
```

```
1350    X = MINX + K * DX
1360    A(K,1) = X
1370    PROCsubcube:
        A(K,2) = F
1380  NEXT K
1390  PROCrootfind
1400  PRINT:
      PRINT"PRESS ANY KEY TO CONTINUE":
      IFGET
1410  XW(N)=X1
1420  REM SYNTHETIC DIVISION
1430  IF N=1 GOTO 1700
1440  B(N-1)=AA(N)
1450  FOR R = 1 TO N-1
1460    B(N-1-R)=AA(N-R)+B(N-R)*X1
1470  NEXT
1480  N=N-1
1490  FOR JJ=N TO 0 STEP -1
1500    AA(JJ) =B(JJ)
1510  NEXT
1520  REM CHECK FOR COMPLEX ROOTS
1530  IF N<>2 GOTO 1680
1540  WW=AA(1)^2-4*AA(2)*AA(0)
1550  IFWW>0 GOTO 1680
1560  PRINT"THIS EQUATION HAS COMPLEX ROOTS":
      PRINT
1570  XW(2)=-AA(1)/(2*AA(2))
1580  XW(1)=SQR(-WW)/(2*AA(2))
1590  PRINT"THE ";NW;" ROOTS ARE:"
1600  FOR JK=NW TO 3 STEP -1
1610    PRINT XW(JK)
1620  NEXT
1630  REM PRINT COMPLEX ROOTS
1640  PRINT XW(2);"+";XW(1);"i"
1650  PRINT XW(2);"-";XW(1);"i"
1660  PRINT:
      PRINT:
      PRINT"PRESS ANY KEY TO CONTINUE":
      IFGET
1670  GOTO 230
1680  IF N>0 GOTO 1320
1690  REM PRINT THE ROOTS
1700  PRINT"THE ";NW;" ROOTS ARE:"
1710  FOR JK = NW TO 1 STEP -1
1720    PRINT XW(JK);"    ";
1730  NEXT
1740  PRINT:
      PRINT"PRESS ANY KEY TO CONTINUE":
      IFGET
1750  ENDPROC
1760  :
      ------------------------------------------------------------------------
-
1770  DEF PROCsubcube
1780  F=0:
      FP=0
1790  FOR KK = N TO 0 STEP -1
1800    F = F + AA(KK) * X^KK
1810    IF KK=0 THEN ENDPROC
1820    FP = FP + KK*AA(KK) * X^(KK-1)
```

```
1830 NEXT KK
1840 ENDPROC
1850 :
     ------------------------------------------------------------------------
-
1860 DEF PROCrootfind
1870 PRINT"CONVERGENCE TO ROOT";(NW-N+1):
     PRINT
1880 FOR ITER=0 TO 400 STEP 2
1890   X=X1:
       PROCsubcube
1900   PRINT"Iteration no. ";ITER;"     x=";X1;"      f(x)";F
1910   A(ITER,3)=X1:
       A(ITER,4)=0
1920   A(ITER+1,3)=X1:
       A(ITER+1,4)=F
1930   IF ABS(F)<EPS THEN 1990 ELSE 1940
1940   X1=X1-F/FP
1950 NEXT ITER
1960 PRINT"EXCEEDS ITERATION LIMIT:  NO CONVERGENCE":
     PRINT:
     PRINT"ITER=";ITER:
     PRINT"EPS=";EPS:
     PRINT"F=";F
1970 INPUT"ENTER NEW CONVERGENCE VALUE ";EPS
1980 GOTO 1860
1990 EPS = 1E-14
2000 ENDPROC
2010 :
     ------------------------------------------------------------------------
-
2020 DEF PROCassign
2030 IF XW(1)>XW(2) AND XW(2)>XW(3) THEN GAMMA=XW(1):
     ALPHA=XW(2):
     BETA=XW(3)
2040 IF XW(1)>XW(3) AND XW(3)>XW(2) THEN GAMMA=XW(1):
     ALPHA=XW(3):
     BETA=XW(2)
2050 IF XW(2)>XW(1) AND XW(1)>XW(3) THEN GAMMA=XW(2):
     ALPHA=XW(1):
     BETA=XW(3)
2060 IF XW(2)>XW(3) AND XW(3)>XW(1) THEN GAMMA=XW(2):
     ALPHA=XW(3):
     BETA=XW(1)
2070 IF XW(3)>XW(1) AND XW(1)>XW(2) THEN GAMMA=XW(3):
     ALPHA=XW(1):
     BETA=XW(2)
2080 IF XW(3)>XW(2) AND XW(2)>XW(1) THEN GAMMA=XW(3):
     ALPHA=XW(2):
     BETA=XW(1)
2090 PRINT:
     PRINT"GAMMA = ";GAMMA;"   ALPHA = ";ALPHA;"   BETA = ";BETA
2100 PRINT:
     PRINT:
     PRINT TAB(20)"PRESS ANY KEY TO CONTINUE":
     IFGET
2110 ENDPROC
2120 :
     ------------------------------------------------------------------------
-
```

```
 2130 DEF PROCtimes
 2140 CLS
 2150 INPUT TAB(20)"TYPE INITIAL TIME (HOURS) ";PHOURS
 2160 INPUT TAB(20)"TYPE FINAL TIME (HOURS) ";QHOURS
 2170 INPUT TAB(20)"TYPE TIME INCREMENT (HOURS) ";RHOURS
 2180 P=PHOURS*60
 2190 Q=QHOURS*60
 2200 R=RHOURS*60
 2210 ENDPROC
 2220 :
      ------------------------------------------------------------------------
-
 2230 DEF PROCcalc
 2240 PRINT"A TABLE OF CP, AP, AL AND AH  INITIALLY WILL BE PRINTED TO SCREEN"
 2250 PRINT"TO ESTABLISH WHETHER THE EXPERIMENTAL TIMES ARE APPROPRIATE"
 2260 PRINT:
      PRINT TAB(20)"PRESS ANY KEY TO CONTINUE":
      IFGET
 2270 CLS
 2280 PRINT "TIME(HOURS)        CP              AP           AL            AH"
 2290 PRINT "-------------------------------------------------------------------
--"
 2300 PRINT
 2310 FOR T=P TO Q STEP R
 2320   CP=(1/VC)*(((K21-GAMMA)*(K31+KM-GAMMA)*(ALPHA-BETA)*EXP(-
GAMMA*T))+((K21-ALPHA)*(ALPHA-(K31+KM))*(GAMMA-BETA)*EXP(-ALPHA*T))+((K21-
BETA)*(K31+KM-BETA)*(GAMMA-ALPHA)*EXP(-BETA*T)))/((GAMMA-ALPHA)*(GAMMA-
BETA)*(ALPHA-BETA))
 2330   AP=(((K21-GAMMA)*(K31+KM-GAMMA)*(ALPHA-BETA)*EXP(-GAMMA*T))+((K21-
ALPHA)*(ALPHA-(K31+KM))*(GAMMA-BETA)*EXP(-ALPHA*T))+((K21-BETA)*(K31+KM-
BETA)*(GAMMA-ALPHA)*EXP(-BETA*T)))/((GAMMA-ALPHA)*(GAMMA-BETA)*(ALPHA-BETA))
 2340   AL=((K12*(K31+KM-GAMMA)*(ALPHA-BETA)*EXP(-GAMMA*T))+(K12*(ALPHA-
(K31+KM))*(GAMMA-BETA)*EXP(-ALPHA*T))+(K12*(K31+KM-BETA)*(GAMMA-ALPHA)*EXP(-
BETA*T)))/((GAMMA-ALPHA)*(GAMMA-BETA)*(ALPHA-BETA))
 2350   AH=((K13*(K21-GAMMA)*(ALPHA-BETA)*EXP(-GAMMA*T))+(K13*(ALPHA-
K21)*(GAMMA-BETA)*EXP(-ALPHA*T))+(K13*(K21-BETA)*(GAMMA-ALPHA)*EXP(-
BETA*T)))/((GAMMA-ALPHA)*(GAMMA-BETA)*(ALPHA-BETA))
 2360   AE=1-AP-AL-AH
 2370   X=((K21-GAMMA)*(K31+KM-GAMMA))/(GAMMA*(GAMMA-ALPHA)*(GAMMA-BETA))
 2380   Y=((K21-ALPHA)*(ALPHA-(K31+KM)))/(ALPHA*(GAMMA-ALPHA)*(ALPHA-BETA))
 2390   Z=((K21-BETA)*(K31+KM-BETA))/(BETA*(GAMMA-BETA)*(ALPHA-BETA))
 2400   AEXCR=KEXCR*(X+Y+Z-(X*EXP(-GAMMA*T))-(Y*EXP(-ALPHA*T))-(Z*EXP(-
BETA*T)))
 2410   U=(K21-GAMMA)/(GAMMA*(GAMMA-ALPHA)*(GAMMA-BETA))
 2420   V=(ALPHA-K21)/(ALPHA*(GAMMA-ALPHA)*(ALPHA-BETA))
 2430   W=(K21-BETA)/(BETA*(GAMMA-BETA)*(ALPHA-BETA))
 2440   AM=(KM*K13)*(U+V+W-(U*EXP(-GAMMA*T))-(V*EXP(-ALPHA*T))-(W*EXP(-
BETA*T)))
 2450   AELIM=AEXCR+AM
 2460   @%=&10607
 2470   PRINT T/60,CP,AP,AL,AH,
 2480 NEXT
 2490 ENDPROC
 2500 :
      ------------------------------------------------------------------------
-
 2510 DEF PROCfilename
 2520 REPEAT
 2530   CLS:
        INPUT TAB(10,5)"Data file name ";FILE$
```

```
 2540 UNTIL FILE$<>""
 2550 REPEAT
 2560   CLS:
        tc$=""
 2570   PRINT "          Insert DATA DISK in drive 0"
 2580   PRINT "           then press C to continue";:
        tc$=GET$
 2590 UNTIL tc$="C"
 2600 LOCAL ERROR
 2610 ON ERROR LOCAL PROCerror
 2620 *MOUNT 0
 2630 OSCLI("SPOOL "+FILE$)
 2640 *SPOOL
 2650 RESTORE ERROR
 2660 *MOUNT 0
 2670 ENDPROC
 2680 :
      ------------------------------------------------------------------------
-
 2690 DEF PROCdisc
 2700 CLS
 2710 LOCAL ERROR
 2720 ON ERROR PROCerror
 2730 OSCLI("SPOOL "+FILE$)
 2740 PRINT TAB(25)"EXPERIMENTAL FILENAME:  ";FILE$
 2750 PRINT
 2760 PRINT"DOSE = ";DOSE": GFR = ";GFR" (ml/min) : BLFR = ";BLFR" (ml/min) :
VC  = ";VC" (ml)"
 2770 PRINT"KFILT = ";KFILT": AFILT = ";AFILT": NFILT = ";NFILT
 2780 PRINT"KLYMPH = ";KLYMPH": ALYMPH = ";ALYMPH": NLYMPH = ";NLYMPH
 2790 PRINT"RADIUS = ";HRADIUS" : K12 = ";K12" : K21 = ";K21" : K13 = ";K13
 2800 PRINT"K31 = ";K31" : KEXCR = ";KEXCR" : KM = ";KM"  (all rate constants
in min^-1)"
 2810 PRINT:
      PRINT "ALPHA = ";ALPHA"    BETA = ";BETA"    GAMMA = ";GAMMA
 2820 PRINT:
      PRINT:
      PRINT:
      PRINT "TIME(HOURS)       CP              AP          AL          AH"
 2830 PRINT "------------------------------------------------------------------
--"
 2840 PRINT
 2850 FOR T=P TO Q STEP R
 2860   CP=(1/VC)*(((K21-GAMMA)*(K31+KM-GAMMA)*(ALPHA-BETA)*EXP(-
GAMMA*T))+((K21-ALPHA)*(ALPHA-(K31+KM))*(GAMMA-BETA)*EXP(-ALPHA*T))+((K21-
BETA)*(K31+KM-BETA)*(GAMMA-ALPHA)*EXP(-BETA*T)))/((GAMMA-ALPHA)*(GAMMA-
BETA)*(ALPHA-BETA))
 2870   AP=(((K21-GAMMA)*(K31+KM-GAMMA)*(ALPHA-BETA)*EXP(-GAMMA*T))+((K21-
ALPHA)*(ALPHA-(K31+KM))*(GAMMA-BETA)*EXP(-ALPHA*T))+((K21-BETA)*(K31+KM-
BETA)*(GAMMA-ALPHA)*EXP(-BETA*T)))/((GAMMA-ALPHA)*(GAMMA-BETA)*(ALPHA-BETA))
 2880   AL=((K12*(K31+KM-GAMMA)*(ALPHA-BETA)*EXP(-GAMMA*T))+(K12*(ALPHA-
(K31+KM))*(GAMMA-BETA)*EXP(-ALPHA*T))+(K12*(K31+KM-BETA)*(GAMMA-ALPHA)*EXP(-
BETA*T)))/((GAMMA-ALPHA)*(GAMMA-BETA)*(ALPHA-BETA))
 2890   AH=((K13*(K21-GAMMA)*(ALPHA-BETA)*EXP(-GAMMA*T))+(K13*(ALPHA-
K21)*(GAMMA-BETA)*EXP(-ALPHA*T))+(K13*(K21-BETA)*(GAMMA-ALPHA)*EXP(-
BETA*T)))/((GAMMA-ALPHA)*(GAMMA-BETA)*(ALPHA-BETA))
 2900   AE=1-AP-AL-AH
 2910   X=((K21-GAMMA)*(K31+KM-GAMMA))/(GAMMA*(GAMMA-ALPHA)*(GAMMA-BETA))
 2920   Y=((K21-ALPHA)*(ALPHA-(K31+KM)))/(ALPHA*(GAMMA-ALPHA)*(ALPHA-BETA))
 2930   Z=((K21-BETA)*(K31+KM-BETA))/(BETA*(GAMMA-BETA)*(ALPHA-BETA))
```

```
 2940    AEXCR=KEXCR*(X+Y+Z-(X*EXP(-GAMMA*T))-(Y*EXP(-ALPHA*T))-(Z*EXP(-
BETA*T)))
 2950    U=(K21-GAMMA)/(GAMMA*(GAMMA-ALPHA)*(GAMMA-BETA))
 2960    V=(ALPHA-K21)/(ALPHA*(GAMMA-ALPHA)*(ALPHA-BETA))
 2970    W=(K21-BETA)/(BETA*(GAMMA-BETA)*(ALPHA-BETA))
 2980    AM=(KM*K13)*(U+V+W-(U*EXP(-GAMMA*T))-(V*EXP(-ALPHA*T))-(W*EXP(-
BETA*T)))
 2990    AELIM=AEXCR+AM
 3000    @%=&10607
 3010    PRINT T/60,CP,AP,AL,AH,
 3020 NEXT
 3030 PRINT:
      PRINT:
      PRINT
 3040 PRINT "TIME(HOURS)       AEXCR           AMET      (AEXCR + AMET)      AE"
 3050 PRINT "-----------------------------------------------------------------
--"
 3060 PRINT:
      FOR T=P TO Q STEP R
 3070    CP=(1/VC)*(((K21-GAMMA)*(K31+KM-GAMMA)*(ALPHA-BETA)*EXP(-
GAMMA*T))+((K21-ALPHA)*(ALPHA-(K31+KM))*(GAMMA-BETA)*EXP(-ALPHA*T))+((K21-
BETA)*(K31+KM-BETA)*(GAMMA-ALPHA)*EXP(-BETA*T)))/((GAMMA-ALPHA)*(GAMMA-
BETA)*(ALPHA-BETA))
 3080    AP=(((K21-GAMMA)*(K31+KM-GAMMA)*(ALPHA-BETA)*EXP(-GAMMA*T))+((K21-
ALPHA)*(ALPHA-(K31+KM))*(GAMMA-BETA)*EXP(-ALPHA*T))+((K21-BETA)*(K31+KM-
BETA)*(GAMMA-ALPHA)*EXP(-BETA*T)))/((GAMMA-ALPHA)*(GAMMA-BETA)*(ALPHA-BETA))
 3090    AL=((K12*(K31+KM-GAMMA)*(ALPHA-BETA)*EXP(-GAMMA*T))+(K12*(ALPHA-
(K31+KM))*(GAMMA-BETA)*EXP(-ALPHA*T))+(K12*(K31+KM-BETA)*(GAMMA-ALPHA)*EXP(-
BETA*T)))/((GAMMA-ALPHA)*(GAMMA-BETA)*(ALPHA-BETA))
 3100    AH=((K13*(K21-GAMMA)*(ALPHA-BETA)*EXP(-GAMMA*T))+(K13*(ALPHA-
K21)*(GAMMA-BETA)*EXP(-ALPHA*T))+(K13*(K21-BETA)*(GAMMA-ALPHA)*EXP(-
BETA*T)))/((GAMMA-ALPHA)*(GAMMA-BETA)*(ALPHA-BETA))
 3110    AE=1-AP-AL-AH
 3120    X=((K21-GAMMA)*(K31+KM-GAMMA))/(GAMMA*(GAMMA-ALPHA)*(GAMMA-BETA))
 3130    Y=((K21-ALPHA)*(ALPHA-(K31+KM)))/(ALPHA*(GAMMA-ALPHA)*(ALPHA-BETA))
 3140    Z=((K21-BETA)*(K31+KM-BETA))/(BETA*(GAMMA-BETA)*(ALPHA-BETA))
 3150    AEXCR=KEXCR*(X+Y+Z-(X*EXP(-GAMMA*T))-(Y*EXP(-ALPHA*T))-(Z*EXP(-
BETA*T)))
 3160    U=(K21-GAMMA)/(GAMMA*(GAMMA-ALPHA)*(GAMMA-BETA))
 3170    V=(ALPHA-K21)/(ALPHA*(GAMMA-ALPHA)*(ALPHA-BETA))
 3180    W=(K21-BETA)/(BETA*(GAMMA-BETA)*(ALPHA-BETA))
 3190    AM=(KM*K13)*(U+V+W-(U*EXP(-GAMMA*T))-(V*EXP(-ALPHA*T))-(W*EXP(-
BETA*T)))
 3200    AELIM=AEXCR+AM
 3210    PRINT T/60,AEXCR,AM,AELIM,AE
 3220 NEXT
 3230 *SPOOL
 3240 OSCLI("ACCESS "+FILE$+" LR")
 3250 RESTORE ERROR
 3260 PRINT:
      PRINT:
      PRINT" Press any key to continue":
      IFGET
 3270 ENDPROC
 3280 :
      ---------------------------------------------------------------------
-
 3290 DEF PROCdiscgraph
 3300 OSCLI("SPOOL G"+FILE$)
 3310 FOR T=P TO Q STEP R
```

```
 3320    CP=(1/VC)*(((K21-GAMMA)*(K31+KM-GAMMA)*(ALPHA-BETA)*EXP(-
GAMMA*T))+((K21-ALPHA)*(ALPHA-(K31+KM))*(GAMMA-BETA)*EXP(-ALPHA*T))+((K21-
BETA)*(K31+KM-BETA)*(GAMMA-ALPHA)*EXP(-BETA*T)))/((GAMMA-ALPHA)*(GAMMA-
BETA)*(ALPHA-BETA))
 3330    AP=(((K21-GAMMA)*(K31+KM-GAMMA)*(ALPHA-BETA)*EXP(-GAMMA*T))+((K21-
ALPHA)*(ALPHA-(K31+KM))*(GAMMA-BETA)*EXP(-ALPHA*T))+((K21-BETA)*(K31+KM-
BETA)*(GAMMA-ALPHA)*EXP(-BETA*T)))/((GAMMA-ALPHA)*(GAMMA-BETA)*(ALPHA-BETA))
 3340    AL=((K12*(K31+KM-GAMMA)*(ALPHA-BETA)*EXP(-GAMMA*T))+(K12*(ALPHA-
(K31+KM))*(GAMMA-BETA)*EXP(-ALPHA*T))+(K12*(K31+KM-BETA)*(GAMMA-ALPHA)*EXP(-
BETA*T)))/((GAMMA-ALPHA)*(GAMMA-BETA)*(ALPHA-BETA))
 3350    AH=((K13*(K21-GAMMA)*(ALPHA-BETA)*EXP(-GAMMA*T))+(K13*(ALPHA-
K21)*(GAMMA-BETA)*EXP(-ALPHA*T))+(K13*(K21-BETA)*(GAMMA-ALPHA)*EXP(-
BETA*T)))/((GAMMA-ALPHA)*(GAMMA-BETA)*(ALPHA-BETA))
 3360    AE=1-AP-AL-AH
 3370    X=((K21-GAMMA)*(K31+KM-GAMMA))/(GAMMA*(GAMMA-ALPHA)*(GAMMA-BETA))
 3380    Y=((K21-ALPHA)*(ALPHA-(K31+KM)))/(ALPHA*(GAMMA-ALPHA)*(ALPHA-BETA))
 3390    Z=((K21-BETA)*(K31+KM-BETA))/(BETA*(GAMMA-BETA)*(ALPHA-BETA))
 3400    AEXCR=KEXCR*(X+Y+Z-(X*EXP(-GAMMA*T))-(Y*EXP(-ALPHA*T))-(Z*EXP(-
BETA*T)))
 3410    U=(K21-GAMMA)/(GAMMA*(GAMMA-ALPHA)*(GAMMA-BETA))
 3420    V=(ALPHA-K21)/(ALPHA*(GAMMA-ALPHA)*(ALPHA-BETA))
 3430    W=(K21-BETA)/(BETA*(GAMMA-BETA)*(ALPHA-BETA))
 3440    AM=(KM*K13)*(U+V+W-(U*EXP(-GAMMA*T))-(V*EXP(-ALPHA*T))-(W*EXP(-
BETA*T)))
 3450    AELIM=AEXCR+AM
 3460    PRINT T/60",";AP",";AL",";AH",";AEXCR",";AM",";AE
 3470 NEXT
 3480  *SPOOL
 3490 ENDPROC
 3500 :
      ------------------------------------------------------------------------
-
 3510 DEFPROCerror
 3520 CASE ERR OF
 3530   WHEN 17
 3540   END
 3550   WHEN 195
 3560   REPEAT
 3570     CLS:
          PRINT:
          INPUT"  FILE ALREADY EXISTS - REUSE";YN1$
 3580   UNTIL YN1$="Y" OR YN1$="N"
 3590   IF YN1$="N" THEN 3670
 3600   OSCLI("ACCESS "+FILE$)
 3610   OSCLI("DELETE "+FILE$)
 3620   OSCLI("ACCESS G"+FILE$)
 3630   OSCLI("DELETE G"+FILE$)
 3640   OSCLI("ACCESS GL"+FILE$)
 3650   OSCLI("DELETE GL"+FILE$)
 3660   ENDPROC
 3670   REPEAT
 3680     FILE1$=FILE$
 3690     CLS:
          PRINT:
          INPUT" New data file name ";FILE$
 3700   UNTIL FILE$<>"" AND FILE$<>FILE1$
 3710   WHEN 201
 3720   CLS:
        PRINT"WRITE PROTECT TAB IS ON - PLEASE REMOVE"
 3730   PRINT"PRESS ANY KEY TO CONTINUE":
```

```
      IFGET
3740  WHEN 67798
3750  REPEAT
3760    CLS:
        PRINT"Data file not found - files on disk are:-"
3770    PRINT:
        PRINT"     ";
3780    *INFO ADFS:
        :
        0.$.*
3790    PRINT:
        PRINT"(1) Enter new filename"
3800    PRINT:
        PRINT"(2) Change the disk"
3810    PRINT:
        PRINT:
        INPUT "Please enter your choice: ";selection$
3820    CASE selection$ OF
3830      WHEN "1"
3840      FILE$=FILE1$
3850      REPEAT
3860        PRINT:
            INPUT"New data file name ";FILE1$
3870      UNTIL FILE1$<>"" AND FILE$<>FILE1$
3880      FILE$="":

3890      WHEN "2"
3900      CLS:
          PRINT TAB(10,10);"Press any key when disk has been changed":
          IFGET
3910      *MOUNT 1
3920    ENDCASE
3930  UNTIL selection$="1" OR selection$="2"
3940  OTHERWISE
3950  PRINT
3960  REPORT:
      PRINT " AT LINE";ERL;" (Error No. ";ERR;")";
3970  PRINT" - PRESS ANY KEY TO CONTINUE":
      IFGET
3980 ENDCASE
3990 ENDPROC
```

Appendix A4.1

Program: PAUL9

```
  10  CLS
  20  INPUT"TYPE VALUE OF B ";B
  30  INPUT"TYPE VALUE OF C ";C
  40  INPUT"TYPE VALUE OF D ";D
  50  CLS
  60  INPUT"ENTER LOWER LIMIT OF X ";P
  70  INPUT"ENTER UPPER LIMIT OF X ";Q
  80  INPUT"ENTER STEP INCREMENT ";R
  90  FOR X=P TO Q STEP R
 100    V=X^3-B*X^2+C*X-D
 110    PRINT X;"      ";V
 120  NEXT
 130  PRINT "DO YOU WISH TO TRY OTHER LIMITS? (Y/N?) "
 140  *FX 15,1
 150  IF GET$="Y" THEN 60 ELSE 160
 160  STOP
 170  END
```

Appendix A4.2

Program: CUBE4

```
  10  CLS
  20  INPUT "TYPE VALUE OF K12";K12
  30  INPUT "TYPE VALUE OF K21";K21
  40  INPUT "TYPE VALUE OF K13";K13
  50  INPUT "TYPE VALUE OF K31";K31
  60  INPUT "TYPE VALUE OF KEL";KEL
  70  INPUT "TYPE VALUE OF KM";KM
  80  CLS
  90  B=K12+K21+K13+K31+KEL+KM
 100
C=(K21*K31)+(K21*KM)+(K12*K31)+(K12*KM)+(K13*KM)+(K13*K21)+(KEL*K31)+(KEL*KM)+
(KEL*K21)
 110  D=(K13*K21*KM)+(KEL*K21*K31)+(KEL*K21*KM)
 115  PRINT "THE COEFFICIENTS OF THE CUBIC EQUATION ARE:"
 120  PRINT B;"          ";C;"          ";D
 140  B1=2*B
 150  R1=(B1+SQR((B1^2)-(12*C)))/6
 160  R2=(B1-SQR((B1^2)-(12*C)))/6
 170  PRINT "ONE OF THE ROOTS OF THE CUBIC EQUATION LIES BETWEEN THE
FOLLOWING VALUES:"
 180  PRINT R1;"          ";R2
 200  PRINT
 210  PRINT
 220  PRINT
 230  PRINT "DO YOU WISH TO CALCULATE FOR A DIFFERENT SET OF RATE CONSTANTS?
(Y/N)"
 240  *FX 15,1
 250  IF GET$="Y" THEN 20 ELSE 260
 260  STOP
 270  END
```

Appendix A5

Skeleton solutions of the physiological one and two-compartment pharmacokinetic models

A5.1 Skeleton solution of the physiological one-compartment pharmacokinetic model.

Using the description presented in 2.3.2.1, the differential equation describing the physiological one-compartment pharmacokinetic model is,

$$\frac{dA_P}{dt} = -k_{excr} A_P \qquad \text{A5.1.1}$$

Taking the Laplace transform of equation A5.1.1 gives

$$sa_1 - D_0 = -k_{excr} a_1$$

therefore,

$$a_1 (s + k_{excr}) = D_0$$

so,

$$a_1 = \frac{D_0}{s + k_{excr}} \qquad \text{A5.1.2}$$

hence taking the inverse Laplace transform gives,

$$A_P = D_0 e^{-k_{excr} t} \qquad \text{A5.1.3}$$

Therefore,

$$C_P = \frac{D_0 e^{-k_{excr} t}}{V_c} \qquad \text{A5.1.4}$$

and $$A_{ELIM} = D_0 - A_P \qquad \text{A5.1.5}$$

where all notation is as defined in subsection 2.3.2, and where the reader is referred to part 2.3.2.3 and Appendix A1 to observe how the principle of Laplace transforms operates.

A5.2 Skeleton solution of the physiological two-compartment pharmacokinetic model

Using the description presented in 2.3.2.1, the differential equations describing the physiological two-compartment pharmacokinetic model are,

$$\frac{dA_P}{dt} = -(k_{12} + k_{excr})A_P + k_{21}A_L \qquad \text{A5.2.1}$$

$$\frac{dA_L}{dt} = k_{12}A_P - k_{21}A_L \qquad \text{A5.2.2}$$

Taking the Laplace transforms of equations A5.2.1 and A5.2.2 respectively and re-arranging gives,

$$(s + k_{12} + k_{excr})a_1 - k_{21}a_2 = D_0 \qquad \text{A5.2.3}$$

$$-k_{12}a_1 + (s + k_{21})a_2 = 0 \qquad \text{A5.2.4}$$

hence the determinant of the system is given by,

$$\Delta = \begin{vmatrix} s + k_{12} + k_{excr} & -k_{21} \\ -k_{12} & s + k_{21} \end{vmatrix}$$

$$= s^2 + (k_{12} + k_{21} + k_{excr})s + k_{21}k_{excr} \qquad \text{A5.2.5}$$

$$\equiv s^2 + (\pi_1 + \pi_2)s + \pi_1\pi_2 = (s + \pi_1)(s + \pi_2) \quad \text{say} \qquad \text{A5.2.6}$$

so that $$\pi_1 + \pi_2 = k_{12} + k_{21} + k_{excr} \qquad \text{A5.2.7}$$

and $$\pi_1\pi_2 = k_{21}k_{excr} \qquad \text{A5.2.8}$$

which upon solving give,

$$\pi_1 = \frac{(k_{12}+k_{21}+k_{excr})+\sqrt{(k_{12}+k_{21}+k_{excr})^2-4k_{21}k_{excr}}}{2} \qquad \text{A5.2.9}$$

$$\pi_2 = \frac{(k_{12}+k_{21}+k_{excr})-\sqrt{(k_{12}+k_{21}+k_{excr})^2-4k_{21}k_{excr}}}{2} \qquad \text{A5.2.10}$$

$$\text{with } \pi_1 > \pi_2 > 0$$

Therefore $$a_1 = \frac{\begin{vmatrix} D_0 & -k_{21} \\ 0 & s+k_{21} \end{vmatrix}}{\Delta} = \frac{(s+k_{21})D_0}{(s+\pi_1)(s+\pi_2)} \qquad \text{A5.2.11}$$

which upon separating by the method of partial fractions and then taking the inverse Laplace transform gives,

$$A_P = \frac{D_0\{(k_{21}-\pi_2)e^{-\pi_2 t}-(k_{21}-\pi_1)e^{-\pi_1 t}\}}{(\pi_1-\pi_2)} \qquad \text{A5.2.12}$$

and therefore $$C_P = \frac{D_o\{(k_{21}-\pi_2)e^{-\pi_2 t}-(k_{21}-\pi_1)e^{-\pi_1 t}\}}{V_c(\pi_1-\pi_2)} \qquad \text{A5.2.13}$$

Similarly $$a_2 = \frac{\begin{vmatrix} s+k_{12}+k_{excr} & D_0 \\ -k_{12} & 0 \end{vmatrix}}{\Delta} = \frac{k_{12}D_0}{(s+\pi_1)(s+\pi_2)} \qquad \text{A5.2.14}$$

which upon separating by the method of partial fractions and then taking the inverse Laplace transform gives,

$$A_L = \frac{D_0 k_{12}\left(e^{-\pi_2 t}-e^{-\pi_1 t}\right)}{(\pi_1-\pi_2)} \qquad \text{A5.2.15}$$

Also, therefore,

$$A_{ELIM} = D_0 - A_p - A_L$$

All notation is as defined in subsection 2.3.2, and the reader is referred to part 2.3.2.3 and Appendix A1 to observe how the principle of Laplace transforms operates.